Fach: Mathematik

Numerical multiscale methods for Maxwell's equations in heterogeneous media

Inaugural-Dissertation

zur Erlangung des Doktorgrades der Naturwissenschaften
im Fachbereich Mathematik und Informatik
der Mathematisch-Naturwissenschaftlichen Fakultät
der Westfälischen Wilhelms-Universität Münster

eingereicht von

Barbara Verfürth

aus Zürich (Schweiz)

– 2018 –

Dekan: Prof. Dr. Xiaoyi Jiang
Erstgutachter: Prof. Dr. Mario Ohlberger (WWU Münster)
Zweitgutachter: Prof. Dr. Olof Runborg (KTH Stockholm)

Tag der mündlichen Prüfung: 05.06.2018
Tag der Promotion: 05.06.2018

Abstract

In this thesis we introduce new numerical multiscale methods for problems arising from time-harmonic Maxwell's equations in heterogeneous media. These problems are used to model electromagnetic wave propagation, for instance, in the context of photonic crystals. Such materials can exhibit unusual optical properties, where we are in particular interested in negative refraction. Although this phenomenon and its effects have been studied in a lot of physical experiments, the mathematical understanding of this topic is still in its infancy.

As a first step, we consider elliptic problems with heterogeneous (rapidly varying) coefficients involving the double application of the curl as differential operator. The corresponding solutions typically admit very low regularity and conventional numerical schemes have arbitrarily bad convergence rates. For locally periodic problems, we suggest a Heterogeneous Multiscale Method and prove a priori error estimates. Numerical experiments are given to confirm the convergence rates and to validate the applicability of the method. In order to cope with more general coefficients, we construct a generalized finite element method in the spirit of the Localized Orthogonal Decomposition. The method decomposes the exact solution into a coarse-scale part (spanned by standard finite element functions) and a fine-scale part. A stable corrector operator, which is quasi-local and thus can be computed efficiently, allows to represent and extract necessary fine-scale features of the solution. We show that this construction enjoys optimal approximation properties in energy and dual norms.

As the next and even more challenging step towards negative refraction, we consider (indefinite) scattering problems with periodic high contrast coefficients. Here, periodically distributed inclusions are associated with a much smaller material coefficient (scaled like the square of the periodicity length) than the rest of the scatterer. Homogenization results show that the high contrast leads to unusual effective parameters in the homogenized equation. Consequently, wave propagation inside the scatterer is physically forbidden for certain wavenumbers; this effect is called a band gap. In the analysis of the homogenized formulation, we particularly prove new wavenumber-explicit stability estimates for solutions to the Helmholtz and Maxwell equations. As numerical discretization scheme we propose a Heterogeneous Multiscale Method, for which we show inf-sup stability, quasi-optimality, and a priori error estimates. These results are obtained under a (standard) resolution condition between the wavenumber and the mesh size. Numerical experiments confirm the convergence rates and give an explanation of the physical phenomenon of band gaps.

Zusammenfassung

In dieser Arbeit präsentieren wir neue numerische Mehrskalen-Methoden für Probleme, die aus den zeitharmonischen Maxwell-Gleichungen in heterogenen Medien entstehen. Diese Probleme werden für die Modellierung elektromagnetischer Wellenausbreitung, zum Beispiel im Kontext photonischer Kristalle, benutzt. Solche Materialien können ungewöhnliche optische Eigenschaften aufweisen, wobei wir besonders an negativer Brechung interessiert sind. Obwohl dieses Phänomen und seine Auswirkungen in vielen physikalischen Experimenten studiert worden sind, steht das mathematische Verständnis dieses Themas noch am Anfang.

Als ersten Schritt betrachten wir elliptische Probleme mit heterogenen Koeffizienten, bei denen die doppelte Anwendung der Rotation den Differentialoperator bildet. Die zugehöri-

gen Lösungen haben typischerweise sehr geringe Regularität und numerische Standardverfahren konvergieren mit beliebig schlechter Rate. Für lokal periodische Probleme präsentieren wir eine Heterogene Mehrskalen-Methode und beweisen a priori Fehlerabschätzungen. Numerische Experimente bestätigen die Konvergenzraten und zeigen die Anwendbarkeit der Methode. Um allgemeinere Koeffizienten zu behandeln, konstruieren wir eine generalisierte Finite-Elemente-Methode im Sinne der Lokalisierten Orthogonalen Zerlegung. Die Methode zerlegt die exakte Lösung in einen grobskaligen Anteil (aufgespannt durch Standard-Finite-Elemente-Funktionen) und einen feinskaligen Anteil. Ein stabiler Korrektor, der quasi-lokal und daher effizient berechenbar ist, ermöglicht es, nötige feinskalige Merkmale der Lösung darzustellen und zu extrahieren. Wir zeigen, dass diese Konstruktion optimale Approximationseigenschaften in Energie- und dualen Normen besitzt.

Als nächsten und weitaus herausfordernderen Schritt Richtung negativer Brechung betrachten wir (indefinite) Streuprobleme mit periodischen Koeffizienten mit hohem Kontrast. Dabei haben periodisch angeordnete Einschlüsse einen wesentlich kleineren Materialkoeffizienten (wie das Quadrat der Periodenlänge skaliert) als der Rest des Streuhindernisses. Homogenisierungsresultate zeigen, dass der hohe Kontrast zu ungewöhnlichen effektiven Parametern in der homogenisierten Gleichung führt. Als Konsequenz ist Wellenausbreitung innerhalb des Streuhindernisses für gewisse Wellenzahlen physikalisch verboten; dieser Effekt wird auch Bandlücke genannt. Bei der Analyse der homogenisierten Formulierung beweisen wir insbesondere neue Stabilitätsabschätzungen (explizit in der Wellenzahl) für Lösungen der Helmholtz- und Maxwell-Gleichungen. Für die numerische Behandlung führen wir eine Heterogene Mehrskalen-Methode ein, für die wir inf-sup-Stabilität, Quasi-Optimalität und a priori Fehlerabschätzungen zeigen. Diese Resultate gelten unter einer (Standard-)Auflösungsbedingung zwischen der Wellenzahl und der Gitterweite. Numerische Experimente bestätigen die Konvergenzraten und erklären das physikalische Phänomen der Bandlücken.

Acknowledgments

First and foremost, I would like to express my gratitude to my supervisor Prof. Dr. Mario Ohlberger for suggesting this interesting topic and for letting me find my way in dealing with it. I sincerely thank him for his strong and kind support, for his numerous advices, and for being a mentor for quite some time. I am also very grateful to my collaborators Dr. Patrick Henning and Dr. Dietmar Gallistl for sharing their ideas and experience, for several advices and comments on our joint work, and for their encouragement.

I would also like to thank my current and former colleagues in the *Institut für Analysis and Numerik* for the pleasant atmosphere, for the friendly interaction, for nice lunch breaks, and for their help. Special thanks go to Julia Brunken and Tim Keil for proofreading this thesis.

I gratefully acknowledge financial support by the *Deutsche Forschungsgemeinschaft (DFG)* through project OH 98/6-1 "Wave propagation in periodic structures and negative refraction mechanisms". I also thank our project partners Prof. Dr. Ben Schweizer, Dr. Agnes Lamacz, and Maik Urban from TU Dortmund for several fruitful discussions and meetings and the exchange of ideas.

Furthermore, I would like to express my gratitude to the *Hausdorff Institute for Mathematics* in Bonn for the possibility to spend 3 months in the trimester program "Multiscale problems: algorithms, numerical analysis and computation". I am very grateful to the other participants, the organizers, and the administration for the inspiring working atmosphere, the hospitality, and the support.

Last but not least, I heartily thank my family and my friends for their encouragement and advice, for their never-ending support, for their belief in me, and for simply being there for me.

Contents

List of Figures

List of Tables

1 Introduction

1.1 Motivation

The behavior and propagation of electromagnetic fields (in heterogeneous media) is studied in many physical applications, for instance, in the large area of wave optics. These problems are modeled by Maxwell's equations and additional material laws. In recent years, heterogeneous materials have been studied with great interest, e.g., in the context of photonic crystals [JJWM08]. They can exhibit unusual and astonishing (optical) properties, such as frequency band gaps [JJWM08], artificial magnetism [OP02], surface plasmons [BDE03], and negative refraction [EP04, PE03].

The latter phenomenon has been described theoretically in 1968 by Veselago [Ves68]. He states that in a material with negative permittivity ε and negative permeability μ, the refractive index is negative. This implies that at the interface to a standard (positive index) material, the refracted light beam lies on the same side of the surface normal as the incident beam. We refer to Figure 1.1 a) and b) for an illustration. This has a lot of interesting applications. For instance, a simple rectangular slab of a negative index material can focus light beams and act as lens, see Figure 1.1 c). In addition, such a perfect lens has no restrictions on the obtainable spatial resolution of the imaged objects, see [Pen00]. Another interesting effect is optical cloaking [PSS06]: If an object is surrounded by a suitable negative index material, light waves seem to propagate undisturbed by the object, meaning that its existence cannot be detected from the outside.

However, Veselago's theoretical work has not been continued for quite a while since no materials with simultaneous negative values of ε and μ were known in practice. By now, the phenomenon of negative refraction has been experimentally confirmed using different setups. We solely focus on constructions based on negative index materials, which rely on *sub-wavelength fine-scale* structures. They can be realized as photonic crystals using, for instance, dielectric composites with high contrast [EP04] or split-ring and wire constructions [SPV$^+$00]. The latter setup is illustrated in Figure 1.2. We refer to the survey article [SPW04] for an overview of different constructions.

Hence, these problems involve microscopic or fine-scale structures as well as macroscopic

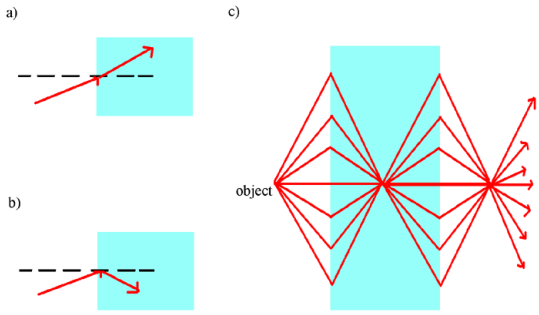

Figure 1.1: Normal (a) versus negative (b) refraction and a perfect lens made out of a negative index material (c); source: `https://commons.wikimedia.org/wiki/File:Negative_refraction_index_focusing.png`

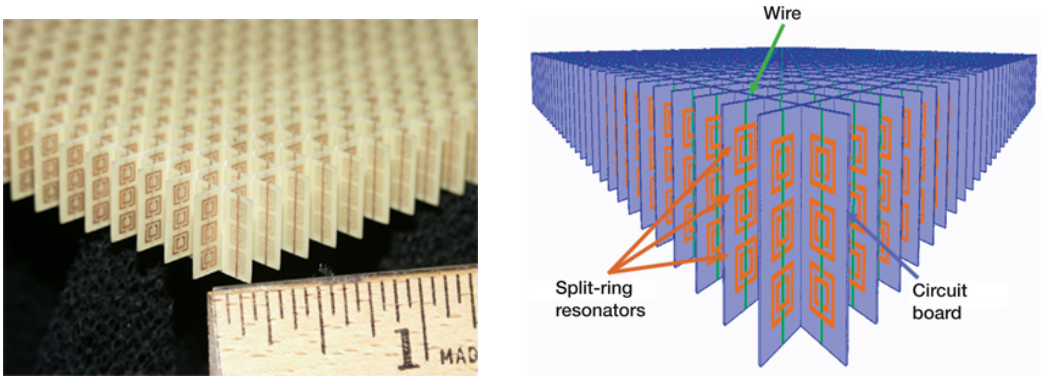

(a) (b)

Figure 1.2: Metamaterial constructed out of split rings and wires: (a) experimental setup, (b) schematic illustration; source: (a) `https://commons.wikimedia.org/wiki/File:Split-ring_resonator_array_10K_sq_nm.jpg`, (b) `https://commons.wikimedia.org/wiki/File:Left-handed_metamaterial_array_configuration.jpg` (both produced by NASA Glenn Research Center)

processes (e.g., wave propagation), so that we deal with two or more scales. As typical size for the finest scale, we introduce the (small) parameter δ. In the context of photonic crystals, δ denotes the length of the periodicity cell, whereas in general heterogeneous materials, δ should simply be seen as an indicator for fine-scale structures and is not uniquely determined. If we want to emphasize that an operator or a function depends on fine-scale features, we equip it with the index δ. In general, a *multiscale problem* has the following (abstract) formulation:

$$\text{Find} \quad u_\delta \in X \quad \text{such that} \qquad \mathcal{L}_\delta u_\delta = f,$$

where $f \in X'$ is a purely macroscopic source term. The multiscale (differential) operator $\mathcal{L}_\delta : X \to X'$ involves rapid spatial oscillations.

Typically, δ is very small in comparison to the length scale of the computational domain. Standard numerical schemes such as the Finite Element Method require to resolve the fine-scale structures in order to produce a faithful approximation of the exact solution. This is (prohibitively) expensive and easily exceeds today's available computer resources. Therefore, there is a need for *multiscale methods*, which have a computational complexity independent of δ. An additional difficulty arises from the wave-type nature of our problems: Typically, solutions are expected to have sine- or cosine-type contributions, where the oscillations become faster for higher frequencies. This again requires a fine resolution of the grid in standard numerical methods, which is known as the resolution condition [Sau06].

1.2 Goal and contribution of this work

The general long-term goal of our research is to (better) understand the mechanisms of negative refraction. As described above, we focus on the approach of effective negative index materials, which use sub-wavelength fine-scale structures. This means that the typical length scale of the material inhomogeneities is much smaller than the wavelength and consequently, we can use homogenization approaches. Furthermore, we concentrate on the time-harmonic setting so that we deal with spatial partial differential equations (PDEs) solely. We emphasize, however, that time dependence can be easily incorporated by using standard time-stepping approaches. We tackle this complex issue in two main steps: First, we deal with rapid oscillations or variations in the coefficients of our PDE and second, we additionally take high contrasts into account.

For the first step, we consider $\mathbf{H}(\mathrm{curl})$-elliptic problems with homogeneous boundary conditions and rapidly oscillating coefficients μ and κ

$$\begin{aligned} \operatorname{curl}\big(\mu(x)\operatorname{curl}\mathbf{u}(x)\big) + \kappa(x)\mathbf{u}(x) &= \mathbf{f}(x) && \text{in} \quad \Omega, \\ \mathbf{u}(x)\times\mathbf{n}(x) &= 0 && \text{on} \quad \partial\Omega. \end{aligned}$$

Such a problem models, for instance, electromagnetic waves in an (ohmic) cavity, surrounded by a perfect electric conductor. Rapidly oscillating coefficients occur, for example, in the context of photonic crystals. For locally periodic materials, we suggest a Heterogeneous Multiscale Method and show a priori convergence rates. The homogenization results as well as the a priori and a posteriori error analysis have been discussed in the author's master thesis. Numerical experiments confirming the convergence results have been conducted during the PhD, so that we summarize the theoretical and numerical findings in this thesis. They are published in *SIAM Journal of Numerical Analysis* [HOV16b] and a second numerical experiment (considering the indefinite $\mathbf{H}(\mathrm{curl})$-problem) is reported in the *Proceedings of Applied Mathematics and Mechanics* [HOV16a]. For general heterogeneous coefficients, beyond the assumption of (local) periodicity and scale separation, we suggest a Localized Orthogonal Decomposition. We analyze the approximation properties of the decomposition and present an efficiently computable localization of the involved corrector. The corresponding results are published in [GHV18]. The adaption of the described numerical scheme and its analysis to the case of indefinite problems are published in the *Proceedings of Equadiff 2017 conference* [Ver17b].

The next and even more challenging step towards negative refraction are time-harmonic scattering problems with high contrast:

$$\begin{cases} -\nabla\cdot\big(\varepsilon_\delta^{-1}(x)\nabla u_\delta(x)\big) - k^2 u_\delta(x) &= 0 \qquad \text{in } G, \\ \nabla u_\delta(x)\cdot\mathbf{n}(x) - iku_\delta(x) &= g(x) \qquad \text{on } \partial G, \end{cases}$$

or

$$\begin{cases} \operatorname{curl}\big(\varepsilon_\delta^{-1}(x)\operatorname{curl}\mathbf{u}_\delta(x)\big) - k^2\mathbf{u}_\delta(x) &= 0 \qquad \text{in } G, \\ \operatorname{curl}\mathbf{u}_\delta(x)\times\mathbf{n}(x) - ik\big(\mathbf{n}(x)\times\mathbf{u}_\delta(x)\big)\times\mathbf{n}(x) &= \mathbf{g}(x) \qquad \text{on } \partial G, \end{cases}$$

where ε_δ^{-1} is 1 outside Ω and inside Ω given by $\varepsilon_\delta^{-1}(x) = \varepsilon_0^{-1}\chi_{\Sigma^*}(\frac{x}{\delta}) + \varepsilon_1^{-1}\chi_\Sigma(\frac{x}{\delta})$. Here Σ and Σ^* form a nonoverlapping partition of the unit cell, see Figure 1.3 for an illustration. We suggest a corresponding Heterogeneous Multiscale Method, formulated as direct discretization of the associated two-scale equation. The homogenized equation includes a nonstandard effective coefficient in the identity term, which can have a positive or negative sign depending on the wavenumber. If this effective permeability is negative, wave propagation inside the scatterer is physically forbidden for the associated wavenumber, which is called a band gap. Stability and quasi-optimality of the method are shown under the assumption of a (standard) resolution condition between the wavenumber k and the mesh width. This resolution condition can become prohibitive for large wavenumbers and we, therefore, study the application of a (two-scale) Localized Orthogonal Decompositions as a remedy. Numerical experiments again confirm the theoretical findings and study the behavior of solutions for different wavenumbers and signs of the effective permeability. This gives an interesting insight into the occurrence of frequency band gaps. The results for the two-dimensional setting (the Helmholtz equation) are published in *Multiscale Modeling and Simulation* [OV18]. The theoretical analysis of the (two-scale) Localized Orthogonal Decomposition is published in *AIMS Mathematics* [OV17]. The results on the Heterogeneous Multiscale Method for the full three-dimensional Maxwell equations are published as a preprint [Ver17a] and are submitted to *ESAIM Mathematical Modeling and Numerical Analysis*.

The implementation of all numerical experiments has been done based on the module dune-gdt [MS15] of the DUNE software framework [BBD+08a, BBD+08b]. The corresponding code can be found on Github[1]. The examples are curlcurl-discretization.cc for Section 3.1.3,

[1] `github.com/BarbaraV/dune-gdt/tree/dissertation`

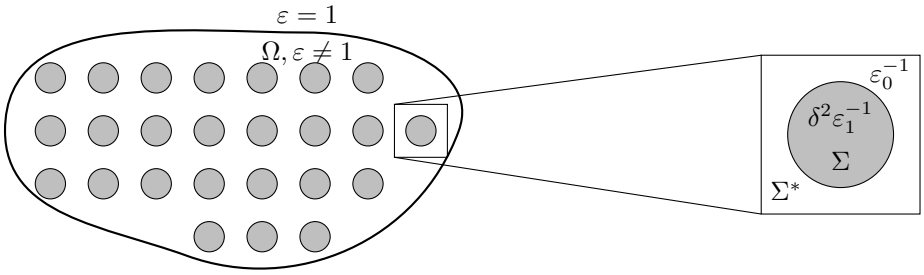

Figure 1.3: Left: Scatterer Ω with inclusions with high permittivity (in gray); Right: Zoom into one unit cell and scaling of the permittivity ε_δ^{-1}.

helmholtz.cc for Section 4.6.1, and hmm-maxwell.cc for Section 4.6.2, all located in the directory test.

1.3 Overview of the literature

There is a large variety of analytical and numerical approaches to cope with multiscale problems. Thus, we only outline the ones most closely related to our work.

Homogenization. Homogenization is an essential analytical tool to reduce the complexity of multiscale problems. Broadly speaking, the main aim is to identify a coarse-scale problem which is cheap to solve and whose solution is close to the exact solution. It considers the limit of δ tending to zero. The question is whether a unique operator $\mathcal{L}_0$ and a function u_0 exist, such that u_0 approximates u_δ and u_0 solves the problem defined by $\mathcal{L}_0$. (General) homogenization results are obtained with the techniques of *G-convergence*, dealing with symmetric linear elliptic operators; *H-convergence*, dealing with nonsymmetric linear operators; and Γ-*convergence* dealing with minimizers of energy functionals. An overview of these techniques is provided in [CD99, JKO94] and the references therein.

Even though these convergences provide the existence of a homogenized problem in very general frameworks, the limit operator $\mathcal{L}_0$ cannot be stated explicitly in most cases. For (locally) periodic problems, explicit limit equations often can be extracted using two specially tailored approaches. The first is the *asymptotic expansion* technique [BLP78] based on the (heuristic) assumption that u_δ can be written as

$$u_\delta(x) = \sum_{j=0}^{\infty} \delta^j u_j\big(x, \frac{x}{\delta}\big),$$

where each u_j is $(0,1)^d$-periodic in the second variable. In a similar spirit the method of *multiscale convergence* gives a rigorous justification of the terms of the above expansion. For a fixed number l of scales, it provides a new notion of convergence which is able to capture oscillations in resonance with δ^j for all $j \leq l-1$. In the limit, homogenized and corrector equations are obtained which can also be coupled in an l-scale limit equation. A very common specific case is two-scale convergence which deals with the first two terms in the above expansion. This method goes back to Nguetseng [Ngu89] and the notion of two-scale convergence has been introduced in the seminal paper by Allaire [All92]. This is also the main analytical homogenization tool we consider in this thesis, see Section 2.3.1 for an introduction.

There are several homogenization results (mainly using two-scale convergence) for wave propagation problems. Dispersive effects occurring for the wave equation over long time are studied in [AP16a, AP17, DLS14, DLS15]. High contrast problems are considered, for

instance, in [All92, Section 4] and [CC15]. Linear Maxwell's equations are homogenized in [CH15, GZN07, Wel01, WK03] in frequency and in time domain. Different limit equations for Maxwell's equations depending on the relation between periodicity length, wavelength and skin depth are discussed in [AS11]. Depending on the shape of the inclusions in the periodic microstructure, [SU17] characterizes the resulting homogenized equations.

To understand negative refraction mechanisms, experimentally known periodic structures are analyzed with homogenization tools. Dielectric structures with high contrast are considered in [BBF09, BBF17, BF04] and frequency-dependent, possibly negative, effective permeabilities are obtained. A qualitatively similar result is obtained for split-ring constructions [BS10, LS13, LS16c]. Wire structures are studied in [BB12, BF06, FB97] and unusual effective permittivities are obtained. Finally, a combination of dielectric structures with high contrasts and wires yields a material with effective negative index in [LS16a]. A good overview on the topic is given in [Sch17].

Homogenization theory for wave propagation is only justified in the regime where the fine-scale features are much smaller than the wavelength. If the heterogeneities of the materials are of the same order as the wavelength, Bloch wave analysis can be used. A Bloch wave is a product of a plane wave and a periodic function, where the latter is the solution to an (elliptic) eigenvalue problem. The (dispersion) relation between the wavevector of the plane wave and the eigenvalue associated to the periodic function is an important (physical) characteristic of the crystal, see, e.g., [EP04, JJWM08, LJJP02]. The use of Bloch wave expansion in the homogenization of multiscale problems goes back to [CV97] and the connections to multiscale convergence are studied, for instance, in [ABV16]. Bloch wave analysis and homogenization is employed to analyze the spectrum of the Maxwell operator in [CG07], to study dispersion effects in the wave equation in [DLS14], or to impose radiation-type boundary conditions in crystals in [DS17, FJ16, LS16b].

Multiscale methods. In addition to purely analytical homogenization tools there also exists a large variety of numerical methods to deal with multiscale problems. In the following, we present a small overview of this large topic. We mainly focus on multiscale methods which can be considered as generalized Finite Element Methods (gFEMs) in the sense of Babuška, Osborn [BO83] and Melenk [Mel95]. They modify standard finite element basis functions and/or they replace the rapidly varying coefficients with macroscopic approximations. In the end, either the exact solution u_δ or the homogenized solution u_0 are approximated, where in the latter case additional corrections can be taken into account in a post-processing step.

In this thesis we focus on two multiscale methods: the Heterogeneous Multiscale Method (HMM), introduced by E and Engquist [EE03], and the Localized Orthogonal Decomposition (LOD), introduced by Målqvist and Peterseim [MP14]. The HMM imitates the analytical homogenization procedure by locally reconstructing the fine-scale behavior of the solution in small cells around quadrature points. An average of this information is passed to a macroscopic bilinear form and the corresponding solver so that the effective (macroscopic) behavior of the solution is extracted. In other words, an approximation of the homogenized solution u_0 is obtained. The method is defined in detail in Section 2.3.3, where we also give a short overview on the associated literature. The key idea of the LOD is to decompose the solution space into a coarse (macroscopic) part and a remainder space using an interpolation operator. Fine-scale information from the kernel of the interpolation operator is extracted by a problem-dependent projection. This correction operator shows exponential decay and can be (quasi-)localized to patches. A detailed introduction to the LOD and a literature survey are given in Section 2.3.4.

This idea to decompose the solution space into a coarse-scale and a fine-scale contribution is motivated from the framework of the Variational Multiscale Method (VMM), introduced by Hughes et al. [HFMQ98, HS07]. The fine-scale equations are formally solved in dependence of the residual of the coarse-scale equation, which is a very general framework and allows for

a lot of specializations. We refer, for instance, to [BC13, OP98] for the Helmholtz equation.

Another popular multiscale method is the Multiscale Finite Element Method (MsFEM), developed by Hou and Wu [HW97]. The method constructs multiscale basis functions by solving local fine-scale problems. The basis functions are coupled in a global variational formulation so that an approximation of the exact solution is obtained, see [EH09] for an overview. Concerning formulations for the wave equation, we refer to [JE12, JEG10]. An MsFEM for elliptic problems with high contrast coefficients is presented in [CGH10]. Photonic crystals are treated with a multiscale *hp*-FEM incorporating Bloch modes in [BSS11].

With view to the question which (generalized) finite element spaces to use for rough and multiscale coefficients, we enumerate a few further suggestions made for elliptic diffusion problems. Owhadi and Zhang [OZ11, OZB14] solve localized fine-scale problems at certain macroscopic points and show optimal convergence independent of the regularity of the solution. The adaptive local (AL) basis [GGS12, Wey17] also uses such local fine-scale computations for each sub-problem, but the contributions are split in so-called near-field and far-field parts, which are approximated differently. In the *p*-FEM method for locally periodic problems [MBS00], standard finite element basis functions of polynomial degree p are modified by fine-scale shape functions, which are determined on the basis of a Fourier-Bochner representation of the exact solution. The two-scale FEM for locally periodic problems [MS02], constructs a two-scale finite element space built from a coarse mesh and a local microscopic space of δ-periodic shape functions for each coarse degree of freedom.

Similar to analytical homogenization, upscaling or averaging methods try to determine effective global properties of an operator. Note that the result of the averaging process highly depends on the chosen triangulation of the domain. The general idea is to perform local fine-scale computations and extract effective global parameters for the coarse-scale from averaging. We refer to [CHHS17] for an approach concerning Maxwell's equations and to [EIL+09] for high contrast problems. The multiscale medium approximation for heterogeneous Helmholtz equations [BCG17] also works in this spirit. Using a fine-scale mesh the wavenumber is projected onto piecewise coarse-scale constants, which are then used in the actual (macroscopic) FEM.

Based on the already mentioned l-scale equation in the context of multiscale convergence, a Sparse Multiscale FEM was suggested by Hoang and Schwab [HS05] for periodic diffusion problems. The discretized l-scale equation can be seen as a (classical) elliptic equation in $\mathbb{R}^{ld}$, where d is the space dimension and $l \geq 2$ the number of scales. Since this may become a very high dimensional system, the use of sparse grids is proposed, making accuracy and memory requirements comparable to the case of only one scale. A sparse multiscale FEM for the wave equation can be found in [XH14].

For (locally) periodic problems, one can also directly discretize (with standard finite element spaces) the terms of the asymptotic expansion or the limit functions of two-scale convergence. This approach is studied for the Helmholtz equation in [CCZ02], for Maxwell's equations in frequency domain in [CZAL10] and in time domain in [CH18, ZCW10].

In the context of *parametric* multiscale problems, where the multiscale coefficients additionally depend on a low-dimensional parameter vector and one is interested in the solution for several configurations, multiscale methods need to be combined with model order reduction approaches. The generalized Multiscale Finite Element Method (gMsFEM) [EGH13] builds a multiscale (snapshot) basis by solving local fine-scale problems in an offline stage as described above for the MsFEM. The dimension of this offline space can be reduced by a spectral decomposition. In the online stage, the solution space for a given parameter is computed using the already determined offline space. We refer to [CEH16] for an overview including adaptivity. The wave equation is studied in [CEL14] and $\mathbf{H}(\mathrm{curl})$-elliptic problems in [CL18]. The Localized Reduced Basis Multiscale Method (LRBMS) [AHKO12, OS15] combines domain decomposition and traditional reduced basis approaches. It constructs a spatially localized reduced basis on each subdomain of a coarse grid. Here, the local reduced bases can be prescribed a priori, computed as solutions to local fine-scale problems, or defined

as restrictions of global reduced bases, which allows for a lot of flexibility. By its locality the computational costs of the basis generation can be much reduced in the LRBMS in comparison to traditional (global) reduced basis methods. Based on this idea of localized reduced bases, the ArbiLoMod [BEOR17a, BEOR17b] allows for fast recomputation after arbitrary local modifications. The reduced model and the reduced basis are only changed in certain subregions, steered by a a local error indicator.

Finally, we refer to [AH17b] for an overview on multiscale methods for the wave equation and to [Li16] for a general survey of mathematical approaches (analytical and numerical) for metamaterials.

1.4 Outline of the work

This thesis is organized as follows. In Chapter 2, we introduce the analytical and numerical background necessary for this thesis. First, we study Maxwell's equations and its variants in Section 2.1. Then, in Section 2.2, we introduce the Finite Element Method for these problems. Section 2.3 finally presents analytical and numerical homogenization approaches and methods.

Chapter 3 is devoted to $\mathbf{H}(\mathrm{curl})$-elliptic problems with rapidly varying coefficients. We introduce and analyze the Heterogeneous Multiscale Method for locally periodic problems in Section 3.1. In Section 3.2, we turn to general oscillating coefficients and motivate, formulate, and analyze a corresponding numerical homogenization scheme in the spirit of the Localized Orthogonal Decomposition.

Chapter 4 deals with scattering problems with locally periodic coefficients with high contrast. We introduce the general setting in Section 4.1. The model problems are homogenized in Section 4.2 and the resulting limit equations are analyzed in Section 4.3. In Section 4.4, we formulate and analyze the corresponding Heterogeneous Multiscale Method. To relax the required resolution between the wavenumber and the mesh size, we study the application of a (two-scale) Localized Orthogonal Decomposition in Section 4.5. Extensive numerical experiments can be found in Section 4.6.

Finally, we draw some conclusions and give a short outlook on possible future research in Chapter 5.

2 Analytical and numerical background

In this chapter, we give the necessary theoretical background for this thesis. We formulate and analyze our model problems derived from Maxwell's equations in Section 2.1. Section 2.2 then deals with the (standard) finite element discretization of the model problems. Finally, Section 2.3 gives an introduction to homogenization and multiscale methods and we motivate the main numerical schemes used in this thesis.

General notation. Throughout this thesis, C denotes a generic constant, which does not depend on the mesh sizes, the oversampling parameter, or the wavenumber. It may vary from line to line in the estimates. We use the short-hand notation $a \lesssim b$ if $a \leq Cb$ with such a generic constant C, and, similarly, $a \gtrsim b$. If $a \lesssim b$ and $a \gtrsim b$, we write $a \approx b$.

2.1 Maxwell's and Helmholtz equations

In this section, we deal with Maxwell's and Helmholtz equations. Section 2.1.1 deduces the considered model problems from the Maxwell's equations in their general form given by the physical theory of electromagnetism. The associated function spaces and their main properties are introduced in Section 2.1.2. With these spaces, we can then formulate the variational problems and study the properties of the (weak) solutions in Section 2.1.3.

2.1.1 Motivation and model problems

Maxwell's equations[1] are the (physical) foundations of electromagnetism. Since they are a topic on their own, we mainly focus on the derivation of our model problems in this section. In order to understand this derivation also from a physical point of view, the important ingredients are constitutive material laws, the behavior of electromagnetic fields at interfaces (between different materials) and simplifications such as the time-harmonic or the two-dimensional case. As this section should motivate the model problems, we postpone exact definitions concerning regularity (of the domain and the coefficients) to later sections.

Maxwell's equations and constitutive laws. In the classical Maxwell equations, the following four time- and space-dependent vector fields are involved as unknowns: the electric field intensity $\mathbf{E}$, the magnetic field intensity $\mathbf{H}$, the electric displacement field $\mathbf{D}$, and the magnetic induction field $\mathbf{B}$. The sources of the electromagnetic fields are the (free) charges and currents, which are denoted by the charge density ρ and the current density $\mathbf{J}$, respectively. The classical formulation of Maxwell's equations reads, see, e.g., [Bos98, Hip02, Mon03, Zag06]:

$$\operatorname{div} \mathbf{D} = \rho, \tag{2.1a}$$

$$\operatorname{div} \mathbf{B} = 0, \tag{2.1b}$$

$$\operatorname{curl} \mathbf{E} + \frac{\partial \mathbf{B}}{\partial t} = 0, \tag{2.1c}$$

$$\operatorname{curl} \mathbf{H} - \frac{\partial \mathbf{D}}{\partial t} = \mathbf{J}. \tag{2.1d}$$

[1] James Clark Maxwell in "A Dynamical Theory of the Electromagnetic Field" (1865) and "Treatise on Electricity and Magnetism" (1873)

The basic interpretations of these laws, which we discuss here shortly, can be seen in their integral form. As there are no magnetic charges ("magnetic monopoles"), the magnetic field is source- (or divergence-) free, equation (2.1b). In contrast, electric charges exist and the electric displacement field (sometimes also called electric flux) through the boundary of a volume equals the enclosed total charge. This relation leads with the divergence theorem by Gauß (also called Gauß's theorem) to equation (2.1a). Faraday's induction law (2.1c) states that the change in time of the magnetic induction field $\mathbf{B}$ (sometimes called magnetic flux) through a surface induces an (opposite) electric field through the boundary of the surface. This can be observed, for instance, in a conductor loop positioned in a time-dependent magnetic field. Ampère's law describes the opposite fact: A current through a surface induces a magnetic field $\mathbf{H}$ in the boundary. Maxwell added a so-called displacement current $\frac{\partial \mathbf{D}}{\partial t}$ to this law, which leads to equation (2.1d). By differentiating equation (2.1a) w.r.t. t and taking the divergence of equation (2.1d), we obtain with $\operatorname{div}\operatorname{curl} = 0$ the continuity equation

$$\operatorname{div} \mathbf{J} + \frac{\partial \rho}{\partial t} = 0, \tag{2.2}$$

which relates the current density and the charge density.

Maxwell's equations (2.1) are only completely determined together with (experimentally derived) material laws. These have the form

$$\mathbf{D} = \varepsilon \mathbf{E} \qquad \text{and} \qquad \mathbf{B} = \mu \mathbf{H} \tag{2.3}$$

with tensors ε and μ. In general these tensors can depend on time, space, and even the fields themselves, but we only admit spatial dependence in the following. The electric permittivity is called ε and the magnetic permeability μ. In an ohmic conductor the current inside the conductor is related to its electric field via $\mathbf{J}_{in} = \sigma \mathbf{E}$ with the electric conductivity σ. The total current density consists of the inner current density and an impressed (or source) density $\mathbf{J} = \mathbf{J}_{in} + \mathbf{J}_s$. The latter can be assumed to be divergence-free (also called consistent), i.e., $\operatorname{div} \mathbf{J}_s = 0$. With the material laws the Maxwell equations have the same number of equations and unknowns. Still, we need initial conditions for the fields in order to have a well-defined system of PDEs. However, we will focus on the time-harmonic case soon and, therefore, we omit a detailed discussion of initial conditions.

Interface and boundary conditions. Gauß's and Stokes' theorem applied to Maxwell's equations (2.1) provide information on the behavior of the electromagnetic fields at the interface between two different materials, see [Mon03, Zag06] for a similar discussion in more detail. Let Γ be a sufficiently smooth (two-dimensional) interface between two domains R_1, R_2 with the normal $\mathbf{n}_\Gamma$ pointing from R_2 to R_1. From the divergence equations (2.1a) and (2.1b), we can deduce with Gauß' theorem that

$$[\mathbf{B} \cdot \mathbf{n}_\Gamma] = 0 \qquad \text{and} \qquad [\mathbf{D} \cdot \mathbf{n}_\Gamma] = \rho_S,$$

where $[\mathbf{B} \cdot \mathbf{n}_\Gamma] := (\mathbf{B}|_{R_2} - \mathbf{B}|_{R_1}) \cdot \mathbf{n}_\Gamma$ denotes the jump and ρ_S is the surface charge. Applying Stokes' theorem to the curl-equations (2.1c) and (2.1d), we deduce that

$$[\mathbf{E} \times \mathbf{n}_\Gamma] = 0 \qquad \text{and} \qquad [\mathbf{H} \times \mathbf{n}_\Gamma] = -\mathbf{j}_\Gamma$$

with the jump $[\cdot]$ defined as above and $\mathbf{j}_\Gamma$ the surface current. Even if $\rho_S = 0$ and $\mathbf{j}_\Gamma = 0$, we see from the material laws (2.3) that the normal components of $\mathbf{E}$ and $\mathbf{H}$ and the tangential components of $\mathbf{D}$ and $\mathbf{B}$ are discontinuous in general. This holds because at an interface between two *different* materials, we have $[\mu] \neq 0$ und $[\varepsilon] \neq 0$ in most cases.

The interface conditions derived above can also serve as a motivation for some frequently used boundary conditions, cf. again [Zag06]. Let $\mathbf{n}$ denote the unit outer normal. By *prescribing the surface quantities* ρ_S or $\mathbf{j}_\Gamma$, we directly arrive at the boundary conditions $\mathbf{D} \cdot \mathbf{n} = \rho_S$

or $\mathbf{H} \times \mathbf{n} = \mathbf{j}_\Gamma$, respectively. A *perfect electric conductor* is a region with very high conductivity σ, so that Ohm's law implies $\mathbf{E} \approx 0$. If such a perfect conductor is situated around the computational domain of interest, we obtain the boundary condition $\mathbf{E} \times \mathbf{n} = 0$. Similarly, a so-called *perfect magnetic conductor* has a high permeability and thus, $\mathbf{H} \approx 0$, which gives the boundary condition $\mathbf{H} \times \mathbf{n} = 0$. Finally, also a coupling of the electric field $\mathbf{E}$ and the magnetic field $\mathbf{H}$ is possible. So-called *impedance boundary conditions* are Robin-type boundary conditions of the form $\mathbf{H} \times \mathbf{n} - z(\mathbf{E} \times \mathbf{n}) \times \mathbf{n} = 0$ with the impedance parameter $z \in \mathbb{C}$. They can, for instance, model the reflections at the interface to a material with high (but still finite) conductivity, where eddy currents are concentrated near the surface. They also appear as approximations of the radiation condition in scattering problems. The exact boundary conditions are given together with our model problems below, but all of them fall into one of the above mentioned (physical) cases.

Simplifications. Often the system of the Maxwell equations is not studied in its full form (2.1), but (problem adapted) reductions are made. First, we replace the time domain by the frequency domain via the so-called *time-harmonic ansatz*, see [Mon03]. This means that we assume $\psi(x,t) = \mathrm{Re}(\exp(i\omega t)\widehat{\psi}(x))$ for all time-dependent quantities $\psi \in \{\mathbf{E}, \mathbf{H}, \mathbf{D}, \mathbf{B}, \rho, \mathbf{J}\}$. Here, ω is the frequency and $\widehat{\psi}$ is complex-valued. In the sequel, we use again ψ instead of $\widehat{\psi}$ for simplicity. The time-harmonic ansatz is justified by the following two common applications: First, a Fourier transform with respect to time can be applied in many cases so that the general solution can be written as the superposition of the solutions at several fixed frequencies. Second, in many physical applications the frequency is a priori known, e.g., by an incoming wave. With the time-harmonic ansatz, all time derivatives reduce to a multiplication by $i\omega$. Hence, Maxwell's equations (2.1) together with the material laws (2.3) simplify to

$$\begin{aligned} \operatorname{curl} \mathbf{E}(x) + i\omega\mu(x)\mathbf{H}(x) &= 0, \\ \operatorname{curl} \mathbf{H}(x) - i\omega\varepsilon(x)\mathbf{E}(x) &= \mathbf{J}(x). \end{aligned} \tag{2.4}$$

The divergence equations (2.1a) and (2.1b) are automatically fulfilled by taking the divergence and using the continuity equation (2.2). The time-harmonic system for $\mathbf{E}$ and $\mathbf{H}$ can be further reduced to a single second-order partial differential equation (PDE) by solving the first equation for $\mathbf{H}$ or the second equation for $\mathbf{E}$ and inserting it into the other equation.

In a *two-dimensional* setting, i.e., a geometry invariant in one direction (e.g., the x_3-direction), all quantities only depend on two space dimensions, denoted here by x_1 and x_2. Assuming a transverse electrical (TE) mode, i.e., $\mathbf{E} = (E_1(x_1, x_2), E_2(x_1, x_2), 0)$, the first equation of (2.4) directly gives $\mathbf{H} = (0, 0, H_3(x_1, x_2))$. We can then solve the second equation of (2.4) for $\mathbf{E}$ and insert it into the first equation. With the knowledge about the structure of $\mathbf{H}$, the curl reduces to a rotated gradient and reveals after a short computation that H_3 is determined as the solution to

$$\nabla \cdot (\varepsilon^{-1} \nabla H_3) + \omega^2 \mu \, H_3 = f, \tag{2.5}$$

where $f = (-\operatorname{curl}(\varepsilon^{-1}\mathbf{J}))_3$ is a source term. This means that H_3 solves a *Helmholtz equation*. Assuming a transverse magnetic (TM) mode, i.e., $\mathbf{H} = (H_1(x_1, x_2), H_2(x_1, x_2), 0)$, we can derive a similar Helmholtz equation for E_3. Therefore, the Helmholtz equation is often studied as the two-dimensional case of time-harmonic Maxwell's equations.

Model problems. With the time-harmonic Maxwell equations and the Helmholtz equation derived above, we have the basic equations at hand for our model problems. We formulate the model problems in their strong form, i.e., as PDEs with boundary conditions and postpone the presentation of the variational formulation to Section 2.1.3, where also more details on the assumptions on the data and the geometry are given.

(1) For the $\mathbf{H}(\mathrm{curl})$-*elliptic* problem, we consider time-harmonic Maxwell's equations in an ohmic conductor: We set $\mathbf{J} = -i\omega\sigma\mathbf{E} + \mathbf{j}$, where $\mathbf{j}$ is a source current density, solve the

first equation of (2.4) for $\mathbf{H}$ and insert it into the second. If the computational domain is surrounded by a perfect electric conductor, we conclude the boundary value problem

$$\begin{aligned} \operatorname{curl}(\tilde{\mu} \operatorname{curl} \mathbf{u}) + \kappa \mathbf{u} &= \mathbf{f} \qquad \text{in} \quad \Omega, \\ \mathbf{u} \times \mathbf{n} &= 0 \qquad \text{on} \quad \partial\Omega, \end{aligned} \tag{2.6}$$

where $\mathbf{u} = \mathbf{E}$, $\tilde{\mu} = \mu^{-1}$, $\kappa = -\omega^2\varepsilon + i\omega\sigma$ and $\mathbf{f} = -i\omega\mathbf{j}$. For simplicity, we write μ instead of $\tilde{\mu}$ and keep in mind that it denotes the inverse permeability when studying an $\mathbf{H}(\operatorname{curl})$-elliptic problem. (2.6) is called $\mathbf{H}(\operatorname{curl})$-elliptic because the associated sesquilinear form is coercive over the space $\mathbf{H}(\operatorname{curl})$ if μ, ε and σ are (uniformly) positive definite, see Definition 2.1.5 for details. A problem of similar structure also has to be solved in every time step of an eddy current computation; then $\mathbf{u}$ is a vector potential for the magnetic field and $\kappa = \sigma/(\Delta t)$ with the time step size Δt.

(2) For the *Helmholtz (scattering) problem*, we take (2.5), set $f = 0$ and equip it with an impedance boundary condition so that we obtain

$$\begin{aligned} -\nabla \cdot (\varepsilon^{-1} \nabla u) - k^2 \mu u &= 0 \qquad \text{in} \quad G, \\ \nabla u \cdot \mathbf{n} - iku &= g \qquad \text{on} \quad \partial G, \end{aligned} \tag{2.7}$$

where $u = H_3$, $G \subset \mathbb{R}^2$ is a two-dimensional domain, ε^{-1} and μ denote the relative permittivity and permeability, respectively, and $k = \omega/c = \omega/\sqrt{\varepsilon_0 \mu_0}$ is the wavenumber. (2.7) models the scattering of an incoming wave at an (embedded) obstacle $\Omega \subset G$. Such a problem is normally posed on the whole space with a (Sommerfeld) radiation condition. Instead, we artificially truncate the domain (by introducing G) here and approximate (at first order) the radiation condition by the impedance boundary condition. g is typically computed from the incoming wave.

(3) The Helmholtz scattering problem presented above can be seen as the two-dimensional reduction of the full *Maxwell (scattering) problem*. For this, we set $\mathbf{J} = 0$ in (2.4), solve the second equation for $\mathbf{E}$ and insert it into the first one. Together with an impedance boundary condition we conclude

$$\begin{aligned} \operatorname{curl}(\varepsilon^{-1} \operatorname{curl} \mathbf{u}) - k^2 \mu \mathbf{u} &= 0 \qquad \text{in} \quad G, \\ \operatorname{curl} \mathbf{u} \times \mathbf{n} - ik(\mathbf{n} \times \mathbf{u}) \times \mathbf{n} &= \mathbf{g} \qquad \text{on} \quad \partial G, \end{aligned} \tag{2.8}$$

where $\mathbf{u} = \mathbf{H}$ and k is again the wavenumber. The impedance boundary condition is the first order approximation of the Silver-Müller radiation condition and $\mathbf{g}$ is typically computed from the incoming wave as in the two-dimensional setting.

2.1.2 Function spaces and their properties

Before we are able to define weak solutions of our model problems (2.6)–(2.8) and prove existence as well as uniqueness, we require appropriate function spaces. Let $R \subset \mathbb{R}^d$, $d \in \{2, 3\}$, be a contractible bounded domain with Lipschitz boundary and (real-valued) outer normal field $\mathbf{n}$. If we need more regularity of the boundary in this section, we will state this explicitly. Vector-valued functions are indicated by bold-face letters and unless otherwise stated, all functions are complex-valued. The dot denotes a normal (real) scalar product, for a complex scalar product we explicitly conjugate the second component by using v^* as the conjugate complex of v. For a general Hilbert space X, we denote its dual space by X'. In this section, we introduce the necessary function spaces, discuss traces on the boundary and present (Helmholtz-type) decompositions of vector functions.

Standard Sobolev spaces. Throughout this thesis, we use standard notation: For $p \in [1, \infty)$ and $m \in \mathbb{N}_0$, $L^p(R)$ denotes the usual complex Lebesgue space with inner product $(\cdot, \cdot)_{L^2(R)}$ and norm $\|\cdot\|_{L^2(R)}$. By $W^{m,p}(R)$ we denote the space of functions on R with weak

derivatives up to order s belonging to $L^p(R)$ and we write $H^m(R) := W^{m,2}(R)$ for the scalar and $\mathbf{H}^m(R) := [H^m(R)]^d$ for the vector-valued case (mostly for $d = 3$). The domain R is omitted from the norms if no confusion can arise and $\|\cdot\|_R$ denotes the $L^2(R)$-norm for short.

The Sobolev spaces can also be defined for non-integers $s \in \mathbb{R}_{\geq 0}$, see [Mon03, p. 42]. Write $s = m + r$ with $m \in \mathbb{N}_0$ and $0 < r < 1$. Then $W^{s,p}(R)$ is the space of functions $v \in W^{m,p}(R)$ with

$$\int_R \int_R \frac{|\partial^{\boldsymbol{\alpha}} v(x) - \partial^{\boldsymbol{\alpha}} v(y)|^p}{|x-y|^{d+rp}}\, dydx < \infty, \qquad \text{for all multi-indices } \boldsymbol{\alpha} \text{ with } |\boldsymbol{\alpha}| = m, \tag{2.9}$$

equipped with the graph norm. Again, we use the abbreviation $H^s(R) = W^{s,2}(R)$ and $\mathbf{H}^s(R)$ for the vector-valued case. Finally $H^{-s}(R)$ for $s \geq 0$ denotes the dual space of $H^s(R)$, i.e., $H^{-s}(R) := (H^s(R))'$.

For the analysis of the Helmholtz scattering problem (2.7), we frequently replace the standard norm of $H^1(R)$ by the k-weighted norm $\|\cdot\|_{1,k}$ defined as

$$\|v\|_{1,k,R} := (\|\nabla v\|^2_{L^2(R)} + k^2 \|v\|^2_{L^2(R)})^{1/2}. \tag{2.10}$$

Moreover, the whole domain G is (naturally) partitioned into the scatterer Ω and the outside $G \setminus \overline{\Omega}$. In this case, it is useful to define

$$H^s_{pw}(G) := H^s(\Omega) \cap H^s(G \setminus \overline{\Omega}) \cap H^1(G) \tag{2.11}$$

for $s \geq 1$ and note that $H^s_{pw}(G) = H^s(G)$ for $1 \leq s < 3/2$, see [Pet10].

Vector functions with weak curl and divergence. Let $R \subset \mathbb{R}^3$. Recall that for a smooth vector field $\mathbf{v} = (v_1, v_2, v_3)^T$ the divergence and the curl are defined as

$$\operatorname{div} \mathbf{v} := \sum_{i=1}^{3} \frac{\partial v_i}{\partial x_i} \qquad \text{and} \qquad \operatorname{curl} \mathbf{v} := \left(\frac{\partial v_3}{\partial x_2} - \frac{\partial v_2}{\partial x_3}, \frac{\partial v_1}{\partial x_3} - \frac{\partial v_3}{\partial x_1}, \frac{\partial v_2}{\partial x_1} - \frac{\partial v_1}{\partial x_2} \right)^T.$$

Using partial integration, we can introduce a weak notion of these differential operators in the following way, see [Mon03, Section 3.5].

- For $\mathbf{v} \in L^2(R; \mathbb{C}^3)$ we call $\operatorname{div} \mathbf{v} \in L^2(R; \mathbb{C})$ the *weak divergence* of $\mathbf{v}$ if it fulfills

$$\int_R \operatorname{div} \mathbf{v}\ \psi^*\, dx = -\int_R \mathbf{v} \cdot \nabla \psi^*\, dx \qquad \forall \psi \in C_0^\infty(R; \mathbb{C}).$$

- For $\mathbf{v} \in L^2(R; \mathbb{C}^3)$ we call $\operatorname{curl} \mathbf{v} \in L^2(R; \mathbb{C}^3)$ the *weak curl* of $\mathbf{v}$ if it fulfills

$$\int_R \operatorname{curl} \mathbf{v} \cdot \boldsymbol{\psi}^*\, dx = \int_R \mathbf{v} \cdot \operatorname{curl} \boldsymbol{\psi}^*\, dx \qquad \forall \boldsymbol{\psi} \in C_0^\infty(R; \mathbb{C}^3).$$

The spaces $\mathbf{H}(\operatorname{curl})$ and $\mathbf{H}(\operatorname{div})$ are defined in a similar way like the standard Sobolev spaces.

Definition 2.1.1 ($\mathbf{H}(\operatorname{curl})$ and $\mathbf{H}(\operatorname{div})$)**.** We define the function spaces

$$\mathbf{H}(\operatorname{curl}, R) := \{\mathbf{v} \in L^2(R; \mathbb{C}^3) | \operatorname{curl} \mathbf{v} \in L^2(R; \mathbb{C}^3)\},$$
$$\mathbf{H}(\operatorname{div}, R) := \{\mathbf{v} \in L^2(R; \mathbb{C}^3) | \operatorname{div} \mathbf{v} \in L^2(R; \mathbb{C})\}$$

with the scalar products

$$(\mathbf{v}, \boldsymbol{\psi})_{\mathbf{H}(\operatorname{curl})} := (\operatorname{curl} \mathbf{v}, \operatorname{curl} \boldsymbol{\psi})_{L^2(R)} + (\mathbf{v}, \boldsymbol{\psi})_{L^2(R)},$$
$$(\mathbf{v}, \boldsymbol{\psi})_{\mathbf{H}(\operatorname{div})} := (\operatorname{div} \mathbf{v}, \operatorname{div} \boldsymbol{\psi})_{L^2(R)} + (\mathbf{v}, \boldsymbol{\psi})_{L^2(R)}.$$

We omit the domain R from the notation of the spaces if no confusion can arise. $\mathbf{H}(\mathrm{curl})$ and $\mathbf{H}(\mathrm{div})$ are Hilbert spaces and furthermore, the space of smooth functions $C^\infty(\overline{R}, \mathbb{C}^3)$ is a dense subspace. Hence, we can define $\mathbf{H}_0(\mathrm{curl}, R)$ and $\mathbf{H}_0(\mathrm{div}, R)$ as the closure of $C_0^\infty(R, \mathbb{C}^3)$ w.r.t. the corresponding norm. These spaces have zero tangential or normal traces, respectively, on the boundary as we see below. To quantify higher regularity, we define for $s \geq 0$ the space $\mathbf{H}^s(\mathrm{curl})$ as follows

$$\mathbf{H}^s(\mathrm{curl}, R) := \{\mathbf{v} \in \mathbf{H}(\mathrm{curl}, R) | \mathbf{v} \in \mathbf{H}^s(R), \mathrm{curl}\, \mathbf{v} \in \mathbf{H}^s(R)\} \tag{2.12}$$

and observe that $\mathbf{H}^0(\mathrm{curl}) = \mathbf{H}(\mathrm{curl})$. The space of divergence-free functions is denoted by $\mathbf{H}(\mathrm{div}\, 0)$.

In order to define a suitable functions space for the Maxwell scattering problem, we introduce the following space of tangential L^2-functions on the boundary

$$L_T^2(\partial R) := \{\mathbf{v} \in [L^2(\partial R)]^3 | \mathbf{v} \cdot \mathbf{n} = 0\}.$$

We denote by $\mathbf{v}_T := (\mathbf{n} \times \mathbf{v}) \times \mathbf{n} = \mathbf{v} - (\mathbf{v} \cdot \mathbf{n})\mathbf{n}$ the tangential component of a vector function $\mathbf{v}$ on the boundary. Then, we define the space for the Maxwell scattering problem as

$$\mathbf{H}_{\mathrm{imp}}(R) := \{\mathbf{v} \in \mathbf{H}(\mathrm{curl}, R) | \mathbf{v}_T \in L_T^2(\partial R)\}, \tag{2.13}$$

equipped with the graph norm, see [Mon03, Section 3.8].

For the analysis of the scattering problem (2.8), we frequently replace the standard norms of $\mathbf{H}(\mathrm{curl})$ and $\mathbf{H}_{\mathrm{imp}}$ by the k-weighted norms $\|\cdot\|_{\mathrm{curl},k}$ and $\|\cdot\|_{\mathrm{imp},k}$ given by

$$\|\mathbf{v}\|_{\mathrm{curl},k,R} := (\|\mathrm{curl}\, \mathbf{v}\|_{L^2(R)}^2 + k^2 \|\mathbf{v}\|_{L^2(R)}^2)^{1/2}, \tag{2.14}$$

$$\|\mathbf{v}\|_{\mathrm{imp},k,R} := (\|\mathrm{curl}\, \mathbf{v}\|_{L^2(R)}^2 + k^2 \|\mathbf{v}\|_{L^2(R)}^2 + k \|\mathbf{v}_T\|_{L^2(\partial R)}^2)^{1/2}. \tag{2.15}$$

Again, the whole domain G is (naturally) partitioned into the scatterer Ω and the outside $G \setminus \overline{\Omega}$. In this case, it is useful to define for $s \geq 0$ the space $\mathbf{H}_{pw}^s(\mathrm{curl})$ as

$$\mathbf{H}_{pw}^s(\mathrm{curl}, G) := \mathbf{H}^s(\mathrm{curl}, \Omega) \cap \mathbf{H}^s(\mathrm{curl}, G \setminus \overline{\Omega}) \cap \mathbf{H}(\mathrm{curl}, G). \tag{2.16}$$

Traces. The definition of Sobolev spaces on Lipschitz domains requires care. For $|s| \leq 1$, the space $H^s(\partial R)$ for a bounded Lipschitz domain $R \subset \mathbb{R}^d$ can be defined via local charts and the definition is well-posed in the sense that it does not depend on the chosen parametrization, see [Mon03, Section 3.2.1] and [Moi11, Section 5.5]. Recall that for $s < 0$, we deal with a dual space. If $0 \leq s < 1$, the definition via local charts is equivalent to the definition of H^s given via (2.9). It is well known (see, e.g., [Mon03, Theorem 3.9]) that there exists a linear, continuous operator $\mathrm{tr} : H^1(R) \to H^{1/2}(\partial R)$ which fulfills

$$\mathrm{tr}(v) = v|_{\partial R} \qquad \forall v \in H^1(R) \cap C^0(\overline{R}).$$

This trace operator is used to define the space $H_0^1(R)$ as the space of all functions in $H^1(R)$ with vanishing traces on the boundary. $H_0^1(R)$ coincides with the closure of $C_0^\infty(R)$ w.r.t. the $H^1(R)$-norm.

From now on, we deal with the three-dimensional case $d = 3$ to identify the traces of functions in $\mathbf{H}(\mathrm{div})$ or $\mathbf{H}(\mathrm{curl})$, see [Mon03, Theorems 3.24, 3.29].

Proposition 2.1.2 (Trace theorems)**.** *Let $R \subset \mathbb{R}^3$ be a bounded Lipschitz domain.*

- *There exists a linear, continuous operator $\mathrm{tr}_{\mathbf{n}} : \mathbf{H}(\mathrm{div}) \to H^{-1/2}(\partial R)$ which fulfills*

$$\mathrm{tr}_{\mathbf{n}}(\mathbf{v}) = (\mathbf{v} \cdot \mathbf{n})|_{\partial R} \qquad \forall \mathbf{v} \in \mathbf{H}(\mathrm{div}) \cap C^0(\overline{R}, \mathbb{C}^3).$$

- *There exists a linear, continuous operator* $\operatorname{tr}_{\boldsymbol{\tau}} : \mathbf{H}(\operatorname{curl}) \to \mathbf{H}^{-1/2}(\partial R)$ *which fulfills*

$$\operatorname{tr}_{\boldsymbol{\tau}}(\mathbf{v}) = (\mathbf{v} \times \mathbf{n})|_{\partial R} \qquad \forall \mathbf{v} \in \mathbf{H}(\operatorname{curl}) \cap C^0(\overline{R}, \mathbb{C}^3).$$

From now on, we write $\mathbf{v} \cdot \mathbf{n}$ and $\mathbf{v} \times \mathbf{n}$ for $\operatorname{tr}_{\mathbf{n}}(\mathbf{v})$ and $\operatorname{tr}_{\boldsymbol{\tau}}(\mathbf{v})$, respectively. With these traces, we can also give an explicit characterization of the spaces $\mathbf{H}_0(\operatorname{curl})$ and $\mathbf{H}_0(\operatorname{div})$ which we introduced as the closure of $C_0^\infty(R)$. In particular, we have

$$\mathbf{H}_0(\operatorname{curl}, R) = \{\mathbf{v} \in \mathbf{H}(\operatorname{curl}, R) |\, \mathbf{v} \times \mathbf{n} = 0\}, \qquad \mathbf{H}_0(\operatorname{div}, R) = \{\mathbf{v} \in \mathbf{H}(\operatorname{div}, R) |\, \mathbf{v} \cdot \mathbf{n} = 0\}.$$

Gauß's theorem gives the following rules of partial integration

$$\begin{aligned}
\int_R \operatorname{div} \mathbf{v}\, \psi^*\, dx &= \int_{\partial R} \operatorname{tr}_{\mathbf{n}}(\mathbf{v})\, \psi^*\, d\sigma - \int_R \mathbf{v} \cdot \nabla \psi^*\, dx && \forall \psi \in H^1(R), \mathbf{v} \in \mathbf{H}(\operatorname{div}, R), \\
\int_R \operatorname{curl} \mathbf{v} \cdot \boldsymbol{\psi}^*\, dx &= -\int_{\partial R} \operatorname{tr}_{\boldsymbol{\tau}}(\mathbf{v}) \cdot \boldsymbol{\psi}^*\, d\sigma + \int_R \mathbf{v} \cdot \operatorname{curl} \boldsymbol{\psi}^*\, dx && \forall \boldsymbol{\psi} \in \mathbf{H}^1(R), \mathbf{v} \in \mathbf{H}(\operatorname{curl}, R).
\end{aligned}$$

With these identities we also deduce the following interface conditions for a piecewise defined function: In order to be in $\mathbf{H}(\operatorname{div})$, the normal traces have to agree; in order to be in $\mathbf{H}(\operatorname{curl})$, the tangential traces have to agree. For a precise formulation we refer to [Mon03, Lemma 5.3]. Note that we obtained similar conditions for the fields in Maxwell's equations in Section 2.1.1.

For the impedance boundary condition in the Maxwell scattering problem (2.8), we need further spaces. For detailed definitions and further properties, we refer to [BC01, BCS02]. First, to quantify higher regularity of a tangential vector field $\mathbf{v} \in L_T^2(\partial R)$, we introduce the space

$$\mathbf{H}_T^s(\partial R) := \{\mathbf{v} \in \mathbf{H}^s(\partial R) | \mathbf{v} \cdot \mathbf{n} = 0\}. \tag{2.17}$$

This is well-defined for $0 \le s \le 1/2$ in the case of a C^2-domain and for $0 \le s < 1/2$ in the case of a polyhedral Lipschitz boundary. In the latter case, the space can also be defined piecewise on each face. Second, there is another (tangential) linear and bounded trace operator $\operatorname{tr}_T : \mathbf{H}^1(R) \to \mathbf{H}^{1/2}(\partial R)$ defined via $\operatorname{tr}_T(\mathbf{v}) := \mathbf{v}_T = \mathbf{v} - (\mathbf{v} \cdot \mathbf{n})\mathbf{n} = (\mathbf{n} \times \mathbf{v}) \times \mathbf{n}$. The operator can be extended to a mapping from $\mathbf{H}(\operatorname{curl}, R)$ to $\mathbf{H}^{-1/2}(\partial R)$. The mapping is not surjective and we simply define the range space as

$$\mathbf{H}_\parallel^s(\partial R) := \operatorname{tr}_T(\mathbf{H}^{s+1/2}(R)), \quad \text{for} \quad s \in (0, 1), \tag{2.18}$$

and refer to [BC01, BCS02] for a characterization. Third, $\operatorname{curl}_{\partial R}$ is defined as the $L^2(\partial R)$-adjoint of $\mathbf{curl}_{\partial R}\, v := \operatorname{tr}_{\boldsymbol{\tau}}(\nabla v)$ for $v \in H^2(R)$, see [BC01] for a precise definition. We define for any Lipschitz surface Γ

$$\mathbf{H}(\operatorname{curl}_\Gamma) := \{\mathbf{v} \in L_T^2(\Gamma) |\, \operatorname{curl}_\Gamma(\mathbf{v}) \in L^2(\Gamma)\}. \tag{2.19}$$

Decompositions. We study the connections between the spaces $H^1(R)$, $\mathbf{H}(\operatorname{curl}, R)$ and $\mathbf{H}(\operatorname{div}, R)$. In this analysis it is important that $R \subset \mathbb{R}^3$ is contractible, i.e., simply connected with connected boundary. The image and kernel of the differential operators is summarized in the so-called de Rham sequence: The de Rham sequence

$$\mathbb{C} \xrightarrow{\text{id}} H^1(R) \xrightarrow{\nabla} \mathbf{H}(\operatorname{curl}, R) \xrightarrow{\operatorname{curl}} \mathbf{H}(\operatorname{div}, R) \xrightarrow{\operatorname{div}} L^2(R) \xrightarrow{0} \{0\}$$

is exact, i.e., the image of one operator is equal to the kernel of the following operator. For zero boundary conditions the modified de Rham sequence

$$\mathbb{C} \xrightarrow{\text{id}} H_0^1(R) \xrightarrow{\nabla} \mathbf{H}_0(\operatorname{curl}, R) \xrightarrow{\operatorname{curl}} \mathbf{H}_0(\operatorname{div}, R) \xrightarrow{\operatorname{div}} L_0^2(R) \xrightarrow{0} \{0\}$$

with $L^2_0(R) := \{v \in L^2(R) | \int_R v\,dx = 0\}$ is still exact. This in particular implies (i) $\operatorname{curl}\nabla = 0$ and $\operatorname{div}\operatorname{curl} = 0$, (ii) a curl-free vector field (i.e., a field $\mathbf{v}$ with $\operatorname{curl}\mathbf{v} = 0$) can be written as a gradient, and (iii) a divergence-free vector field (i.e., a field $\mathbf{v}$ with $\operatorname{div}\mathbf{v} = 0$) can be written as a curl.

The Helmholtz decomposition states that every vector field can be decomposed into a curl-free and a divergence-free part. We only give one of the many variants and refer to [ABDG98] for more details, also in the case of a noncontractible domain.

Proposition 2.1.3 (Helmholtz decomposition)**.** *For every vector field $\mathbf{v} \in L^2(R, \mathbb{C}^3)$ there exists the (unique) orthogonal decomposition*

$$\mathbf{v} = \operatorname{curl}\mathbf{w} + \nabla\theta \qquad \text{with} \quad \theta \in H^1(R), \mathbf{w} \in \mathbf{H}(\operatorname{curl}, R).$$

In particular, if $\mathbf{v} \in \mathbf{H}_0(\operatorname{curl}, R)$ we have the orthogonal decomposition

$$\mathbf{v} = \mathbf{z} + \nabla\theta \qquad \text{with} \quad \theta \in H^1_0(R), \mathbf{z} \in \mathbf{H}_0(\operatorname{curl}, R) \cap \mathbf{H}(\operatorname{div} 0, R),$$

where $\mathbf{H}(\operatorname{div} 0, R)$ is the space of the divergence-free functions.

The orthogonality is meant w.r.t. $L^2(R)$. The scalar potential θ is characterized as solution to the following problem: Find $\theta \in H^1_0(R)$ such that $(\nabla\theta, \nabla\psi)_{L^2(R)} = (\mathbf{v}, \nabla\psi)_{L^2(R)}$ for all $\psi \in H^1_0(R)$.

The second part of the proposition immediately rises the question how $\mathbf{H}_0(\operatorname{curl}, R) \cap \mathbf{H}(\operatorname{div} 0, R)$ is connected to $\mathbf{H}^1(R)$. Partial integration directly shows that $\mathbf{H}_0(\operatorname{curl}, R) \cap \mathbf{H}_0(\operatorname{div}, R)$ coincides with $\mathbf{H}^1_0(R)$. If only parts of the traces are known, the situation is more complicated and additional conditions on the domain are required. More precisely, if R has a C^2-boundary or if R is a *convex* polyhedral Lipschitz domain, then $\mathbf{H}_0(\operatorname{curl}, R) \cap \mathbf{H}(\operatorname{div}, R)$ and $\mathbf{H}_0(\operatorname{div}, R) \cap \mathbf{H}(\operatorname{curl}, R)$ are both continuously embedded in $\mathbf{H}^1(R)$, see [ABDG98]. Even for general Lipschitz domains, a *regular* decomposition with $\mathbf{z} \in \mathbf{H}^1_0(R)$ can be obtained, but the uniqueness and the L^2-orthogonality are lost. More precisely, we have the following results, see [Hip02, Hip15, PZ02].

Proposition 2.1.4 (Regular decomposition)**.** *For every $\mathbf{v} \in \mathbf{H}_0(\operatorname{curl}, R)$, there exist $\mathbf{z} \in \mathbf{H}^1_0(R)$ and $\theta \in H^1_0(R)$ such that $\mathbf{v} = \mathbf{z} + \nabla\theta$.*

The Helmholtz as well as the regular decompositions are important tools in the analysis of $\mathbf{H}(\operatorname{curl})$-problems such as (2.6) and (2.8), since they admit a splitting into the kernel of the curl-operator and its complement.

2.1.3 Weak solutions: Existence, uniqueness, stability and regularity

With the knowledge of the function spaces from the previous section, we can define and analyze the variational formulations of our model problems (2.6)–(2.8). We also (briefly) discuss the existence and uniqueness of solutions as well as stability and (higher) regularity results that are available in the literature.

Weak solutions. The weak (or variational) formulations of the (strong) equations (2.6)–(2.8) are obtained by multiplying with a test function and integrating by parts. In our cases, one order of the derivative is shifted to the test function so that the weak problems require less regularity of the solutions. In the sequel, we give precise assumptions on the domain and the data for each problem.

Definition 2.1.5 ($\mathbf{H}(\operatorname{curl})$-elliptic problem)**.** Let $\Omega \subset \mathbb{R}^3$ be an open, bounded, contractible domain with polyhedral Lipschitz boundary. Let $\mathbf{f} \in \mathbf{H}(\operatorname{div}, \Omega)$, $\mu \in L^\infty(\Omega; \mathbb{R}^{3\times3})$ and $\kappa \in L^\infty(\Omega; \mathbb{C}^{3\times3})$. We define the sesquilinear form $\mathcal{B} : \mathbf{H}(\operatorname{curl}, \Omega) \times \mathbf{H}(\operatorname{curl}, \Omega) \to \mathbb{C}$ as

$$\mathcal{B}(\mathbf{v}, \boldsymbol{\psi}) := (\mu \operatorname{curl}\mathbf{v}, \operatorname{curl}\boldsymbol{\psi})_{L^2(\Omega)} + (\kappa\mathbf{v}, \boldsymbol{\psi})_{L^2(\Omega)}.$$

The form $\mathcal{B}$ is obviously continuous, i.e., there is $C_B > 0$ such that

$$|\mathcal{B}(\mathbf{v}, \boldsymbol{\psi})| \leq C_B \|\mathbf{v}\|_{\mathbf{H}(\mathrm{curl},\Omega)} \|\boldsymbol{\psi}\|_{\mathbf{H}(\mathrm{curl},\Omega)} \qquad \forall \mathbf{v}, \boldsymbol{\psi} \in \mathbf{H}(\mathrm{curl}, \Omega).$$

We furthermore assume that $\mathcal{B}$ is $\mathbf{H}(\mathrm{curl})$-elliptic, i.e., there is $\alpha > 0$ such that

$$|\mathcal{B}(\mathbf{v}, \mathbf{v})| \geq \alpha \|\mathbf{v}\|^2_{\mathbf{H}(\mathrm{curl})} \qquad \forall \mathbf{v} \in \mathbf{H}_0(\mathrm{curl}).$$

We then seek $\mathbf{u} \in \mathbf{H}_0(\mathrm{curl}, \Omega)$ such that

$$\mathcal{B}(\mathbf{u}, \boldsymbol{\psi}) = (\mathbf{f}, \boldsymbol{\psi})_{L^2(\Omega)} \qquad \forall \boldsymbol{\psi} \in \mathbf{H}_0(\mathrm{curl}, \Omega). \tag{2.20}$$

This is the weak formulation associated with (2.6). The ellipticity assumption on $\mathcal{B}$ is a condition on μ and κ. It is, for instance, fulfilled if (i) $\mathrm{Im}(\kappa)$ is uniformly positive definite or if (ii) $\kappa \in L^\infty(\Omega, \mathbb{R}^{3\times 3})$ and it is again uniformly positive definite. Case (i) occurs in an ohmic conductor and case (ii) is attained in each time step of an eddy current simulation, see the discussion in Section 2.1.1. For other settings yielding an $\mathbf{H}(\mathrm{curl})$-elliptic problem we refer to [FR05]. In Chapter 3, we study the $\mathbf{H}(\mathrm{curl})$-elliptic problem of Definition 2.1.5 in detail.

Definition 2.1.6 (Helmholtz problem)**.** Let $G \subset \mathbb{R}^2$ be an open, bounded, contractible domain with C^2-boundary. Let $\varepsilon^{-1}, \mu \in L^\infty(G; \mathbb{R})$ be uniformly positive, $g \in L^2(\partial G)$ and $k \in \mathbb{R}$ with $k \geq k_0 > 0$. We define the sesquilinear form $\mathcal{B}_1 : H^1(G) \times H^1(G) \to \mathbb{C}$ as

$$\mathcal{B}_1(v, \psi) := (\varepsilon^{-1} \nabla v, \nabla \psi)_{L^2(G)} - k^2 (\mu v, \psi)_{L^2(G)} - ik (v, \psi)_{L^2(\partial G)},$$

which is continuous. We then seek $u \in H^1(G)$ such that

$$\mathcal{B}_1(u, \psi) = (g, \psi)_{L^2(\partial G)} \qquad \forall \psi \in H^1(G). \tag{2.21}$$

This is the weak formulation associated with (2.7). The definition for the three-dimensional generalization (2.8) is similar.

Definition 2.1.7 (Maxwell problem)**.** Let $G \subset \mathbb{R}^3$ be an open, bounded, contractible domain with C^2-boundary. Let $\varepsilon^{-1}, \mu \in L^\infty(G; \mathbb{R})$ be uniformly positive and piecewise constant, $\mathbf{g} \in L^2_T(\partial G)$ and $k \in \mathbb{R}$ with $k \geq k_0 > 0$. We define the sesquilinear form $\mathcal{B}_2 : \mathbf{H}_{\mathrm{imp}}(G) \times \mathbf{H}_{\mathrm{imp}}(G) \to \mathbb{C}$ as

$$\mathcal{B}_2(\mathbf{v}, \boldsymbol{\psi}) := (\varepsilon^{-1} \operatorname{curl} \mathbf{v}, \operatorname{curl} \boldsymbol{\psi})_{L^2(G)} - k^2 (\mu \mathbf{v}, \boldsymbol{\psi})_{L^2(G)} - ik (\mathbf{v}_T, \boldsymbol{\psi}_T)_{L^2(\partial G)},$$

which is continuous. We then seek $\mathbf{u} \in \mathbf{H}_{\mathrm{imp}}(G)$ such that

$$\mathcal{B}_2(\mathbf{u}, \boldsymbol{\psi}) = (\mathbf{g}, \boldsymbol{\psi}_T)_{L^2(\partial G)} \qquad \forall \boldsymbol{\psi} \in \mathbf{H}_{\mathrm{imp}}(G). \tag{2.22}$$

For the scattering problems, the domain is called G because we will later on have a second (embedded) domain Ω, which is the actual scatterer. G is the (artificial) computational domain introduced to truncate the whole space. Note that we include the wave propagation inside the scatterer in our model and do not only set a condition on the boundary of the scatterer. The assumption $k \geq k_0$ means that we are interested in medium and high frequencies and thus, the explicit dependency of all constants on k is of interest. In Chapter 4, the scattering problems of Definitions 2.1.6 and 2.1.7 are studied in detail.

Remark 2.1.8. In Definitions 2.1.6 and 2.1.7, we assume that the coefficients ε^{-1} and μ are real- and scalar-valued. The existence and uniqueness results presented below can be extended to the matrix-valued case and furthermore, ε^{-1} and μ may also be complex-valued with $\mathrm{Im}(\varepsilon^{-1})$ negative semidefinite and $\mathrm{Im}(\mu)$ positive semidefinite. Combinations of these situations occur in Chapter 4. However, we present the existence and uniqueness results only for the scalar- and real-valued case for simplicity as this is in agreement with the literature.

Existence and uniqueness of solutions. For the $\mathbf{H}(\mathrm{curl})$-elliptic problem of Definition 2.1.5, existence and uniqueness directly follows from the Theorem of Lax-Milgram-Babuška [Bab71], repeated below for convenience.

Theorem 2.1.9 (Lax-Milgram-Babuška)**.** *Let X be a (complex) Hilbert space and $B : X \times X \to \mathbb{C}$ a sesquilinear form which is continuous and coercive, i.e., there exist $c, C > 0$ such that for all $v, \psi \in X$*

$$|B(v,\psi)| \leq C\|v\|_X\|\psi\|_X \qquad \textit{(continuity)} \qquad \textit{and} \qquad |B(v,v)| \geq c\|v\|_X^2 \qquad \textit{(coercivity).}$$

Given $F \in X'$, there exists a unique $u \in X$ such that

$$B(u,\psi) = F(\psi) \qquad \forall \psi \in X.$$

Since the sesquilinear forms for the Helmholtz problem in Definition 2.1.6 and the Maxwell problem in Definition 2.1.7 are not coercive, the existence and uniqueness of a solution cannot be proved with the Theorem of Lax-Milgram-Babuška. In fact, in most cases uniqueness is shown first, i.e., it exists *at most* one solution. For that, it has to be proved that for a zero right-hand side the solution (if it exists) is necessarily zero. For the Helmholtz as well as the Maxwell equation, we obtain by inserting $\psi = v$ in the corresponding sesquilinear form and taking the imaginary part that $v \in H_0^1(G)$ for the Helmholtz problem and that $\mathbf{v}_T = 0$ for the Maxwell problem. Unique continuation principles [Ale12, Mon03, NW12] then give that v or $\mathbf{v}$ are already zero on the whole domain.

The existence of solutions to (2.21) and (2.22) is proved with Fredholm theory. We repeat the main theorem of the Fredholm alternative in the formulation of [Hip15, Theorem 13] below.

Theorem 2.1.10 (Fredholm alternative)**.** *Let X, Y be Banach spaces, $T : X \to Y$ a bijective bounded linear operator and $K : X \to Y$ a compact linear operator. Then,*

$$T + K \quad \textit{injective} \quad \Leftrightarrow \quad T + K \quad \textit{bijective} \quad \Leftrightarrow \quad T + K \quad \textit{surjective.}$$

The sesquilinear forms $\mathcal{B}_1$ and $\mathcal{B}_2$ can be identified with an operator, which one then tries to split in the way required by the Fredholm alternative. Note that we have already proved that $T + K$ is injective by proving the uniqueness of a solution. The splitting in $T + K$ with T bijective and K compact is accomplished by a so-called Gårding inequality: We add a term to the original sesquilinear form so that is becomes coercive. The added term must give rise to a compact operator in order to make Fredholm alternative applicable. For instance, for the Helmholtz problem of Definition 2.1.6 we have the following result, see [Hip15].

Lemma 2.1.11 (Gårding inequality for the Helmholtz problem)**.** *Let the assumptions of Definition 2.1.6 be fulfilled. There exist $C, c > 0$ (independent of k) such that for all $v \in H^1(G)$*

$$\mathrm{Re}\{\mathcal{B}_1(v,v) + Ck^2\|v\|_{L^2(G)}^2\} \geq c\|v\|_{1,k,G}^2.$$

The term $Ck^2\|v\|_{L^2(G)}^2$ can be identified with a compact operator because of the compact embedding of $H^1(G)$ into $L^2(G)$. The constant C only depends on the upper bound of μ.

For the Maxwell problem of Definition 2.1.7, the same idea is not applicable, since the embedding of $\mathbf{H}_{\mathrm{imp}}$ into L^2 is not compact due to the large kernel of the curl-operator. Instead, we have to use a Helmholtz decomposition (similar to Proposition 2.1.3) and a so-called sign-flip isomorphism. To be more precise, we have the following result.

Lemma 2.1.12 (Gårding-type inequality for the Maxwell problem)**.** *Let the assumption of Definition 2.1.7 be fulfilled. Decompose $\mathbf{v} \in \mathbf{H}_{\mathrm{imp}}$ as $\mathbf{v} = \mathbf{z} + \nabla\theta$ with $\theta \in H_0^1(G)$ and $\mathbf{z} \in \mathbf{H}_{\mathrm{imp}}(G) \cap \mathbf{H}(\mathrm{div}\,0, G)$. Define the sign-flip isomorphism $SF(\mathbf{v}) := \mathbf{z} - \nabla\theta$. There exist $C, c > 0$ such that for all $\mathbf{v} \in \mathbf{H}_{\mathrm{imp}}$*

$$|\mathcal{B}_2(\mathbf{v}, SF(\mathbf{v})) + C(k^2\|\mathbf{z}\|_{L^2(G)}^2 + k\|\mathbf{z}_T\|_{L^2(\partial G)}^2)| \geq c\|\mathbf{v}\|_{\mathrm{imp},k,G}^2.$$

The sign-flip isomorphism corrects the wrong sign of $\mathcal{B}_2$ on the subspace of gradients and the added term corrects the sign for the remainder part. Mixed terms between $\mathbf{z}$ and $\nabla\theta$ in $\mathcal{B}_2$ either vanish due to the L^2-orthogonality or can be absorbed using Cauchy-Schwarz and Young's inequality. The added term $C(k^2\|\mathbf{z}\|^2_{L^2(G)} + k\|\mathbf{z}_T\|^2_{L^2(\partial G)})$ can be identified with a compact operator, see [Mon03, Theorem 4.7]. See [GM12] and [Hip15] (with the regular decomposition) for similar Gårding-type inequalities.

Stability and higher regularity. Lax-Milgram-Babuška as well as Fredholm theory immediately imply stability, i.e., the solution depends continuously on the data. For instance, the solution $\mathbf{u} \in \mathbf{H}_0(\mathrm{curl})$ to (2.20) fulfills

$$\|\mathbf{u}\|_{\mathbf{H}(\mathrm{curl})} \leq C/c \; \|\mathbf{f}\|_{L^2}.$$

For the scattering problems of Definitions 2.1.6 and 2.1.7, however, this stability constant depends on the wavenumber k. Since we are interested in the behavior for large k, the explicit dependency on k needs to be known. This cannot be achieved by Fredholm theory, but by explicit calculations, mostly using special test functions or the so-called Rellich-Morawetz identities (see [MS14] and the original papers [ML68, Mor75]).

At first, constant coefficients have been studied with the result that the stability constant for the Helmholtz equation behaves like

- k^0 for G polygonal and star-shaped with respect to a ball, see [Mel95] for $d = 2$ and [CF06, Het07] for $d \geq 2$;
- k^0 for a C^∞-domain G, see [BSW16];
- k^1 for a general Lipschitz domain, see [Spe14], which improves the earlier result of $k^{5/2}$, see [EM12].

However, such a polynomial stability does not always exist as the counter-example of a so-called trapping domain constructed in [BCG$^+$11] shows. More recently, extensions to non-constant coefficients have been studied such as scalar-valued Lipschitz coefficients in [BGP17] or scalar and piecewise constant coefficients in [BCG17]. Detailed stability analysis is conducted for the transmission problem in [MS17] and for general matrix-valued coefficients in [GPS18]. The latter two works also discuss in how far the assumptions on the jumps of the coefficients are necessary to avoid an exponential-type k-dependency of the stability constant. In this spirit, [ST17] analyzes the one-dimensional case for coefficients with several jumps. Nothing worse than exponential stability is possible, while the well-behaved polynomial stability is even the dominant case. For the three-dimensional case of Maxwell's equation (2.22) less results are available. All works show a dependency of k^0 for constant coefficients [FW14b, HMP11, Moi11, WW14]. We study the issue of stability for problems like those of Definitions 2.1.6 and 2.1.7 in more detail in Section 4.3.2 and obtain some generalizations of the above mentioned results for matrix-valued, nonconstant coefficients.

Since the scattering problems of Definitions 2.1.6 and 2.1.7 are not coercive, the well-posedness (provided by Fredholm theory) is expressed via *inf-sub stability*. For instance, for the Helmholtz equation there exists a constant $C > 0$, which depends on k, such that

$$\inf_{v \in H^1(G)\setminus\{0\}} \sup_{\psi \in H^1(G)\setminus\{0\}} \frac{\mathrm{Re}\, \mathcal{B}_1(v,\psi)}{\|v\|_{1,k}\|\psi\|_{1,k}} \geq C.$$

It can be shown, see, e.g., [EM12], that $C \approx (kC_{\mathrm{stab}})^{-1}$, where C_{stab} denotes the k-dependent stability constant for the problem. A similar result also holds for Maxwell's equation (2.22). Hence, the knowledge of the k-dependency of the stability constant is also important for the inf-sup constant.

Often the solutions to variational problems admit higher regularity than required in the problem. From elliptic regularity theory we can deduce that the solution u of the Helmholtz

problem of Definition 2.1.6 admits $H^2(G)$ regularity if $\varepsilon^{-1} \in W^{1,\infty}(G)$, $g \in H^{1/2}(\partial G)$ and G is either a C^2-domain or convex. If ε is discontinuous or G not convex, the maximal regularity depends on the shape of the interfaces or the boundary, respectively. We refer to [Gri85, GT77, Pet10] for more details and discuss the higher regularity for our example of the (homogenized) Helmholtz equation in Section 4.3. Using the Helmholtz or regular decomposition, the regularity of solutions to problems in $\mathbf{H}(\mathrm{curl})$ can be re-traced to elliptic regularity. For problems as in Definition 2.1.5, the solution $\mathbf{u}$ admits $\mathbf{H}^1(\mathrm{curl})$-regularity if $\mu, \kappa \in W^{1,\infty}(\Omega)$, $\mathbf{f} \in \mathbf{H}(\mathrm{div})$ and Ω is either a C^2-domain or convex, see [Hip02]. In the case of discontinuous coefficients or nonconvex domains, the regularity is reduced, for details see [BGL13, CD00, CDN99]. These results also apply to Neumann-type boundary conditions. In the case of impedance boundary conditions as in Definition 2.1.7, however, the maximal regularity $\mathbf{H}^1(\mathrm{curl})$ is only achieved for Lipschitz-continuous coefficients and $\mathbf{g} \in \mathbf{H}_T^{1/2}(\partial G)$ on C^2-domains, see [Moi11]. For polyhedral domains, even if they are convex, the regularity is reduced, see [Moi11] and the results in Proposition 4.3.8.

2.2 Finite element discretizations

In this section, we present the standard discretization of our model problems, based on the Finite Element Method (FEM). We only consider lowest order methods and (uniform) mesh refinement, the latter is commonly denoted by h-FEM. In Section 2.2.1, we recall the main ingredients for the FEM and some basic notations on meshes. In Section 2.2.2, we introduce the finite element spaces for our model problems which approximate the spaces H^1, $\mathbf{H}(\mathrm{curl})$, $\mathbf{H}(\mathrm{div})$ and L^2. In Section 2.2.3, we study stable interpolation operators on these spaces more closely because they are an essential ingredient for one of our multiscale methods, the Localized Orthogonal Decomposition.

2.2.1 Basic concepts of the Finite Element Method

Galerkin approximation. Our model problems can be abstractly written as variational problems over a Hilbert space: Let X be a Hilbert space with dual X', $\mathcal{B} : X \times X \to \mathbb{C}$ a sesquilinear form and $F \in X'$. Find $u \in X$ such that

$$\mathcal{B}(u, \psi) = F(\psi) \qquad \forall \psi \in X. \tag{2.23}$$

The Galerkin projection, see, e.g., [Cia78, Section 2.1], provides a general technique for a discrete approximation of the above problem. Let X_h be a finite-dimensional Hilbert space and find $u_h \in X_h$ such that

$$\mathcal{B}(u_h, \psi_h) = F(\psi_h) \qquad \forall \psi_h \in X_h. \tag{2.24}$$

Here, h denotes a discretization parameter and typically, a sequence of spaces X_h with $h \to 0$ is considered. Important questions are (i) whether u_h is well-defined and (ii) how well u_h approximates u.

We only consider *conforming* methods, i.e., $X_h \subset X$. Since X_h is finite-dimensional, a basis can be chosen so that the determination of the discrete solution u_h is equivalent to the solution of a linear system. For conforming methods the error fulfills the *Galerkin orthogonality*

$$\mathcal{B}(u - u_h, \psi_h) = 0 \qquad \forall \psi_h \in X_h.$$

For coercive and continuous sesquilinear forms u_h is automatically well-defined and the Galerkin orthogonality directly gives the first abstract error estimate, the *Céa lemma*, see [BS08, Theorem 2.8.1] and [Cia78, Theorem 2.4.1].

Lemma 2.2.1 (Céa)**.** *Let $\mathcal{B}$ be coercive and continuous, u the solution to* (2.23) *and $u_h \in X_h \subset X$ the discrete solution to* (2.24)*. It holds that*

$$\|u - u_h\|_X \lesssim \inf_{v_h \in X_h} \|u - v_h\|_X.$$

This means that the error of the conforming Galerkin approximation is determined by the best approximation error. For convergence results (and rates) it is then sufficient to study the approximation properties of the discrete space X_h. In the case of an indefinite sesquilinear form fulfilling a Gårding inequality, however, already the well-posedness of the discrete problem (2.24) is not directly given. For sufficiently fine meshes well-posedness and also quasi-optimality results similar to the Céa lemma can be established, see [Sch74]. This constraint on h eventually leads to so-called resolution conditions for the discretization of the scattering problems of Definitions 2.1.6 and 2.1.7.

Meshes. The construction of the discrete finite element (FE) spaces X_h depends on an underlying mesh of the computational domain (called Ω in this section). We make the following assumptions on our mesh, see [Cia78, Section 2.1].

Definition 2.2.2 (Triangulation)**.** A triangulation $\mathcal{T}_h$ (simplicial mesh) is a finite subdivision $\mathcal{T}_h = \{T_j | j \in I\}$ of Ω with an index set I into simplices T_j (triangles for $d = 2$ and tetrahedra for $d = 3$). $\mathcal{T}_h$ is called regular if

1. it is nonoverlapping, i.e., $\operatorname{int}(T_j) \cap \operatorname{int}(T_l) = \emptyset$ for $j \neq l$;
2. it is a covering of Ω, i.e., $\bigcup_{j \in I} T_j = \overline{\Omega}$;
3. it has no hanging nodes, i.e., $T_j \cap T_l$ for $j \neq l$ is either empty, or a vertex or an edge or a face of both elements.

We define the local mesh size $h_j := \operatorname{diam}(T_j)$ and the global mesh size $h = \max_{j \in I} h_j$. Instead of h_j, we sometimes write h_T.

Definition 2.2.3 (Shape regular and quasi-uniform)**.** Let $\mathcal{T}_h$ be a regular triangulation of Ω. For an element $T_j \in \mathcal{T}_h$, we denote by ρ_j the incircle radius, i.e., the maximal number such that a ball of radius ρ_j completely fits into T_j.

- $\mathcal{T}_h$ is called shape regular if $h_j/\rho_j \leq C$ for all $j \in I$ with C independent of h.
- $\mathcal{T}_h$ is called quasi-uniform if $h_j = Ch$ for all $j \in I$ with C independent of h.

We always assume shape regularity of our triangulations, while quasi-uniformity is only required in special cases. Shape regularity means that the minimal angle in the triangulation is bounded away from zero, uniformly in h, i.e., it does not degenerate under mesh refinement.

It is useful to have a notion of neighboring elements. We directly quantify the "distance" between elements of the triangulation by introducing mth level patches as follows, see Figure 2.1 for an illustration and cf., e.g., [GHV18, Pet17].

Definition 2.2.4 (Patches)**.** Given any (possibly even not connected) subdomain $R \subset \overline{\Omega}$ define its neighborhood via

$$\mathrm{N}(R) := \operatorname{int}(\cup\{T \in \mathcal{T}_h | T \cap \overline{R} \neq \emptyset\})$$

and for any $m \geq 2$ the patches

$$\mathrm{N}^1(R) := \mathrm{N}(R) \qquad \text{and} \qquad \mathrm{N}^m(R) := \mathrm{N}(\mathrm{N}^{m-1}(R)).$$

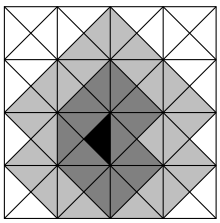

Figure 2.1: Triangle T (in black) and its first and second order patches (additional elements for $\mathrm{N}(T)$ in dark gray and additional elements for $\mathrm{N}^2(T)$ in light gray).

Shape regularity implies that there is a uniform bound $C_{\mathrm{ol},m}$ on the number of elements in the mth level patch

$$\max_{T\in\mathcal{T}_h} \operatorname{card}\{K \in \mathcal{T}_h | K \subset \overline{\mathrm{N}^m(T)}\} \leq C_{\mathrm{ol},m} \tag{2.25}$$

and (additional) quasi-uniformity implies that $C_{\mathrm{ol},m}$ depends polynomially on m.

Finite element. Our Galerkin approximation is based on a shape regular triangulation $\mathcal{T}_h$ as introduced above, so that h is the essential discretization parameter. It remains to define the spaces X_h, which is done separately for each element $T \in \mathcal{T}_h$. As already mentioned, we consider Finite Element Methods as special case of a Galerkin approximation. In this context a finite element is defined in general as follows, see [Cia78, Section 2.3] and [BS08, Definition 3.1.1].

Definition 2.2.5 (Finite Element)**.** A finite element is a triple $(K, P_K, \mathcal{D}_K)$, where

1. the geometric domain K is bounded and closed with nonempty interior and piecewise smooth boundary;
2. the space of shape functions P_K is a finite-dimensional space of functions on K;
3. the set of degrees of freedoms $\mathcal{D}_K = \{L_j\}_j$ is a basis of the dual space P_K'.

In this thesis, K will be a simplex (triangle or tetrahedron) and P_K a set of polynomials of total degree at most 1. Of course, for the same K and P_K several choices of $\mathcal{D}_K$ are still possible. Since the degrees of freedom form a basis of the dual spaces, they can be utilized to define a so-called *nodal basis* $\{\phi_j\}_j$ of $\mathcal{P}_K$ which fulfills $L_j(\phi_l) = \delta_{jl}$, see [BS08, Definition 3.1.2]. A so-called *nodal interpolation operator* I_K can be defined for sufficiently smooth functions v as

$$I_K(v) = \sum_j L_j(v)\phi_j. \tag{2.26}$$

The next step is to connect the local finite elements on each simplex $T \in \mathcal{T}_h$ to a global space. A global set of degrees of freedom $\mathcal{D}$ is obtained by identifying degrees of freedom at interfaces between elements of the mesh. The local nodal bases can then be glued together to a global basis, see [Cia78, Section 2.3] for details. Note that the global basis functions only have a small support, which is one key feature of the FEM. Since we want to consider conforming Galerkin methods only, the (local) degrees of freedom of the finite element have to be chosen appropriately, so that the global finite element space is a subspace of X. Then we can equivalently define X_h as

$$X_h = \{v_h \in X \,|\, v_h|_T \in P_T \quad \forall T \in \mathcal{T}_h\}.$$

A global nodal interpolation operator I_H can be defined via the local nodal interpolation operator (2.26) on each element.

2.2.2 Lowest order elements for H^1, $\mathbf{H}(\mathrm{curl})$, $\mathbf{H}(\mathrm{div})$ and L^2

In this section, we define the conforming finite element spaces for H^1, $\mathbf{H}(\mathrm{curl})$, $\mathbf{H}(\mathrm{div})$ and L^2. Our main focus lies on H^1 and $\mathbf{H}(\mathrm{curl})$ as these are the spaces for our model problems. Although we repeat the main definitions, we assume that the reader is familiar with the standard Lagrange finite elements for H^1. As described in the previous section, we begin with the local finite elements. Let K be a simplex in $\mathbb{R}^d$ with $d \in \{2, 3\}$ and denote by $\mathcal{P}^p(K)$ the polynomials of (total) degree at most p on K.

Definition 2.2.6 (Local Finite Element)**.**

1. The FE for H^1 (see [Mon03, Def. 5.46]) is given by the local space $P_K = \mathcal{P}^1$ and the degrees of freedom $\mathcal{D}_K = \{L_j\}_{j=1}^{d+1}$ are defined by $L_j(p) = p(a_j)$, where a_j are the vertices of K. The nodal basis is denoted by λ_j.

2. Let $d = 3$. The FE for $\mathbf{H}(\mathrm{curl})$ (see [Mon03, Def. 5.33]) is given by the local space $P_K = \mathcal{N} := \{\mathbf{a} + \mathbf{b} \times x \mid \mathbf{a}, \mathbf{b} \in \mathbb{C}^3\}$ and the degrees of freedom $\mathcal{D}_K = \{L_j\}_{j=1}^{6}$ are defined by $L_j(\mathbf{p}) = \fint_{E_j} \mathbf{p} \cdot \mathbf{t}\, ds$, where E_j are the edges of K and $\mathbf{t}$ is the unit tangent. The nodal basis $\boldsymbol{\phi}_j$ for the edge $E_j = \mathrm{conv}\{a_{i_0}, a_{i_1}\}$ with tangent from a_{i_0} to a_{i_1} is given by (see [Mon03, Section 5.5.1])
$$\boldsymbol{\phi}_j = |E_j|(\lambda_{i_0} \nabla \lambda_{i_1} - \lambda_{i_1} \nabla \lambda_{i_0}).$$

3. The FE for $\mathbf{H}(\mathrm{div})$ (see [Mon03, Def. 5.14]) is given by the local space $P_K = \mathcal{RT} := \{\mathbf{a} + bx \mid \mathbf{a} \in \mathbb{C}^d, b \in \mathbb{C}\}$ and the degrees of freedom $\mathcal{D}_K = \{L_j\}_{j=1}^{d+1}$ are defined by $L_j(\mathbf{p}) = \fint_{F_j} \mathbf{p} \cdot \mathbf{n}\, d\sigma$, where F_j are the faces of K.

4. The FE for L^2 is given by the local space $P_K = \mathcal{P}^0$ and the local degree of freedom $\mathcal{D}_K = \{L_1\}$ is defined by $L_1(p) = \fint_K p\, dx$.

For the case of vector-valued functions in $\mathbf{H}^1$ or $L^2(\Omega; \mathbb{C}^3)$, the presented scalar spaces are applied component-wise. Note that the local spaces $\mathcal{N}$ and $\mathcal{RT}$ lie inbetween zeroth and first order polynomials.

For a simple implementation of the FEM, local FE spaces and the shape (basis) function should only be given on the so-called reference element $\widehat{T} = \mathrm{conv}\{0, \mathbf{e}_1, \ldots, \mathbf{e}_d\}$, where $\mathbf{e}_j$ is the jth unit vector. A general simplex is the image of the reference element under an affine map $F_T : \widehat{T} \to T$, $F_T(\widehat{x}) = A\widehat{x} + \mathbf{b}$. Using this affine map, transformations for shape functions on the reference element to a general simplex can be defined. In order to also preserve the degrees of freedom, we define the following (conforming) transformations, see [Zag06, Lemmas 4.10, 4.15].

Lemma 2.2.7 (Conforming transformations)**.** *Let $\widehat{T}$ be the reference element and F_T the reference map as above.*

1. *Let $\widehat{v} \in H^1(\widehat{T})$ and define $v := \widehat{v} \circ F_T^{-1}$. Then $v \in H^1(T)$ and $\nabla_x v = (A^{-1})^T \nabla_{\widehat{x}} \widehat{v} \circ F_T^{-1}$.*

2. *Let $\widehat{\mathbf{v}} \in \mathbf{H}(\mathrm{curl}, \widehat{T})$ and define $\mathbf{v} := (A^{-1})^T\, \widehat{\mathbf{v}} \circ F_T^{-1}$. Then $\mathbf{v} \in \mathbf{H}(\mathrm{curl}, T)$ with $\mathrm{curl}_x \mathbf{v} = \det(A)^{-1} A\, (\mathrm{curl}_{\widehat{x}} \widehat{\mathbf{v}}) \circ F_T^{-1}$.*

Identifying degrees of freedom associated with global edges or vertices of the mesh, we can glue together the local finite elements to global spaces. Let Δ_0, Δ_1 be the set of vertices and edges of $\mathcal{T}_h$, respectively. Then we define
$$\mathcal{S}(\mathcal{T}_h) = \bigoplus_{a_j \in \Delta_0} \mathrm{span}\{\lambda_j\} \qquad \text{and} \qquad \mathcal{N}(\mathcal{T}_h) = \bigoplus_{E_j \in \Delta_1} \mathrm{span}\{\boldsymbol{\phi}_j\}.$$
These spaces are conforming, i.e., they are subspaces of $H^1(\Omega)$ and $\mathbf{H}(\mathrm{curl}, \Omega)$, respectively. The global basis is denoted by $\{\lambda_a\}_{a \in \Delta_0}$ and $\{\boldsymbol{\phi}_E\}_{E \in \Delta_1}$, respectively. The same procedure can be applied to the finite elements for $\mathbf{H}(\mathrm{div})$ and L^2. Thus, we can alternatively define the spaces as follows, see [Mon03, Chapter 5].

Definition 2.2.8 (Global spaces)**.** We define the following global FE spaces

$$\begin{aligned}\mathcal{S}(\mathcal{T}_h) &= \{v \in H^1(\Omega)|\ v|_T \in \mathcal{P}^1(T) \quad \forall T \in \mathcal{T}_h\}\\ \mathcal{N}(\mathcal{T}_h) &= \{\mathbf{v} \in \mathbf{H}(\mathrm{curl},\Omega)|\ \mathbf{v}|_T \in \mathcal{N}(T) \quad \forall T \in \mathcal{T}_h\}\\ \mathcal{RT}(\mathcal{T}_h) &= \{\mathbf{v} \in \mathbf{H}(\mathrm{div},\Omega)|\ \mathbf{v}|_T \in \mathcal{RT}(T) \quad \forall T \in \mathcal{T}_h\}\\ \mathcal{P}^0(\mathcal{T}_h) &= \{v \in L^2(\Omega)|\ v|_T \in \mathcal{P}^0(T) \quad \forall T \in \mathcal{T}_h\}.\end{aligned}$$

Finite element spaces with zero traces can be obtained by setting the degrees of freedom on the boundary to zero. They are denoted by $\mathring{\mathcal{S}}(\mathcal{T}_h)$, $\mathring{\mathcal{N}}(\mathcal{T}_h)$ and $\mathring{\mathcal{RT}}(\mathcal{T}_h)$. The L^2-conforming space is sometimes generalized to other polynomial orders as $\mathcal{P}^p(\mathcal{T}_h) := \{v \in L^2(\Omega)|\ v|_T \in \mathcal{P}^p(T)\}$.

The FE spaces are constructed such that the exact de Rham sequence of the continuous spaces carries over to the discrete case. Let $\Omega \subset \mathbb{R}^3$ be simply connected with connected boundary. Then the discrete de Rham sequence

$$\mathbb{R} \xrightarrow{\mathrm{id}} \mathcal{S}(\mathcal{T}_h) \xrightarrow{\nabla} \mathcal{N}(\mathcal{T}_h) \xrightarrow{\mathrm{curl}} \mathcal{RT}(\mathcal{T}_h) \xrightarrow{\mathrm{div}} \mathcal{P}^0(\mathcal{T}_h) \xrightarrow{0} \{0\}$$

is exact, see [AFW06]. The same also holds true for the FE spaces with zero boundary conditions. The sequence in particular implies the relations $\nabla\mathcal{S}(\mathcal{T}_h) \subset \mathcal{N}(\mathcal{T}_h)$ and $\mathrm{curl}\mathcal{N}(\mathcal{T}_h) \subset \mathcal{RT}(\mathcal{T}_h)$.

In Section 2.2.1, we have already discussed the construction of nodal interpolation operators I_h. For instance, for the spaces $\mathcal{S}(\mathcal{T}_h)$ and $\mathcal{N}(\mathcal{T}_h)$, the nodal interpolation operators I_h^L and I_h^E, respectively, are defined for sufficiently smooth functions v and $\mathbf{v}$ as

$$I_h^L(v) = \sum_{a\in\Delta_0} v(a)\lambda_a \qquad \text{and} \qquad I_h^E(\mathbf{v}) = \sum_{E\in\Delta_1} \Big(\fint_E \mathbf{v}\cdot\mathbf{t}\,ds\Big)\boldsymbol{\phi}_E.$$

In the same way also I_h^F for $\mathcal{RT}(\mathcal{T}_h)$ and I_h^P for $\mathcal{P}^0(\mathcal{T}_h)$ are defined. Note that I_h^P is simply the local L^2-projection. Except for I_h^P, all other nodal interpolation operators need higher regularity than H^1, $\mathbf{H}(\mathrm{curl})$ or $\mathbf{H}(\mathrm{div})$. In particular, I_h^L is well-defined on $H^{3/2+\delta}(\Omega)$, I_h^E on $\mathbf{H}^{1/2+\delta}(\mathrm{curl},\Omega)$, and I_h^F on $\mathbf{H}(\mathrm{div}) \cap \mathbf{H}^{1/2+\delta}(\Omega)$ for $\delta > 0$. Moreover, the following diagram commutes, see [Mon03, (5.59)]:

$$\begin{array}{ccccccc}
H^1(\Omega) & \xrightarrow{\nabla} & \mathbf{H}(\mathrm{curl}) & \xrightarrow{\mathrm{curl}} & \mathbf{H}(\mathrm{div}) & \xrightarrow{\mathrm{div}} & L^2(\Omega) \\
\cup & & \cup & & \cup & & \\
H^{3/2+\delta}(\Omega) & & \mathbf{H}^{1/2+\delta}(\mathrm{curl}) & & \mathbf{H}^{1/2+\delta}(\Omega)\cap\mathbf{H}(\mathrm{div}) & & \\
\downarrow{\scriptstyle I_h^L} & & \downarrow{\scriptstyle I_h^E} & & \downarrow{\scriptstyle I_h^F} & & \downarrow{\scriptstyle I_h^P} \\
\mathcal{S}(\mathcal{T}_h) & \xrightarrow{\nabla} & \mathcal{N}(\mathcal{T}_h) & \xrightarrow{\mathrm{curl}} & \mathcal{RT}(\mathcal{T}_h) & \xrightarrow{\mathrm{div}} & \mathcal{P}^0(\mathcal{T}_h)
\end{array}$$

Using this commuting diagram, the scaling properties of the transformations (from and to the reference element), and the Bramble-Hilbert lemma, the interpolation errors can be estimated.

Proposition 2.2.9 (Estimates for the interpolation error)**.** *Let $\mathcal{T}_h$ be a (three-dimensional) regular and shape regular simplicial mesh and recall the spaces of Definition 2.2.8.*

1. *If $v \in H^s(\Omega)$ for $s \in (\frac{3}{2}, 2]$, I_h^L satisfies (see [Mon03, Thm. 5.48])*

$$h^{-1}\|v - I_h^L v\|_{L^2(\Omega)} + \|\nabla(v - I_h^L v)\|_{L^2(\Omega)} \lesssim h^{s-1}\|v\|_{H^s(\Omega)}.$$

2. *If $\mathbf{v} \in \mathbf{H}^s(\mathrm{curl},\Omega)$ for $s \in (\frac{1}{2}, 1]$, I_h^E satisfies (see [Mon03, Thm. 5.41, Rem. 5.42])*

$$\|\mathbf{v} - I_h^E\mathbf{v}\|_{L^2(\Omega)} \lesssim h^s\|\mathbf{v}\|_{\mathbf{H}^s(\mathrm{curl})} \qquad \text{and} \qquad \|\,\mathrm{curl}(\mathbf{v} - I_h^E\mathbf{v})\|_{L^2(\Omega)} \lesssim h^s\|\,\mathrm{curl}\,\mathbf{v}\|_{\mathbf{H}^s(\Omega)}.$$

3. *If* $\mathbf{v} \in \mathbf{H}^s(\Omega)$ *and* $\operatorname{div} \mathbf{v} \in H^s(\Omega)$ *for* $s \in (\frac{1}{2}, 1]$, I_h^F *satisfies (see [Mon03, Thm. 5.25, Rem. 5.26])*

$$\|\mathbf{v} - I_h^F \mathbf{v}\|_{L^2(\Omega)} \lesssim h^s \|\mathbf{v}\|_{\mathbf{H}^s(\Omega)} \qquad \text{and} \qquad \|\operatorname{div}(\mathbf{v} - I_h^F \mathbf{v})\|_{L^2(\Omega)} \lesssim h^s \|\operatorname{div} \mathbf{v}\|_{H^s(\Omega)}.$$

All estimates also hold elementwise. (Similar) best approximation estimates are given in [EG17b]. Furthermore, nodal-type interpolation operators for $\mathbf{H}(\operatorname{curl})$ can also be constructed based on the Helmholtz decomposition, see [Cia16]. We refer to the next section for a detailed discussion on (quasi-)interpolation operators, which are already well-defined on the spaces H^1 and $\mathbf{H}(\operatorname{curl})$, respectively.

2.2.3 Stable interpolation operators

The nodal interpolation operators introduced in the previous section are utilized for a priori error estimates, where we can expect some higher regularity of the analytical solution, see Section 2.1.3. However, in situations where no additional regularity can (reasonably) be assumed, the nodal operators lack the required stability (they may even not be well-defined) and new approaches are needed. Examples of such situations are a posteriori error estimates and decompositions of the function spaces in the spirit of the Local Orthogonal Decomposition (LOD), see Section 2.3.4. We focus on interpolation operators for the latter situation and introduce appropriate choices for the spaces H^1 and $\mathbf{H}(\operatorname{curl})$, which are used in Sections 3.2 and 4.5.

Stable interpolation in H^1. We seek an interpolation operator $\Pi_h : H_0^1(\Omega) \to \mathring{\mathcal{S}}(\mathcal{T}_h)$ which is a projection, i.e., $\Pi_h \circ \Pi_h = \Pi_h$, and has the following stability property: It fulfills for all $T \in \mathcal{T}_h$ and all $v \in H_0^1(\Omega)$

$$h_T^{-1} \|v - \Pi_h(v)\|_{L^2(T)} + \|\nabla(v - \Pi_h(v))\|_{L^2(T)} \lesssim \|\nabla v\|_{L^2(\mathrm{N}(T))}. \tag{2.27}$$

The previous estimate implies that Π_h is H^1-stable. Moreover, the scaling in h is consistent with scaling estimates for the L^2-norm and H^1-seminorm of discrete functions. Indeed, one possible construction satisfying the required properties is the following: We concatenate the L^2-projection onto discontinuous affine elements $\mathcal{P}^1(\mathcal{T}_h)$ (as defined in Section 2.2.2) with the Oswald interpolation operator $I_h^O : \mathcal{P}^1(\mathcal{T}_h) \to \mathring{\mathcal{S}}(\mathcal{T}_h)$. The Oswald interpolation operator takes the average of the different nodal values of a function in $\mathcal{P}^1(\mathcal{T}_h)$. Let $v \in \mathcal{P}^1(\mathcal{T}_h)$ and define $I_h^O(v)$ for any (interior) vertex $a \in \mathring{\Delta}_0$ via

$$I_h^O(v)(a) = \frac{1}{\operatorname{card}\{K \in \mathcal{T}_h | a \in K\}} \sum_{T \in \mathcal{T}_h : a \in T} v|_T(a).$$

Estimate (2.27) follows from the properties of the L^2-projection and the Oswald interpolation operator, see [DE12, Pet16]. We emphasize that the kernel of this interpolation operator Π_h can be computed efficiently because the construction only involves local problems. Other possible choices are the local L^2-projection and Clément-type operators, see [EHMP16] for a detailed discussion. Note that the projection property can be relaxed by only requiring the existence of a quasi-local and stable right inverse, see, e.g., [HP13, MP14].

Stable interpolation in $\mathbf{H}(\operatorname{curl})$. For $\mathbf{H}(\operatorname{curl})$, we also require a stable, (quasi-)local interpolation operator which fits into a commuting diagram (as the nodal interpolation operators do). Constructing an operator that enjoys such properties is a very delicate task and a lot of operators have been suggested with different backgrounds and applications in mind. The nodal interpolation operator and the interpolation operators introduced in [DB05] are not well-defined on $\mathbf{H}(\operatorname{curl})$ and hence lack the required stability. Various (quasi)-interpolation operators are constructed as composition of smoothing and some (nodal) interpolation, such as [Chr07, CW08, DH14, EG16, Sch05, Sch08]. For all of them, the kernel of the operator is

practically hard or even impossible to compute and they only fulfill the projection *or* the locality property. Finally, we mention the interpolation operator of [EG17b] which is local and a projection, however, which does not commute with the exterior derivative. A suitable candidate (and to the author's best knowledge, the only one) that enjoys all required properties is proposed by Falk and Winther in [FW14a] and it is called π^E from now on. We briefly describe the construction of [FW14a] for the present case of the space $\mathbf{H}(\mathrm{curl})$ in three space dimensions. The two-dimensional case is thoroughly described in the gentle introductory paper [FW15].

Let again Δ_0 and Δ_1 denote the set of vertices and edges of $\mathcal{T}_h$, respectively, and let $\mathring{\Delta}_0$ and $\mathring{\Delta}_1$ denote the interior vertices and edges, i.e., the elements of Δ_0 and Δ_1 that are not a subset of $\partial\Omega$. As introduced in Section 2.2.2, the space $\mathring{\mathcal{N}}(\mathcal{T}_h)$ is spanned by the well-known edge-oriented basis $(\boldsymbol{\phi}_E)_{E\in\mathring{\Delta}_1}$. Any vertex $a \in \Delta_0$ possesses a nodal patch (sometimes also called macroelement)

$$\omega_a := \mathrm{int}\big(\cup\{T \in \mathcal{T}_h : a \in T\}\big).$$

For any edge $E \in \Delta_1$ being the convex hull of the two vertices $a_1, a_2 \in \Delta_0$, i.e., $E = \mathrm{conv}\{a_1, a_2\}$, the extended edge patch reads $\omega_E^{ext} := \omega_{a_1} \cup \omega_{a_2}$. The restriction of the mesh $\mathcal{T}_h$ to ω_E^{ext} is denoted by $\mathcal{T}_h(\omega_E^{ext})$ and the restrictions of the finite element spaces $\mathcal{S}$, $\mathcal{N}$, and $\mathcal{RT}$ are denoted accordingly. The operator $Q_E^1 : \mathbf{H}(\mathrm{curl}, \omega_E^{ext}) \to \mathcal{N}(\mathcal{T}_h(\omega_E^{ext}))$ is defined for any $\mathbf{v} \in \mathbf{H}(\mathrm{curl}, \omega_E^{ext})$ via

$$\begin{aligned}(\mathbf{v} - Q_E^1\mathbf{v}, \nabla\tau) &= 0 \qquad && \forall \tau \in \mathcal{S}^1(\mathcal{T}_h(\omega_E^{ext})),\\ (\mathrm{curl}(\mathbf{v} - Q_E^1\mathbf{v}), \mathrm{curl}\,\boldsymbol{\psi}) &= 0 && \forall \boldsymbol{\psi} \in \mathcal{N}(\mathcal{T}_h(\omega_E^{ext})).\end{aligned}$$

Given any vertex $a \in \Delta_0$, define the piecewise constant function z_a^0 by

$$z_a^0 = \begin{cases} |\omega_a|^{-1} & \text{in } \omega_a,\\ 0 & \text{in } \Omega \setminus \omega_a,\end{cases}$$

where $|\omega_a|$ is the measure of the patch ω_a. For an edge $E \in \Delta_1$ shared by vertices $a_1, a_2 \in \Delta_0$ such that $E = \mathrm{conv}\{a_1, a_2\}$, define

$$(\delta z^0)_E := z_{a_2}^0 - z_{a_1}^0.$$

Let for any $E \in \Delta_1$ the field $\mathbf{z}_E^1 \in \mathring{\mathcal{RT}}(\mathcal{T}_h(\omega_E^{ext}))$ be defined by

$$\begin{aligned}\mathrm{div}\,\mathbf{z}_E^1 &= -(\delta z^0)_E,\\ (\mathbf{z}_E^1, \mathrm{curl}\,\boldsymbol{\psi}) &= 0, \qquad && \forall \boldsymbol{\psi} \in \mathring{\mathcal{N}}(\mathcal{T}_h(\omega_E^{ext})).\end{aligned}$$

The operator $M^1 : L^2(\Omega;\mathbb{C}^3) \to \mathring{\mathcal{N}}(\mathcal{T}_h)$ maps any $\mathbf{v} \in L^2(\Omega;\mathbb{C}^3)$ to

$$M^1\mathbf{v} := \sum_{E\in\mathring{\Delta}_1} |E|^{-1}\Big(\int_{\omega_E^{ext}} \mathbf{v}\cdot\mathbf{z}_E^1\,dx\Big)\boldsymbol{\phi}_E.$$

Recall that the weights in the (modified) Clément interpolation of a function $v \in H_0^1$ are $|\omega_z|^{-1}\int_{\omega_z} v\,dx$ for all vertices z. The operator M^1 generalizes this (local) averaging process of the Clément operator to the case of edge elements. However, M^1 is not a projection onto the edge elements yet.

The operator $Q_{a,-}^1 : \mathbf{H}(\mathrm{curl}, \omega_E^{ext}) \to \mathcal{S}^1(\mathcal{T}_h(\omega_E^{ext}))$ associated with a vertex $a \in E$ is the solution operator of a local discrete Neumann problem. For any $\mathbf{v} \in \mathbf{H}(\mathrm{curl}, \omega_E^{ext})$, the function $Q_{a,-}^1\mathbf{v}$ solves

$$\begin{aligned}(\mathbf{v} - \nabla Q_{a,-}^1\mathbf{v}, \nabla\tau) &= 0 \qquad && \forall \tau \in \mathcal{S}^1(\mathcal{T}_h(\omega_E^{ext}))\\ \int_{\omega_E^{ext}} Q_{a,-}^1\mathbf{v}\,dx &= 0.\end{aligned}$$

Define the operator $S^1 : \mathbf{H}_0(\operatorname{curl}, \Omega) \to \mathring{\mathcal{N}}(\mathcal{T}_h)$ via

$$S^1\mathbf{v} := M^1\mathbf{v} + \sum_{a \in \mathring{\Delta}_0} (Q^1_{a,-}\mathbf{v})(a)\nabla\lambda_a, \tag{2.28}$$

where λ_a are the nodal basis functions of $\mathcal{S}(\mathcal{T}_h)$ as introduced in Section 2.2.2. S^1 preserves the degrees of freedom of $\mathcal{N}(\mathcal{T}_h)$ for all gradient functions $\nabla\mathcal{S}(\mathcal{T}_h)$, which is a first step to the projection property. However, S^1 does not commute with the exterior derivative in general and hence, needs to be further modified. The second sum on the right-hand side of (2.28) can be rewritten in terms of the basis functions $\boldsymbol{\phi}_E$. The inclusion $\nabla\mathring{\mathcal{S}}^1(\mathcal{T}_h) \subseteq \mathring{\mathcal{N}}(\mathcal{T}_h)$ follows from the principles of finite element exterior calculus [AFW06, AFW10]. Given an interior vertex $a \in \mathring{\Delta}_0$, the expansion in terms of the basis $(\boldsymbol{\phi}_E)_{E \in \mathring{\Delta}_1}$ reads

$$\nabla\lambda_a = \sum_{E \in \mathring{\Delta}_1} \Big(\fint_E \nabla\lambda_a \cdot \mathbf{t}_E \, ds \Big) \boldsymbol{\phi}_E = \sum_{E \in \Delta_1(a)} \frac{\operatorname{sign}(\mathbf{t}_E \cdot \nabla\lambda_a)}{|E|} \boldsymbol{\phi}_E$$

where $\Delta_1(a) \subseteq \mathring{\Delta}_1$ is the set of all edges that contain a. Thus, S^1 from (2.28) can be rewritten as

$$S^1\mathbf{v} := M^1\mathbf{v} + \sum_{E \in \mathring{\Delta}_1} |E|^{-1} \big((Q^1_{a_2(E),-}\mathbf{u})(a_2(E)) - (Q^1_{a_1(E),-}\mathbf{u})(a_1(E)) \big) \boldsymbol{\phi}_E, \tag{2.29}$$

where $a_1(E)$ and $a_2(E)$ denote the endpoints of E (with the orientation convention $\mathbf{t}_E = (a_2(E) - a_1(E))/|E|$). The Falk-Winter interpolation operator $\pi^E_H : \mathbf{H}_0(\operatorname{curl}, \Omega) \to \mathring{\mathcal{N}}(\mathcal{T}_h)$ is defined as

$$\pi^E_h\mathbf{v} := S^1\mathbf{v} + \sum_{E \in \mathring{\Delta}_1} \Big(\fint_E \big((\mathrm{id} - S^1) Q^1_E \mathbf{v} \big) \cdot \mathbf{t}_E \, ds \Big) \boldsymbol{\phi}_E. \tag{2.30}$$

The interpolation operator can be constructed in a similar manner without the homogeneous boundary values, i.e., in $\mathbf{H}(\operatorname{curl})$. Falk and Winther [FW14a] also construct corresponding interpolation operators mapping onto $\mathcal{S}(\mathcal{T}_h)$ and $\mathcal{RT}(\mathcal{T}_h)$, which are omitted here for simplicity. Note that the Falk-Winther projection onto $\mathcal{S}(\mathcal{T}_h)$ does not coincide with Π_h presented above, but fulfills (almost) the same estimates. The most important properties of π^E_h are summarized in the following proposition.

Proposition 2.2.10. *The projection $\pi^E_h : \mathbf{H}_0(\operatorname{curl}) \to \mathring{\mathcal{N}}(\mathcal{T}_h)$ from (2.30) satisfies: For all $\mathbf{v} \in \mathbf{H}_0(\operatorname{curl})$ and all $T \in \mathcal{T}_h$ it holds that*

$$\|\pi^E_h(\mathbf{v})\|_{L^2(T)} \leq C_\pi \big(\|\mathbf{v}\|_{L^2(\mathrm{N}(T))} + h \|\operatorname{curl}\mathbf{v}\|_{L^2(\mathrm{N}(T))} \big), \tag{2.31}$$

$$\|\operatorname{curl}\pi^E_h(\mathbf{v})\|_{L^2(T)} \leq C_\pi \|\operatorname{curl}\mathbf{v}\|_{L^2(\mathrm{N}(T))}. \tag{2.32}$$

Furthermore, there exists a projection $\pi^F_h : \mathbf{H}_0(\operatorname{div}) \to \mathring{\mathcal{RT}}(\mathcal{T}_h)$ to the Raviart-Thomas space such that the following commutation property holds

$$\operatorname{curl}\pi^E_h(\mathbf{v}) = \pi^F_h(\operatorname{curl}\mathbf{v}).$$

A corresponding proof that is also valid (verbatim) in the case of homogeneous boundary values can be found in [FW14a]. The interpolation operator π^E_h and its properties play a crucial role in the Localized Orthogonal Decomposition for $\mathbf{H}(\operatorname{curl})$-problems in Section 3.2. Further (new) properties are proved in Lemma 3.2.1 and the representation of π^E_h as a matrix is discussed in Section 3.2.6.

2.3 Homogenization and Multiscale Methods

As explained in the introduction, our model problems have a multiscale structure, i.e., the coefficients in the PDE may vary rapidly on small spatial scales. In this setting, standard FE discretizations fail to yield good approximations to the exact solution unless the underlying mesh is very fine which, however, is computationally infeasible. In this section, we therefore present analytical and numerical homogenization procedures. In Section 2.3.1, we introduce the analytical homogenization tool of two-scale convergence. Section 2.3.2 presents a general framework of numerical multiscale methods and gives a short overview of different schemes fitting into this framework. We then focus on two multiscale methods, the Heterogeneous Multiscale Method (HMM) in Section 2.3.3 and the Localized Orthogonal Decompositon (LOD) in Section 2.3.4. Throughout this section, we consider a simple diffusion problem with Dirichlet boundary conditions as model problem: Find $u_\delta \in H_0^1(\Omega)$ such that

$$\int_\Omega A_\delta \nabla u_\delta \cdot \nabla \psi \, dx = \int_\Omega f\psi \, dx \qquad \forall \psi \in H_0^1(\Omega). \tag{2.33}$$

with a given right-hand side $f \in L^2(\Omega)$ and a diffusion tensor $A_\delta \in L^\infty(\Omega; \mathbb{R}^{d\times d})$, where the index δ emphasizes the multiscale nature. We assume that A_δ is uniformly elliptic independent of δ.

2.3.1 Two-scale convergence

Two-scale convergence is a type of convergence for *rapidly oscillating, (locally) periodic* functions, i.e., functions with a period $\delta \ll 1$. We present the main function spaces and the important theorems concerning two-scale convergence without proofs. Furthermore, we present the (by now standard) homogenization results for the diffusion problem (2.33) with $A_\delta(x) = A(x, \frac{x}{\delta})$ for a locally periodic function. These results should be compared with the homogenization of the $\mathbf{H}$(curl)-elliptic problem in Section 3.1.1 and the high contrast problems in Section 4.2.

Periodic functions. First, we precisely define periodic functions and introduce some associated function spaces. From now on let $Y := (-\frac{1}{2}, \frac{1}{2})^d$ be the unit cell.

Definition 2.3.1 (Periodic function spaces)**.** A continuous function $v \in C^0(\mathbb{R}^d)$ is called Y-periodic if it fulfills

$$v(y) = v(y + \mathbf{e}_j), \quad \text{for } 1 \le j \le d \text{ and all } y \in \mathbb{R}^d.$$

Here, $\mathbf{e}_j$ are the standard unit vectors. Let $l \in \mathbb{N}_0 \cup \{\infty\}$, $1 \le p \le \infty$ and $s \in \mathbb{N}_0$. We define the following spaces of periodic functions: $C_\sharp^l(Y)$ as the functions in $C^l(\mathbb{R}^d)$ which are Y-periodic, $L_\sharp^\infty(Y)$ as the functions in $L^\infty(\mathbb{R}^d)$ which are Y-periodic for almost all y, $H_\sharp^s(Y)$ and $\mathbf{H}_\sharp(\mathrm{curl}, Y)$ as the closure of $C_\sharp^\infty(Y)$ w.r.t. the corresponding norms. The Sobolev space of functions with zero average is defined as

$$H_{\sharp,0}^s(Y) := \Big\{ v \in H_\sharp^s(Y) \Big| \int_Y v(y)\, dy = 0 \Big\}.$$

The subscript $\sharp$ thus indicates periodic functions. They can also be seen as functions on the (flat) torus.

Bochner-Lebesgue spaces are a generalization of the well-known L^p-spaces to functions with values in a Banach space.

Definition 2.3.2 (Bochner-Lebesgue space)**.** Let $1 \le p < \infty$ and X be a Banach space. The Bochner-Lebesgue space is defined as

$$L^p(\Omega; X) := \{ v : \Omega \to X | v \text{ is measurable and } \|v\|_X \in L^p(\Omega) \}$$

with the norm

$$\|v\|_{L^p(\Omega;X)} := \left(\int_\Omega \|v(x)\|_X^p \, dx \right)^{\frac{1}{p}}.$$

We use the short notation $v(x,y) := v(x)(y)$ for $v \in L^p(\Omega;X)$. Finally, the space $C_0^\infty(\Omega; C_\sharp^\infty(Y))$ consists of all functions $v(x,y)$ for which we have $v(x,\cdot) \in C_\sharp^\infty(Y)$ for fixed $x \in \Omega$ and for which the map $x \in \Omega \mapsto v(x,\cdot) \in C_\sharp^\infty(Y)$ has Fréchet derivatives of all orders and a compact support.

Two-scale convergence. The term "two-scale convergence" was first used by Allaire [All92] for a result derived by Nguetseng [Ngu89]. We present the definition and the main properties and refer to [All92, LNW02] for details. We denote weak convergence by $\rightharpoonup$.

Definition 2.3.3 (Two-scale convergence)**.** A sequence $(v_\delta)_{\delta>0} \subset L^2(\Omega)$ two-scale converges to a function $v_0 \in L^2(\Omega \times Y)$ if it fulfills

$$\lim_{\delta\to 0} \int_\Omega v_\delta(x) \psi\Big(x, \frac{x}{\delta}\Big)\, dx = \int_\Omega \int_Y v_0(x,y)\psi(x,y)\, dydx \qquad \forall \psi \in L^2(\Omega; C_\sharp^0(Y)).$$

In short form we write $v_\delta \overset{2}{\rightharpoonup} v_0$ for the two-scale convergence.

The two-scale limit is always unique. An example for two-scale convergence is the so-called asymptotic expansion: If v_δ is of the form $v_\delta(x) = v_0(x, \frac{x}{\delta}) + \delta v_1(x, \frac{x}{\delta})$ with smooth functions v_0, v_1, we have $v_\delta \overset{2}{\rightharpoonup} v_0$. The test functions allowed in the definition of the two-scale convergence can be slightly changed, where we mention the notion of admissible test functions [All92, Definition 1.4]. Two-scale convergence can be considered as inbetween strong and weak convergence, i.e., strong (norm) convergences implies two-scale convergence, which again implies weak convergence, see [LNW02, Theorems 5 and 6] for details.

Finally, we give compactness results in L^2 and H^1, see [LNW02, Theorems 7 and 13].

Theorem 2.3.4 (Compactness in L^2)**.** *Let $(v_\delta)_{\delta>0} \subset L^2(\Omega)$ be bounded. Then there exists a subsequence $(v_{\delta'})_{\delta'>0}$ and $v_0 \in L^2(\Omega \times Y)$ such that $v_{\delta'} \overset{2}{\rightharpoonup} v_0$.*

Theorem 2.3.5 (Compactness in H^1)**.** *Let $v_\delta \rightharpoonup v_0$ in $H^1(\Omega)$. Then we have $v_\delta \overset{2}{\rightharpoonup} v_0$ and there exists a subsequence $(v_{\delta'})_{\delta'>0}$ and $v_1 \in L^2(\Omega; H^1_{\sharp,0}(Y))$ such that $\nabla v_{\delta'} \overset{2}{\rightharpoonup} \nabla v_0 + \nabla_y v_1$.*

As $\mathbf{H}(\mathrm{curl})$ is not compactly embedded in $L^2(\Omega)$ (in contrast to $H^1(\Omega)$), the two-scale limit in L^2 does not coincide with the weak limit, see [Vis07, p. 44]. We have the following result for two-scale convergence in $\mathbf{H}(\mathrm{curl})$ from the literature [CH15, Wel01, Wel09, WK03].

Theorem 2.3.6 (Compactness in $\mathbf{H}(\mathrm{curl})$)**.** *Let $(\mathbf{v}_\delta)_{\delta>0} \subset \mathbf{H}(\mathrm{curl})$ be a bounded sequence. Then there exists a subsequence and functions $\mathbf{v}_0 \in \mathbf{H}(\mathrm{curl})$, $\mathbf{v}_1 \in L^2(\Omega; \mathbf{H}^1_{\sharp,0}(Y))$ with $\operatorname{div}_y \mathbf{v}_1 = 0$ a.e. and $v_2 \in L^2(\Omega; H^1_{\sharp,0}(Y))$ such that*

$$\mathbf{v}_\delta \overset{2}{\rightharpoonup} \mathbf{v}_0 + \nabla_y v_2 \qquad \text{and} \qquad \operatorname{curl} \mathbf{v}_\delta \overset{2}{\rightharpoonup} \operatorname{curl} \mathbf{v}_0 + \operatorname{curl}_y \mathbf{v}_1.$$

Homogenization of the diffusion problem. We present the typical homogenization results at the example of the diffusion problem (2.33). In particular, this reveals the application of the compactness results of Theorems 2.3.4 and 2.3.5. We assume (only for the rest of this subsection) that $A_\delta(x) = A(x, \frac{x}{\delta})$ in (2.33), where $A \in C^0(\Omega; L_\sharp^\infty(Y; \mathbb{R}^{d\times d}))$ is uniformly elliptic and each matrix entry is an admissible test function.

Proposition 2.3.7. *The sequence $(u_\delta)_{\delta>0}$ of weak solutions to (2.33) converges weakly in $H^1_0(\Omega)$ to u_0 and we have $\nabla u_\delta \overset{2}{\rightharpoonup} \nabla u_0 + \nabla_y u_1$, where $(u_0, u_1) \in H^1_0(\Omega) \times L^2(\Omega; H^1_{\sharp,0}(Y))$ is the unique solution to*

$$\int_\Omega \int_Y A(x,y)(\nabla u_0(x) + \nabla_y u_1(x,y)) \cdot (\nabla \psi_0(x) + \nabla_y \psi_1(x,y))\, dydx = \int_\Omega f(x)\psi_0(x)\, dx \qquad \forall (\psi_0, \psi_1) \in H^1_0(\Omega) \times L^2(\Omega; H^1_{\sharp,0}(Y)). \tag{2.34}$$

Problem (2.34) is called the two-scale equation and is derived from the original PDE (2.33) through the application of Theorem 2.3.5, for details see [All92]. The two-scale equation is again well-posed because its left-hand side is coercive and bounded over the space $H^1_0(\Omega) \times L^2(\Omega; H^1_{\sharp,0}(Y))$. The influence of the macroscopic scale in x and the microscopic scale in y can be decoupled as follows.

Proposition 2.3.8. *Define the homogenized matrix A_{hom} via*

$$A_{\mathrm{hom}}(x)\mathbf{e}_j = \int_Y A(x,y)(\mathbf{e}_j + \nabla_y w_j(x,y))\,dy \quad \text{for } j = 1,\dots,d,$$

where $w_j \in L^2(\Omega; H^1_{\sharp,0}(Y))$ solves the cell problem

$$\int_Y A(x,y)(\mathbf{e}_j + \nabla_y w_j(x,y)) \cdot \nabla_y \psi_1(y)\,dx = 0 \qquad \forall \psi_1 \in H^1_{\sharp,0}(Y),\ \text{a.e. in } \Omega.$$

Then, (u_0, u_1) is the solution to (2.34) if and only if $u_0 \in H^1_0(\Omega)$ is the unique solution to

$$\int_\Omega A_{\mathrm{hom}}(x)\nabla u_0(x) \cdot \nabla\psi(x)\,dx = \int_\Omega f(x)\psi(x)\,dx \qquad \forall \psi \in H^1_0(\Omega) \tag{2.35}$$

and $u_1(x,y) = \sum_{j=1}^d w_j(x,y)\frac{\partial}{\partial x_j}u_0(x)$.

Note that the homogenized equation (2.35) has the same structure as the original equation (2.33). However, the (effective) diffusion tensor A_{hom} is not given in closed form, but requires the solution of an additional PDE (at each point x).

2.3.2 General idea of multiscale methods

In this section we give a general motivation for numerical multiscale methods, see also [Hen11]. We again consider model problem (2.33) with diffusion tensor $A_\delta \in L^\infty(\Omega; \mathbb{R}^{d\times d})$ over a general Hilbert space X, which is either $H^1_0(\Omega)$ or a finite-dimensional approximation space. In the finite-dimensional case we assume that the corresponding (Galerkin) solution (which we call again u_δ) is a good approximation to the true solution. The basic idea is to split the space into $X = X_c \oplus X_f$. Here, X_c is a coarse-scale space which does not contain rapidly oscillating functions, and X_f is a fine-scale space. Writing $u_\delta = u_c + u_f$ and also splitting the test functions gives the system: Find $u_\delta = u_c + u_f \in X$ such that

$$\begin{aligned}
\int_\Omega A_\delta(\nabla u_c + \nabla u_f) \cdot \nabla\psi_c\,dx &= \int_\Omega f\psi_c\,dx \qquad \forall \psi_c \in X_c,\\
\int_\Omega A_\delta(\nabla u_c + \nabla u_f) \cdot \nabla\psi_f\,dx &= \int_\Omega f\psi_f\,dx \qquad \forall \psi_f \in X_f.
\end{aligned}$$

Inspired by the second equation, we define the corrector operator $\mathcal{Q} : X_c \to X_f$. For given $\psi_c \in X_c$, find $\mathcal{Q}(\psi_c) \in X_f$ such that

$$\int_\Omega A_\delta(\nabla\psi_c + \nabla\mathcal{Q}(\psi_c)) \cdot \nabla\psi_f\,dx = \int_\Omega f\psi_f\,dx \qquad \forall \psi_f \in X_f.$$

Obviously, we have $\mathcal{Q}(u_c) = u_f$. Defining then the reconstruction operator $\mathcal{R}(\psi) := \mathcal{Q}(\psi) + \psi$, we have $u_\delta = \mathcal{R}(u_c)$. Consequently, the system can be rewritten as: Find $u_c \in X_c$ such that

$$\begin{aligned}
\int_\Omega A_\delta\nabla\mathcal{R}(u_c) \cdot \nabla\psi_c\,dx &= \int_\Omega f\psi_c\,dx \qquad \forall \psi_c \in X_c,\\
\int_\Omega A_\delta\nabla\mathcal{R}(u_c) \cdot \nabla\psi_f\,dx &= \int_\Omega f\psi_f\,dx \qquad \forall \psi_f \in X_f.
\end{aligned}$$

The different multiscale methods deal with the following questions: (i) what should be chosen as X_c and X_f? (ii) how to solve the macro-scale equation (evaluation of the integrals etc.)? (iii) how to compute the reconstructions *efficiently*? The third question plays an essential role since we still have to solve *global fine-scale* equations in order to determine the reconstructions. Most work in the numerical methods is thus devoted to a suitable localization (and discretization) of the fine-scale equation.

The above motivation is closely inspired by the framework of the Variational Multiscale Method (VMM), where we refer to [HFMQ98, HS07, LM05, LM07] for further details, especially concerning localization strategies. From this framework the Localized Orthogonal Decomposition (LOD) arose and we refer to [BFHR97, HFMQ98, HS07, MP14, Pet16] for historically important steps. The idea of the LOD [HP13, MP14] is to take $X_c = \mathring{\mathcal{S}}(\mathcal{T}_H)$ as a standard finite element space on a coarse mesh, i.e., a mesh which does not resolve the oscillations of A_δ. The fine-scale space X_f is defined as the kernel of a stable interpolation operator $\Pi : H^1_0(\Omega) \to X_c$. The corrector $\mathcal{Q} : X_c \to X_f$ is chosen as the $(A_\delta \nabla \cdot, \nabla \cdot)$-orthogonal projection (i.e., $\int_\Omega f \psi_f$ is set to zero). It turns out that the corrector $\mathcal{Q}$ can be localized to patches of macroscopic simplices leading to a computable numerical scheme. This localization and the choice of the right-hand side for the fine-scale problems both contribute to question (iii) raised above. Further details are explained in Section 2.3.4 and we refer to [Pet16] for an overview. The idea to compute local reconstructions on each macroscopic element $T \in \mathcal{T}_H$ by solving the fine-scale equation in a neighborhood of this element is also the central idea in the Multiscale Finite Element Method (MsFEM). However, it simply takes $X_f = \mathring{\mathcal{S}}(\mathcal{T}_h)$, i.e., the standard FE space with Dirichlet conditions on a fine mesh. The left-hand side of the macroscopic equation then involves averages of $A_\delta \nabla \mathcal{R}_T(u_c) \cdot \nabla \psi_c$, where $\mathcal{R}_T$ is the local reconstruction described above. We refer to [EH09, EHG04, HW97] for details on this method. The Heterogeneous Multiscale (Finite Element) Method (HMM) [EE03, EE05] is closely related to the MsFEM. It differs in the choice of the local reconstructions and the averaging as follows: The local problems are solved on small unit cells $Y_j^\delta = x_j + \delta Y$ around the macroscopic quadrature points x_j with periodic boundary conditions. The averaging takes place over similar scaled and shifted (smaller) cells. In general, the domain for averaging is a subset of the computational domain for the local fine-scale problems in the MsFEM and the HMM. This so-called oversampling is employed to reduce the effects of the incorrect boundary conditions in the local problems. The procedure of the HMM is strongly inspired by the findings of analytical homogenization in Section 2.3.1. We give further details on the HMM and in particular on this connection in Section 2.3.3.

2.3.3 Heterogeneous Multiscale Method

In this section, we present the HMM for the diffusion problem (2.33). For simplicity, we restrict ourselves to lowest order Lagrange finite elements and hence also to zeroth order quadrature rules. In the case of a locally periodic diffusion coefficient $A_\delta(x) = A(x, \frac{x}{\delta})$, the method can be reformulated as a direct discretization of the two-scale equation, which is a crucial technique also for the problems considered in Chapters 3 and 4. We end this section by a short literature overview.

Formulations of the HMM. Let $Y = (-\frac{1}{2}, \frac{1}{2})^d$ be the unit cell. Denote with $\mathcal{T}_H$ and $\mathcal{T}_h$ regular and shape regular simplicial partitions of Ω and Y, respectively. We assume that $\mathcal{T}_h$ is periodic in the sense that it can be wrapped to a regular triangulation of the torus, i.e., no hanging nodes and edges occur over the periodic boundary. Introduce appropriate index sets such that $\mathcal{T}_H = \{T_j \,|\, j \in J\}$ and $\mathcal{T}_h = \{K_l \,|\, l \in I\}$. The barycenter of T_j is denoted by x_j. The δ-scaled and shifted unit cells are denoted by $Y_j^\delta = \delta Y + x_j$, together with the mappings $y_j^\delta : Y_j^\delta \to Y$ and $x_j^\delta = (y_j^\delta)^{-1} : Y \to Y_j^\delta$. A triangulation of the shifted unit cells is then given by $\mathcal{T}_h(Y_j^\delta) = \{\widetilde{K} \,|\, \widetilde{K} = x_k^\delta(K), K \in \mathcal{T}_h\}$. The global mesh sizes are defined as $H := \max_{j \in J} \operatorname{diam}(T_j)$ and $h := \max_{l \in I} \operatorname{diam}(K_l)$. Note that h denotes the mesh width of

the partition of the unit cell Y. We stress that it is in no way related to δ and can be of the same order as H. The δ-scaled cubes Y_j^δ consequently have a mesh size of δh. A coarse-scale space is given by $\mathring{\mathcal{S}}(\mathcal{T}_H)$ consisting of linear finite elements. The fine-scale spaces are given by $\widetilde{\mathcal{S}}(\mathcal{T}_h(Y_j^\delta))$, which consist of periodic, piecewise affine functions with zero average.

In the HMM [EE05, Ohl05] we seek $u_H \in \mathring{\mathcal{S}}(\mathcal{T}_H)$ such that

$$\sum_{j\in J} |T_j| \fint_{Y_j^\delta} A_\delta(x)\nabla_x R_j(u_H)(x)\cdot\nabla R_j(\psi_H)(x)\,dx = (f,\psi_H)_{L^2(\Omega)} \qquad \forall \psi_H \in \mathring{\mathcal{S}}(\mathcal{T}_H). \quad (2.36)$$

The reconstruction $R_j(\psi_H) \in \psi_H + \widetilde{\mathcal{S}}(\mathcal{T}_h(Y_j^{\delta_1}))$ of $\psi_H \in \mathring{\mathcal{S}}(\mathcal{T}_H)$ solves

$$\int_{Y_j^{\delta_1}} A_\delta(x)\nabla_x R_j(\psi_H)(x)\cdot\nabla_x\phi_h(x)\,dx = 0 \qquad \forall \phi_h \in \widetilde{\mathcal{S}}(\mathcal{T}_h(Y_j^{\delta_1})).$$

As already mentioned, we take $\delta_1 \geq \delta$ (oversampling). The formulation (2.36) can be naturally extended to higher order quadratures; then the reconstruction has to be determined for each quadrature point. Note that the diffusion tensor A_δ needs to be approximated for the computation of the integrals in practice.

In the locally periodic case with $A_\delta(x) = A(x, \frac{x}{\delta})$, we can choose $\delta_1 = \delta$. There is no need for oversampling as the periodic boundary conditions imposed in the reconstruction problems are exact. Moreover, in this case we define a piecewise constant approximation $A_{\delta,h}$ for (2.36) as follows $A_{\delta,h}(x)|_{x_j^\delta(K_l)} := A\big(x_j, \frac{x_j^\delta(y_l)}{\delta}\big)$ for all $T_j \in \mathcal{T}_H$ and all $K_l \in \mathcal{T}_h$. The HMM strongly resembles a discretized version of Proposition 2.3.8. The homogenized matrix is determined at each macroscopic quadrature point by the solution of discretized cell problems. Then, a discrete solution to the homogenized equation (2.35) is computed. This correspondence between the analytical homogenization result and the numerical scheme is made precise at the level of the two-scale equation in the following proposition, see [Ohl05].

Proposition 2.3.9. *Define the piecewise constant approximation A_h as $A_h(x,y)|_{T_j\times K_l} := A(x_j, y_l)$ for all $T_j \in \mathcal{T}_H$ and all $K_l \in \mathcal{T}_h$. Let $u_H \in \mathring{\mathcal{S}}(\mathcal{T}_H)$ be the HMM-approximation of* (2.36) *(with the modifications for the periodic case mentioned above). Then u_H is also the solution to the discrete two-scale-equation: Find $(u_H, u_h) \in \mathring{\mathcal{S}}(\mathcal{T}_H) \times \mathcal{P}^0(\Omega; \widetilde{\mathcal{S}}(\mathcal{T}_h))$ such that*

$$\int_\Omega \int_Y A_h(x,y)(\nabla_x u_H(x) + \nabla_y u_h(x,y))\cdot(\nabla_x\psi_H(x) + \nabla_y\psi_h(x,y))\,dydx = (f,\psi_H)_{L^2(\Omega)}$$
$$\forall (\psi_H,\psi_h) \in \mathring{\mathcal{S}}(\mathcal{T}_H) \times L^2(\Omega;\widetilde{\mathcal{S}}(\mathcal{T}_h)).$$

We furthermore have the relation $u_h(x,y)|_{T_j\times Y} = \frac{1}{\delta}(R_j(u_H) - u_H)(\delta y)$.

The proof uses the transformation and chain rule and the mappings y_j^δ and x_j^δ to switch the integration from Y_j^δ to Y. Finally, we employ the periodicity of A and the fact that the chosen quadrature rule is exact for the integrand. For details of the proof we refer to [Ohl05]. This reformulation means that, at least in the locally periodic case, we can consider the HMM as a direct discretization of the two-scale equation with numerical quadrature. We take this viewpoint for new formulations of HMMs in this thesis and emphasize that we can always reformulate them in the "traditional" way. This interpretation is also very useful for error analysis as standard arguments directly lead to a priori estimates and also a posteriori estimators.

Literature survey. The Heterogeneous Multiscale Method as introduced by Engquist and E in [EE03] is a very general concept and allows for a lot of different realizations. It is based on a framework of reconstructions and local averaging, where only the local averages are passed as fine-scale information to the coarse-scale problem. Hence, the HMM tries to extract effective

macroscopic information, but it is always possible to locally recover fine-scale information via the reconstructions. For a specific HMM, one has the choice of the macroscopic and microscopic solvers, the boundary conditions of the local fine-scale problems, and even of the coupling between coarse- and fine-scale. We focus on the HMM based on the standard finite element approach (sometimes also called FE-HMM, Finite Element Heterogeneous Multiscale Method), but also finite volume or finite difference methods are possible, see [AE03, EEL+07]. Furthermore, we note that our formulation of the HMM in (2.36) is a Galerkin approach, as the test function ψ_H is also reconstructed. Petrov-Galerkin formulations, where only the ansatz function is reconstructed, are also possible and in particular interesting for nonlinear problems [HO15].

For a general and detailed overview of the HMM, specifications, implementation, stability and different applications, we refer to the original paper by Engquist and E [EE03], as well as the survey articles [Abd09, AEEV12, EE05], where also the available error estimates are given. First detailed a priori error theory is presented in [EMZ05] for linear and nonlinear elliptic problems with locally periodic or random coefficients. The analysis is performed in a semi-discrete setting, i.e., it is assumed that the local fine-scale problems are solved analytically. The results, still in the semi-discrete setting, are improved later in [AS05]. The HMM-approximation with piecewise polynomials of order p converges to the homogenized solution with rate p in the H^1-norm and rate $p+1$ in the L^2-norm, i.e., the rates known for standard FEM. The first contributions on an optimal fully discrete error analysis are [Ohl05] in an energy norm and [Abd05] in the L^2-norm. As already mentioned, [Ohl05] also introduces the reformulation technique, which enables the first a posteriori error estimate. The result is again achieved in an energy norm assuming locally periodic coefficients. A general a posteriori error result in dependence on the homogenized matrix is given in [AN09].

Concerning wave propagation problems, we mention the works on the acoustic and elastic wave equation [AG11, AH17b, EHR11] and [AGJ17], long-time effects in the wave equation [AGS14, AP16a, AP16b, AP17, AR14, EHR12], the Helmholtz equation [CS14], and Maxwell's equations in frequency and time domain [CFS17, HS17]. We note that the HMM in [CFS17] is very similar to the one studied in Section 3.1, but with a different treatment of the divergence-free constraint in one of the cell problems and with a different approach to the a priori error analysis. An HMM for perforated domains is analyzed in [HO09] and flow problems in porous media are treated, for instance, in [AB15, AB16]. We emphasize that the HMM and its analysis are not limited to (locally) periodic problems, see [Glo06, HO15].

2.3.4 Localized Orthogonal Decomposition

In this section, we present the LOD for the diffusion problem (2.33). For this method no periodicity of A_δ is assumed. We even do not require scale separation of a coarse- and a fine-scale and therefore, drop δ from the notation of A and the solution u.

Formulation of the LOD. Let $\mathcal{T}_H$ be a coarse triangulation of Ω in the sense that it does not resolve the rapid variations of A. We denote by $\mathcal{A} : H_0^1(\Omega) \times H_0^1(\Omega) \to \mathbb{R}$ the bilinear form induced by the left-hand side of (2.33), i.e., $\mathcal{A}(v,\psi) := (A\nabla v, \nabla\psi)_{L^2(\Omega)}$. As already mentioned, the idea is to write $H_0^1(\Omega) = \mathring{\mathcal{S}}(\mathcal{T}_H) \oplus W$ with $W = \ker \Pi_H$, where $\Pi_H : H_0^1(\Omega) \to \mathring{\mathcal{S}}(\mathcal{T}_H)$ is a suitable projection, such as described in Section 2.2.3. We define the correction operator $\mathcal{Q} : H_0^1(\Omega) \to W$ as the $\mathcal{A}$-orthogonal projection via

$$\mathcal{A}(\mathcal{Q}v, w) = -\mathcal{A}(v, w) \qquad \forall w \in W. \tag{2.37}$$

Introducing the multiscale space $V_H^{ms} := (\mathrm{id} + \mathcal{Q})\mathring{\mathcal{S}}(\mathcal{T}_H)$, we have the direct sum splitting $H_0^1(\Omega) = V_H^{ms} \oplus W$, which is orthogonal w.r.t. $\mathcal{A}$. The (ideal) LOD is then a generalized FEM (gFEM) over the space V_H^{ms}, i.e., we seek $u_H \in \mathring{\mathcal{S}}(\mathcal{T}_H)$ such that

$$\mathcal{A}\big((\mathrm{id} + \mathcal{Q})u_H, (\mathrm{id} + \mathcal{Q})\psi_H\big) = \big(f, (\mathrm{id} + \mathcal{Q})\psi_H\big)_{L^2(\Omega)} \qquad \forall \psi_H \in \mathring{\mathcal{S}}(\mathcal{T}_H). \tag{2.38}$$

Denoting $e = u - (\mathrm{id} + \mathcal{Q})u_H$, where u solves (2.33), we observe $\Pi_H e = 0$, i.e., $e \in W$. With the orthogonality of V_H^{ms} and W, we obtain

$$\|\nabla e\|_{L^2(\Omega)}^2 \lesssim \mathcal{A}(e,e) = \mathcal{A}(u,e) = (f,e)_{L^2(\Omega)} = (f, e - \Pi_H e)_{L^2(\Omega)}.$$

At this point, the approximation properties of Π_H play a crucial role. With (2.27), we obtain a convergence rate of H for the error *independent of the oscillations of A and the regularity of u.*

Problem (2.37), however, is global and therefore very costly to solve. In order to obtain a localized method the computation has to be truncated to patches $\mathrm{N}^m(T)$ of diameter approximately mH, see Definition 2.2.4. For a discrete function $v_H \in \mathring{\mathcal{S}}(\mathcal{T}_H)$ this localized corrector is computed as follows: For all $T \in \mathcal{T}_H$, we solve for $\mathcal{Q}_{T,m}(v_H) \in W(\mathrm{N}^m(T))$ such that

$$\mathcal{A}_{\mathrm{N}^m(T)}(\mathcal{Q}_{T,m}(v_H), w) = -\mathcal{A}_T(v_H, w) \qquad \forall w \in W(\mathrm{N}^m(T)). \tag{2.39}$$

Here $\mathcal{A}_{\mathrm{N}^m(T)}$ and $\mathcal{A}_T$ denote the restriction of $\mathcal{A}$ to $\mathrm{N}^m(T)$ and T, respectively, and $W(\mathrm{N}^m(T))$ are the functions in W vanishing outside $\mathrm{N}^m(T)$. Defining the corrector operator $\mathcal{Q}_m$ via

$$\mathcal{Q}_m(v_H) = \sum_{T \in \mathcal{T}_H} \mathcal{Q}_{T,m}(v_H),$$

we seek the solution $u_{H,m} \in \mathring{\mathcal{S}}(\mathcal{T}_H)$ to (2.38) with $\mathcal{Q}$ replaced by $\mathcal{Q}_m$. Observe that $\mathcal{Q}_m$ is computed by solving local decoupled problems. The question is how this truncation to the patches $\mathrm{N}^m(T)$ affects the approximation properties of the corrector. For the diffusion model problem, we have the following crucial estimate, see, e.g., [MP14]: There is $0 < \beta < 1$, independent of H and m, such that for all $v_H \in \mathring{\mathcal{S}}(\mathcal{T}_H)$

$$\|\nabla(\mathcal{Q} - \mathcal{Q}_m)(v_H)\|_{L^2(\Omega)} \lesssim \sqrt{C_{ol,m}}\,\beta^m \|\nabla v_H\|_{L^2(\Omega)}$$

with the overlap constant $C_{\mathrm{ol},m}$ from (2.25). This means that the error introduced by localization is decaying exponentially in the so-called oversampling parameter m. Choosing $m \approx |\log H|$, the LOD-approximation $u_{H,m}$ still converges to u with rate H. Note that the localized corrector problems (2.39) still need to be discretized since the spaces $W(\mathrm{N}^m(T))$ are infinite dimensional. For this step, a fine triangulation $\mathcal{T}_h$ of Ω is used, which resolves the rapid variations of A.

Summarizing, we see that the error estimates for the LOD crucially depend on the properties of the interpolation operator and the exponential decay of the corrector, see [Pet16].

Literature survey. As already mentioned, the LOD as introduced in [MP14] arose from the VMM framework [HFMQ98, HS07]. It reuses the idea of decomposing the solution space into a coarse and a fine part and in particular studies the localization of the fine-scale corrector problems. It is based on simplicial or quadrilateral partitions of the domain, but also meshless methods are possible [HMP15]. The LOD as presented in (2.38) uses a Galerkin ansatz, but also Petrov-Galerkin methods show the same stability and convergence behavior while requiring less communication at the correctors, see [EGH15, Pet16]. The correction on the right-hand side of (2.38) can be omitted and still some error estimates remain valid, see [GP17a] for details. The LOD has been extensively studied for Lagrange finite elements, with a wide range of applications such as elliptic diffusion problems [HM14,HP13,MP14], eigenvalue problems [MP15] and parabolic equations [MP18], amongst others. We refer to [Pet16] and [EHMP16] for details on the method and its implementation, where also a lot of application cases are mentioned. Aside from Lagrange finite elements, an LOD in Raviart-Thomas spaces is given in [HHM16].

The acoustic wave equation was treated in [AH17a, AH17b, PS17]. Elliptic diffusion problems with high contrast are studied in [HM17, PS16]. For high-frequency wave propagation the LOD is not only able to deal with rapidly varying coefficients, but also to relax the

resolution condition between the mesh size and the wavenumber. Instead of the standard condition $k^\alpha H \lesssim 1$ with $\alpha > 1$, only a natural mesh resolution of $kH \lesssim 1$ is needed, provided that the oversampling parameter is chosen as $m \approx |\log k|$. This has been analyzed in [BGP17, GP15, Pet17] for the Helmholtz equation and in [BG16] for elastodynamics. Section 4.5 also discusses this issue for two-scale Helmholtz-type problems.

The methodology of the LOD can be re-interpreted and connected to other existing methods in various ways. With a different localization strategy, it can be viewed as an iterative method (additive subspace correction method), which also yields a new technique for proving the exponential decay of the corrector, see [KPY18, KY16]. A game-theoretic interpretation, using so-called gamblets, was recently given in [Owh17], see also [OZ17]. Finally, the LOD is also strongly connected to the computation of homogenized matrices as they occur in periodic and stochastic homogenization, see [GP17a, GP17b].

3 Multiscale methods for H(curl)-problems

In this chapter, we present and analyze two multiscale methods for the $\mathbf{H}(\mathrm{curl})$-elliptic problem (2.20) with possibly rapidly varying coefficients. Specifically, we study the situation of Definition 2.1.5. We recall that we assumed $\mathbf{f} \in \mathbf{H}(\mathrm{div}, \Omega)$, $\mu \in L^\infty(\Omega; \mathbb{R}^{3\times 3})$, and $\kappa \in L^\infty(\Omega; \mathbb{C}^{3\times 3})$, where $\Omega \subset \mathbb{R}^3$ is an open, bounded, contractible domain with polyhedral Lipschitz boundary. We defined a sesquilinear form $\mathcal{B}$ over Ω. This can be generalized to any open subset $R \subset \Omega$ as follows: $\mathcal{B}_R : \mathbf{H}(\mathrm{curl}, R) \times \mathbf{H}(\mathrm{curl}, R) \to \mathbb{C}$ is defined as

$$\mathcal{B}_R(\mathbf{v}, \boldsymbol{\psi}) := (\mu \operatorname{curl} \mathbf{v}, \operatorname{curl} \boldsymbol{\psi})_{L^2(R)} + (\kappa \mathbf{v}, \boldsymbol{\psi})_{L^2(R)}, \tag{3.1}$$

and we set $\mathcal{B} := \mathcal{B}_\Omega$. We recall that $\mathcal{B}_R$ is continuous and that $\mathcal{B}$ is assumed to be $\mathbf{H}(\mathrm{curl})$-coercive. The weak solution $\mathbf{u} \in \mathbf{H}_0(\mathrm{curl}, \Omega)$ solves

$$\mathcal{B}(\mathbf{u}, \boldsymbol{\psi}) = (\mathbf{f}, \boldsymbol{\psi})_{L^2(\Omega)} \qquad \forall \boldsymbol{\psi} \in \mathbf{H}_0(\mathrm{curl}, \Omega).$$

We refer to Section 2.1.1 for a derivation of the model problem and the relations of μ, κ, and $\mathbf{f}$ to physical quantities. Rapidly varying coefficients occur in composite materials with fine-scale features or photonic crystals.

The assumption of contractibility of Ω is only required to ensure the existence of local regular decompositions later used in the proof of Lemma 3.2.1. We note that this assumption can be relaxed by assuming that Ω is simply connected in certain local subdomains formed by unions of tetrahedra (i.e., in patches of the form $\mathrm{N}(\Omega_P)$, using the notation from Lemma 3.2.1).

If we discretize the model problem from Definition 2.1.5 in the lowest order Nédélec finite element space $\mathring{\mathcal{N}}(\mathcal{T}_H)$, we have the classical error estimate of the form (see Section 2.2.2):

$$\inf_{\mathbf{v}_H \in \mathring{\mathcal{N}}(\mathcal{T}_H)} \|\mathbf{u} - \mathbf{v}_H\|_{\mathbf{H}(\mathrm{curl})} \leq CH\big(\|\mathbf{u}\|_{\mathbf{H}^1(\Omega)} + \|\operatorname{curl} \mathbf{u}\|_{\mathbf{H}^1(\Omega)}\big).$$

However, if the coefficients μ and κ are discontinuous, the necessary regularity for this estimate is not available, see [BGL13, CDN99, Cos90]. On the other hand, if μ and κ are sufficiently regular but rapidly oscillating on a fine scale, then we face the "blow-up" with $\|\mathbf{u}\|_{\mathbf{H}^1(\Omega)} + \|\operatorname{curl} \mathbf{u}\|_{\mathbf{H}^1(\Omega)} \to \infty$ for the oscillation length going to zero. This makes the estimate useless in practice, unless the mesh size H becomes very small to compensate for the blow-up. The observation does not change if we replace the $\mathbf{H}(\mathrm{curl})$-norm by the $L^2(\Omega)$-norm since both norms are equivalent in the kernel of the curl-operator, i.e., on the subspace of gradient functions. Therefore, we want to decompose the exact solution into a macroscopic part, which does not involve fast oscillations and can thus be approximated on a rather coarse mesh, and a fine-scale corrector contribution. Two main questions then arise: (i) What approximation properties does the macroscopic part have? (ii) Can we find a *computable* approximation for the fine-scale corrector? Both questions are tackled in this chapter.

Section 3.1 considers locally periodic coefficients and analyzes a Heterogeneous Multiscale Method (HMM). In Section 3.2, we extend our findings to the general multiscale $\mathbf{H}(\mathrm{curl})$-problem beyond the assumptions of (local) periodicity and scale separation by the means of a Localized Orthogonal Decomposition (LOD). The results presented in this chapter are published in [GHV18, HOV16a, HOV16b, Ver17b].

3.1 Heterogeneous Multiscale Method for locally periodic problems

In this section we study the $\mathbf{H}(\mathrm{curl})$-elliptic problem from Definition 2.1.5 for so-called locally periodic coefficients. In particular, we introduce the periodicity length $\delta \ll 1$, which is small in comparison to the wavelength and the typical length scale of the computational domain Ω. We make the following additional assumptions on the coefficients.

Assumption 3.1.1. Let the assumptions of Definition 2.1.5 be fulfilled. Define $\kappa_\delta(x) := \kappa(x, \frac{x}{\delta})$, $\mu_\delta(x) := \mu(x, \frac{x}{\delta})$, where the coefficients μ and κ fulfill $\mu \in C^0(\Omega; L^\infty_\sharp(Y; \mathbb{R}^{3\times 3}))$ and $\kappa \in C^0(\Omega; L^\infty_\sharp(Y; \mathbb{C}^{3\times 3}))$. We assume that the upper and lower bounds on μ and κ (implicitly contained in the assumptions of Definition 2.1.5) are uniform in x and y.

The regularity assumptions on μ and κ imply that these functions are admissible test functions for two-scale convergence in the sense of Allaire, see [All92, Def. 1.4 and Cor. 5.4]. This is needed for the homogenization results in Section 3.1.1. We indicate the coefficients and the solution of our locally periodic problem with the subscript δ. More precisely, we seek $\mathbf{u}_\delta \in \mathbf{H}_0(\mathrm{curl})$ such that

$$\int_\Omega \mu_\delta \operatorname{curl} \mathbf{u}_\delta \cdot \operatorname{curl} \boldsymbol{\psi}^* + \kappa_\delta \mathbf{u}_\delta \cdot \boldsymbol{\psi}^* \, dx = \int_\Omega \mathbf{f} \cdot \boldsymbol{\psi}^* \, dx \qquad \forall \boldsymbol{\psi} \in \mathbf{H}_0(\mathrm{curl}). \tag{3.2}$$

The sesquilinear form on the left-hand side is uniformly coercive in δ and hence, we have the uniform estimate $\|\mathbf{u}_\delta\|_{\mathbf{H}(\mathrm{curl})} \leq C\|\mathbf{f}\|_{L^2}$ with $C = C(\mu, \kappa, \Omega)$.

We present homogenization results for this problem in Section 3.1.1. In Section 3.1.2, the Heterogeneous Multiscale Method is introduced and its numerical analysis is presented. Numerical experiments in Section 3.1.3 confirm our theoretical findings. All proofs are detailed in [HOV16b].

3.1.1 Homogenization results

In this section we present homogenization results for time-harmonic Maxwell's equations in a two-scale formulation, a formulation with cell problems and macroscopic equations, and a corrector result. We emphasize that although Maxwell's equations have been homogenized in the literature [AS11, Wel01, WK03], amongst others, the focus has mostly been on macroscopic (homogenized) problems as (3.7), but not on two-scale limit equations. A two-scale result similar to the following theorem has been presented recently in [CFS17, CH15] and for the coupled system of first-order equations in [WK03]. The latter includes some incorrect terms as remarked in [Wel09].

Theorem 3.1.2 (Two-scale equation)**.** *Under Assumption 3.1.1, let $\mathbf{u}_\delta \in \mathbf{H}_0(\mathrm{curl})$ be a solution to (3.2). Then there exists a solution triple $\underline{\mathbf{u}} = (\mathbf{u}_0, \mathbf{u}_1, u_2)$ of functions $\mathbf{u}_0 \in \mathbf{H}_0(\mathrm{curl})$, $\mathbf{u}_1 \in L^2(\Omega; \mathbf{H}^1_{\sharp,0}(Y))$ with $\operatorname{div}_y \mathbf{u}_1 = 0$ a.e., and $u_2 \in L^2(\Omega; H^1_{\sharp,0}(Y))$ such that*

$$\mathbf{u}_\delta \rightharpoonup \mathbf{u}_0 \quad \text{in } \mathbf{H}_0(\mathrm{curl}), \qquad \mathbf{u}_\delta \overset{2}{\rightharpoonup} \mathbf{u}_0 + \nabla_y u_2, \qquad \operatorname{curl} \mathbf{u}_\delta \overset{2}{\rightharpoonup} \operatorname{curl} \mathbf{u}_0 + \operatorname{curl}_y \mathbf{u}_1.$$

Considered in $\mathcal{H} := \mathbf{H}_0(\mathrm{curl}) \times L^2(\Omega; \mathbf{H}^1_{\sharp,0}(Y)) \times L^2(\Omega; H^1_{\sharp,0}(Y))$, the triple $\underline{\mathbf{u}}$ is the unique solution to

$$\boldsymbol{\mathcal{B}}(\underline{\mathbf{u}}, \underline{\boldsymbol{\psi}}) = (\mathbf{f}, \boldsymbol{\psi}_0)_{L^2(\Omega)} \qquad \forall \underline{\boldsymbol{\psi}} = (\boldsymbol{\psi}_0, \boldsymbol{\psi}_1, \psi_2) \in \mathcal{H} \tag{3.3}$$

with the two-scale sesquilinear form $\boldsymbol{\mathcal{B}}$ defined by

$$\begin{aligned}\boldsymbol{\mathcal{B}}(\underline{\mathbf{v}}, \underline{\boldsymbol{\psi}}) := \int_\Omega \int_Y \mu \left(\operatorname{curl} \mathbf{v}_0 + \operatorname{curl}_y \mathbf{v}_1\right) \cdot \left(\operatorname{curl} \boldsymbol{\psi}_0^* + \operatorname{curl}_y \boldsymbol{\psi}_1^*\right) + \operatorname{div}_y \mathbf{v}_1 \operatorname{div}_y \boldsymbol{\psi}_1^* \\ + \kappa \left(\mathbf{v}_0 + \nabla_y v_2\right) \cdot \left(\boldsymbol{\psi}_0^* + \nabla_y \psi_2^*\right) dy dx.\end{aligned}$$

In order to determine $\mathbf{u}_1$ in the two-scale equation, we have to solve the following problem: Find $\mathbf{u} \in \mathbf{H}(\operatorname{curl}, Y) \cap \mathbf{H}(\operatorname{div}, Y)$ with $\operatorname{div} \mathbf{u} = 0$ a.e. in Y such that

$$\int_Y \mu \operatorname{curl} \mathbf{u} \cdot \operatorname{curl} \boldsymbol{\psi}^* \, dy = 0 \qquad \forall \boldsymbol{\psi} \in \mathbf{H}(\operatorname{curl}, Y)$$

with appropriate boundary conditions. The divergence-free constraint $\operatorname{div} \mathbf{u} = 0$ is necessary to guarantee the uniqueness of the solution, as otherwise the solution is only determined up to a gradient term. However, divergence-free finite elements are quite rare and thus, it is more convenient to include the constraint implicitly in the equation.

Using divergence-regularization, we seek $\mathbf{u} \in \mathbf{H}^1(Y)$ such that

$$\int_Y \mu \operatorname{curl} \mathbf{u} \cdot \operatorname{curl} \boldsymbol{\psi}^* + \operatorname{div} \mathbf{u} \operatorname{div} \boldsymbol{\psi}^* \, dy = 0 \qquad \forall \boldsymbol{\psi} \in \mathbf{H}^1(Y).$$

Both problems are equivalent for convex domains, see [CD00]. This geometrical condition is no constraint here as the cell problem is always posed on the obviously convex unit cube Y. There are other possibilities to deal with a divergence-free constraint, cf. [CFS17]. The introduction of Lagrange multipliers (see [CD00]) leads to a mixed problem, which increases the computational costs and complicates the error analysis. The s-regularization suggested in [DLTZ12] makes the reformulation of the HMM later on (Proposition 3.1.8) impossible, since different orders of derivatives appear.

Definition 3.1.3 (Cell problems and homogenized matrices)**.** The cell problems are defined as follows: Find $\mathbf{w}_k \in L^2(\Omega; \mathbf{H}^1_{\sharp,0}(Y))$, $w_k \in L^2(\Omega; H^1_{\sharp,0}(Y))$ such that a.e. in Ω there holds

$$\int_Y \mu \left(\mathbf{e}_k + \operatorname{curl}_y \mathbf{w}_k\right) \cdot \operatorname{curl} \boldsymbol{\psi}^* + \operatorname{div}_y \mathbf{w}_k \operatorname{div} \boldsymbol{\psi}^* \, dy = 0 \qquad \forall \boldsymbol{\psi} \in \mathbf{H}^1_{\sharp,0}(Y), \tag{3.4}$$

$$\int_Y \kappa \left(\mathbf{e}_k + \nabla_y w_k\right) \cdot \nabla \psi^* \, dy = 0 \qquad \forall \psi \in H^1_{\sharp,0}(Y). \tag{3.5}$$

With the (unique) solutions to the cell problems (3.4)–(3.5) we define the homogenized matrices

$$\begin{aligned} \left(\mu_{\mathrm{hom}}(x)\right)_{j,k} &= \int_Y \mu(x,y)(\mathbf{e}_k + \operatorname{curl}_y \mathbf{w}_k(x,y)) \cdot \mathbf{e}_j \, dy, \\ \left(\kappa_{\mathrm{hom}}(x)\right)_{j,k} &= \int_Y \kappa(x,y)(\mathbf{e}_k + \nabla_y w_k(x,y)) \cdot \mathbf{e}_j \, dy, \qquad j,k = 1,2,3. \end{aligned} \tag{3.6}$$

The homogenized matrices are used to formulate the macro-scale problem for $\mathbf{u}_0$, which has the same structure as our original problem.

Theorem 3.1.4 (Equivalence of two-scale and homogenized equation)**.** *The triple* $(\mathbf{u}_0, \mathbf{u}_1, u_2)$ *is the unique solution to* (3.3) *if and only if* $\mathbf{u}_0 \in \mathbf{H}_0(\operatorname{curl})$ *solves*

$$\int_\Omega \mu_{\mathrm{hom}} \operatorname{curl} \mathbf{u}_0 \cdot \operatorname{curl} \boldsymbol{\psi}^* + \kappa_{\mathrm{hom}} \mathbf{u}_0 \cdot \boldsymbol{\psi}^* \, dx = \int_\Omega \mathbf{f} \cdot \boldsymbol{\psi}^* \, dx \qquad \forall \boldsymbol{\psi} \in \mathbf{H}_0(\operatorname{curl}) \tag{3.7}$$

with the correctors $\mathbf{u}_1, u_2$ *defined as* $\mathbf{u}_1 = \sum_{k=1}^3 (\operatorname{curl} \mathbf{u}_0)_k \, \mathbf{w}_k$, $u_2 = \sum_{k=1}^3 (\mathbf{u}_0)_k \, w_k$. *Here, the matrices* $\mu_{\mathrm{hom}}, \kappa_{\mathrm{hom}}$ *are defined through* (3.6) *and* $\mathbf{w}_k$ *and* w_k *are the solutions to the cell problems* (3.4) *and* (3.5)*, respectively.*

We end this section by a corrector-type result, which relates the two-scale solution to the asymptotic expansion. The assumption in the theorem below can, for instance, be fulfilled if the mentioned functions belong to $C^0(\overline{\Omega}; L^2_\sharp(Y))$, which is a regularity assumption on the geometry and the material parameters. Other function spaces giving admissible test functions for two-scale convergence are mentioned in [LNW02, Theorem 3]. See also the related corrector result in [WK03] for the coupled first-order system of equations for the electric and magnetic field.

Theorem 3.1.5 (Strong convergence in $\mathbf{H}(\mathrm{curl})$)**.** *Let μ, κ, $\mathbf{u}_1$, $\mathrm{curl}_x \mathbf{u}_1$, $\mathrm{curl}_y \mathbf{u}_1$, $\nabla_x u_2$, and $\nabla_y u_2$ be admissible test functions for two-scale convergence in the sense of Allaire [All92, Definition 1.4]. Then it holds that*

$$\left\| \mathbf{u}_\delta - \left(\mathbf{u}_0 + \delta \left(\mathbf{u}_1 \left(\cdot, \frac{\cdot}{\delta} \right) + \nabla u_2 \left(\cdot, \frac{\cdot}{\delta} \right) \right) \right) \right\|_{\mathbf{H}(\mathrm{curl})} \xrightarrow{\delta \to 0} 0.$$

The theorem shows that the correctors $\mathbf{u}_1$ and u_2 represent a Helmholtz decomposition of the first order term in the asymptotic expansion. Since on the gradient subspace, the $\mathbf{H}(\mathrm{curl})$-norm and the $L^2(\Omega)$-norm are equivalent, we see that in particular u_2 carries important information about the solution $\mathbf{u}_\delta$ itself. Thus, in contrast to the case of diffusion problems, the correctors $\mathbf{u}_1$, u_2 have to be considered as well (and not only the weak limit $\mathbf{u}_0$) in order to get a good approximation of the heterogeneous solution $\mathbf{u}_\delta$. This is a crucial observation. Consequently, the HMM is not only constructed to approximate $\mathbf{u}_0$, but requires to approximate $\mathbf{u}_1$ and u_2 as well.

This convergence result is not only interesting for the design of the HMM, but also serves as a good motivation for the general considerations in Section 3.2. Under the assumptions of Theorem 3.1.5 we derive the estimates

$$\begin{aligned} \delta^{-1} \left\| \delta \mathbf{u}_1 \left(\cdot, \frac{\cdot}{\delta} \right) \right\|_{L^2(\Omega)} + \left\| \delta \mathbf{u}_1 \left(\cdot, \frac{\cdot}{\delta} \right) \right\|_{\mathbf{H}(\mathrm{curl})} &\lesssim \|\mathbf{u}_0\|_{\mathbf{H}(\mathrm{curl})}, \\ \delta^{-1} \left\| \delta u_2 \left(\cdot, \frac{\cdot}{\delta} \right) \right\|_{L^2(\Omega)} + \left\| \delta \nabla u_2 \left(\cdot, \frac{\cdot}{\delta} \right) \right\|_{L^2(\Omega)} &\lesssim \|\mathbf{u}_0\|_{\mathbf{H}(\mathrm{curl})} \end{aligned} \tag{3.8}$$

from the boundedness of the cell problem solutions and the homogenized solution $\mathbf{u}_0$. These two estimates reveal that the first-order corrector $\mathbf{K}_\delta := \delta \mathbf{u}_1 + \delta \nabla u_2$ is $\mathbf{H}(\mathrm{curl})$-stable and that $\mathbf{u}_0$ *must* be a good approximation of $\mathbf{u}_\delta$ in $H^{-1}(\Omega)$. In fact, using (3.8) we have for any $\mathbf{v} \in \mathbf{H}_0^1(\Omega)$ with $\|\mathbf{v}\|_{\mathbf{H}^1} = 1$ that

$$\left| \int_\Omega \mathbf{K}_\delta \cdot \mathbf{v} \right| = \delta \left| \int_\Omega \mathbf{u}_1 \left(\cdot, \frac{\cdot}{\delta} \right) \cdot \mathbf{v} - \int_\Omega u_2 \left(\cdot, \frac{\cdot}{\delta} \right) \operatorname{div} \mathbf{v} \right| \leq \delta (\|\mathbf{u}_1\|_{L^2(\Omega)} + \|u_2\|_{L^2(\Omega)}) \lesssim \delta \|\mathbf{u}_0\|_{\mathbf{H}(\mathrm{curl})}.$$

This implies strong convergence in $H^{-1}(\Omega)$, i.e., $\|\mathbf{u}_\delta - \mathbf{u}_0\|_{H^{-1}(\Omega)} \to 0$ for $\delta \to 0$. Section 3.2 is concerned with the question whether these approximation results can be transferred to a discrete setting beyond the assumption of periodicity.

Moreover, a δ-explicit estimate for the homogenization error has been proved in [CH15, Theorem 3.1]. Assuming sufficient regularity of the data and the analytical two-scale solution, we have

$$\left\| \mathbf{u}_\delta - \left(\mathbf{u}_0 + \delta \left(\mathbf{u}_1 \left(\cdot, \frac{\cdot}{\delta} \right) + \nabla u_2 \left(\cdot, \frac{\cdot}{\delta} \right) \right) \right) \right\|_{\mathbf{H}(\mathrm{curl})} \leq C \delta^{1/2}. \tag{3.9}$$

3.1.2 Heterogeneous Multiscale Method and numerical analysis

In this section we introduce the Heterogeneous Multiscale Method (HMM) for problem (3.2), reformulate it as a discretization for the two-scale equation (3.3) and present its main a priori error estimates.

The HMM. We reuse the notation and the ideas already introduced in Section 2.3.3. Let $\mathcal{T}_H = \{T_j | j \in J\}$ and $\mathcal{T}_h = \{S_l | l \in I\}$ with index sets J, I denote regular and shape regular, simplicial partitions of Ω and Y, respectively, where $\mathcal{T}_H$ is periodic in the sense of Section 2.3.3 (i.e, no hanging nodes or edges over the periodic boundary). The δ-scaled and x_j-shifted unit cubes are denoted by $Y_j^\delta = \delta Y + x_j$, together with the mappings $y_j^\delta : Y_j^\delta \to Y$ and $x_j^\delta = (y_j^\delta)^{-1} : Y \to Y_j^\delta$. A triangulation of the shifted unit cubes is then given by $\mathcal{T}_h(Y_j^\delta) = \{\tilde{S} | \tilde{S} = x_j^\delta(S), S \in \mathcal{T}_h\}$. We define the global mesh sizes $H := \max_{j \in J} \operatorname{diam}(T_j)$ and $h := \max_{l \in I} \operatorname{diam}(S_l)$. Finally, we choose discrete function spaces $\mathring{\mathcal{N}}(\mathcal{T}_H) \subset \mathbf{H}_0(\mathrm{curl})$,

$\widetilde{\mathcal{S}}(\mathcal{T}_h(Y_j^\delta)) \subset H^1_{\sharp,0}(Y_j^\delta)$, and $\widetilde{\boldsymbol{\mathcal{S}}}(\mathcal{T}_h) := (\widetilde{\mathcal{S}}(\mathcal{T}_h))^3$. The Nédélec edge elements $\mathcal{N}$ and the linear Lagrange elements $\mathcal{S}$ are defined as in Section 2.2.2. We denote by $\widetilde{\mathcal{S}}$ the linear Lagrange elements with periodic boundary values and zero mean value. We pick numerical quadrature rules that are exact for the given test and ansatz spaces: In our case of piecewise linear functions, it suffices to choose the one-point rule $\{x_j, |T_j|\}$ with the barycenter x_j for the curl-part and a second order quadrature rule $Q_j^{(2)} := \{q_l, x_l\}_l$ with $l = 1, \dots, 4$ for the identity part.

With these preliminaries we are able to define the HMM (see also [EE03, EE05, Ohl05]).

Definition 3.1.6 (HMM)**.** The HMM-approximation of (3.2) is a discrete solution triple $(\mathbf{u}_H, \mathbf{R}_1(\mathbf{u}_H), \mathbf{R}_2(\mathbf{u}_H))$, where $\mathbf{u}_H \in \mathring{\mathcal{N}}(\mathcal{T}_H)$ is defined as the solution to

$$B_H(\mathbf{u}_H, \boldsymbol{\psi}_H) = (\mathbf{f}, \boldsymbol{\psi}_H)_{L^2(\Omega)} \qquad \forall \boldsymbol{\psi}_H \in \mathring{\mathcal{N}}(\mathcal{T}_H), \tag{3.10}$$

where the discrete sesquilinear form is given by

$$\begin{aligned} B_H(\mathbf{v}_H, \boldsymbol{\psi}_H) := &\sum_{j\in J} \frac{|T_j|}{\delta^3} \int_{Y_j^\delta} \mu_h^\delta(x) \operatorname{curl} \mathbf{R}_{j,1}(\mathbf{v}_H)(x) \cdot \operatorname{curl} \boldsymbol{\psi}_H^*(x)\, dx \\ &+ \sum_{j\in J} \sum_{l\in Q_j^{(2)}} \frac{q_l}{\delta^3} \int_{Y_l^\delta} \kappa_h^\delta(x) \mathbf{R}_{l,2}(\mathbf{v}_H)(x) \cdot \mathbf{R}_{l,2}(\boldsymbol{\psi}_H)^*(x)\, dx \end{aligned} \tag{3.11}$$

with the piecewise constant approximations $\kappa_h^\delta|_{x_j^\delta(S_l)}(x) := \kappa\big(x_j, \frac{x_j^\delta(y_l)}{\delta}\big)$ for all $S_l \in \mathcal{T}_h$ and μ_h^δ defined analogously. The local reconstructions $\mathbf{R}_{j,1}(\mathbf{v}_H) \in \mathbf{v}_H|_{Y_j^\delta} + \widetilde{\boldsymbol{\mathcal{S}}}(\mathcal{T}_h(Y_j^\delta))$, $\mathbf{R}_{j,2}(\mathbf{v}_H) = \mathbf{v}_H(x_j)|_{Y_j^\delta} + \nabla_y v_h$ with $v_h \in \widetilde{\mathcal{S}}(\mathcal{T}_h(Y_j^\delta))$ are defined as the solutions to the local cell problems

$$\int_{Y_j^\delta} \mu_h^\delta(x) \operatorname{curl} \mathbf{R}_{j,1}(\mathbf{v}_H) \cdot \operatorname{curl} \boldsymbol{\psi}_h^* + \operatorname{div}(\mathbf{R}_{j,1}(\mathbf{v}_H) - \mathbf{v}_H) \operatorname{div} \boldsymbol{\psi}_h^*\, dx = 0 \quad \forall \boldsymbol{\psi}_h \in \widetilde{\boldsymbol{\mathcal{S}}}(\mathcal{T}_h(Y_j^\delta)),$$

$$\int_{Y_j^\delta} \kappa_h^\delta(x) \mathbf{R}_{j,2}(\mathbf{v}_H) \cdot \nabla \psi_h^*\, dx = 0 \quad \forall \psi_h \in \widetilde{\mathcal{S}}(\mathcal{T}_h(Y_j^\delta)).$$

We reformulate the reconstructions of the HMM solution triple to draw a parallel between them and the analytical correctors.

Remark 3.1.7 (Role of the reconstructions)**.** Let $(\mathbf{u}_H, \mathbf{R}_1(\mathbf{u}_H), \mathbf{R}_2(\mathbf{u}_H))$ denote the HMM-approximation from Definition 3.1.6. Setting $\mathbf{K}_{j,1}(\mathbf{u}_H) = \mathbf{R}_{j,1}(\mathbf{u}_H) - \mathbf{u}_H$, we have $\mathbf{K}_{j,1}(\mathbf{u}_H) \in \widetilde{\boldsymbol{\mathcal{S}}}(\mathcal{T}_h(Y_j^\delta))$. Denote by $K_{j,2}(\mathbf{u}_H) \in \widetilde{\mathcal{S}}(\mathcal{T}_h(Y_j^\delta))$ the function fulfilling $\nabla K_{j,2}(\mathbf{u}_H) = \mathbf{R}_{j,2}(\mathbf{u}_H) - \mathbf{u}_H(x_j)$. We then define the discrete fine-scale corrections $\mathbf{u}_{h,1} \in \mathcal{P}^0(\mathcal{T}_H; \widetilde{\boldsymbol{\mathcal{S}}}(\mathcal{T}_h))$ and $u_{h,2} \in \mathcal{P}^1(\mathcal{T}_H; \widetilde{\mathcal{S}}(\mathcal{T}_h))$ as

$$\begin{aligned} \mathbf{u}_{h,1}(x, y) &:= \frac{1}{\delta} \mathbf{K}_{j,1}(\mathbf{u}_H)(\delta y), \quad \forall x \in T_j \quad \forall T_j \in \mathcal{T}_H \\ u_{h,2}(x_l, y) &:= \frac{1}{\delta} K_{l,2}(\mathbf{u}_H)(\delta y) \quad \forall x_l \in Q_j^{(2)} \quad \forall T_j \in \mathcal{T}_H, \end{aligned}$$

where the space of piecewise p-polynomial (w.r.t. x) discrete functions $\mathcal{P}^p(\mathcal{T}_H; X_h)$ is defined in Section 2.2.2. The discrete fine-scale corrections $\mathbf{u}_{h,1}$, $u_{h,2}$ are discrete counterparts of the analytical correctors $\mathbf{u}_1$ and u_2 introduced in Theorem 3.1.2. The specific relation of both will be clear from Proposition 3.1.8 below. Therefore, these corrections (or equivalently the reconstructions) are an important part of the HMM-approximation. As discussed at the end of Section 3.1.1, the correctors carry important information on the solution and cannot be neglected as higher order terms (in contrast to diffusion problems). In form of the fine-scale corrections, the observation transfers to the numerical scheme and the discrete setting.

Having observed this correspondence, we can reformulate the whole HMM as a direct discretization with numerical quadrature of the two-scale equation (3.3), see Section 2.3.3 and [Ohl05].

Proposition 3.1.8 (Reformulation of the HMM)**.** *Define the piecewise constant approximations κ_h on $\Omega \times Y$ by $\kappa_h|_{T_j \times S_l} := \kappa(x_j, y_l)$ and μ_h in the same way. Furthermore, let $\mathbf{u}_{h,1}$, $u_{h,2}$ be the discrete fine-scale corrections as defined in Remark 3.1.7. Then $(\mathbf{u}_H, \mathbf{u}_{h,1}, u_{h,2}) \in \mathring{\mathcal{N}}(\mathcal{T}_H) \times \mathcal{P}^0(\mathcal{T}_H; \widetilde{\boldsymbol{\mathcal{S}}}(\mathcal{T}_h)) \times \mathcal{P}^1(\mathcal{T}_H; \widetilde{\mathcal{S}}(\mathcal{T}_h))$ is a solution to*

$$\begin{aligned}\mathcal{B}_h\big((\mathbf{u}_H, \mathbf{u}_{h,1}, u_{h,2}), (\boldsymbol{\psi}_H, \boldsymbol{\psi}_{h,1}, \psi_{h,2})\big) &= (\mathbf{f}, \boldsymbol{\psi}_H)_{L^2(\Omega)} \\ \forall (\boldsymbol{\psi}_H, \boldsymbol{\psi}_{h,1}, \psi_{h,2}) &\in \mathring{\mathcal{N}}(\mathcal{T}_H) \times L^2(\Omega; \widetilde{\boldsymbol{\mathcal{S}}}(\mathcal{T}_h)) \times L^2(\Omega; \widetilde{\mathcal{S}}(\mathcal{T}_h))\end{aligned}$$

with the discrete sesquilinear form $\mathcal{B}_h$ given as in (3.3) *with μ and κ replaced by μ_h and κ_h, respectively.*

Conclusion 3.1.9. *Let us note that the result of Theorem 3.1.5 is still valid if we replace ∇u_2 by $\delta^{-1} \nabla_y u_2$. This implies that we can approximate $\mathbf{u}_\delta$ in $\mathbf{H}(\mathrm{curl})$ by $\mathbf{u}(x) + \delta \mathbf{u}_1\left(x, \frac{x}{\delta}\right) + \nabla_y u_2\left(x, \frac{x}{\delta}\right)$. Consequently, exploiting Proposition 3.1.8, we see that our final HMM-approximation $\mathbf{u}_{\mathrm{HMM}}$ to $\mathbf{u}_\delta$ can be written as*

$$\mathbf{u}_{\mathrm{HMM}}(x) := \mathbf{u}_H(x) + \delta \mathbf{u}_{h,1}\left(x, \frac{x}{\delta}\right) + \nabla_y u_{h,2}\left(x, \frac{x}{\delta}\right).$$

Numerical analysis. Based on the reformulation of the HMM in Proposition 3.1.8, we give the main a priori error estimates in Theorems 3.1.11 and 3.1.12. All error estimates are derived in the two-scale energy norm $\|\cdot\|_e$ defined as

$$\|(\mathbf{v}_0, \mathbf{v}_1, v_2)\|_e := \|\operatorname{curl} \mathbf{v}_0 + \operatorname{curl}_y \mathbf{v}_1\|_{L^2(\Omega \times Y)} + \|\operatorname{div}_y \mathbf{v}_1\|_{L^2(\Omega \times Y)} + \|\mathbf{v}_0 + \nabla_y v_2\|_{L^2(\Omega \times Y)}.$$

Let us furthermore define the error terms $e_0 := \mathbf{u}_0 - \mathbf{u}_H$, $e_1 := \mathbf{u}_1 - \mathbf{u}_{h,1}$, and $e_2 := u_2 - u_{h,2}$. We only estimate these (discretization) errors and leave the modeling error $\mathbf{u}_\delta - \big(\mathbf{u}_0 + \delta\left(\mathbf{u}_1\left(\cdot, \frac{\cdot}{\delta}\right) + \nabla u_2\left(\cdot, \frac{\cdot}{\delta}\right)\right)\big)$, introduced by homogenization, apart. Conclusion 3.1.9 together with Theorem 3.1.5 as well as the explicit rate (3.9) from [CH15] show that we can neglect the modeling error if δ is sufficiently small. More explicitly, we have the following estimate for the total error:

$$\left\|\mathbf{u}_\delta - \left(\mathbf{u}_H + \delta\left(\mathbf{u}_{h,1}\left(\cdot, \frac{\cdot}{\delta}\right) + \nabla u_{h,2}\left(\cdot, \frac{\cdot}{\delta}\right)\right)\right)\right\|_{\mathbf{H}(\mathrm{curl})} \leq C\delta^{1/2} + \|(e_0, e_1, e_2)\|_e.$$

The numerical experiments in Section 3.1.3 also justify this concentration on the discretization error.

Assumption 3.1.10. On top of the periodicity of the coefficients, we also assume

$$\mu, \kappa \in W^{1,\infty}(\Omega \times Y),$$

i.e., the coefficient functions are globally Lipschitz. Furthermore, let Ω be a convex domain.

Theorem 3.1.11 (A priori estimate in the energy norm)**.** *Under Assumptions 3.1.1 and 3.1.10, the following a priori estimate for the error between the discrete and the analytical two-scale solution holds:*

$$\|(e_0, e_1, e_2)\|_e \leq C(H + h)\|\mathbf{f}\|_{L^2(\Omega)}.$$

The constant C only depends on the domain Ω, the coefficients μ and κ, but not on the periodicity parameter δ or the mesh sizes.

Theorem 3.1.12 (A priori error estimate with dual problems)**.** *Under the same assumptions as in Theorem 3.1.11, the Helmholtz decomposition of the error between the homogenized solution* $\mathbf{u}_0$ *and the HMM-approximation* $\mathbf{u}_H$

$$\mathbf{u}_0 - \mathbf{u}_H = \nabla\theta + \mathbf{z} \qquad \text{with} \quad \theta \in H_0^1(\Omega), \quad \mathbf{z} \perp \nabla H_0^1(\Omega)$$

satisfies

$$\|\theta\|_{L^2(\Omega)} + \|\mathbf{z}\|_{L^2(\Omega)} \leq C(H^2 + h^2)\|\mathbf{f}\|_{L^2(\Omega)} + Ce_{\text{approx}}\|\mathbf{f}\|_{L^2(\Omega)},$$

where $e_{\text{approx}} = \max\{\|\mu - \mu_h\|_{L^\infty(\Omega\times Y)}, \|\kappa - \kappa_h\|_{L^\infty(\Omega\times Y)}\}$ *is a data approximation error arising from numerical quadrature. The constant* C *only depends on the domain* Ω*, the coefficients* μ *and* κ*, but not on the periodicity parameter* δ *or the mesh sizes.*

For elliptic diffusion problems posed on $H^1(\Omega)$, the $L^2(\Omega)$-norm of the error converges with quadratic rate. This better convergence is obtained by posing a dual problem and using the Aubin-Nitsche trick. The above theorem shows how the result can be transferred to problems in $\mathbf{H}(\text{curl})$: On the gradient subspace, the $L^2(\Omega)$-norm is of the same order as the $\mathbf{H}(\text{curl})$-norm, so that only on the complement a better convergence is obtained. Hence, the quadratic convergence here is (only) obtained in $H^{-1}(\Omega)$.

Both a priori error estimates are proved using standard Galerkin orthogonality and interpolation estimates, see [HOV16b] for details. The reformulation of the HMM from Proposition 3.1.8 also enables us to derive robust and efficient local residual-based a posteriori error estimators presented in [HOV16b].

3.1.3 Numerical experiments

In this section we analyze the HMM numerically and verify the theoretical a priori estimates given in Theorems 3.1.11 and 3.1.12. The implementation has been done based on the module dune-gdt [MS15] of the DUNE software framework [BBD+08a, BBD+08b]. The corresponding code can be found on Github[1]. The example is located in test/curlcurl-discretization.cc. We consider a test case with analytically known homogenized solution and a test case inspired by [CZAL10], where this is not available. Besides the (absolute) errors we also give the experimental order of convergence (EOC), which is defined for two mesh sizes $H_1 > H_2$ and the corresponding error values $e_{H,1}$ and $e_{H,2}$ as $\text{EOC}(e) := \ln(\frac{e_{H,1}}{e_{H,2}})/\ln(\frac{H_1}{H_2})$. In the tables, we list the EOC for $H_1 > H_2$ in the row of the smaller mesh size H_2.

Academic test case. The parameters μ and κ are periodic and quasi-one-dimensional, given by

$$\mu(y) = \frac{1}{2 + \cos(2\pi y_1)} \quad \text{and} \quad \kappa(y) = -\frac{1}{2 + \cos(2\pi y_1) + i(2 + \sin(2\pi y_1))}.$$

Cell problem (3.4) then has the solutions

$$\mathbf{v}_1 = 0, \qquad \mathbf{v}_2 = -\frac{1}{4\pi}\sin(2\pi y_1)\mathbf{e}_3, \qquad \mathbf{v}_3 = \frac{1}{4\pi}\sin(2\pi y_1)\mathbf{e}_2$$

and cell problem (3.5) has the solutions

$$v_1 = \frac{1-i}{8\pi}(\sin(2\pi y_1) - i\cos(2\pi y_1)), \qquad v_2 = v_3 = 0.$$

We obtain the homogenized matrices

$$\mu_{\text{hom}} = \text{diag}\Big(\frac{1}{\sqrt{3}}, \frac{1}{2}, \frac{1}{2}\Big) \qquad \text{and} \qquad \kappa_{\text{hom}} = \frac{i-1}{4}\,\text{Id}\,.$$

[1] github.com/BarbaraV/dune-gdt/tree/dissertation

Table 3.1: Convergence history and EOC for the energy error between the HMM-approximation and the analytical two-scale solution for the academic test case.

$H = 0.5h$	$\|e_0\|_{\mathbf{H}(\mathrm{curl})}$	$\|\nabla_y e_1\|_{\Omega\times Y}$	$\|\nabla_y e_2\|_{\Omega\times Y}$	EOC(e_0)	EOC(e_1)	EOC(e_2)
$\sqrt{3}\cdot 1/4$	0.8525680	1.1779100	0.1453250	—	—	—
$\sqrt{3}\cdot 1/6$	0.5536540	0.6539270	0.1070710	1.065	1.452	0.753
$\sqrt{3}\cdot 1/8$	0.4123370	0.5105090	0.0826501	1.024	0.860	0.900
$\sqrt{3}\cdot 1/12$	0.2737220	0.3465770	0.0563304	1.011	0.955	0.946

Table 3.2: Convergence history and EOC for the $L^2(\Omega)$- and $H^{-1}(\Omega)$-norm of the macroscopic error for the academic test case.

$H = 0.5h$	$\|e_0\|_{L^2(\Omega)}$	$\|\theta_{0.5H}\|_{L^2(\Omega)}$	EOC($\|e_0\|_{L^2}$)	EOC($\|\theta_{0.5H}\|_{L^2}$)
$\sqrt{3}\cdot 1/4$	0.289838	0.01016380	—	—
$\sqrt{3}\cdot 1/6$	0.198130	0.00547900	0.938	1.524
$\sqrt{3}\cdot 1/8$	0.150250	0.00286401	0.961	2.255
$\sqrt{3}\cdot 1/12$	0.100898	0.00139175	0.982	1.780

For the computational (macroscopic) domain $\Omega = (0,1)^3$ and an appropriate volume term $\mathbf{f}$ the homogenized solution $\mathbf{u}_0$ is given by

$$\mathbf{u}_0(x) = (\sin(\pi x_2)\sin(\pi x_3),\, \sin(\pi x_1)\sin(\pi x_3),\, \sin(\pi x_1)\sin(\pi x_2))^T.$$

In fact the corresponding $\mathbf{f}$ is similar to $\mathbf{u}_0$ up to a prefactor, related to the homogenized matrices, in each component. Note that $\mathbf{u}_0$ has zero tangential traces as required and that μ, κ, and $\mathbf{f}$ fulfill Assumption 3.1.1. As it is explicitly known, the analytical two-scale solution is used as reference solution for the error computation, but we also compute a reference solution as direct discretization to the heterogeneous problem (3.2) on a well resolved mesh.

The energy norm for a two-scale triple $(\mathbf{v}_0, \mathbf{v}_1, v_2)$ in principle consists of the $\mathbf{H}(\mathrm{curl})$-norm of $\mathbf{v}_0$ and the $H^1(Y)$-seminorms of $\mathbf{v}_1$ and v_2. Table 3.1 shows the behavior of these contributions for the error (e_0, e_1, e_2) between the analytical two-scale solution $(\mathbf{u}_0, \mathbf{u}_1, u_2)$ and the HMM-approximation $(\mathbf{u}_H, \mathbf{u}_{h,1}, u_{h,2})$ (as defined in Section 3.1.2) when decreasing H and h simultaneously. One can clearly see a linear decay (the EOC is close to 1) for all three parts of the energy error as predicted by Theorem 3.1.11.

In order to verify Theorem 3.1.12, the Helmholtz decomposition of the error $\mathbf{u}_0 - \mathbf{u}_H$ has to be computed. As it is well known, the gradient part $\theta \in H^1_0(\Omega)$ can be characterized as solution to $(\nabla\theta, \nabla v)_{L^2(\Omega)} = (\mathbf{u}_0 - \mathbf{u}_H, \nabla v)_{L^2(\Omega)}$ for all $v \in H^1_0(\Omega)$. We solve the variational problem using linear Lagrange finite elements on a refined macroscopic grid with mesh size $0.5H$. The obtained approximation $\theta_{0.5H}$ of θ is considered in Table 3.2 and we verify the predicted quadratic convergence of Theorem 3.1.12 (the EOC is close to 2). We emphasize that this consideration of the $H^{-1}(\Omega)$-norm is necessary to obtain a higher convergence order by dual problems: Table 3.2 reveals that the $L^2(\Omega)$-norm only shows linear convergence (the EOC is close to 1). The theoretical reasons for this difference have been discussed in Section 3.1.2.

Furthermore, we justify our assumption that the homogenization error can be neglected and show that the correctors are needed to approximate the heterogeneous solution $\mathbf{u}_\delta$. For the rather large parameter $\delta = 0.2$, we compute a fine reference solution $\mathbf{u}_\delta$ by a standard discretization with edge elements on a well resolved grid with 82,944 entities. The "homogenization" error between this reference solution and the homogenized solution $\mathbf{u}_0$ in the $\mathbf{H}(\mathrm{curl})$-norm is 1.1175. Table 3.3 shows that the correctors are important parts of the approximation, as predicted in Conclusion 3.1.9. While the $L^2(\Omega)$-norm and $\mathbf{H}(\mathrm{curl})$-seminorm between the reference solution and the macroscopic HMM-approximation $\mathbf{u}_H$ decrease only

Table 3.3: Errors between the reference solution for $\delta = 0.2$ and the HMM- and zeroth order approximations for the academic test case.

$H = 0.5h$	$\|\mathbf{u}_\delta - \mathbf{u}_H\|$	$\|\operatorname{curl}(\mathbf{u}_\delta - \mathbf{u}_H)\|$	$\|\mathbf{u}_\delta - \mathbf{u}^0_{\mathrm{HMM}}\|$	$\|\operatorname{curl}\mathbf{u}_\delta - \operatorname{curl}\mathbf{u}^0_{\mathrm{HMM}}\|$
$\sqrt{3}\cdot 1/4$	0.335398	1.506500	0.327844	1.506500
$\sqrt{3}\cdot 1/6$	0.238788	1.298450	0.223458	0.968140
$\sqrt{3}\cdot 1/8$	0.213063	1.195330	0.174381	0.734586
$\sqrt{3}\cdot 1/12$	0.185121	1.136130	0.127631	0.486497

(a) Behavior of the L^2-norms

$H = 0.5h$	$\mathrm{EOC}(\|\mathbf{u}_\delta - \mathbf{u}_H\|)$	$\mathrm{EOC}(\|\mathbf{u}_\delta - \mathbf{u}^0_{\mathrm{HMM}}\|)$	$\mathrm{EOC}(\|\operatorname{curl}\mathbf{u}_\delta - \operatorname{curl}\mathbf{u}^0_{\mathrm{HMM}}\|)$
$\sqrt{3}\cdot 1/4$	—	—	—
$\sqrt{3}\cdot 1/6$	0.838	0.945	1.091
$\sqrt{3}\cdot 1/8$	0.396	0.862	0.960
$\sqrt{3}\cdot 1/12$	0.347	0.770	1.016

(b) Experimental order of convergence (EOC)

very slowly (Table 3.4a, columns 2–3, and Table 3.4b, column 2), the errors to the zeroth order approximations $\mathbf{u}^0_{\mathrm{HMM}} := \mathbf{u}_H + \nabla_y u_{h,2}(\cdot, \frac{\cdot}{\delta})$ and $\operatorname{curl}\mathbf{u}^0_{\mathrm{HMM}} := \operatorname{curl}\mathbf{u}_H + \operatorname{curl}_y \mathbf{u}_{h,1}(\cdot, \frac{\cdot}{\delta})$ converge (almost) linearly as predicted, see the EOCs in Table 3.4b. The convergence slows down slightly in the end because the regime where the modeling error dominates over the discretization error is approached.

Finally, we visualize the differences between a homogenized and heterogeneous solution and their approximations by the HMM. Figure 3.1 shows the magnitude of four different fields in the plane $z = 0.5$: The expected homogenized solution $\mathbf{u}_0$ (top left) on a grid with $H = \sqrt{3}\cdot 1/12$, the macroscopic part of the HMM-approximation $\mathbf{u}_H$ (top right) for $H = 0.5h = \sqrt{3}\cdot 1/12$, the reference solution $\mathbf{u}_\delta$ (bottom left) for $\delta = 0.2$ on a mesh with size $H = \sqrt{3}\cdot 1/24$, and the zeroth order approximation $\mathbf{u}^0_{\mathrm{HMM}}$ (bottom right), as defined above, computed with $H = 0.5h = \sqrt{3}\cdot 1/12$ and depicted on the fine-scale reference mesh. The figure shows a good correspondence between the HMM-approximation and the expected homogenized or reference solution (the left vs. right picture in the top and bottom row of Figure 3.1, respectively). Moreover, by comparing the reference solution and the expected homogenized solution (the left column of Figure 3.1), one can see how the periodic features related to the oscillations in the parameters are in some sense "averaged" in the homogenization procedure. This can also be seen in Figure 3.2, which shows the zeroth order approximation $\mathbf{u}^0_{\mathrm{HMM}}$ for three different values of δ. With decreasing δ from left to right, we see that the oscillations get "faster" (shorter length of a period), while their amplitudes remain the same. This also corresponds to the fact that the convergence of $\mathbf{u}_\delta$ to $\mathbf{u}_0$ is *not* strong, but only weak in $L^2(\Omega)$.

Test case inspired by [CZAL10]. We chose a situation inspired by [CZAL10, Case 5.1.1]: The macroscopic domain is $\Omega = (0,1)^3$, $\kappa = -1$ and $\mathbf{f} = (30, 30, 30)^T$ are constant, and μ_δ is given as $\mu_\delta(x) = \mu(\frac{x}{\delta})$ with the periodic function

$$\mu(y) = \frac{20}{(2 + 1.5\sin(2\pi y_1 + 0.75))(2 + 1.5\sin(2\pi y_2 + 0.75))(2 + 1.5\sin(2\pi y_3 + 0.75))}.$$

Neither the exact nor the homogenized solution are known analytically. Moreover, due to the choice of κ, we deal with an indefinite problem. Formally, this is not covered by our error analysis, but we still expect the same rates for sufficiently fine meshes, see [CFS17] for

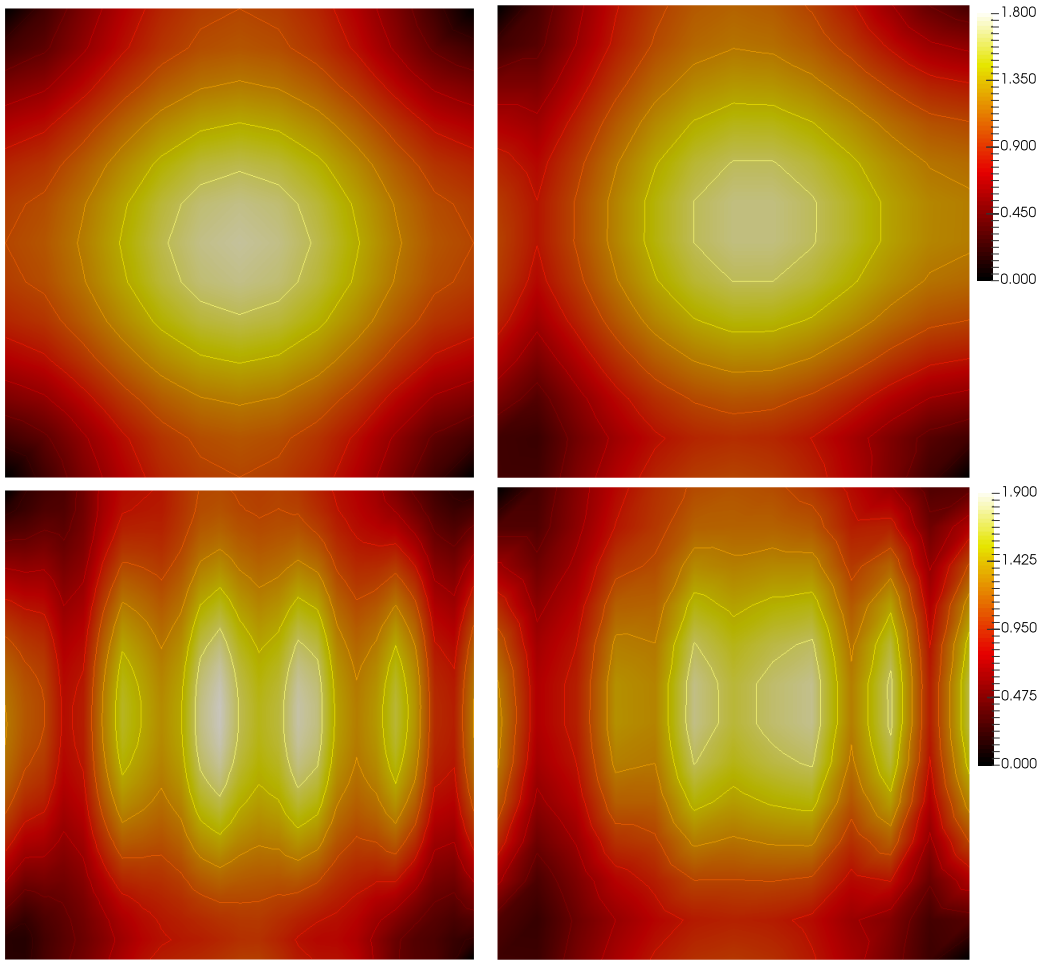

Figure 3.1: In the plane $z = 0.5$: magnitudes of the homogenized solution $\mathbf{u}_0$ (top left), of the macroscopic part of the HMM-approximation $\mathrm{Re}(\mathbf{u}_H)$ (top right), of the reference solution $\mathrm{Re}(\mathbf{u}_\delta)$ on fine grid for $\delta = 0.2$ (bottom left), and of the zeroth order approximation $\mathrm{Re}(\mathbf{u}^0_{\mathrm{HMM}})$ (bottom right), all for the academic test case.

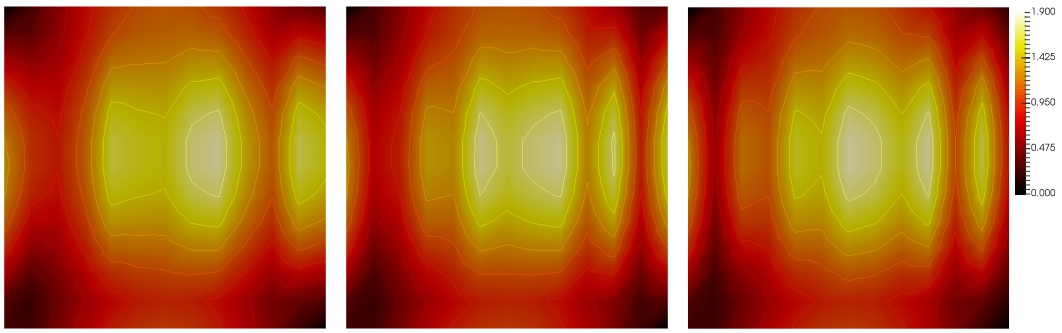

Figure 3.2: In the plane $z = 0.5$: magnitudes of the zeroth order approximations $\mathrm{Re}(\mathbf{u}^0_{\mathrm{HMM}})$ for $\delta = 0.3$ (left), $\delta = 0.2$ (middle), and $\delta = 0.15$ (right) for the academic test case.

Table 3.4: Convergence history and EOC for the error $e_0 = \mathbf{u}_0 - \mathbf{u}_H$ between the HMM-approximation and the reference homogenized solution for the test case of [CZAL10].

$H = 0.5h$	$\|\operatorname{curl} e_0\|$	$\|e_0\|$	$\|\theta(e_0)\|$	EOC(e_0)	EOC($\operatorname{curl} e_0$)	EOC($\theta(e_0)$)
$\sqrt{3} \cdot 1/4$	1.030690	0.233979	0.00665521	—	—	—
$\sqrt{3} \cdot 1/6$	0.579060	0.139066	0.00387697	1.283	1.422	1.333
$\sqrt{3} \cdot 1/8$	0.452262	0.108110	0.00219004	0.875	0.859	1.985
$\sqrt{3} \cdot 1/12$	0.250834	0.062329	0.00094402	1.358	1.454	2.076

Table 3.5: Convergence history and EOC for the error between the HMM-approximation $\mathbf{u}_H$, the curl zeroth order approximation $\operatorname{curl} \mathbf{u}^0_{\mathrm{HMM}} := \operatorname{curl} \mathbf{u}_H + \operatorname{curl}_y \mathbf{u}_{h,1}(\cdot, \frac{\cdot}{\delta})$, and the reference solution $\mathbf{u}_\delta$ for the test case of [CZAL10].

$H = 0.5h$	$\|\operatorname{curl}(\mathbf{u}_\delta - \mathbf{u}_H)\|$	$\|\operatorname{curl} \mathbf{u}_\delta - \operatorname{curl} \mathbf{u}^0_{\mathrm{HMM}}\|$	$\|\mathbf{u}_\delta - \mathbf{u}_H\|$	$\|\theta(\mathbf{u}_\delta - \mathbf{u}_H)\|$
$\sqrt{3} \cdot 1/4$	2.407260	2.138060	0.266706	0.006656590
$\sqrt{3} \cdot 1/6$	2.238660	1.586240	0.186146	0.003878270
$\sqrt{3} \cdot 1/8$	2.193030	1.239650	0.163394	0.002191250
$\sqrt{3} \cdot 1/12$	2.140620	1.002660	0.135681	0.000945141

a rigorous proof using T-coercivity. Since κ is constant, the second corrector u_2 vanishes and we expect strong convergence of $\mathbf{u}_\delta$ to $\mathbf{u}_0$ in $L^2(\Omega)$.

We first compare the HMM-approximation to a reference homogenized solution (approximating $\mathbf{u}_0$), which is computed in the following way. The effective parameter μ_{hom} is calculated by solving cell problem (3.4) on a mesh with 82,944 elements (κ_{hom} is simply the negative identity). Afterwards, the macroscopic equation (3.7) is solved with the same number of elements yielding the reference homogenized solution $\mathbf{u}_0$. Table 3.4 confirms the predictions of Theorems 3.1.11 and 3.1.12: We observe linear convergence in the $\mathbf{H}(\mathrm{curl})$-seminorm and the $L^2(\Omega)$-norm and quadratic convergence for the Helmholtz decomposition. The gradient part θ is computed as finite element approximation of the associated Poisson problem on the reference mesh, as already described for the academic test case. The table not only confirms the a priori error estimates, but also shows that solving the cell problems first, then assembling the effective parameters, and finally solving the macroscopic homogenized equation on a rather fine mesh gives a good approximation to the homogenized solution $\mathbf{u}_0$, which is useful for other numerical experiments.

The reference mesh with 82,944 elements is also used to compute a reference solution $\mathbf{u}_\delta$ for $\delta = 1/3$. The homogenization error between this (heterogeneous) reference solution and the reference homogenized solution described above amounts to 2.11517 in the full $\mathbf{H}(\mathrm{curl})$- and 0.119217 in the $L^2(\Omega)$-norm. Since u_2 vanishes, the macroscopic part of the HMM-approximation $\mathbf{u}_H$ already forms the zeroth order L^2-approximation to $\mathbf{u}_\delta$, so that the error $\mathbf{u}_\delta - \mathbf{u}_H$ equals the error $\mathbf{u}_\delta - \mathbf{u}^0_{\mathrm{HMM}}$. Table 3.5 summarizes the errors between $\mathbf{u}_\delta$ and the HMM-approximation and reveals various interesting aspects. First, $\mathbf{u}_1$ has to be considered for the error in the $\mathbf{H}(\mathrm{curl})$-seminorm: While the error $\operatorname{curl}(\mathbf{u}_\delta - \mathbf{u}_H)$ is only slowly decreasing, we almost regain linear convergence when considering $\operatorname{curl} \mathbf{u}_\delta - \operatorname{curl} \mathbf{u}^0_{\mathrm{HMM}}$ with $\operatorname{curl} \mathbf{u}^0_{\mathrm{HMM}} := \operatorname{curl} \mathbf{u}_H + \operatorname{curl}_y \mathbf{u}_h(\cdot, \frac{\cdot}{\delta})$. The convergence is slowing down slightly at the end probably because the homogenization error is dominating. Second, because of the vanishing corrector u_2, we obtain some (sublinear) convergence in the $L^2(\Omega)$-norm of $\mathbf{u}_\delta - \mathbf{u}_H$. This convergence is certainly more than we obtained for the academic test case, where the corrector has to be considered. The sublinearity of the rate may be explained by a dominance of the homogenization error. However, it could also be that the heterogeneous reference solution is still not well resolved enough. Third, we obtain quadratic convergence for the Helmholtz

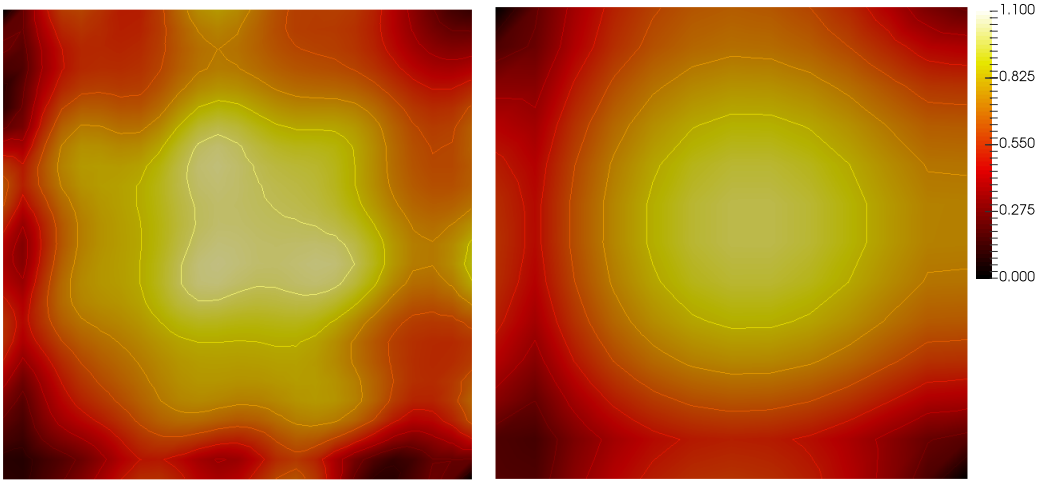

Figure 3.3: In the plane $z = 0.5$: Magnitude of the reference solution $\mathbf{u}_\delta$ for $\delta = 1/3$ (left) and HMM-approximation $\mathbf{u}_H$ (right) for the test case of [CZAL10].

decomposition of $\mathbf{u}_\delta - \mathbf{u}_H$, which is in accordance with Theorem 3.1.12 and also due to the vanishing corrector u_2.

Finally, we visualize the reference solution (for $\delta = 1/3$ on a mesh with 82,944 elements) and the HMM-approximation $\mathbf{u}_H$ (with $H = 0.5h = \sqrt{3} \cdot 1/12$) in Figure 3.3. Note that the HMM-approximation $\mathbf{u}_H$ equals the zeroth order approximation $\mathbf{u}^0_{\mathrm{HMM}}$ in this case and moreover, it is also close to the homogenized solution. We see that some oscillatory behavior of the reference solution is not captured and would need higher order correctors. However, in contrast to the academic case, due to the strong convergence $\mathbf{u}_\delta$ to $\mathbf{u}_0$ in $L^2(\Omega)$, the amplitudes of these oscillations are decreasing for $\delta \to 0$. Therefore, we already have a good agreement between the reference solution and the HMM-approximation for the parameter $\delta = 1/3$.

3.2 Numerical homogenization beyond periodicity

In this section, we study the $\mathbf{H}(\mathrm{curl})$-elliptic problem of Definition 2.1.5 without the assumption of (local) periodicity or scale separation. For better readability, we assume that $\mu \in L^\infty(\Omega; \mathbb{R}^{3\times 3})$ and $\kappa \in L^\infty(\Omega; \mathbb{C}^{3\times 3})$ are self-adjoint because in this case the discretization is a Galerkin method instead of a Petrov-Galerkin method. This is not an essential restriction.

This section is organized as follows. In Section 3.2.1, we give a short motivation of our approach from two perspectives: periodic homogenization and the (ideal) Localized Orthogonal Decomposition. Section 3.2.2 presents some more details about the Falk-Winther interpolation operator. In Section 3.2.3, we introduce the Corrector Green's Operator and show its approximation properties. We localize the corrector operator in Section 3.2.4 and present the main a priori error estimates. The proofs of the decay of the correctors are given in Section 3.2.5. Details on the implementation of the Falk-Winther interpolation operator are given in Section 3.2.6. The extension to indefinite $\mathbf{H}(\mathrm{curl})$-problems is discussed in Section 3.2.7. We only consider homogeneous essential boundary conditions, the incorporation of impedance boundary conditions, in particular for the indefinite case, is an open question for future work.

3.2.1 Motivation of the approach

Motivation via homogenization. For the sake of argument, let us again look at periodically oscillating coefficients $\mu_\delta(x) = \mu(x/\delta)$ and $\kappa_\delta(x) = \kappa(x/\delta)$. Classical homogenization theory in Section 3.1.1 shows that the sequence of exact solutions $\mathbf{u}_\delta$ converges weakly in $\mathbf{H}_0(\mathrm{curl})$ to

a *homogenized* function $\mathbf{u}_0$. Since $\mathbf{u}_0 \in \mathbf{H}_0(\mathrm{curl})$ is δ-independent, it can be well approximated in $\mathring{\mathcal{N}}(\mathcal{T}_H)$. Furthermore, there exists a *corrector* $\mathbf{K}_\delta(\mathbf{u}_0)$ such that $\mathbf{u}_\delta \approx (\mathrm{id} + \mathbf{K}_\delta)\mathbf{u}_0$ is a good approximation in $\mathbf{H}(\mathrm{curl})$, i.e., the error converges strongly to zero with

$$\|\mathbf{u}_\delta - (\mathbf{u}_0 + \mathbf{K}_\delta(\mathbf{u}_0))\|_{\mathbf{H}(\mathrm{curl})} \to 0 \qquad \text{for } \delta \to 0.$$

Moreover, the corrector $\mathbf{K}_\delta(\mathbf{u}_0)$ admits a decomposition into a gradient part and part with small amplitude, see (3.8). We deduced that $\mathbf{K}_\delta(\mathbf{u}_0)$ is $\mathbf{H}(\mathrm{curl})$-stable and that $\mathbf{u}_0$ *must* be a good approximation of the exact solution in the space $H^{-1}(\Omega;\mathbb{C}^3)$. Consequently we have strong convergence in $H^{-1}(\Omega)$ with

$$\|\mathbf{u}_\delta - \mathbf{u}_0\|_{H^{-1}(\Omega)} \overset{\delta\to 0}{\longrightarrow} 0.$$

Rephrasing this, we concluded two things. First, even though the coarse space $\mathring{\mathcal{N}}(\mathcal{T}_H)$ does not contain good $\mathbf{H}(\mathrm{curl})$- or L^2-approximations, it still contains meaningful approximations in $H^{-1}(\Omega)$. Second, the fact that the coarse part $\mathbf{u}_0$ is a good H^{-1}-approximation of $\mathbf{u}_\delta$ is an intrinsic conclusion from the properties of the correction $\mathbf{K}_\delta(\mathbf{u}_0)$. A refined analysis reveals that the numerical homogenization method presented here allows for estimates in the stronger $\mathbf{H}(\mathrm{div})'$-norm.

In this section we are concerned with the question if the above considerations can be transferred to a discrete setting beyond the assumption of periodicity. More precisely, defining a coarse level of resolution through the space $\mathring{\mathcal{N}}(\mathcal{T}_H)$, we ask if it is possible to find a coarse function $\mathbf{u}_H$ and an (efficiently computable) $\mathbf{H}(\mathrm{curl})$-stable operator $\mathcal{K}$, such that

$$\|\mathbf{u}_\delta - \mathbf{u}_H\|_{H^{-1}(\Omega)} \leq CH \qquad \text{and} \qquad \|\mathbf{u}_\delta - (\mathrm{id} + \mathcal{K})\mathbf{u}_H\|_{\mathbf{H}(\mathrm{curl})} \leq CH, \tag{3.12}$$

with C being independent of the oscillations in terms of δ. A natural ansatz for the coarse part is $\mathbf{u}_H = \pi_H(\mathbf{u})$ for a suitable projection $\pi_H : \mathbf{H}(\mathrm{curl}) \to \mathring{\mathcal{N}}(\mathcal{T}_H)$. From the considerations above it is desirable that the interpolation error $\mathbf{u}_\delta - \pi_H(\mathbf{u}_\delta)$ fulfills a discrete analog to the estimates (3.8). Hence, we seek a projector π_H with the following property: There are $\mathbf{z} \in \mathbf{H}_0^1(\Omega)$ and $\theta \in H_0^1(\Omega)$ such that $\mathbf{v} - \pi_H\mathbf{v} = \mathbf{z} + \nabla\theta$ with

$$\begin{aligned} H^{-1}\|\mathbf{z}\|_{L^2(\Omega)} + \|\nabla\mathbf{z}\|_{L^2(\Omega)} &\leq C\|\operatorname{curl}\mathbf{v}\|_{L^2(\Omega)}, \\ H^{-1}\|\theta\|_{L^2(\Omega)} + \|\nabla\theta\|_{L^2(\Omega)} &\leq C\|\mathbf{v}\|_{\mathbf{H}(\mathrm{curl})}. \end{aligned} \tag{3.13}$$

Note that the above properties are not fulfilled for, e.g., the L^2-projection. We conclude this paragraph by summarizing that we want to have a projection π_H fulfilling (3.13). We can then define a coarse scale numerically through the space $\mathring{\mathcal{N}}(\mathcal{T}_H) = \mathrm{im}(\pi_H)$. Moreover, the corrector $\mathcal{K}$ should be constructed such that it maps into the kernel of the projection operator, i.e., $\mathrm{im}(\mathcal{K}) \subset \ker(\pi_H)$ in order to inherit the estimates (3.12).

Motivation via the Localized Orthogonal Decomposition. As described in Section 2.3.4, the decomposition of the solution space into a coarse and a fine part is also the key motivation for the Localized Orthogonal Decomposition (LOD). In our setting, the idea is to write $\mathbf{H}_0(\mathrm{curl}) = \mathring{\mathcal{N}}(\mathcal{T}_H) \oplus \mathbf{W}$ with $\mathbf{W} = \ker\pi_H$, where $\pi_H : \mathbf{H}_0(\mathrm{curl}) \to \mathring{\mathcal{N}}(\mathcal{T}_H)$ is a suitable projection. We can define a correction operator $\mathcal{K} : \mathbf{H}_0(\mathrm{curl}) \to \mathbf{W}$ via

$$\mathcal{B}(\mathcal{K}\mathbf{v}, \boldsymbol{\psi}) = -\mathcal{B}(\mathbf{v}, \mathbf{w}) \qquad \forall \mathbf{w} \in \mathbf{W}. \tag{3.14}$$

The (ideal) LOD is then a Galerkin method over the space $(\mathrm{id} + \mathcal{K})\mathring{\mathcal{N}}(\mathcal{T}_H)$, i.e., we seek $\mathbf{u}_H \in \mathring{\mathcal{N}}(\mathcal{T}_H)$ such that

$$\mathcal{B}\big((\mathrm{id} + \mathcal{K})\mathbf{u}_H, (\mathrm{id} + \mathcal{K})\mathbf{v}_H\big) = \big(\mathbf{f}, (\mathrm{id} + \mathcal{K})\mathbf{v}_H\big)_{L^2(\Omega)} \qquad \forall \mathbf{v}_H \in \mathring{\mathcal{N}}(\mathcal{T}_H). \tag{3.15}$$

Problem (3.14), however, is global and therefore very costly to solve. In order to obtain a localized method, we truncate the computation to patches $\mathrm{N}^m(T)$ as in Section 2.3.4. The overall scheme can then be described as follows: Consider a basis $\{\mathbf{\Phi}_l |\ 1 \leq l \leq N\}$ of $\mathring{\mathcal{N}}(\mathcal{T}_H)$. For all $T \in \mathcal{T}_H$ with $T \subset \mathrm{supp}(\mathbf{\Phi}_l)$, we solve for $\mathcal{K}_{T,m}(\mathbf{\Phi}_l) \in \mathbf{W}(\mathrm{N}^m(T))$ such that

$$\mathcal{B}_{\mathrm{N}^m(T)}(\mathcal{K}_{T,m}(\mathbf{\Phi}_l), \mathbf{w}) = -\mathcal{B}_T(\mathbf{\Phi}_l, \mathbf{w}) \qquad \forall \mathbf{w} \in \mathbf{W}(\mathrm{N}^m(T)),$$

where $\mathbf{W}(\mathrm{N}^m(T))$ denotes the space of functions in $\mathbf{W}$ which vanish outside $\mathrm{N}^m(T)$. Defining the corrector operator $\mathcal{K}_m$ via

$$\mathcal{K}_m(\mathbf{\Phi}_l) = \sum_{\substack{T \in \mathcal{T}_H \\ T \subset \mathrm{supp}(\mathbf{\Phi}_l)}} \mathcal{K}_{T,m}(\mathbf{\Phi}_l),$$

we seek the solution $\mathbf{u}_{H,m} \in \mathring{\mathcal{N}}(\mathcal{T}_H)$ to (3.15) with $\mathcal{K}$ replaced by $\mathcal{K}_m$, see Section 3.2.4 for details.

As discussed in Section 2.3.4, we have to analyze (i) what approximation properties $\mathbf{u}_H$ and $(\mathrm{id}+\mathcal{K})\mathbf{u}_H$ have, and, (ii) whether the computation in (3.14) can be truncated to patches of elements without losing the approximation properties. With regard to these two questions, we briefly describe the main challenges for $\mathbf{H}(\mathrm{curl})$-problems in contrast to elliptic diffusion problems (cf. Section 2.3.4). Concerning (i), denoting $e = \mathbf{u} - (\mathrm{id}+\mathcal{K})\mathbf{u}_H$ with the exact solution $\mathbf{u}$ of Definition 2.1.5, we observe $\pi_H e = 0$ and quickly deduce the estimate

$$\|e\|^2_{\mathbf{H}(\mathrm{curl})} \lesssim |(\mathbf{f}, e)| = |(\mathbf{f}, e - \pi_H e)|.$$

In Section 2.3.4, we used estimates of the form $\|v - \pi_H v\|_{L^2(\Omega)} \lesssim H\|\nabla v\|_{L^2(\Omega)}$ for $v \in H^1_0(\Omega)$. Such an estimate (with the gradient replaced by the curl), however, cannot hold in $\mathbf{H}(\mathrm{curl})$ because of the large kernel of the curl-operator. Instead, we require estimates like (3.13) in order to deduce

$$|(\mathbf{f}, e - \pi_H e)| = |(\mathbf{f}, \mathbf{z} + \nabla\theta)| \leq |(\mathbf{f}, \mathbf{z})| + |(\mathrm{div}\,\mathbf{f}, \theta)| \lesssim H\|\mathbf{f}\|_{\mathbf{H}(\mathrm{div})}\|e\|_{\mathbf{H}(\mathrm{curl})},$$

where we also see the role of the assumption $\mathbf{f} \in \mathbf{H}(\mathrm{div})$. This difference between the gradient subspace and its complement also has to be considered when studying the exponential decay of $\mathcal{K}$ in order to answer (ii).

3.2.2 Basic notation and the interpolation operator

We recall the basic notation on meshes and finite element spaces from Sections 2.2.1 and 2.2.2 and show that the Falk-Winther interpolation operator fulfills the condition (3.13) derived above.

Let $\mathcal{T}_H$ be a regular, shape regular, and quasi-uniform partition of Ω into tetrahedra with global mesh size $H := \max\{\mathrm{diam}(T) | T \in \mathcal{T}_H\}$. $\mathcal{T}_H$ is a coarse mesh in the sense that it does not resolve the fine-scale oscillations of the parameters. We recall the notation of patches $\mathrm{N}^m(T)$ (Definition 2.2.4) and the uniform upper bound $C_{\mathrm{ol},m}$ on the number of elements in the mth order patch (2.25), which depends polynomially on m due to quasi-uniformity. We abbreviate $C_{\mathrm{ol}} := C_{\mathrm{ol},1}$. We use the space of linear Lagrange elements $\mathring{\mathcal{S}}(\mathcal{T}_H)$, the lowest order Nédélec finite elements $\mathring{\mathcal{N}}(\mathcal{T}_H)$, and the space of Raviart–Thomas fields $\mathring{\mathcal{RT}}(\mathcal{T}_H)$, as defined in Definition 2.2.8.

We use the Falk-Winther interpolation operator $\pi^E_H : \mathbf{H}_0(\mathrm{curl}) \to \mathring{\mathcal{N}}(\mathcal{T}_H)$ defined in Section 2.2.3, see also [FW14a], for our numerical method. It is $\mathbf{H}(\mathrm{curl})$-stable, local and fits into a commuting diagram with other stable interpolation operators for lowest order $H^1(\Omega)$, $\mathbf{H}(\mathrm{div})$ and $L^2(\Omega)$ elements, see Proposition 2.2.10. As explained in the motivation above, we also require that π^E_H allows for a regular decomposition in the sense of (3.13). The first proof of

such a local and H-weighted decomposition was given by Schöberl [Sch08]. In the following we shall use his results and the locality of the Falk-Winther operator to recover a similar decomposition for the projection π_H^E. More precisely, we have the following lemma which is crucial for our analysis.

Lemma 3.2.1 (Localized regular decomposition of the interpolation error)**.** *Let π_H^E denote the projection from Proposition 2.2.10. For any $\mathbf{v} \in \mathbf{H}_0(\operatorname{curl}, \Omega)$, there are $\mathbf{z} \in \mathbf{H}_0^1(\Omega)$ and $\theta \in H_0^1(\Omega)$ such that*

$$\mathbf{v} - \pi_H^E(\mathbf{v}) = \mathbf{z} + \nabla\theta$$

with the local bounds for every $T \in \mathcal{T}_H$

$$\begin{aligned} H^{-1}\|\mathbf{z}\|_{L^2(T)} + \|\nabla\mathbf{z}\|_{L^2(T)} &\leq C_z \|\operatorname{curl}\mathbf{v}\|_{L^2(\mathrm{N}^3(T))}, \\ H^{-1}\|\theta\|_{L^2(T)} + \|\nabla\theta\|_{L^2(T)} &\leq C_\theta\big(\|\mathbf{v}\|_{L^2(\mathrm{N}^3(T))} + H\|\operatorname{curl}\mathbf{v}\|_{L^2(\mathrm{N}^3(T))}\big), \end{aligned} \tag{3.16}$$

where $\nabla\mathbf{z}$ stands for the Jacobi matrix of $\mathbf{z}$. Here C_z and C_θ are generic constants that only depend on the regularity of the coarse mesh.

Observe that (3.16) implies the earlier formulated condition (3.13).

Proof. Let $\mathbf{v} \in \mathbf{H}_0(\operatorname{curl}, \Omega)$. Denote by $I_H^S : \mathbf{H}_0(\operatorname{curl}, \Omega) \to \mathring{\mathcal{N}}(\mathcal{T}_H)$ the quasi-interpolation operator introduced by Schöberl in [Sch08]. It is shown in [Sch08, Theorem 6] that there exists a decomposition

$$\mathbf{v} - I_H^S(\mathbf{v}) = \sum_{\substack{P \text{ vertex} \\ \text{of } \mathcal{T}_H}} \mathbf{v}_P \tag{3.17}$$

where, for any vertex P, $\mathbf{v}_P \in \mathbf{H}_0(\operatorname{curl}, \Omega_P)$ and Ω_P the support of the local hat function associated with P. Moreover, [Sch08, Theorem 6] provides the stability estimates

$$\|\mathbf{v}_P\|_{L^2(\Omega_P)} \lesssim \|\mathbf{v}\|_{L^2(\mathrm{N}(\Omega_P))} \quad \text{and} \quad \|\operatorname{curl}\mathbf{v}_P\|_{L^2(\Omega_P)} \lesssim \|\operatorname{curl}\mathbf{v}\|_{L^2(\mathrm{N}(\Omega_P))} \tag{3.18}$$

for any vertex P. With these results we deduce, since π_H^E is a projection onto the finite element space, that

$$\mathbf{v} - \pi_H^E(\mathbf{v}) = \mathbf{v} - I_H^S(\mathbf{v}) - \pi_H^E(\mathbf{v} - I_H^S(\mathbf{v})) = \sum_{\substack{P \text{ vertex} \\ \text{of } \mathcal{T}_H}} (\mathrm{id} - \pi_H^E)(\mathbf{v}_P).$$

Due to the locality of π_H^E, we have $(\mathrm{id} - \pi_H^E)(\mathbf{v}_P) \in \mathbf{H}_0(\operatorname{curl}, \mathrm{N}(\Omega_P))$. The local stability of π_H^E, (2.31) and (2.32), and the stability (3.18) imply

$$\begin{aligned} \|(\mathrm{id} - \pi_H^E)(\mathbf{v}_P)\|_{L^2(\mathrm{N}(\Omega_P))} &\lesssim \|\mathbf{v}\|_{L^2(\mathrm{N}(\Omega_P))} + H\|\operatorname{curl}\mathbf{v}\|_{L^2(\mathrm{N}(\Omega_P))}, \\ \|\operatorname{curl}(\mathrm{id} - \pi_H^E)(\mathbf{v}_P)\|_{L^2(\mathrm{N}(\Omega_P))} &\lesssim \|\operatorname{curl}\mathbf{v}\|_{L^2(\mathrm{N}(\Omega_P))}. \end{aligned}$$

We can now apply the regular splitting to $(\mathrm{id} - \pi_H^E)(\mathbf{v}_P)$ (cf. [PZ02]), i.e., there are $\mathbf{z}_P \in \mathbf{H}_0^1(\mathrm{N}(\Omega_P))$, $\theta_P \in H_0^1(\mathrm{N}(\Omega_P))$ such that $(\mathrm{id} - \pi_H^E)(\mathbf{v}_P) = \mathbf{z}_P + \nabla\theta_P$ satisfying

$$\begin{aligned} H^{-1}\|\mathbf{z}_P\|_{L^2(\mathrm{N}(\Omega_P))} + \|\nabla\mathbf{z}_P\|_{L^2(\mathrm{N}(\Omega_P))} &\lesssim \|\operatorname{curl}((\mathrm{id} - \pi_H^E)(\mathbf{v}_P))\|_{L^2(\mathrm{N}(\Omega_P))}, \\ H^{-1}\|\theta_P\|_{L^2(\mathrm{N}(\Omega_P))} + \|\nabla\theta_P\|_{L^2(\mathrm{N}(\Omega_P))} &\lesssim \|(\mathrm{id} - \pi_H^E)(\mathbf{v}_P)\|_{L^2(\mathrm{N}(\Omega_P))}. \end{aligned}$$

Set $\mathbf{z} = \sum_P \mathbf{z}_P$ and $\theta = \sum_P \theta_P$, which is a regular decomposition of $\mathbf{v} - \pi_H^E(\mathbf{v})$. The local estimate follows from the foregoing estimates for $\mathbf{v}_P$ and the decomposition (3.17) which yields

$$\begin{aligned} H^{-1}\|\mathbf{z}\|_{L^2(T)} + \|\nabla\mathbf{z}\|_{L^2(T)} &\leq \sum_{\substack{P \text{ vertex} \\ \text{of } T}} \big(H^{-1}\|\mathbf{z}_P\|_{L^2(\Omega_P)} + \|\nabla\mathbf{z}_P\|_{L^2(\Omega_P)}\big) \\ &\lesssim \sum_{\substack{P \text{ vertex} \\ \text{of } T}} \|\operatorname{curl}(\mathrm{id} - \pi_H^E)(\mathbf{v}_P)\|_{L^2(\mathrm{N}(\Omega_P))} \lesssim \|\operatorname{curl}\mathbf{v}\|_{L^2(\mathrm{N}^3(T))}. \end{aligned}$$

The local estimate for θ follows analogously. □

3.2.3 Corrector Green's Operator

In this section we introduce an ideal *Corrector Green's Operator* (also known as fine-scale Green's operator in the context of the Variational Multiscale Method, see [HS07]) that allows us to derive a decomposition of the exact solution into a coarse part (which is a good approximation in $H^{-1}(\Omega)$) and two different corrector contributions. For simplicity, we let from now on $\mathcal{L} : \mathbf{H}_0(\mathrm{curl}) \to \mathbf{H}_0(\mathrm{curl})'$ denote the differential operator associated with the sesquilinear form $\mathcal{B}(\cdot,\cdot)$, i.e., $\mathcal{L}(v)(w) = \mathcal{B}(v,w)$.

Using the Falk-Winter interpolation operator π_H^E for the Nédélec elements, we split the space $\mathbf{H}_0(\mathrm{curl})$ into the finite, low-dimensional coarse space $\mathring{\mathcal{N}}(\mathcal{T}_H) = \mathrm{im}(\pi_H^E)$ and a corrector space given as the kernel of π_H^E, i.e., we set $\mathbf{W} := \ker(\pi_H^E) \subset \mathbf{H}_0(\mathrm{curl})$. This yields the direct sum splitting $\mathbf{H}_0(\mathrm{curl}) = \mathring{\mathcal{N}}(\mathcal{T}_H) \oplus \mathbf{W}$. Note that $\mathbf{W}$ is closed since it is the kernel of a continuous (i.e., $\mathbf{H}(\mathrm{curl})$-stable) operator. With this the ideal Corrector Green's Operator is defined as follows.

Definition 3.2.2 (Corrector Green's Operator)**.** For $\mathbf{F} \in \mathbf{H}_0(\mathrm{curl})'$, we define the Corrector Green's Operator

$$\mathcal{G} : \mathbf{H}_0(\mathrm{curl})' \to \mathbf{W} \qquad \text{by} \qquad \mathcal{B}(\mathcal{G}(\mathbf{F}), \mathbf{w}) = \mathbf{F}(\mathbf{w}) \qquad \forall \mathbf{w} \in \mathbf{W}. \tag{3.19}$$

It is well-defined by the Lax-Milgram-Babuška theorem, which is applicable since $\mathcal{B}(\cdot,\cdot)$ is $\mathbf{H}_0(\mathrm{curl})$-elliptic and since $\mathbf{W}$ is a closed subspace of $\mathbf{H}_0(\mathrm{curl})$.

Using the Corrector Green's Operator we obtain the following decomposition of the exact solution.

Lemma 3.2.3 (Ideal decomposition)**.** *The exact solution $\mathbf{u} \in \mathbf{H}_0(\mathrm{curl})$ from Definition 2.1.5 and $\mathbf{u}_H := \pi_H^E(\mathbf{u})$ admit the decomposition*

$$\mathbf{u} = \mathbf{u}_H - (\mathcal{G} \circ \mathcal{L})(\mathbf{u}_H) + \mathcal{G}(\mathbf{f}).$$

Proof. Since $\mathbf{H}_0(\mathrm{curl}) = \mathring{\mathcal{N}}(\mathcal{T}_H) \oplus \mathbf{W}$, we can write $\mathbf{u}$ uniquely as

$$\mathbf{u} = \pi_H^E(\mathbf{u}) + (\mathrm{id} - \pi_H^E)(\mathbf{u}) = \mathbf{u}_H + (\mathrm{id} - \pi_H^E)(\mathbf{u}),$$

where $(\mathrm{id} - \pi_H^E)(\mathbf{u}) \in \mathbf{W}$ by the projection property of π_H^E. Using the differential equation for test functions $\mathbf{w} \in \mathbf{W}$ yields that

$$\mathcal{B}((\mathrm{id} - \pi_H^E)(\mathbf{u}), \mathbf{w}) = -\mathcal{B}(\mathbf{u}_H, \mathbf{w}) + (\mathbf{f}, \mathbf{w})_{L^2(\Omega)} = -\mathcal{B}((\mathcal{G} \circ \mathcal{L})(\mathbf{u}_H), \mathbf{w}) + \mathcal{B}(\mathcal{G}(\mathbf{f}), \mathbf{w}).$$

Since this holds for all $\mathbf{w} \in \mathbf{W}$ and since $\mathcal{G}(\mathbf{f}) - (\mathcal{G} \circ \mathcal{L})(\mathbf{u}_H) \in \mathbf{W}$, we conclude that

$$(\mathrm{id} - \pi_H^E)(\mathbf{u}) = \mathcal{G}(\mathbf{f}) - (\mathcal{G} \circ \mathcal{L})(\mathbf{u}_H). \qquad \square$$

The Corrector Green's Operator has the following approximation and stability properties, which reveal that its contribution is always negligible in the $\mathbf{H}(\mathrm{div})'$-norm and negligible in the $\mathbf{H}(\mathrm{curl})$-norm if applied to a function in $\mathbf{H}(\mathrm{div})$.

Lemma 3.2.4 (Ideal corrector estimates)**.** *Any $\mathbf{F} \in \mathbf{H}_0(\mathrm{curl})'$ satisfies*

$$H\|\mathcal{G}(\mathbf{F})\|_{\mathbf{H}(\mathrm{curl})} + \|\mathcal{G}(\mathbf{F})\|_{\mathbf{H}(\mathrm{div})'} \leq CH\alpha^{-1}\|\mathbf{F}\|_{\mathbf{H}_0(\mathrm{curl})'}. \tag{3.20}$$

If $\mathbf{F} = \mathbf{f} \in \mathbf{H}(\mathrm{div})$, we even have

$$H\|\mathcal{G}(\mathbf{f})\|_{\mathbf{H}(\mathrm{curl})} + \|\mathcal{G}(\mathbf{f})\|_{\mathbf{H}(\mathrm{div})'} \leq CH^2\alpha^{-1}\|\mathbf{f}\|_{\mathbf{H}(\mathrm{div})}. \tag{3.21}$$

The constant C only depends on C_{ol} and the generic constants appearing in Lemma 3.2.1.

Remark 3.2.5. We phrase all results in the $\mathbf{H}(\mathrm{div})'$-norm because we do not require more. Note, however, that all results are still valid if we replace the $\mathbf{H}(\mathrm{div})'$-norm by the $H^{-1}(\Omega;\mathbb{C}^3)$-norm, which is the norm we used in the motivation in Section 3.2.1.

Proof. The stability estimate $\|\mathcal{G}(\mathbf{F})\|_{\mathbf{H}(\mathrm{curl})} \leq \alpha^{-1}\|\mathbf{F}\|_{\mathbf{H}_0(\mathrm{curl})'}$ is obvious. Next, with $\mathcal{G}(\mathbf{F}) \in \mathbf{W}$ and Lemma 3.2.1 we have

$$\begin{aligned}\|\mathcal{G}(\mathbf{F})\|_{\mathbf{H}(\mathrm{div})'} &= \sup_{\substack{\mathbf{v}\in\mathbf{H}(\mathrm{div})\\ \|\mathbf{v}\|_{\mathbf{H}(\mathrm{div})}=1}} \left|\int_\Omega \mathbf{z}\cdot\mathbf{v} - \int_\Omega \theta(\nabla\cdot\mathbf{v})\right| \\ &\leq (\|\mathbf{z}\|^2_{L^2(\Omega)} + \|\theta\|^2_{L^2(\Omega)})^{1/2} \leq CH\|\mathcal{G}(\mathbf{F})\|_{\mathbf{H}(\mathrm{curl})} \leq CH\alpha^{-1}\|\mathbf{F}\|_{\mathbf{H}_0(\mathrm{curl})'},\end{aligned} \tag{3.22}$$

which proves (3.20). Note that this estimate exploited $\theta \in H^1_0(\Omega)$, which is why we do not require the function $\mathbf{v}$ to have a vanishing normal trace. Let us consider the case that $\mathbf{F} = \mathbf{f} \in \mathbf{H}(\mathrm{div})$. The coercivity, the relation (3.19), and (3.22) imply that

$$\alpha\|\mathcal{G}(\mathbf{f})\|^2_{\mathbf{H}(\mathrm{curl})} \leq \|\mathcal{G}(\mathbf{f})\|_{\mathbf{H}(\mathrm{div})'}\|\mathbf{f}\|_{\mathbf{H}(\mathrm{div})} \leq CH\|\mathcal{G}(\mathbf{f})\|_{\mathbf{H}(\mathrm{curl})}\|\mathbf{f}\|_{\mathbf{H}(\mathrm{div})}.$$

We conclude $\|\mathcal{G}(\mathbf{f})\|_{\mathbf{H}(\mathrm{curl})} \leq CH\alpha^{-1}\|\mathbf{f}\|_{\mathbf{H}(\mathrm{div})}$. Finally, we can use this estimate again in (3.22) to obtain

$$\|\mathcal{G}(\mathbf{f})\|_{\mathbf{H}(\mathrm{div})'} \leq CH\|\mathcal{G}(\mathbf{f})\|_{\mathbf{H}(\mathrm{curl})} \leq CH^2\alpha^{-1}\|\mathbf{f}\|_{\mathbf{H}(\mathrm{div})}.$$ □

An immediate conclusion of Lemmas 3.2.3 and 3.2.4 is the following.

Conclusion 3.2.6. *Let $\mathbf{u}$ denote the exact solution from Definition 2.1.5. Then with the coarse part $\mathbf{u}_H := \pi^E_H(\mathbf{u})$ and corrector operator $\mathcal{K} := -\mathcal{G}\circ\mathcal{L}$ it holds*

$$H^{-1}\|\mathbf{u} - (\mathrm{id}+\mathcal{K})\mathbf{u}_H\|_{\mathbf{H}(\mathrm{div})'} + \|\mathbf{u} - (\mathrm{id}+\mathcal{K})\mathbf{u}_H\|_{\mathbf{H}(\mathrm{curl})} + \|\mathbf{u}-\mathbf{u}_H\|_{\mathbf{H}(\mathrm{div})'} \leq CH\|\mathbf{f}\|_{\mathbf{H}(\mathrm{div})}.$$

Here, C only depends on α, the mesh regularity and on the constants appearing in Lemma 3.2.1.

Proof. The estimates for $\mathbf{u} - (\mathrm{id}+\mathcal{K})\mathbf{u}_H = \mathcal{G}(\mathbf{f})$ directly follow from (3.21). For the estimate of $\mathbf{u} - \mathbf{u}_H = \mathcal{K}(\mathbf{u}_H) + \mathcal{G}(\mathbf{f})$ observe that (3.20) and Proposition 2.2.10 imply

$$\|\mathcal{K}(\mathbf{u}_H)\|_{\mathbf{H}(\mathrm{div})'} \lesssim H\|\mathcal{L}\mathbf{u}_H\|_{\mathbf{H}_0(\mathrm{curl})'} \lesssim H\|\mathbf{u}_H\|_{\mathbf{H}(\mathrm{curl})} = H\|\pi^E_H\mathbf{u}\|_{\mathbf{H}(\mathrm{curl})} \lesssim H\|\mathbf{u}\|_{\mathbf{H}(\mathrm{curl})}.$$

Thus, the proof follows from the stability of the problem and the triangle inequality. □

It only remains to derive an equation that characterizes $(\mathrm{id}+\mathcal{K})\mathbf{u}_H$ as the unique solution of a variational problem. This is done in the following theorem.

Theorem 3.2.7 (Ideal numerical homogenization scheme)**.** *We consider the setting of Conclusion 3.2.6. Then $\mathbf{u}_H = \pi^E_H(\mathbf{u}) \in \mathring{\mathcal{N}}(\mathcal{T}_H)$ is characterized as the unique solution to*

$$\mathcal{B}\big((\mathrm{id}+\mathcal{K})\mathbf{u}_H, (\mathrm{id}+\mathcal{K})\boldsymbol{\psi}_H\big) = \big(\mathbf{f}, (\mathrm{id}+\mathcal{K})\boldsymbol{\psi}_H\big)_{L^2(\Omega)} \qquad \forall\boldsymbol{\psi}_H \in \mathring{\mathcal{N}}(\mathcal{T}_H). \tag{3.23}$$

The sesquilinear form $\mathcal{B}((\mathrm{id}+\mathcal{K})\cdot, (\mathrm{id}+\mathcal{K})\cdot)$ is $\mathbf{H}(\mathrm{curl})$-elliptic on $\mathring{\mathcal{N}}(\mathcal{T}_H)$.

We mention that, in the non self-adjoint case, the correction operator for the test functions would be the adjoint $\mathcal{K}^*$.

Proof. Since Lemma 3.2.3 guarantees $\mathbf{u} = \mathbf{u}_H - (\mathcal{G}\circ\mathcal{L})(\mathbf{u}_H) + \mathcal{G}(\mathbf{f})$, Definition 2.1.5 yields

$$\mathcal{B}(\mathbf{u}_H - (\mathcal{G}\circ\mathcal{L})(\mathbf{u}_H) + \mathcal{G}(\mathbf{f}), \boldsymbol{\psi}_H) = (\mathbf{f}, \boldsymbol{\psi}_H)_{L^2(\Omega)} \qquad \forall\boldsymbol{\psi}_H \in \mathring{\mathcal{N}}(\mathcal{T}_H).$$

We observe that by definition of $\mathcal{G}$ we have

$$\mathcal{B}(\mathcal{G}(\mathbf{f}), \boldsymbol{\psi}_H) = (\mathbf{f}, (\mathcal{G} \circ \mathcal{L})\boldsymbol{\psi}_H)_{L^2(\Omega)}$$

and

$$\mathcal{B}(\mathbf{u}_H - (\mathcal{G} \circ \mathcal{L})(\mathbf{u}_H), (\mathcal{G} \circ \mathcal{L})\boldsymbol{\psi}_H) = 0.$$

Combining the three equations shows that $(\mathrm{id} + \mathcal{K})\mathbf{u}_H$ is a solution to (3.23). The uniqueness follows from the following norm equivalence

$$\|\mathbf{u}_H\|_{\mathbf{H}(\mathrm{curl})} = \|\pi_H^E((\mathrm{id} + \mathcal{K})\mathbf{u}_H)\|_{\mathbf{H}(\mathrm{curl})} \leq C\|(\mathrm{id} + \mathcal{K})\mathbf{u}_H\|_{\mathbf{H}(\mathrm{curl})} \leq C\|\mathbf{u}_H\|_{\mathbf{H}(\mathrm{curl})}.$$

This is also the reason why the $\mathbf{H}(\mathrm{curl})$-ellipticity of $\mathcal{B}(\cdot, \cdot)$ implies the $\mathbf{H}(\mathrm{curl})$-ellipticity of $\mathcal{B}((\mathrm{id} + \mathcal{K}) \cdot, (\mathrm{id} + \mathcal{K}) \cdot)$ on $\mathring{\mathcal{N}}(\mathcal{T}_H)$. □

Dropping the correction on the right-hand side of (3.23) still allows for a numerical homogenization result. However, not all estimates from Conclusion 3.2.6 can be recovered in this case, as the quadratic order convergence for $\|\mathbf{u} - (\mathrm{id} + \mathcal{K})\widetilde{\mathbf{u}}_H\|_{\mathbf{H}(\mathrm{div})'}$ is typically lost (at least in the asymptotic regime). In general, the following result is available.

Conclusion 3.2.8. *For $\mathbf{f} \in \mathbf{H}(\mathrm{div})$, let $\widetilde{\mathbf{u}}_H \in \mathring{\mathcal{N}}(\mathcal{T}_H)$ denote the unique solution to*

$$\mathcal{B}\big((\mathrm{id} + \mathcal{K})\widetilde{\mathbf{u}}_H, (\mathrm{id} + \mathcal{K})\mathbf{v}_H\big) = (\mathbf{f}, \mathbf{v}_H)_{L^2(\Omega)} \qquad \forall \mathbf{v}_H \in \mathring{\mathcal{N}}(\mathcal{T}_H). \tag{3.24}$$

Then we have the error estimate

$$\|\mathbf{u} - (\mathrm{id} + \mathcal{K})\widetilde{\mathbf{u}}_H\|_{\mathbf{H}(\mathrm{curl})} + \|\mathbf{u} - \widetilde{\mathbf{u}}_H\|_{\mathbf{H}(\mathrm{div})'} \leq CH\|\mathbf{f}\|_{\mathbf{H}(\mathrm{div})}.$$

Proof. We estimate the error $\mathbf{u}_H - \widetilde{\mathbf{u}}_H$, where $\mathbf{u}_H$ solves (3.23). For any $\mathbf{v}_H \in \mathring{\mathcal{N}}(\mathcal{T}_H)$, we have that

$$\mathcal{B}((\mathrm{id} + \mathcal{K})(\mathbf{u}_H - \widetilde{\mathbf{u}}_H), (\mathrm{id} + \mathcal{K})\mathbf{v}_H) = (\mathbf{f}, \mathcal{K}\mathbf{v}_H)_{L^2(\Omega)}.$$

Hence, we conclude with the coercivity and continuity of $\mathcal{B}$ and Lemma 3.2.4 that

$$\begin{aligned}\|\mathbf{u}_H - \widetilde{\mathbf{u}}_H\|^2_{\mathbf{H}(\mathrm{curl})} &\lesssim \|(\mathrm{id} + \mathcal{K})(\mathbf{u}_H - \widetilde{\mathbf{u}}_H)\|^2_{\mathbf{H}(\mathrm{curl})} \lesssim \|\mathbf{f}\|_{\mathbf{H}(\mathrm{div})}\|\mathcal{K}(\mathbf{u}_H - \widetilde{\mathbf{u}}_H)\|_{\mathbf{H}(\mathrm{div})'} \\ &\lesssim H\|\mathbf{f}\|_{\mathbf{H}(\mathrm{div})}\|\mathcal{L}(\mathbf{u}_H - \widetilde{\mathbf{u}}_H)\|_{\mathbf{H}_0(\mathrm{curl})'} \lesssim H\|\mathbf{f}\|_{\mathbf{H}(\mathrm{div})}\|\mathbf{u}_H - \widetilde{\mathbf{u}}_H\|_{\mathbf{H}(\mathrm{curl})}.\end{aligned}$$

The estimate for $\|\mathbf{u} - \widetilde{\mathbf{u}}_H\|_{\mathbf{H}(\mathrm{div})'}$ follows with the triangle inequality and the properties of the corrector $\mathcal{K}$. □

The result from Conclusion 3.2.8 reflects the fact that in periodic homogenization, correctors typically do not appear on the right-hand side. However, as mentioned before, problem (3.24) has the disadvantage that its suffers from a slight loss in accuracy which is expected to cause reduced convergence rates for $\|\mathbf{u} - (\mathrm{id} + \mathcal{K})\widetilde{\mathbf{u}}_H\|_{\mathbf{H}(\mathrm{div})'}$.

Numerical homogenization. We summarize the most important findings and relate them to (numerical) homogenization. We defined a *homogenization scale* via the coarse FE space $\mathring{\mathcal{N}}(\mathcal{T}_H)$. We proved that there exists a numerically homogenized function $\mathbf{u}_H \in \mathring{\mathcal{N}}(\mathcal{T}_H)$ which approximates the exact solution well in $\mathbf{H}(\mathrm{div})'$ with

$$\|\mathbf{u} - \mathbf{u}_H\|_{\mathbf{H}(\mathrm{div})'} \leq CH\|\mathbf{f}\|_{\mathbf{H}(\mathrm{div})}.$$

From the periodic homogenization theory (cf. Sections 3.1.1 and 3.2.1) we know that this is the best we can expect and that $\mathbf{u}_H$ is typically not a good L^2-approximation due to the large kernel of the curl-operator. Furthermore, we showed the existence of an $\mathbf{H}(\mathrm{curl})$-stable

corrector operator $\mathcal{K} : \mathring{\mathcal{N}}(\mathcal{T}_H) \to \mathbf{W}$ that corrects the homogenized solution in such a way that the approximation is also accurate in $\mathbf{H}(\mathrm{curl})$ with

$$\|\mathbf{u} - (\mathrm{id} + \mathcal{K})\mathbf{u}_H\|_{\mathbf{H}(\mathrm{curl})} \leq CH\|\mathbf{f}\|_{\mathbf{H}(\mathrm{div})}.$$

Since $\mathcal{K} = -\mathcal{G} \circ \mathcal{L}$, we know that we can characterize $\mathcal{K}(\mathbf{v}_H) \in \mathbf{W}$ as the unique solution to the (ideal) corrector problem

$$\mathcal{B}(\mathcal{K}(\mathbf{v}_H), \mathbf{w}) = -\mathcal{B}(\mathbf{v}_H, \mathbf{w}) \qquad \forall \mathbf{w} \in \mathbf{W}. \tag{3.25}$$

The above result shows that $(\mathrm{id} + \mathcal{K})\mathbf{u}_H$ approximates the analytical solution with linear rate without any assumptions on the regularity of the problem or the structure of the coefficients that define $\mathcal{B}(\cdot, \cdot)$. Also it does not assume that the mesh resolves the possible fine-scale features of the coefficient. On the other hand, the ideal corrector problem (3.25) is global, which significantly limits its practical usability in terms of real computations.

However, as we see next, the Corrector Green's function associated with problem (3.19) shows an exponential decay measured in units of H. This property allows the splitting of the global corrector problem (3.25) into several smaller problems on subdomains, similar to how we encounter it in classical homogenization theory.

3.2.4 Quasi-local numerical homogenization

In this section we describe how the ideal corrector $\mathcal{K}$ can be approximated by a sum of local correctors without destroying the overall approximation order. This is of central importance for an efficient computability. Furthermore, it also reveals that the new corrector is a quasi-local operator, which is in line with homogenization theory. We follow the standard procedure for the localization in the LOD, as displayed for instance in [AH17a, HM14, MP14, Pet17], just to name a few.

Exponential decay and localized corrector. The property that $\mathcal{K}$ can be approximated by local correctors is directly linked to the decay properties of the Green's function associated with problem (3.19). These decay properties can be quantified explicitly by measuring distances between points in units of the coarse mesh size H. We have the following result, which states – loosely speaking – in which distance from the support of a source term $\mathbf{F}$, becomes the $\mathbf{H}(\mathrm{curl})$-norm of $\mathcal{G}(\mathbf{F})$ negligibly small. A proof of the following proposition is given in Section 3.2.5.

Proposition 3.2.9 (Decay of the corrector)**.** *Let $T \in \mathcal{T}_H$ denote a coarse element and $m \in \mathbb{N}$ a number of layers. Furthermore, let $\mathbf{F}_T \in \mathbf{H}_0(\mathrm{curl})'$ denote a local source functional in the sense that $\mathbf{F}_T(\mathbf{v}) = 0$ for all $\mathbf{v} \in \mathbf{H}_0(\mathrm{curl})$ with $\mathrm{supp}(\mathbf{v}) \subset \Omega \setminus T$. Then there exists $0 < \tilde{\beta} < 1$, independent of H, T, m, and $\mathbf{F}_T$, such that*

$$\|\mathcal{G}(\mathbf{F}_T)\|_{\mathbf{H}(\mathrm{curl}, \Omega \setminus \mathrm{N}^m(T))} \lesssim \tilde{\beta}^m \|\mathbf{F}_T\|_{\mathbf{H}_0(\mathrm{curl})'}. \tag{3.26}$$

In order to use this result to approximate $\mathcal{K}(\mathbf{v}_H) = -(\mathcal{G} \circ \mathcal{L})\mathbf{v}_H$ (which has a nonlocal argument), we introduce, for any $T \in \mathcal{T}_H$, localized differential operators $\mathcal{L}_T : \mathbf{H}(\mathrm{curl}, T) \to \mathbf{H}(\mathrm{curl}, \Omega)'$ such that

$$\langle \mathcal{L}_T(\mathbf{u}), \mathbf{v} \rangle := \mathcal{B}_T(\mathbf{u}, \mathbf{v}),$$

where $\mathcal{B}_T(\cdot, \cdot)$ denotes the restriction of $\mathcal{B}(\cdot, \cdot)$ to the element T. By linearity of $\mathcal{G}$ we can consequently write

$$\mathcal{K}(\mathbf{v}_H) = -(\mathcal{G} \circ \mathcal{L})\mathbf{v}_H = -\sum_{T \in \mathcal{T}_H} (\mathcal{G} \circ \mathcal{L}_T)\mathbf{v}_H = \sum_{T \in \mathcal{T}_H} \mathcal{G}(\mathbf{F}_T) \qquad \text{with } \mathbf{F}_T := -\mathcal{L}_T(\mathbf{v}_H).$$

Obviously, $\mathcal{G}(\mathbf{F}_T)$ fits into the setting of Proposition 3.2.9. This suggests to truncate the individual computations of $\mathcal{G}(\mathbf{F}_T)$ to a small patch $\mathrm{N}^m(T)$ and then collect the results to construct a global approximation for the corrector. Typically, m is referred to as *oversampling parameter*. The strategy is detailed in the following definition.

Definition 3.2.10 (Localized Corrector Approximation)**.** For an element $T \in \mathcal{T}_H$ we define the element patch $\Omega_T := \mathrm{N}^m(T)$ of order $m \in \mathbb{N}$. Let $\mathbf{F} \in \mathbf{H}_0(\mathrm{curl})'$ be the sum of local functionals with $\mathbf{F} = \sum_{T\in\mathcal{T}_H} \mathbf{F}_T$, where $\mathbf{F}_T \in \mathbf{H}_0(\mathrm{curl})'$ is as in Proposition 3.2.9. Furthermore, let $\mathbf{W}(\Omega_T) \subset \mathbf{W}$ denote the space of functions from $\mathbf{W}$ that vanish outside Ω_T, i.e.,

$$\mathbf{W}(\Omega_T) = \{\mathbf{w} \in \mathbf{W} | \mathbf{w} = 0 \text{ outside } \Omega_T\}.$$

We call $\mathcal{G}_{T,m}(\mathbf{F}_T) \in \mathbf{W}(\Omega_T)$ the *localized corrector* if it solves

$$\mathcal{B}(\mathcal{G}_{T,m}(\mathbf{F}_T), \mathbf{w}) = \mathbf{F}_T(\mathbf{w}) \qquad \forall \mathbf{w} \in \mathbf{W}(\Omega_T). \tag{3.27}$$

With this, the global corrector approximation is given by

$$\mathcal{G}_m(\mathbf{F}) := \sum_{T\in\mathcal{T}_H} \mathcal{G}_{T,m}(\mathbf{F}_T).$$

Observe that problem (3.27) is only formulated on the patch Ω_T and that it admits a unique solution by the Lax-Milgram-Babuška theorem.

Based on the decay properties stated in Proposition 3.2.9, we can derive the following error estimate for the difference between the exact corrector $\mathcal{G}(\mathbf{F})$ and its approximation $\mathcal{G}_m(\mathbf{F})$ obtained by an mth level truncation. The proof of the following result is again postponed to Section 3.2.5.

Theorem 3.2.11 (Error of the corrector approximation)**.** *We consider the setting of Definition 3.2.10 with ideal Green's Corrector $\mathcal{G}(\mathbf{F})$ and its mth level truncated approximation $\mathcal{G}_m(\mathbf{F})$. Then there exist constants $C_d > 0$ and $0 < \beta < 1$ (both independent of H and m) such that*

$$\|\mathcal{G}(\mathbf{F}) - \mathcal{G}_m(\mathbf{F})\|_{\mathbf{H}(\mathrm{curl})} \leq C_d \sqrt{C_{\mathrm{ol},m}}\, \beta^m \Big(\sum_{T\in\mathcal{T}_H} \|\mathbf{F}_T\|^2_{\mathbf{H}_0(\mathrm{curl})'} \Big)^{1/2} \tag{3.28}$$

and

$$\|\mathcal{G}(\mathbf{F}) - \mathcal{G}_m(\mathbf{F})\|_{\mathbf{H}(\mathrm{div})'} \leq C_d \sqrt{C_{\mathrm{ol},m}}\, \beta^m H \Big(\sum_{T\in\mathcal{T}_H} \|\mathbf{F}_T\|^2_{\mathbf{H}_0(\mathrm{curl})'} \Big)^{1/2}. \tag{3.29}$$

As a direct conclusion from Theorem 3.2.11 we obtain the main result of this section.

The quasi-local corrector and homogenization. Following the above motivation we split the ideal corrector $\mathcal{K}(\mathbf{v}_H) = -(\mathcal{G} \circ \mathcal{L})\mathbf{v}_H$ into a sum of quasi-local contributions of the form $\sum_{T\in\mathcal{T}_H} (\mathcal{G} \circ \mathcal{L}_T)\mathbf{v}_H$. Applying Theorem 3.2.11, we obtain the following result.

Conclusion 3.2.12. *Let $\mathcal{K}_m := -\sum_{T\in\mathcal{T}_H} (\mathcal{G}_{T,m} \circ \mathcal{L}_T) : \mathring{\mathcal{N}}(\mathcal{T}_H) \to \mathbf{W}$ denote the localized corrector operator obtained by truncation of mth order. Then it holds*

$$\inf_{\mathbf{v}_H \in \mathring{\mathcal{N}}(\mathcal{T}_H)} \|\mathbf{u} - (\mathrm{id} + \mathcal{K}_m)\mathbf{v}_H\|_{\mathbf{H}(\mathrm{curl})} \leq C\big(H + \sqrt{C_{\mathrm{ol},m}}\beta^m\big)\|\mathbf{f}\|_{\mathbf{H}(\mathrm{div})}. \tag{3.30}$$

Note that even though the ideal corrector $\mathcal{K}$ is a nonlocal operator, we can approximate it by a quasi-local corrector $\mathcal{K}_m$. Here, the quasi-locality is seen by the fact that, if $\mathcal{K}$ is applied to a function $\mathbf{v}_H$ with local support, the image $\mathcal{K}(\mathbf{v}_H)$ will typically still have a global support in Ω. On the other hand, if $\mathcal{K}_m$ is applied to a locally supported function, the support will only increase by a layer with thickness of order mH.

Proof of Conclusion 3.2.12. With $\mathcal{K}_m = -\sum_{T\in\mathcal{T}_H}(\mathcal{G}_{T,m}\circ\mathcal{L}_T)$ we apply Conclusion 3.2.6 and Theorem 3.2.11 to obtain

$$\begin{aligned}\inf_{\mathbf{v}_H\in\mathring{\mathcal{N}}(\mathcal{T}_H)}\|\mathbf{u}-(\mathrm{id}+\mathcal{K}_m)\mathbf{v}_H\|_{\mathbf{H}(\mathrm{curl})} &\leq \|\mathbf{u}-(\mathrm{id}+\mathcal{K})\mathbf{u}_H\|_{\mathbf{H}(\mathrm{curl})}+\|(\mathcal{K}-\mathcal{K}_m)\mathbf{u}_H\|_{\mathbf{H}(\mathrm{curl})}\\ &\leq CH\|\mathbf{f}\|_{\mathbf{H}(\mathrm{div})}+C\sqrt{C_{\mathrm{ol},m}}\,\beta^m\Big(\sum_{T\in\mathcal{T}_H}\|\mathcal{L}_T(\mathbf{u}_H)\|^2_{\mathbf{H}_0(\mathrm{curl})'}\Big)^{1/2},\end{aligned}$$

where we observe with $\|\mathcal{L}_T(\mathbf{v}_H)\|_{\mathbf{H}_0(\mathrm{curl})'}\leq C\|\mathbf{v}_H\|_{\mathbf{H}(\mathrm{curl},T)}$ that

$$\sum_{T\in\mathcal{T}_H}\|\mathcal{L}_T(\mathbf{u}_H)\|^2_{\mathbf{H}_0(\mathrm{curl})'}\leq C\|\mathbf{u}_H\|^2_{\mathbf{H}(\mathrm{curl})}=C\|\pi_H^E(\mathbf{u})\|^2_{\mathbf{H}(\mathrm{curl})}\leq C\|\mathbf{u}\|^2_{\mathbf{H}(\mathrm{curl})}\leq C\|\mathbf{f}\|^2_{\mathbf{H}(\mathrm{div})}.$$

In the last line, the second last inequality is due to the stability of π_H^E and the last inequality is the energy estimate for the original problem of Definition 2.1.5. □

Conclusion 3.2.12 has immediate implications from the computational point of view. First, we observe that $\mathcal{K}_m$ can be computed by solving local decoupled problems. Considering a basis $\{\mathbf{\Phi}_l|\ 1\leq l\leq N\}$ of $\mathring{\mathcal{N}}(\mathcal{T}_H)$, we require to determine $\mathcal{K}_m(\mathbf{\Phi}_l)$. For that, we consider all $T\in\mathcal{T}_H$ with $T\subset\mathrm{supp}(\mathbf{\Phi}_l)$ and solve for $\mathcal{K}_{T,m}(\mathbf{\Phi}_l)\in\mathbf{W}(\mathrm{N}^m(T))$ such that

$$\mathcal{B}_{\mathrm{N}^m(T)}(\mathcal{K}_{T,m}(\mathbf{\Phi}_l),\mathbf{w})=-\mathcal{B}_T(\mathbf{\Phi}_l,\mathbf{w})\qquad\forall\mathbf{w}\in\mathbf{W}(\mathrm{N}^m(T)).\tag{3.31}$$

The global corrector approximation is then given by

$$\mathcal{K}_m(\mathbf{\Phi}_l)=\sum_{\substack{T\in\mathcal{T}_H\\ T\subset\mathrm{supp}(\mathbf{\Phi}_l)}}\mathcal{K}_{T,m}(\mathbf{\Phi}_l),$$

as already presented in the motivation in Section 3.2.1. Next, we observe that selecting the localization parameter m such that

$$m\gtrsim|\log H|/|\log\beta|\approx|\log H|,$$

we have with Conclusion 3.2.12 that

$$\inf_{\mathbf{v}_H\in\mathring{\mathcal{N}}(\mathcal{T}_H)}\|\mathbf{u}-(\mathrm{id}+\mathcal{K}_m)\mathbf{v}_H\|_{\mathbf{H}(\mathrm{curl})}\leq CH\|\mathbf{f}\|_{\mathbf{H}(\mathrm{div})},\tag{3.32}$$

which is of the same order as for the ideal corrector $\mathcal{K}$. Note that the polynomial (in m) growth of $C_{\mathrm{ol},m}$ does only influence the constant hidden in $\gtrsim$ in the selection rule $m\gtrsim|\log H|$, but not (3.32). The choice $m\approx|\log H|$ is the standard condition for the oversampling parameter m in LOD-type methods. However, numerical experiments for other types of problems show that moderate sizes of m such as $m=1,2,3$ are often sufficient in practice, cf. [HM14, Pet17]. This indicates that there is hope for similar observations for $\mathbf{H}(\mathrm{curl})$-problems, although this still remains open for investigations.

Consequently, we can consider the Galerkin finite element method, where we seek $\mathbf{u}_{H,m}\in\mathring{\mathcal{N}}(\mathcal{T}_H)$ such that

$$\mathcal{B}\big((\mathrm{id}+\mathcal{K}_m)\mathbf{u}_{H,m},(\mathrm{id}+\mathcal{K}_m)\boldsymbol{\psi}_H\big)=\big(\mathbf{f},(\mathrm{id}+\mathcal{K}_m)\boldsymbol{\psi}_H\big)_{L^2(\Omega)}\qquad\forall\boldsymbol{\psi}_H\in\mathring{\mathcal{N}}(\mathcal{T}_H).$$

Since a Galerkin method yields the $\mathbf{H}(\mathrm{curl})$ quasi-best approximation of $\mathbf{u}$ in the space $(\mathrm{id}+\mathcal{K}_m)\mathring{\mathcal{N}}(\mathcal{T}_H)$ we have with (3.32) that

$$\|\mathbf{u}-(\mathrm{id}+\mathcal{K}_m)\mathbf{u}_{H,m}\|_{\mathbf{H}(\mathrm{curl})}\leq CH\|\mathbf{f}\|_{\mathbf{H}(\mathrm{div})}$$

and we have with (3.20), (3.29), and the $\mathbf{H}(\mathrm{curl})$-stability of π_H^E that

$$\|\mathbf{u}-\mathbf{u}_{H,m}\|_{\mathbf{H}(\mathrm{div})'} \leq CH\|\mathbf{f}\|_{\mathbf{H}(\mathrm{div})}.$$

This result is a homogenization result in the sense that it yields a coarse function $\mathbf{u}_{H,m}$ that approximates the exact solution in $\mathbf{H}(\mathrm{div})'$. Furthermore, it yields an appropriate (quasi-local) corrector $\mathcal{K}_m(\mathbf{u}_{H,m})$ that is required for an accurate approximation in $\mathbf{H}(\mathrm{curl})$.

Finally, we note that the error estimate in $\mathbf{H}(\mathrm{curl})$ above can also be obtained for the Galerkin method without corrector $\mathcal{K}_m$ on the right-hand side, see Conclusion 3.2.8. Moreover, the assumption $\mathbf{f}\in\mathbf{H}(\mathrm{div})$ is essential to obtain a linear rate: If we only have $\mathbf{f}\in\mathbf{H}_0(\mathrm{curl})'$, the results of Conclusion 3.2.12 do not hold. As seen in Lemma 3.2.4, we lose a power of H for less regular right-hand sides.

Remark 3.2.13 (Refined estimates)**.** With a more careful proof, the constants in the estimate of Conclusion 3.2.12 can be specified as

$$\begin{aligned}&\inf_{\mathbf{v}_H\in\mathring{\mathcal{N}}(\mathcal{T}_H)}\|\mathbf{u}-(\mathrm{id}+\mathcal{K}_m)\mathbf{v}_H\|_{\mathbf{H}(\mathrm{curl})}\\&\quad\leq\alpha^{-1}(1+H)\big(H\max\{C_z,C_\theta\}\sqrt{C_{\mathrm{ol},3}}+C_dC_\pi C_B^2\sqrt{C_{\mathrm{ol},m}C_{\mathrm{ol}}}\,\beta^m\big)\|\mathbf{f}\|_{\mathbf{H}(\mathrm{div})},\end{aligned}$$

where α and C_B are as in Definition 2.1.5, C_d is the constant appearing in the decay estimate (3.28), C_π is as in Proposition 2.2.10, C_z and C_θ are from (3.16). Note that if m is large enough so that $\mathrm{N}^m(T)=\Omega$ for all $T\in\mathcal{T}_H$, we have as a refinement of Conclusion 3.2.6 that

$$\inf_{\mathbf{v}_H\in\mathring{\mathcal{N}}(\mathcal{T}_H)}\|\mathbf{u}-(\mathrm{id}+\mathcal{K})\mathbf{v}_H\|_{\mathbf{H}(\mathrm{curl})}\leq\alpha^{-1}(1+H)\big(H\max\{C_z,C_\theta\}\sqrt{C_{\mathrm{ol},3}}\big)\|\mathbf{f}\|_{\mathbf{H}(\mathrm{div})}.$$

A fully discrete localized multiscale method. The procedure described above is still not yet applicable in practice as the local corrector problems (3.31) involve the infinite dimensional spaces $\mathbf{W}(\Omega_T)$. Hence, we require an additional fine-scale discretization of the corrector problems (just like the cell problems in periodic homogenization theory can typically not be solved analytically).

For a fully discrete formulation, we introduce a second shape regular partition $\mathcal{T}_h$ of Ω into tetrahedra. This partition may be nonuniform and is assumed to be obtained from $\mathcal{T}_H$ by at least one global refinement. It is a fine discretization in the sense that $h<H$ and that $\mathcal{T}_h$ resolves all fine-scale features of the coefficients. Let $\mathring{\mathcal{N}}(\mathcal{T}_h)\subset\mathbf{H}_0(\mathrm{curl})$ denote the space of Nédélec elements w.r.t. the partition $\mathcal{T}_h$. We then introduce the space

$$\mathbf{W}_h(\Omega_T):=\mathbf{W}(\Omega_T)\cap\mathring{\mathcal{N}}(\mathcal{T}_h)=\{\mathbf{v}_h\in\mathring{\mathcal{N}}(\mathcal{T}_h)|\mathbf{v}_h=0\text{ outside }\Omega_T,\pi_H^E(\mathbf{v}_h)=0\}$$

and discretize the corrector problem (3.31) with this new space. The corresponding correctors are denoted by $\mathcal{K}_{T,m,h}$ and $\mathcal{K}_{m,h}$. With this modification we can prove analogously to the error estimate (3.30) that it holds

$$\inf_{\mathbf{v}_H\in\mathring{\mathcal{N}}(\mathcal{T}_H)}\|\mathbf{u}_h-(\mathrm{id}+\mathcal{K}_{m,h})\mathbf{v}_H\|_{\mathbf{H}(\mathrm{curl})}\leq C\left(H+\sqrt{C_{\mathrm{ol},m}}\tilde{\beta}^m\right)\|\mathbf{f}\|_{\mathbf{H}(\mathrm{div})},\tag{3.33}$$

where $\mathbf{u}_h$ is the Galerkin approximation of $\mathbf{u}$ in the discrete fine space $\mathring{\mathcal{N}}(\mathcal{T}_h)$. If $\mathcal{T}_h$ is fine enough, we can assume that $\mathbf{u}_h$ is a good $\mathbf{H}(\mathrm{curl})$-approximation to the true solution $\mathbf{u}$. Consequently, it is justified to formulate a fully discrete (localized) multiscale method by seeking $\mathbf{u}_{H,h,m}\in\mathring{\mathcal{N}}(\mathcal{T}_H)$ such that

$$\mathcal{B}\big((\mathrm{id}+\mathcal{K}_{m,h})\mathbf{u}_{H,h,m},(\mathrm{id}+\mathcal{K}_{m,h})\boldsymbol{\psi}_H\big)=\big(\mathbf{f},(\mathrm{id}+\mathcal{K}_{m,h})\boldsymbol{\psi}_H\big)_{L^2(\Omega)}\qquad\forall\boldsymbol{\psi}_H\in\mathring{\mathcal{N}}(\mathcal{T}_H).$$

As before, we can conclude from (3.33) together with the choice $m\gtrsim|\log H|/|\log\beta|$, that it holds

$$\|\mathbf{u}_h-(\mathrm{id}+\mathcal{K}_{m,h})\mathbf{u}_{H,h,m}\|_{\mathbf{H}(\mathrm{curl})}+\|\mathbf{u}_h-\mathbf{u}_{H,h,m}\|_{\mathbf{H}(\mathrm{div})'}\leq CH\|\mathbf{f}\|_{\mathbf{H}(\mathrm{div})}.$$

Thus, the additional fine-scale discretization does not affect the overall error estimates and we therefore concentrate in the proofs on the semi-discrete case (for simplicity). Only some small modifications are needed in the proofs for the decay of the correctors, which are outlined at the end of Section 3.2.5. Note that the fine-scale reference solution $\mathbf{u}_h$ is not needed in the practical implementation of the method.

3.2.5 Main proofs

In this section, we prove Proposition 3.2.9 and Theorem 3.2.11. Since the latter one is based on the first result, we start with proving the exponential decay of the Green's function associated with $\mathcal{G}$. Recall that we quantified the decay indirectly through estimates of the form

$$\|\mathcal{G}(\mathbf{F}_T)\|_{\mathbf{H}(\mathrm{curl},\Omega\setminus \mathrm{N}^m(T))} \lesssim \tilde{\beta}^m \|\mathbf{F}_T\|_{\mathbf{H}_0(\mathrm{curl})'},$$

where $\mathbf{F}_T$ is a T-local functional and $0<\tilde{\beta}<1$. The proof techniques rely on the multiplication of a corrector function with a cut-off function η and Caccioppoli-type argument, as it is the usual strategy for LOD methods, see, e.g., [MP14,Pet17]. Alternatively, the LOD has been recently re-interpreted in form of an iterative method (additive subspace correction method) and a new technique for proving the exponential decay has been proposed, see [KPY18,KY16]. However, this modified approach would require a different localization strategy than the one that we chose in Section 3.2.4.

Proof of Proposition 3.2.9. Let $\eta \in \mathcal{S}^1(\mathcal{T}_H) \subset H^1(\Omega)$ be a scalar-valued, piecewise linear and globally continuous cut-off function with

$$\eta = 0 \qquad \text{in} \quad \mathrm{N}^{m-6}(T), \qquad\qquad \eta = 1 \qquad \text{in} \quad \Omega \setminus \mathrm{N}^{m-5}(T).$$

Denote $\mathcal{R} = \mathrm{supp}(\nabla\eta)$ and $\boldsymbol{\phi} := \mathcal{G}(\mathbf{F}_T) \in \mathbf{W}$. In the following we use $\mathrm{N}^k(\mathcal{R}) = \mathrm{N}^{m-5+k}(T) \setminus \mathrm{N}^{m-6-k}(T)$. Note that $\|\nabla\eta\|_{L^\infty(\mathcal{R})} \sim H^{-1}$. Furthermore, let $\boldsymbol{\phi} = \boldsymbol{\phi} - \pi_H^E\boldsymbol{\phi} = \mathbf{z} + \nabla\theta$ be the splitting from Lemma 3.2.1.

Set $\mathbf{w} := (\mathrm{id} - \pi_H^E)(\eta\mathbf{z} + \nabla(\eta\theta))$ and note that (i) $\operatorname{curl}\mathbf{w} = \operatorname{curl}(\mathrm{id} - \pi_H^E)(\eta\mathbf{z})$, (ii) $\mathbf{w} \in \mathbf{W}$, (iii) $\mathrm{supp}\,\mathbf{w} \subset \Omega\setminus T$. Property (i) holds because of $\operatorname{curl}\nabla = 0$ and $\operatorname{curl}\pi_H^E\nabla v = \pi_H^F(\operatorname{curl}\nabla v) = 0$ for all $v \in H_0^1(\Omega)$ due to the commuting property of π_H^E. Since $\pi_H^E\boldsymbol{\phi} = 0$, $\eta = 1$ in $\Omega\setminus \mathrm{N}^m(T)$ and because of the coercivity, we obtain that

$$\begin{aligned}\|\boldsymbol{\phi}\|^2_{\mathbf{H}(\mathrm{curl},\Omega\setminus \mathrm{N}^m(T))} &= \|(\mathrm{id} - \pi_H^E)(\mathbf{z} + \nabla\theta)\|^2_{\mathbf{H}(\mathrm{curl},\Omega\setminus \mathrm{N}^m(T))} \le \|\mathbf{w}\|^2_{\mathbf{H}(\mathrm{curl},\Omega)} \\ &\le \alpha^{-1}|\mathcal{B}(\mathbf{w},\mathbf{w})|.\end{aligned}$$

Using the definition of the Corrector Green's Operator in (3.19) and the fact that $\mathbf{F}_T(\mathbf{w}) = 0$ due to $\mathrm{supp}\,\mathbf{w} \subset \Omega\setminus T$ yields $\mathcal{B}(\boldsymbol{\phi},\mathbf{w}) = 0$. Using that $\mathrm{supp}\,\mathbf{w} \cap \mathrm{supp}(\boldsymbol{\phi} - \mathbf{w}) \subset \mathrm{N}(\mathcal{R})$, we obtain with the continuity of $\mathcal{B}$

$$\begin{aligned}\alpha\|\boldsymbol{\phi}\|^2_{\mathbf{H}(\mathrm{curl},\Omega\setminus \mathrm{N}^m(T))} &\le |\mathcal{B}(\mathbf{w},\mathbf{w})| = |\mathcal{B}(\mathbf{w}-\boldsymbol{\phi},\mathbf{w})| \\ &\lesssim \|\mathbf{w}-\boldsymbol{\phi}\|_{\mathbf{H}(\mathrm{curl},\mathrm{N}(\mathcal{R}))}\|\mathbf{w}\|_{\mathbf{H}(\mathrm{curl},\mathrm{N}(\mathcal{R}))} \\ &\le \|\mathbf{w}-\boldsymbol{\phi}\|_{\mathbf{H}(\mathrm{curl},\mathrm{N}(\mathcal{R}))}\big(\|\mathbf{w}-\boldsymbol{\phi}\|_{\mathbf{H}(\mathrm{curl},\mathrm{N}(\mathcal{R}))} + \|\boldsymbol{\phi}\|_{\mathbf{H}(\mathrm{curl},\mathrm{N}(\mathcal{R}))}\big).\end{aligned}$$

We estimate $\boldsymbol{\phi} - \mathbf{w} = (\mathrm{id} - \pi_H^E)(\boldsymbol{\phi} - \eta\mathbf{z} - \nabla(\eta\theta))$. We deduce with the stability of π_H^E, (2.31) and (2.32), and Lemma 3.2.1

$$\begin{aligned}&\|\boldsymbol{\phi}-\mathbf{w}\|_{\mathbf{H}(\mathrm{curl},\mathrm{N}(\mathcal{R}))} \\ &\lesssim \|\boldsymbol{\phi} - \eta\mathbf{z} - \nabla(\eta\theta)\|_{L^2(\mathrm{N}^2(\mathcal{R}))} + H\|\operatorname{curl}(\boldsymbol{\phi}-\eta\mathbf{z})\|_{L^2(\mathrm{N}^2(\mathcal{R}))} \\ &\lesssim (\|\boldsymbol{\phi}\|_{L^2(\mathrm{N}^2(\mathcal{R}))} + H\|\operatorname{curl}\boldsymbol{\phi}\|_{L^2(\mathrm{N}^2(\mathcal{R}))} + \|\eta\mathbf{z}\|_{L^2(\mathrm{N}^2(\mathcal{R}))} \\ &\quad + \|\nabla\eta\|_{L^\infty(\mathcal{R})}\|\theta\|_{L^2(\mathcal{R})} + \|\eta\|_{L^\infty(\mathrm{N}^2(\mathcal{R}))}\|\nabla\theta\|_{L^2(\mathrm{N}^{m-3}(T)\setminus \mathrm{N}^{m-6}(T))} \\ &\quad + H\big(\|\nabla\eta\|_{L^\infty(\mathcal{R})}\|\mathbf{z}\|_{L^2(\mathcal{R})} + \|\eta\|_{L^\infty(\mathrm{N}^2(\mathcal{R}))}\|\operatorname{curl}\mathbf{z}\|_{L^2(\mathrm{N}^{m-3}(T)\setminus \mathrm{N}^{m-6}(T))}\big) \\ &\lesssim \|\boldsymbol{\phi}\|_{L^2(\mathrm{N}^m(T)\setminus \mathrm{N}^{m-9}(T))} + H\|\operatorname{curl}\boldsymbol{\phi}\|_{L^2(\mathrm{N}^m(T)\setminus \mathrm{N}^{m-9}(T))}.\end{aligned}$$

All in all, this gives

$$\|\boldsymbol{\phi}\|^2_{\mathbf{H}(\mathrm{curl},\Omega\setminus \mathrm{N}^m(T))} \leq \tilde{C}\|\boldsymbol{\phi}\|^2_{\mathbf{H}(\mathrm{curl},\mathrm{N}^m(T)\setminus \mathrm{N}^{m-9}(T))}$$

for some $\tilde{C} > 0$. Moreover, it holds that

$$\|\boldsymbol{\phi}\|^2_{\mathbf{H}(\mathrm{curl},\Omega\setminus \mathrm{N}^m(T))} = \|\boldsymbol{\phi}\|^2_{\mathbf{H}(\mathrm{curl},\Omega\setminus \mathrm{N}^{m-9}(T))} - \|\boldsymbol{\phi}\|^2_{\mathbf{H}(\mathrm{curl},\mathrm{N}^m(T)\setminus \mathrm{N}^{m-9}(T))}.$$

Thus, we obtain finally with $\tilde{\beta}_{\mathrm{pre}} := (1+\tilde{C}^{-1})^{-1} < 1$, a re-iteration of the above argument, and Lemma 3.2.4 that

$$\|\boldsymbol{\phi}\|^2_{\mathbf{H}(\mathrm{curl},\Omega\setminus \mathrm{N}^m(T))} \lesssim \tilde{\beta}_{\mathrm{pre}}^{\lfloor m/9 \rfloor}\|\boldsymbol{\phi}\|^2_{\mathbf{H}(\mathrm{curl})} \lesssim \tilde{\beta}_{\mathrm{pre}}^{\lfloor m/9 \rfloor}\|\mathbf{F}_T\|^2_{\mathbf{H}_0(\mathrm{curl})'}.$$

Algebraic manipulations give the assertion. □

Proof of Theorem 3.2.11. We start by proving the following local estimate

$$\|\mathcal{G}(\mathbf{F}_T) - \mathcal{G}_{T,m}(\mathbf{F}_T)\|_{\mathbf{H}(\mathrm{curl})} \leq C_1\tilde{\beta}^m\|\mathbf{F}_T\|_{\mathbf{H}_0(\mathrm{curl})'} \tag{3.34}$$

for some constant $C_1 > 0$ and $0 < \tilde{\beta} < 1$. Let $\eta \in \mathcal{S}^1(\mathcal{T}_H)$ be a piecewise linear and globally continuous cut-off function with

$$\eta = 0 \quad \text{in} \quad \Omega \setminus \mathrm{N}^{m-1}(T), \qquad\qquad \eta = 1 \quad \text{in} \quad \mathrm{N}^{m-2}(T).$$

Due to Céa's Lemma we have

$$\|\mathcal{G}(\mathbf{F}_T) - \mathcal{G}_{T,m}(\mathbf{F}_T)\|_{\mathbf{H}(\mathrm{curl})} \lesssim \inf_{\mathbf{w}_{T,m}\in\mathbf{W}(\Omega_T)} \|\mathcal{G}(\mathbf{F}_T) - \mathbf{w}_{T,m}\|_{\mathbf{H}(\mathrm{curl})}.$$

We use the splitting of Lemma 3.2.1 and write $\mathcal{G}(\mathbf{F}_T) = (\mathrm{id} - \pi_H^E)(\mathcal{G}(\mathbf{F}_T)) = \mathbf{z} + \nabla\theta$. Then we choose $\mathbf{w}_{T,m} = (\mathrm{id} - \pi_H^E)(\eta\mathbf{z} + \nabla(\eta\theta)) \in \mathbf{W}(\Omega_T)$ and derive with the stability of π_H^E and (3.16)

$$\begin{aligned}
\|\mathcal{G}(\mathbf{F}_T) - \mathcal{G}_{T,m}(\mathbf{F}_T)\|_{\mathbf{H}(\mathrm{curl})} &\lesssim \|(\mathrm{id} - \pi_H^E)(\mathcal{G}(\mathbf{F}_T) - \eta\mathbf{z} - \nabla(\eta\theta))\|_{\mathbf{H}(\mathrm{curl})} \\
&= \|(\mathrm{id} - \pi_H^E)((1-\eta)\mathbf{z} + \nabla((1-\eta)\theta))\|_{\mathbf{H}(\mathrm{curl})} \\
&\lesssim \|(1-\eta)\mathbf{z}\|_{L^2(\Omega\setminus\{\eta=1\})} + \|\nabla((1-\eta)\theta)\|_{L^2(\Omega\setminus\{\eta=1\})} \\
&\quad + (1+H)\|\operatorname{curl}((1-\eta)\mathbf{z})\|_{L^2(\Omega\setminus\{\eta=1\})} \\
&\lesssim (1+H)\,\|\mathcal{G}(\mathbf{F}_T)\|_{\mathbf{H}(\mathrm{curl},\mathrm{N}^3(\Omega\setminus\{\eta=1\}))}.
\end{aligned}$$

Combination with Proposition 3.2.9 gives estimate (3.34).

To prove the main estimate of Theorem 3.2.11, i.e., estimate (3.28), we define, for a given simplex $T \in \mathcal{T}_H$, the piecewise linear, globally continuous cut-off function $\eta_T \in \mathcal{S}^1(\mathcal{T}_H)$ via

$$\eta_T = 0 \quad \text{in} \quad \mathrm{N}^{m+1}(T), \qquad\qquad \eta_T = 1 \quad \text{in} \quad \Omega \setminus \mathrm{N}^{m+2}(T).$$

Denote $\mathbf{w} := (\mathcal{G} - \mathcal{G}_m)(\mathbf{F}) = \sum_{T\in\mathcal{T}_H}\mathbf{w}_T$ with $\mathbf{w}_T := (\mathcal{G} - \mathcal{G}_{T,m})(\mathbf{F}_T)$ and split $\mathbf{w}$ according to Lemma 3.2.1 as $\mathbf{w} = \mathbf{w} - \pi_H^E(\mathbf{w}) = \mathbf{z} + \nabla\theta$. Due to the ellipticity of $\mathcal{B}$ and its sesquilinearity, we have

$$\alpha\|\mathbf{w}\|^2_{\mathbf{H}(\mathrm{curl})} \leq \Big|\sum_{T\in\mathcal{T}_H}\mathcal{B}(\mathbf{w}_T,\mathbf{w})\Big| \leq \sum_{T\in\mathcal{T}_H}|\mathcal{B}(\mathbf{w}_T,\mathbf{z}+\nabla\theta)| \leq \sum_{T\in\mathcal{T}_H}(A_T + B_T)$$

where, for any $T \in \mathcal{T}_H$, we abbreviate

$$A_T := \big|\mathcal{B}\big(\mathbf{w}_T,(1-\eta_T)\mathbf{z} + \nabla((1-\eta_T)\theta)\big)\big| \quad \text{and} \quad B_T := \big|\mathcal{B}\big(\mathbf{w}_T,\eta_T\mathbf{z} + \nabla(\eta_T\theta)\big)\big|.$$

For the term A_T, we derive by using the properties of the cut-off function and the regular decomposition (3.16)

$$\begin{aligned} A_T &\lesssim \|\mathbf{w}_T\|_{\mathbf{H}(\mathrm{curl})} \|(1-\eta_T)\mathbf{z} + \nabla((1-\eta_T)\theta)\|_{\mathbf{H}(\mathrm{curl},\{\eta_T\neq 1\})} \\ &\leq \|\mathbf{w}_T\|_{\mathbf{H}(\mathrm{curl})} \, (1+H) \, \|\mathbf{w}\|_{\mathbf{H}(\mathrm{curl},\mathrm{N}^3(\{\eta_T\neq 1\}))}. \end{aligned}$$

The term B_T can be split as

$$B_T \leq \Big|\mathcal{B}\big(\mathbf{w}_T, (\mathrm{id}-\pi_H^E)(\eta_T\mathbf{z}+\nabla(\eta_T\theta))\big)\Big| + \Big|\mathcal{B}\big(\mathbf{w}_T, \pi_H^E(\eta_T\mathbf{z}+\nabla(\eta_T\theta))\big)\Big|.$$

Denoting $\boldsymbol{\phi} := (\mathrm{id}-\pi_H^E)(\eta_T\mathbf{z}+\nabla(\eta_T\theta))$, we observe $\boldsymbol{\phi}\in\mathbf{W}$ and $\operatorname{supp}\boldsymbol{\phi}\subset\Omega\setminus\mathrm{N}^m(T)$. Because $\boldsymbol{\phi}\in\mathbf{W}$ with support outside T, we have $\mathcal{B}(\mathcal{G}(\mathbf{F}_T),\boldsymbol{\phi}) = \mathbf{F}_T(\boldsymbol{\phi}) = 0$. Since $\boldsymbol{\phi}$ has support outside $\mathrm{N}^m(T)=\Omega_T$, but $\mathcal{G}_{T,m}(\mathbf{F}_T)\in\mathbf{W}(\Omega_T)$, we also have $\mathcal{B}(\mathcal{G}_{T,m}(\mathbf{F}_T),\boldsymbol{\phi})=0$. All in all, this means $\mathcal{B}(\mathbf{w}_T,\boldsymbol{\phi})=0$. Using the stability of π_H^E (2.31), (2.32) and the regular decomposition (3.16), we obtain

$$\begin{aligned} B_T &\leq |\mathcal{B}(\mathbf{w}_T, \pi_H^E(\eta_T\mathbf{z}+\nabla(\eta_T\theta)))| \\ &\lesssim \|\mathbf{w}_T\|_{\mathbf{H}(\mathrm{curl})}\big(\|\eta_T\mathbf{z}+\nabla(\eta_T\theta)\|_{L^2(\mathrm{N}^2(\{\eta_T\neq1\}))} + (1+H)\|\operatorname{curl}(\eta_T\mathbf{z})\|_{L^2(\mathrm{N}^2(\{\eta_T\neq1\}))}\big) \\ &\lesssim \|\mathbf{w}_T\|_{\mathbf{H}(\mathrm{curl})}(1+H)\,\|\mathbf{w}\|_{\mathbf{H}(\mathrm{curl},\mathrm{N}^5(\{\eta_T\neq1\}))}. \end{aligned}$$

Combining the estimates for A_T and B_T and observing that $\{\eta_T\neq1\}=\mathrm{N}^{m+2}(T)$, we deduce

$$\alpha\|\mathbf{w}\|^2_{\mathbf{H}(\mathrm{curl})} \lesssim \sum_{T\in\mathcal{T}_H}\|\mathbf{w}_T\|_{\mathbf{H}(\mathrm{curl})}\,\|\mathbf{w}\|_{\mathbf{H}(\mathrm{curl},\mathrm{N}^{m+7}(T))} \lesssim \sqrt{C_{\mathrm{ol},m}}\,\|\mathbf{w}\|_{\mathbf{H}(\mathrm{curl})}\sqrt{\sum_{T\in\mathcal{T}_H}\|\mathbf{w}_T\|^2_{\mathbf{H}(\mathrm{curl})}}.$$

Combination with estimate (3.34) finishes the proof of (3.28). Finally, estimate (3.29) follows with

$$\|\mathbf{w}\|_{\mathbf{H}(\mathrm{div})'} \leq CH\|\mathbf{w}\|_{\mathbf{H}(\mathrm{curl})}. \qquad \square$$

Changes for the fully discrete localized method. Let us briefly consider the fully-discrete setting described at the end of Section 3.2.4. We note that, up to a modification of the constants, Theorem 3.2.11 also holds for the difference $(\mathcal{G}_h-\mathcal{G}_{h,m})(\mathbf{F})$. Here, $\mathcal{G}_h(\mathbf{F})$ is the Galerkin approximation of $\mathcal{G}(\mathbf{F})$ in the discrete space $\mathbf{W}_h := \{\mathbf{v}_h\in\mathring{\mathcal{N}}(\mathcal{T}_h)|\pi_H^E(\mathbf{v}_h)=0\}$ and $\mathcal{G}_{h,m}(\mathbf{F})$ is defined analogously to $\mathcal{G}_m(\mathbf{F})$ but where $\mathbf{W}_h(\Omega_T) := \{\mathbf{w}_h\in\mathbf{W}_h|\ \mathbf{w}_h = 0 \text{ in } \Omega\setminus\Omega_T\}$ replaces $\mathbf{W}(\Omega_T)$ in the local problems. Again, the central observation is a decay result similar to Proposition 3.2.9, but now for $\mathcal{G}_h(\mathbf{F}_T)$. A few modifications to the proof have to be made, though: The product of the cut-off function η and the regular decomposition $\mathbf{z}+\nabla\theta$ does not lie in $\mathring{\mathcal{N}}(\mathcal{T}_h)$. Therefore, an additional interpolation operator into $\mathring{\mathcal{N}}(\mathcal{T}_h)$ has to be applied. Here it is tempting to just use the nodal interpolation operator and its stability on piecewise polynomials, since $\eta\,\mathcal{G}_h(\mathbf{F}_T)$ is a piecewise (quadratic) polynomial. However, the regular decomposition employed is no longer piecewise polynomial and we hence have to use the Falk-Winther operator π_h^E onto the fine space $\mathring{\mathcal{N}}(\mathcal{T}_h)$ here. This means that we have to modify $\mathbf{w}$ to $\widetilde{\mathbf{w}} := (\mathrm{id}-\pi_H^E)\pi_h^E(\eta\mathbf{z}+\nabla(\eta\theta))$. Note that the additional interpolation operator π_h^E enlarges the patches slightly, so that we should define η via

$$\eta = 0 \qquad \text{in} \quad \mathrm{N}^{m-8}(T), \qquad\qquad \eta = 1 \qquad \text{in} \quad \Omega\setminus\mathrm{N}^{m-7}(T).$$

With the same arguments as in the proof of Proposition 3.2.9, we deduce that

$$\alpha\|\boldsymbol{\phi}\|^2_{\mathbf{H}(\mathrm{curl},\Omega\setminus\mathrm{N}^m(T)} \leq |\mathcal{B}(\widetilde{\mathbf{w}},\widetilde{\mathbf{w}})| = |\mathcal{B}(\widetilde{\mathbf{w}}-\boldsymbol{\phi},\widetilde{\mathbf{w}})|.$$

Note that $\boldsymbol{\phi}-\widetilde{\mathbf{w}} = (\mathrm{id}-\pi_h^E)(\boldsymbol{\phi}-\eta\mathbf{z}-\nabla(\eta\theta)) + (\mathrm{id}-\pi_H^E)(\mathrm{id}-\pi_h^E)(\eta\mathbf{z}+\nabla(\eta\theta))$. The first term is the same as in the proof of Proposition 3.2.9. The second term can be estimated simply using the stability of π_h^E, the properties of η, and the regular decomposition (3.16).

3.2.6 Implementation of the Falk-Winther interpolation operator

Given a mesh $\mathcal{T}_H$ and a refinement $\mathcal{T}_h$, the linear projection $\pi_H^E : \mathring{\mathcal{N}}(\mathcal{T}_h) \to \mathring{\mathcal{N}}(\mathcal{T}_H)$ can be represented by a matrix $\mathsf{P} \in \mathbb{C}^{\dim \mathring{\mathcal{N}}(\mathcal{T}_H) \times \dim \mathring{\mathcal{N}}(\mathcal{T}_h)}$. This subsection briefly sketches the assembling of that matrix. The procedure involves the solution of local discrete problems on the macroelements. It is important to note that these problems are of small size. We recall the detailed definition of the Falk-Winther interpolation operator in Section 2.2.3 and stick to the notation used there.

Given an interior edge $e \in \mathring{\Delta}_1^h$ of $\mathcal{T}_h$, the interpolation $\pi_H^E \boldsymbol{\phi}_e$ of the edge element basis function $\boldsymbol{\phi}_e$ has an expansion

$$\pi_H^E \boldsymbol{\phi}_e = \sum_{E' \in \mathring{\Delta}_1^H} c_{E'} \boldsymbol{\phi}_{E'}$$

for coefficients $(c_{E'})_{E' \in \mathring{\Delta}_1^H}$. The coefficient c_E is zero whenever e is not contained in the closure of the extended edge patch $\overline{\omega}_E^{ext}$. The assembling can therefore be organized in a loop over all interior edges in $\mathring{\Delta}_1^H$. Given a global numbering of the edges in $\mathring{\Delta}_1^H$, each edge $E \in \mathring{\Delta}_1^H$ is equipped with a unique index $\mathcal{I}_H(E) \in \{1, \dots, \mathrm{card}(\mathring{\Delta}_1^H)\}$. Similarly, the numbering of edges in $\mathring{\Delta}_1^h$ is denoted by $\mathcal{I}_h$.

The matrix $\mathsf{P} = \mathsf{P}_1 + \mathsf{P}_2$ is composed as the sum of matrices P_1, P_2 that represent the two summands on the right-hand side of (2.30). These are assembled in loops over the interior edges. Matrices P_1, P_2 are initialized as empty sparse matrices.

Operator P_1. for $E \in \mathring{\Delta}_1^H$ do

Let the interior edges in $\mathring{\Delta}_1^h$ that lie inside $\overline{\omega}_E^{ext}$ be denoted with $\{e_1, e_2, \dots, e_N\}$ for some $N \in \mathbb{N}$. The entries $\mathsf{P}_1(\mathcal{I}_H(E), [\mathcal{I}_h(e_1) \dots \mathcal{I}_h(e_N)])$ of the matrix P_1 are determined as follows. Compute $\mathbf{z}_E^1 \in \mathring{\mathcal{RT}}(\mathcal{T}_H(\omega_E^{ext}))$. The matrix $\mathsf{M}_E \in \mathbb{C}^{1 \times N}$ defined via

$$\mathsf{M}_E := |E|^{-1} \left[\int_{\omega_E^{ext}} \mathbf{z}_E^1 \cdot \boldsymbol{\phi}_{e_j} \, dx \right]_{j=1}^{N}$$

represents the map of the basis functions on the fine mesh to the coefficient of M^1 contributing to $\boldsymbol{\phi}_E$ on the coarse mesh. For the vertices $y_j(E)$ of E, denote by $\mathsf{A}_{y_j(E)}$ and $\mathsf{B}_{y_j(E)}$ $(j = 1, 2)$ the stiffness and right-hand side matrix representing the system for the operator $Q_{y_j(E),-}$

$$\mathsf{A}_{y_j(E)} := \left[\int_{\omega_{y_j(E)}} \nabla \lambda_y \cdot \nabla \lambda_z \, dx \right]_{y,z \in \Delta_0(\mathcal{T}_H(\omega_{y_j(E)}))},$$

$$\mathsf{B}_{y_j(E)} := \left[\int_{\omega_{y_j(E)}} \nabla \lambda_y \cdot \boldsymbol{\phi}_{e_j} \, dx \right]_{y \in \Delta_0(\mathcal{T}_H(\omega_{y_j(E)})), \, j=1,\dots,N}.$$

We recall that λ_y is the linear Lagrange element basis function (hat function) associated with the vertex y. After enhancing the system to $\tilde{\mathsf{A}}_{y_j(E)}$ and $\tilde{\mathsf{B}}_{y_j(E)}$ (with a Lagrange multiplier accounting for the mean constraint), it is uniquely solvable. Set $\tilde{\mathsf{Q}}_{y_j(E)} = \tilde{\mathsf{A}}_{y_j(E)}^{-1} \tilde{\mathsf{B}}_{y_j(E)}$ and extract the row corresponding to the vertex $y_j(E)$

$$\mathsf{Q}_j := |E|^{-1} \tilde{\mathsf{Q}}_{y_j(E)}[y_j(E), :] \in \mathbb{C}^{1 \times N}.$$

Set

$$\mathsf{P}_1(\mathcal{I}_H(E), [\mathcal{I}_h(e_1) \dots \mathcal{I}_h(e_N)]) = \mathsf{M}_E + \mathsf{Q}_1 - \mathsf{Q}_2.$$

end

Operator P_2. for $E \in \mathring{\Delta}_1^H$ do

Denote the matrices – where indices j,k run from 1 to $\operatorname{card}(\Delta_1(\mathcal{T}_H(\omega_E^{ext})))$, y through $\Delta_0(\mathcal{T}_H(\omega_E^{ext}))$, and $\ell = 1,\dots,N$ –

$$\mathsf{S}_E := \left[\int_{\omega_E^{ext}} \operatorname{curl}\boldsymbol{\phi}_{E_j}\cdot\operatorname{curl}\boldsymbol{\phi}_{E_k}\,dx\right]_{j,k} \quad \mathsf{T}_E := \left[\int_{\omega_E^{ext}} \boldsymbol{\phi}_{E_j}\cdot\nabla\lambda_y\,dx\right]_{j,y}$$

and

$$\mathsf{F}_E := \left[\int_{\omega_E^{ext}} \operatorname{curl}\boldsymbol{\phi}_{E_j}\cdot\operatorname{curl}\boldsymbol{\phi}_{e_\ell}\,dx\right]_{j,\ell} \quad \mathsf{G}_E := \left[\int_{\omega_E^{ext}} \boldsymbol{\phi}_{e_\ell}\cdot\nabla\lambda_y\,dx\right]_{y,\ell}.$$

Solve the saddle-point system

$$\begin{bmatrix}\mathsf{S} & \mathsf{T}^*\\ \mathsf{T} & 0\end{bmatrix}\begin{bmatrix}\mathsf{U}\\ \mathsf{V}\end{bmatrix} = \begin{bmatrix}\mathsf{F}\\ \mathsf{G}\end{bmatrix}.$$

(This requires an additional one-dimensional gauge condition because the sum of the test functions $\sum_y \nabla\lambda_y$ equals zero.) Assemble the operator S^1 (locally) as described in the previous step and denote this matrix by P_1^{loc}. Compute $\mathsf{U} - \mathsf{P}_1^{loc}\mathsf{U}$ and extract the line X corresponding to the edge E

$$\mathsf{P}_2(\mathcal{I}_H(E), [\mathcal{I}_h(e_1)\dots\mathcal{I}_h(e_N)]) = \mathsf{X}.$$

end

We note that this representation of the Falk-Winther operator as a matrix is an essential step towards a practical implementation: Computations requiring test or ansatz functions in the kernel space $\mathbf{W}$ or its modifications can be written as saddle-point problems, see [EHMP16]. As the rest of our construction follows the LOD framework, we refer to [EHMP16] for a discussion of an efficient implementation.

3.2.7 Indefinite H(curl)-problems

The error estimates for the Localized Orthogonal Decomposition in Sections 3.2.3 and 3.2.4 essentially use the coercivity of the sesquilinear form $\mathcal{B}$. In this section, we extend the presented results to the indefinite case. As discussed in Section 2.1.3, the well-posedness of the corresponding (standard) discrete problems is only given for sufficiently fine meshes. This resolution condition between the frequency ω and the mesh size can be reduced with the Localized Orthogonal Decomposition, as we will see in this section.

The indefinite case roughly sets $\kappa = -\omega^2\varepsilon$ in (2.6). To be more precise, we replace the sesquilinear form $\mathcal{B}$ (3.1) in the following way. Let $\mu \in L^\infty(\Omega;\mathbb{R}^{3\times3})$, $\varepsilon \in L^\infty(\Omega;\mathbb{R}^{3\times3})$ and $\omega \in \mathbb{R}_+$ and we assume $\omega \gtrsim 1$, i.e., we study the high frequency case. We then seek $\mathbf{u} \in \mathbf{H}_0(\operatorname{curl})$ such that

$$\mathcal{B}(\mathbf{u},\boldsymbol{\psi}) := (\mu\operatorname{curl}\mathbf{u},\operatorname{curl}\boldsymbol{\psi})_{L^2(\Omega)} - \omega^2(\varepsilon\mathbf{u},\boldsymbol{\psi})_{L^2(\Omega)} = (\mathbf{f},\boldsymbol{\psi})_{L^2(\Omega)} \quad \forall\boldsymbol{\psi}\in\mathbf{H}_0(\operatorname{curl},\Omega). \tag{3.35}$$

Fredholm theory guarantees the existence of a unique solution $\mathbf{u}$ to (3.35) provided that ω is not an eigenvalue of the curl-curl-operator, which we assume from now on. This in particular implies that there is $\gamma(\omega) > 0$ such that $\mathcal{B}$ is inf-sup stable with constant $\gamma(\omega)$, i.e.,

$$\inf_{\mathbf{v}\in\mathbf{H}_0(\operatorname{curl})\setminus\{0\}}\sup_{\boldsymbol{\psi}\in\mathbf{H}_0(\operatorname{curl})\setminus\{0\}}\frac{|\mathcal{B}(\mathbf{v},\boldsymbol{\psi})|}{\|\mathbf{v}\|_{\operatorname{curl},\omega}\|\boldsymbol{\psi}\|_{\operatorname{curl},\omega}} \geq \gamma(\omega). \tag{3.36}$$

Here and in the following, we use the ω-dependent inner product on $\mathbf{H}_0(\operatorname{curl},R)$ for $R\subset\Omega$

$$(\mathbf{v},\boldsymbol{\psi})_{\operatorname{curl},\omega,R} := (\operatorname{curl}\mathbf{v},\operatorname{curl}\boldsymbol{\psi})_{L^2(R)} + \omega^2(\mathbf{v},\boldsymbol{\psi})_{L^2(R)}.$$

Ideal numerical homogenization. As in Section 3.2.3, we would like to decompose the exact solution into a coarse part, which is a good approximation in $\mathbf{H}(\mathrm{div})'$, and a corrector contribution using the direct sum splitting $\mathbf{H}_0(\mathrm{curl}) = \mathring{\mathcal{N}}(\mathcal{T}_H) \oplus \mathbf{W}$ with $\mathbf{W} := \ker(\pi_H^E)$. The crucial point here is to prove the inf-sup stability of $\mathcal{B}$ over $\mathbf{W}$ in order to have a well-defined *Corrector Green's Operator*.

For this, we first observe that the regular decomposition estimates (3.16) directly imply for any $\mathbf{w} \in \mathbf{W}$

$$\|\mathbf{w}\|_{\mathbf{H}(\mathrm{div})'} \lesssim H \|\mathbf{w}\|_{\mathbf{H}(\mathrm{curl})}. \tag{3.37}$$

Moreover, the stability estimates (2.31), (2.32) imply that following stability of π_H^E:

$$\|\pi_H^E \mathbf{v}\|_{\mathrm{curl},\omega} \lesssim \|\mathbf{v}\|_{\mathrm{curl},\omega} \qquad \text{if} \quad \omega H \lesssim 1.$$

From now on, we assume this resolution condition

$$\omega H \lesssim 1. \tag{3.38}$$

It reflects that a few degrees of freedom per wavelength are always required to represent a wave. The constant hidden in $\lesssim$ only depends on interpolation constants and the bounds on the material coefficients μ and κ. Under this resolution condition (3.38), $\mathcal{B}$ is stable on $\mathbf{W}$, as details the next lemma.

Lemma 3.2.14 (Properties of $\mathbf{W}$). *Let $\mathbf{w} \in \mathbf{W}$ be decomposed as $\mathbf{w} = \mathbf{z} + \nabla\theta$ and (3.38) be satisfied. Then*

- *we have a (ω-independent) norm equivalence between $\|\cdot\|_{\mathrm{curl},\omega}$ and $|||\mathbf{w}|||^2 := \|\operatorname{curl}\mathbf{z}\|^2 + \omega^2\|\nabla\theta\|^2$;*
- *there is $\alpha > 0$ independent of ω such that*

$$\inf_{\mathbf{w}\in\mathbf{W}\setminus\{0\}} \sup_{\boldsymbol{\phi}\in\mathbf{W}\setminus\{0\}} \frac{|\mathcal{B}(\mathbf{w},\boldsymbol{\phi})|}{\|\mathbf{w}\|_{\mathrm{curl},\omega}\|\boldsymbol{\phi}\|_{\mathrm{curl},\omega}} \geq \alpha.$$

Proof. For the norm equivalence we obtain using (3.16) and $\operatorname{curl}\mathbf{w} = \operatorname{curl}\mathbf{z}$

$$\begin{aligned}
|||\mathbf{w}|||^2 &= \|\operatorname{curl}\mathbf{z}\|^2 + \omega^2\|\nabla\theta\|^2 \lesssim \|\operatorname{curl}\mathbf{w}\|^2 + \omega^2\|\mathbf{w}\|^2 + \omega^2 H^2 \|\operatorname{curl}\mathbf{w}\|^2 \lesssim \|\mathbf{w}\|^2_{\mathrm{curl},\omega}, \\
\|\mathbf{w}\|^2_{\mathrm{curl},\omega} &\leq \|\mathbf{z}\|^2_{\mathrm{curl},\omega} + \|\nabla\theta\|^2_{\mathrm{curl},\omega} \lesssim \|\operatorname{curl}\mathbf{z}\|^2 + \omega^2 H^2 \|\operatorname{curl}\mathbf{z}\|^2 + \omega^2\|\nabla\theta\|^2 \lesssim |||\mathbf{w}|||^2.
\end{aligned}$$

For the inf-sup constant, define the sign-flip isomorphism $SF(\mathbf{w}) = \mathbf{z} - \nabla\theta$. Observe that $\operatorname{curl}\pi_H^E\mathbf{z} = \operatorname{curl}\pi_H^E\mathbf{w} = 0$ because of the commuting property of π_H^E. Then

$$\begin{aligned}
\mathrm{Re}\{\mathcal{B}(\mathbf{w}, (\mathrm{id} - \pi_H^E)SF(\mathbf{w}))\} \gtrsim{}& \|\operatorname{curl}\mathbf{z}\|^2 + \omega^2\|\nabla\theta\|^2 - \omega^2\|\mathbf{z}\|^2 - 2\omega^2|(\varepsilon\mathbf{z}, \nabla\theta)| \\
&- 2\omega^2|(\varepsilon\mathbf{z}, \pi_H^E\mathbf{z})| - 2\omega^2|(\varepsilon\nabla\theta, \pi_H^E\mathbf{z})|,
\end{aligned}$$

where we used $\pi_H^E\nabla\theta = -\pi_H^E\mathbf{z}$ because of $\pi_H^E\mathbf{w} = 0$. Applying Young's inequality, the stability of π_H^E (2.31)–(2.32), estimate (3.16) and using the resolution condition (3.38), we arrive at

$$\mathrm{Re}\{\mathcal{B}(\mathbf{w}, (\mathrm{id} - \pi_H^E)SF(\mathbf{w}))\} \gtrsim \|\operatorname{curl}\mathbf{z}\|^2 + \omega^2\|\nabla\theta\|^2 \gtrsim \|\mathbf{w}\|^2_{\mathrm{curl},\omega}$$

because of the norm equivalence. The estimate $\|(\mathrm{id} - \pi_H^E)SF(\mathbf{w})\|_{\mathrm{curl},\omega} \lesssim \|\mathbf{w}\|_{\mathrm{curl},\omega}$ finally gives the claim. □

With this inf-sup stability of $\mathcal{B}$ over $\mathbf{W}$ the Corrector Green's Operator $\mathcal{G}$ from Definition 3.2.2 is well-defined. Moreover, the stability and approximation properties from Lemma 3.2.4 directly transfer to the indefinite case. Therefore, an ideal numerical homogenization scheme consists in solving the variational problem over the "multiscale" space $(\mathrm{id} + \mathcal{K})\mathring{\mathcal{N}}(\mathcal{T}_H)$ with $\mathcal{K} = -\mathcal{G} \circ \mathcal{L}$ defined as in Section 3.2.3. The well-posedness of this scheme is proved in the next lemma.

Lemma 3.2.15 (Well-posedness of the ideal scheme)**.** *Under the resolution condition* (3.38)*, we have with* $\gamma(\omega)$ *from* (3.36) *that*

$$\inf_{\mathbf{v}_H \in \mathring{\mathcal{N}}(\mathcal{T}_H)\setminus\{0\}} \sup_{\boldsymbol{\psi}_H \in \mathring{\mathcal{N}}(\mathcal{T}_H)\setminus\{0\}} \frac{|\mathcal{B}((\mathrm{id}+\mathcal{K})\mathbf{v}_H, (\mathrm{id}+\mathcal{K})\boldsymbol{\psi}_H)|}{\|\mathbf{v}_H\|_{\mathrm{curl},\omega}\|\boldsymbol{\psi}_H\|_{\mathrm{curl},\omega}} \gtrsim \gamma(\omega). \tag{3.39}$$

Proof. Fix $\mathbf{v}_H \in \mathring{\mathcal{N}}(\mathcal{T}_H)$. From (3.36), there exists $\boldsymbol{\psi} \in \mathbf{H}_0(\mathrm{curl})$ with $\|\boldsymbol{\psi}\|_{\mathrm{curl},\omega} = 1$ such that

$$|\mathcal{B}((\mathrm{id}+\mathcal{K})\mathbf{v}_H, \boldsymbol{\psi})| \geq \gamma(\omega)\|(\mathrm{id}+\mathcal{K})\mathbf{v}_H\|_{\mathrm{curl},\omega}.$$

By the definition of $\mathcal{K}$, it holds that $(\mathrm{id}+\mathcal{K})\pi_H^E\boldsymbol{\psi} = (\mathrm{id}+\mathcal{K})\boldsymbol{\psi}$ and $\mathcal{B}((\mathrm{id}+\mathcal{K})\mathbf{v}_H, \mathbf{w}) = 0$ for all $\mathbf{w} \in \mathbf{W}$. Thus, we obtain

$$\begin{aligned}|\mathcal{B}((\mathrm{id}+\mathcal{K})\mathbf{v}_H, (\mathrm{id}+\mathcal{K})\pi_H^E\boldsymbol{\psi})| &= |\mathcal{B}((\mathrm{id}+\mathcal{K})\mathbf{v}_H, (\mathrm{id}+\mathcal{K})\boldsymbol{\psi})| = |\mathcal{B}((\mathrm{id}+\mathcal{K})\mathbf{v}_H, \boldsymbol{\psi})| \\ &\geq \gamma(\omega)\|(\mathrm{id}+\mathcal{K})\mathbf{v}_H\|_{\mathrm{curl},\omega}.\end{aligned}$$

The claim follows by the norm equivalence

$$\|\mathbf{v}_H\|_{\mathrm{curl},\omega} = \|\pi_H^E(\mathrm{id}+\mathcal{K})\mathbf{v}_H\|_{\mathrm{curl},\omega} \lesssim \|(\mathrm{id}+\mathcal{K})\mathbf{v}_H\|_{\mathrm{curl},\omega},$$

which is a result of the stability of π_H^E. □

Then, the main results (Lemma 3.2.3 and Conclusion 3.2.6) of Section 3.2.3 also hold for the indefinite case in the following way.

Theorem 3.2.16 (Ideal decomposition)**.** *Let* $\mathbf{u}$ *denote the exact solution to* (3.35) *and* $\mathbf{u}_H = \pi_H^E\mathbf{u}$*. Then*

- *it holds that* $\mathbf{u} = \mathbf{u}_H + \mathcal{K}(\mathbf{u}_H) + \mathcal{G}(\mathbf{f})$*;*
- *assuming* (3.38)*,* $\mathbf{u}_H$ *is characterized as the unique solution to*

$$\mathcal{B}((\mathrm{id}+\mathcal{K})\mathbf{u}_H, (\mathrm{id}+\mathcal{K})\boldsymbol{\psi}_H) = (\mathbf{f}, (\mathrm{id}+\mathcal{K})\boldsymbol{\psi}_H) \qquad \forall \boldsymbol{\psi}_H \in \mathring{\mathcal{N}}(\mathcal{T}_H); \tag{3.40}$$

- *assuming* (3.38)*, it holds that*

$$\|\mathbf{u} - (\mathrm{id}+\mathcal{K})\mathbf{u}_H\|_{\mathrm{curl},\omega} + \|\mathbf{u} - \mathbf{u}_H\|_{\mathbf{H}(\mathrm{div})'} \lesssim H\|\mathbf{f}\|_{\mathbf{H}(\mathrm{div})}. \tag{3.41}$$

The theorem shows that $(\mathrm{id}+\mathcal{K})\mathbf{u}_H$ approximates the analytical solution with linear rate without assumptions on the regularity of the problem. What is more, only the reasonable resolution condition $\omega H \lesssim 1$ is required, which is less restrictive than the condition for standard finite element methods. However, the determination of $\mathcal{K}$ requires (again) the solution of global problems, which limits the practical usability of the scheme.

Quasi-local numerical homogenization. Using the inf-sup stability of $\mathcal{B}$ over $\mathbf{W}$, the exponential decay result of Proposition 3.2.9 generalizes to the indefinite case. Therefore, we can approximate $\mathcal{K}$ by local correctors in a similar manner as in Section 3.2.4. For the indefinite case, however, we have to guarantee the well-posedness of the localized corrector problems. When trying to carry over the proof of the inf-sup stability of Lemma 3.2.14 to local patches $\Omega_T := \mathrm{N}^m(T)$, we observe that the test function $(\mathrm{id}-\pi_H^E)SF(\mathbf{w})$ is no longer supported in Ω_T, but on a slightly larger patch. Therefore, we have to modify the definition of the localized corrector in the following way.

Definition 3.2.17 (Localized Corrector Approximation)**.** For any element $T \in \mathcal{T}_H$ we define its patch $\Omega_T := \mathrm{N}^m(T)$. Let $\mathbf{F} \in \mathbf{H}_0(\mathrm{curl})'$ be the sum of local functionals, i.e., $\mathbf{F} = \sum_{T\in\mathcal{T}_H} \mathbf{F}_T$ with $\mathbf{F}_T$ as in Proposition 3.2.9. Denote by $\pi^E_{H,\Omega_T} : \mathbf{H}_0(\mathrm{curl},\Omega) \to \mathring{\mathcal{N}}(\mathcal{T}_H(\Omega_T))$ the Falk-Winther interpolation operator which enforces essential boundary conditions (i.e., zero tangential traces) on $\partial\Omega_T$. We then define

$$\mathbf{W}(\Omega_T) := \{\mathbf{w} \in \mathbf{H}_0(\mathrm{curl}) | \mathbf{w} = 0 \text{ outside } \Omega_T, \pi^E_{H,\Omega_T}\mathbf{w} = 0\} \not\subseteq \mathbf{W}. \tag{3.42}$$

We call $\mathcal{G}_{T,m}(\mathbf{F}_T) \in \mathbf{W}(\Omega_T)$ the *localized corrector* if it solves

$$\mathcal{B}(\mathcal{G}_{T,m}(\mathbf{F}_T), \mathbf{w}) = \mathbf{F}_T(\mathbf{w}) \qquad \forall \mathbf{w} \in \mathbf{W}(\Omega_T). \tag{3.43}$$

The global corrector approximation is then given by

$$\mathcal{G}_m(\mathbf{F}) = \sum_{T\in\mathcal{T}_H} \mathcal{G}_{T,m}(\mathbf{F}_T).$$

Observe that problem (3.43) is only formulated on the patch Ω_T. Its well-posedness can be proved as in Lemma 3.2.14: For $\mathbf{w} \in \mathbf{W}(\Omega_T)$, use $(\mathrm{id} - \pi^E_{H,\Omega_T})SF(\mathbf{w}) \in \mathbf{W}(\Omega_T)$ as test function (with the sign-flip isomorphism SF). This is a nonconforming definition of the localized corrector (i.e., $\pi^E_H \mathcal{G}_m(\cdot) \neq 0$), so that additional terms appear in the error analysis. However, the nonconformity error only plays a role near the boundary of $\partial\Omega_T$ and can therefore be controlled very well.

Theorem 3.2.18 (Error of the corrector approximation)**.** *Let $\mathcal{G}(\mathbf{F})$ be the ideal Green's corrector and $\mathcal{G}_m(\mathbf{F})$ the localized corrector from Definition 3.2.17. Under resolution condition* (3.38)*, there exists $0 < \beta < 1$ such that*

$$\|\mathcal{G}(\mathbf{F}) - \mathcal{G}_m(\mathbf{F})\|_{\mathrm{curl},\omega} \lesssim \sqrt{C_{\mathrm{ol},m}}\,\beta^m \Big(\sum_{T\in\mathcal{T}_H} \|\mathbf{F}_T\|^2_{\mathbf{H}_0(\mathrm{curl})'}\Big)^{1/2}, \tag{3.44}$$

$$\|\pi^E_H \mathcal{G}_m(\mathbf{F})\|_{\mathrm{curl},\omega} \lesssim \sqrt{C_{\mathrm{ol},m}}\,\beta^m \Big(\sum_{T\in\mathcal{T}_H} \|\mathbf{F}_T\|^2_{\mathbf{H}_0(\mathrm{curl})'}\Big)^{1/2}. \tag{3.45}$$

The proof is given in the next paragraph.

Following the above motivation, we define a quasi-local numerical homogenization scheme by replacing $\mathcal{K}$ in the ideal scheme (3.40) with $\mathcal{K}_m = -\sum_{T\in\mathcal{T}_H} \mathcal{G}_{T,m} \circ \mathcal{L}_T$ with the localized corrector $\mathcal{G}_{T,m}$ from Definition 3.2.17.

Definition 3.2.19 (Quasi-local numerical homogenization scheme)**.** In the *quasi-local numerical homogenization scheme* we seek $\mathbf{u}_{H,m} \in \mathring{\mathcal{N}}(\mathcal{T}_H)$ such that

$$\mathcal{B}((\mathrm{id}+\mathcal{K}_m)\mathbf{u}_{H,m}, (\mathrm{id}+\mathcal{K}_m)\mathbf{v}_H) = (\mathbf{f}, (\mathrm{id}+\mathcal{K}_m)\mathbf{v}_H) \qquad \forall \mathbf{v}_H \in \mathring{\mathcal{N}}(\mathcal{T}_H). \tag{3.46}$$

We observe that $\mathcal{K}_m$ can be computed by solving local decoupled problems and that the spaces $\mathbf{W}(\Omega_T)$ still need to be discretized, see Section 3.2.4 for a detailed discussion.

We then prove the well-posedness and the a priori error estimate for the quasi-local numerical homogenization scheme.

Theorem 3.2.20 (Well-posedness of (3.46))**.** *If the resolution condition* (3.38) *and the oversampling condition*

$$m \gtrsim |\log\big(\gamma(\omega)/\sqrt{C_{\mathrm{ol},m}}\big)|/|\log(\beta)| \tag{3.47}$$

are fulfilled, $\mathcal{B}$ is inf-sup stable over $(\mathrm{id}+\mathcal{K}_m)\mathring{\mathcal{N}}(\mathcal{T}_H)$, i.e.,

$$\inf_{\mathbf{v}_H\in\mathring{\mathcal{N}}(\mathcal{T}_H)\setminus\{0\}} \sup_{\boldsymbol{\psi}_H\in\mathring{\mathcal{N}}(\mathcal{T}_H)\setminus\{0\}} \frac{|\mathcal{B}((\mathrm{id}+\mathcal{K}_m)\mathbf{v}_H, (\mathrm{id}+\mathcal{K}_m)\boldsymbol{\psi}_H)|}{\|\mathbf{v}_H\|_{\mathrm{curl},\omega}\|\boldsymbol{\psi}\|_{\mathrm{curl},\omega}} \geq \gamma_{\mathrm{LOD}}(\omega) \approx \gamma(\omega).$$

Theorem 3.2.21 (A priori estimate)**.** *Let* $\mathbf{u}$ *denote the solution to* (3.35) *and* $\mathbf{u}_{H,m}$ *the solution to* (3.46)*. If the resolution condition* (3.38) *and the oversampling condition*

$$m \gtrsim |\log\big(\gamma_{\mathrm{LOD}}(\omega)/\sqrt{C_{\mathrm{ol},m}}\big)|/|\log(\beta)| \tag{3.48}$$

are fulfilled, then

$$\|\mathbf{u} - (\mathrm{id} + \mathcal{K}_m)\mathbf{u}_{H,m}\|_{\mathrm{curl},\omega} \lesssim (H + \beta^m \gamma^{-1}(\omega))\|\mathbf{f}\|_{\mathbf{H}(\mathrm{div})}. \tag{3.49}$$

Note that the oversampling condition (3.48) is – up to constants independent of H and ω – the same as condition (3.47). Since $C_{\mathrm{ol},m}$ grows polynomially in m for quasi-uniform meshes, it is satisfiable and depends on the behavior of $\gamma(\omega)$. If $\gamma(\omega) \lesssim \omega^q$, we derive $m \approx |\log(\omega)|$. Note that in (3.49), we can replace $\gamma^{-1}(\omega)$ with $C_{\mathrm{stab}}(\omega)$, the stability constant of the original problem (3.35). This is exactly the same a priori estimate as for Helmholtz problems in [Pet17]. To sum up, an oversampling parameter $m \approx |\log(\omega)|$ is sufficient for the stability of the LOD. Requiring additionally $m \approx |\log(H)|$, we obtain a linear convergence rate for the error.

Main Proofs. Theorem 3.2.18 results from the exponential decay of $\mathcal{G}$ in Proposition 3.2.9.

Proof of Theorem 3.2.18. We start by proving the following local estimate

$$\|\mathcal{G}(\mathbf{F}_T) - \mathcal{G}_{T,m}(\mathbf{F}_T)\|_{\mathrm{curl},\omega} \lesssim \tilde{\beta}^m \|\mathbf{F}_T\|_{\mathbf{H}_0(\mathrm{curl})'}. \tag{3.50}$$

By Strang's second lemma we obtain

$$\begin{aligned}&\|\mathcal{G}(\mathbf{F}_T) - \mathcal{G}_{T,m}(\mathbf{F}_T)\|_{\mathrm{curl},\omega}\\ &\quad\lesssim \inf_{\mathbf{w}_{T,m}\in\mathbf{W}(\Omega_T)} \|\mathcal{G}(\mathbf{F}_T) - \mathbf{w}_{T,m}\|_{\mathrm{curl},\omega} + \sup_{\substack{\boldsymbol{\phi}_{T,m}\in\mathbf{W}(\Omega_T)\\ \|\boldsymbol{\phi}_{T,m}\|_{\mathrm{curl},\omega}=1}} |\mathcal{B}(\mathcal{G}(\mathbf{F}_T), \boldsymbol{\phi}_{T,m}) - \mathbf{F}_T(\boldsymbol{\phi}_{T,m})|.\end{aligned}$$

The first term can be estimated as in Section 3.2.5 for Theorem 3.2.11. For the second term, we have due to (3.19) that it is equal to

$$\sup_{\boldsymbol{\phi}_{T,m}\in\mathbf{W}(\Omega_T),\|\boldsymbol{\phi}_{T,m}\|_{\mathrm{curl},\omega}=1} |\mathcal{B}(\mathcal{G}(\mathbf{F}_T), \boldsymbol{\phi}_{T,m} - \boldsymbol{\phi}) - \mathbf{F}_T(\boldsymbol{\phi}_{T,m} - \boldsymbol{\phi})|$$

for any $\boldsymbol{\phi} \in \mathbf{W}$. Fixing $\boldsymbol{\phi}_{T,m} = \mathbf{z}_{T,m} + \nabla\theta_{T,m}$, we choose $\boldsymbol{\phi} = (\mathrm{id} - \pi_H^E)(\eta\mathbf{z}_{T,m} + \nabla(\eta\theta_{T,m}))$ with a cut-off function such that $\boldsymbol{\phi}_{T,m} - \boldsymbol{\phi} = 0$ in $\mathrm{N}^{m-2}(T)$. Then $\mathbf{F}_T(\boldsymbol{\phi}_{T,m} - \boldsymbol{\phi}) = 0$ and we get with the stability of π_H^E and (3.16)

$$\begin{aligned}|\mathcal{B}(\mathcal{G}(\mathbf{F}_T), \boldsymbol{\phi}_{T,m} - \boldsymbol{\phi})| &\lesssim \|\mathcal{G}(\mathbf{F}_T)\|_{\mathrm{curl},\omega,\Omega\setminus\mathrm{N}^{m-2}(T)}\|\boldsymbol{\phi}_{T,m} - \boldsymbol{\phi}\|_{\mathrm{curl},\omega}\\ &\lesssim \|\mathcal{G}(\mathbf{F}_T)\|_{\mathrm{curl},\omega,\Omega\setminus\mathrm{N}^{m-2}(T)}.\end{aligned}$$

Combination with Proposition 3.2.9 gives (3.50).

For (3.44), we split the error as

$$\|\mathcal{G}(\mathbf{F}) - \mathcal{G}_m(\mathbf{F})\|_{\mathrm{curl},\omega} \le \|(\mathrm{id} - \pi_H^E)(\mathcal{G}(\mathbf{F}) - \mathcal{G}_m(\mathbf{F}))\|_{\mathrm{curl},\omega} + \|\pi_H^E\mathcal{G}_m(\mathbf{F})\|_{\mathrm{curl},\omega}.$$

The first term can be estimated with the procedure for Theorem 3.2.11 from Section 3.2.5. The second term is the left-hand side of (3.45) and thus, it suffices to prove (3.45). We observe that $\pi_H^E\mathcal{G}_{T,m}(\mathbf{F}_T) \neq 0$ only on a small ring $R \subset \mathrm{N}^{m+1}(T)$ because π_H^E and π_{H,Ω_T}^E only differ near the boundary of Ω_T. Hence, we get

$$\begin{aligned}\|\pi_H^E\mathcal{G}_m(\mathbf{F})\|_{\mathrm{curl},\omega}^2 &\le \sum_{T\in\mathcal{T}_H} |(\pi_H^E\mathcal{G}_m(\mathbf{F}), \pi_H^E\mathcal{G}_{T,m}(\mathbf{F}_T))_{\mathrm{curl},\omega}|\\ &\lesssim \sum_T \|\pi_H^E\mathcal{G}_m(\mathbf{F})\|_{\mathrm{curl},\omega,\mathrm{N}^{m+1}(T)}\|\pi_H^E(\mathcal{G}(\mathbf{F}_T) - \mathcal{G}_{T,m}(\mathbf{F}_T))\|_{\mathrm{curl},\omega}\\ &\lesssim \sqrt{C_{\mathrm{ol},m}}\|\pi_H^E\mathcal{G}_m(\mathbf{F})\|_{\mathrm{curl},\omega}\Big(\sum_T \|\mathcal{G}(\mathbf{F}_T) - \mathcal{G}_{T,m}(\mathbf{F}_T)\|_{\mathrm{curl},\omega}\Big)^{1/2}.\end{aligned}$$

Application of (3.50) gives the claim. □

The well-posedness of the quasi-local numerical scheme comes from the well-posedness of the ideal scheme (Theorem 3.2.16) and the fact that the localized corrector is exponentially close to the ideal corrector.

Proof of Theorem 3.2.20. Fix $\mathbf{v}_H \in \mathring{\mathcal{N}}(\mathcal{T}_H)$ and set $\tilde{\mathbf{v}}_H = \pi_H^E(\mathrm{id}+\mathcal{K}_m)(\mathbf{v}_H)$. According to Theorem 3.2.16, there exists $\boldsymbol{\psi}_H \in \mathring{\mathcal{N}}(\mathcal{T}_H)$ with $\|\boldsymbol{\psi}_H\|_{\mathrm{curl},\omega} = 1$ such that

$$|\mathcal{B}((\mathrm{id}+\mathcal{K})\tilde{\mathbf{v}}_H, (\mathrm{id}+\mathcal{K})\boldsymbol{\psi}_H)| \geq \gamma(\omega)\|\tilde{\mathbf{v}}_H\|_{\mathrm{curl},\omega}.$$

As $\mathcal{B}(\mathbf{w}, (\mathrm{id}+\mathcal{K})\boldsymbol{\psi}_H) = 0$ for all $\mathbf{w} \in \mathbf{W}$, we derive

$$\begin{aligned}\mathcal{B}((\mathrm{id}+\mathcal{K}_m)\mathbf{v}_H, (\mathrm{id}+\mathcal{K})\boldsymbol{\psi}_H) &= \mathcal{B}((\mathrm{id}+\mathcal{K}_m)\mathbf{v}_H - (\mathrm{id}-\pi_H^E)((\mathrm{id}+\mathcal{K}_m)\mathbf{v}_H), (\mathrm{id}+\mathcal{K})\boldsymbol{\psi}_H)\\ &= \mathcal{B}(\tilde{\mathbf{v}}_H, (\mathrm{id}+\mathcal{K})\boldsymbol{\psi}_H) = \mathcal{B}((\mathrm{id}+\mathcal{K})\tilde{\mathbf{v}}_H, (\mathrm{id}+\mathcal{K})\boldsymbol{\psi}_H).\end{aligned}$$

This yields together with Theorem 3.2.18

$$\begin{aligned}&|\mathcal{B}((\mathrm{id}+\mathcal{K}_m)\mathbf{v}_H, (\mathrm{id}+\mathcal{K}_m)\boldsymbol{\psi}_H)|\\ &\quad= |\mathcal{B}((\mathrm{id}+\mathcal{K}_m)\mathbf{v}_H, (\mathcal{K}_m-\mathcal{K})\boldsymbol{\psi}_H) + \mathcal{B}((\mathrm{id}+\mathcal{K})\mathbf{v}_H, (\mathrm{id}+\mathcal{K})\boldsymbol{\psi}_H)|\\ &\quad= |\mathcal{B}((\mathrm{id}+\mathcal{K}_m)\mathbf{v}_H, (\mathcal{K}_m-\mathcal{K})\boldsymbol{\psi}_H) + \mathcal{B}((\mathrm{id}+\mathcal{K})\tilde{\mathbf{v}}_H, (\mathrm{id}+\mathcal{K})\boldsymbol{\psi}_H)|\\ &\quad\geq \gamma(\omega)\|\tilde{\mathbf{v}}_H\|_{\mathrm{curl},\omega} - C\sqrt{C_{\mathrm{ol},m}}\,\beta^m\|(\mathrm{id}+\mathcal{K}_m)\mathbf{v}_H\|_{\mathrm{curl},\omega}.\end{aligned}$$

Moreover, we have

$$\|(\mathrm{id}+\mathcal{K}_m)\mathbf{v}_H\|_{\mathrm{curl},\omega} \lesssim (1+\beta^m)\|\mathbf{v}_H\|_{\mathrm{curl},\omega} \lesssim \|\mathbf{v}_H\|_{\mathrm{curl},\omega},$$

since $\beta < 1$, and

$$\begin{aligned}\|\mathbf{v}_H\|_{\mathrm{curl},\omega} &= \|\pi_H^E(\mathrm{id}+\mathcal{K})\mathbf{v}_H\|_{\mathrm{curl},\omega} = \|\pi_H^E(\mathrm{id}+\mathcal{K}_m)\mathbf{v}_H + \pi_H^E(\mathcal{K}-\mathcal{K}_m)\mathbf{v}_H\|_{\mathrm{curl},\omega}\\ &\lesssim \|\tilde{\mathbf{v}}_H\|_{\mathrm{curl},\omega} + C\sqrt{C_{\mathrm{ol},m}}\,\beta^m\|\mathbf{v}_H\|_{\mathrm{curl},\omega}.\end{aligned}$$

If m is large enough (indirectly implied by the oversampling condition), the second term can be hidden on the left-hand side. Thus, we finally obtain

$$|\mathcal{B}((\mathrm{id}+\mathcal{K}_m)\mathbf{v}_H, (\mathrm{id}+\mathcal{K}_m)\boldsymbol{\psi}_H)| \gtrsim (\gamma(\omega) - C\sqrt{C_{\mathrm{ol},m}}\,\beta^m)\|\mathbf{v}_H\|_{\mathrm{curl},\omega}.$$

Application of the oversampling condition (3.47) gives the assertion. □

The proof of the a priori error estimate is inspired by the procedure for the Helmholtz equation [Pet17] and uses duality arguments.

Proof of Theorem 3.2.21. Define $\mathbf{e} := \mathbf{u} - (\mathrm{id}+\mathcal{K}_m)\mathbf{u}_{H,m}$ and set $\mathbf{e}_{H,m} := (\mathrm{id}+\mathcal{K}_m)\pi_H^E(\mathbf{e})$. Let $\mathbf{z}_H \in \mathring{\mathcal{N}}(\mathcal{T}_H)$ be the solution to the dual problem

$$\mathcal{B}((\mathrm{id}+\mathcal{K}_m)\mathbf{v}_H, (\mathrm{id}+\mathcal{K}_m)\mathbf{z}_H) = (\mathbf{e}_{H,m}, (\mathrm{id}+\mathcal{K}_m)\mathbf{v}_H)_{\mathrm{curl},\omega} \qquad \forall \mathbf{v}_H \in \mathring{\mathcal{N}}(\mathcal{T}_H).$$

Using the fact that $\mathcal{B}(\mathbf{w}, (\mathrm{id}+\mathcal{K})\mathbf{z}_H) = 0$ for all $\mathbf{w} \in \mathbf{W}$ and employing the Galerkin orthogonality $\mathcal{B}(\mathbf{e}, (\mathrm{id}+\mathcal{K}_m)\mathbf{z}_H) = 0$, we obtain that

$$\begin{aligned}\|\mathbf{e}_{H,m}\|_{\mathrm{curl},\omega}^2 &= \mathcal{B}(\mathbf{e}_{H,m}, (\mathrm{id}+\mathcal{K}_m)\mathbf{z}_H)\\ &= \mathcal{B}(\mathbf{e}_{H,m}, (\mathcal{K}_m-\mathcal{K})\mathbf{z}_H) + \mathcal{B}(\mathbf{e}_{H,m}, (\mathrm{id}+\mathcal{K})\mathbf{z}_H)\\ &= \mathcal{B}(\mathbf{e}-\mathbf{e}_{H,m}, (\mathcal{K}-\mathcal{K}_m)\mathbf{z}_H) - \mathcal{B}(\pi_H^E(\mathbf{e}-\mathbf{e}_{H,m}), (\mathrm{id}+\mathcal{K})\mathbf{z}_H).\end{aligned}$$

Observe that $\pi_H^E(\mathbf{e}-\mathbf{e}_{H,m}) = \pi_H^E\mathcal{K}_m\pi_H^E(\mathbf{e})$. Theorems 3.2.18 and 3.2.20 yield

$$\begin{aligned}\|\mathbf{e}_{H,m}\|_{\mathrm{curl},\omega}^2 &\lesssim \sqrt{C_{\mathrm{ol},m}}\,\beta^m\|\mathbf{e}-\mathbf{e}_{H,m}\|_{\mathrm{curl},\omega}\|\mathbf{z}_H\|_{\mathrm{curl},\omega} + \sqrt{C_{\mathrm{ol},m}}\,\beta^m\|\mathbf{e}\|_{\mathrm{curl},\omega}\|\mathbf{z}_H\|_{\mathrm{curl},\omega}\\ &\lesssim \sqrt{C_{\mathrm{ol},m}}\,\beta^m\,\gamma_{\mathrm{LOD}}^{-1}(\omega)\,(\|\mathbf{e}-\mathbf{e}_{H,m}\|_{\mathrm{curl},\omega} + \|\mathbf{e}\|_{\mathrm{curl},\omega})\|\mathbf{e}_{H,m}\|_{\mathrm{curl},\omega}.\end{aligned}$$

The triangle inequality gives

$$\|\mathbf{e}\|_{\mathrm{curl},\omega} \leq \|(\mathrm{id}-\pi_H^E)(\mathbf{e}-\mathbf{e}_{H,m})\|_{\mathrm{curl},\omega} + \|\pi_H^E(\mathbf{e}-\mathbf{e}_{H,m})\|_{\mathrm{curl},\omega} + \|\mathbf{e}_{H,m}\|_{\mathrm{curl},\omega}.$$

The above computations and (3.45) imply with the resolution condition (3.48)

$$\|\mathbf{e}\|_{\mathrm{curl},\omega} \lesssim \|(\mathrm{id}-\pi_H^E)(\mathbf{e}-\mathbf{e}_{H,m})\|_{\mathrm{curl},\omega}.$$

Observe that $\mathbf{e}-\mathbf{e}_{H,m} = \mathbf{u} - (\mathrm{id}+\mathcal{K}_m)\pi_H^E(\mathbf{u}) - (\mathrm{id}+\mathcal{K}_m)\pi_H^E\mathcal{K}_m\mathbf{u}_{H,m}$. Since $(\mathrm{id}-\pi_H^E)(\mathbf{e}-\mathbf{e}_{H,m}) \in \mathbf{W}$, Lemma 3.2.14 gives $\mathbf{w} \in \mathbf{W}$ with $\|\mathbf{w}\|_{\mathrm{curl},\omega} = 1$ such that

$$\begin{aligned}
&\|(\mathrm{id}-\pi_H^E)(\mathbf{e}-\mathbf{e}_{H,m})\|_{\mathrm{curl},\omega} \\
&\quad\lesssim |\mathcal{B}((\mathrm{id}-\pi_H^E)(\mathbf{e}-\mathbf{e}_{H,m}),\mathbf{w})| \\
&\quad= |\mathcal{B}(\mathbf{u},\mathbf{w}) - \mathcal{B}((\mathrm{id}+\mathcal{K}_m)\pi_H^E\mathbf{u},\mathbf{w}) - \mathcal{B}((\mathrm{id}+\mathcal{K}_m)\pi_H^E\mathcal{K}_m\mathbf{u}_{H,m},\mathbf{w}) - \mathcal{B}(\pi_H^E\mathcal{K}_m\pi_H^E\mathbf{e},\mathbf{w})| \\
&\quad= |(\mathbf{f},\mathbf{w}) - \mathcal{B}((\mathcal{K}_m-\mathcal{K})\pi_H^E\mathbf{u},\mathbf{w}) - \mathcal{B}((\mathcal{K}_m-\mathcal{K})\pi_H^E\mathcal{K}_m\mathbf{u}_{H,m},\mathbf{w}) - \mathcal{B}(\pi_H^E\mathcal{K}_m\pi_H^E\mathbf{e},\mathbf{w})|.
\end{aligned}$$

Theorems 3.2.18 and 3.2.20 give together with the stability of π_H^E and (3.37)

$$\begin{aligned}
&\|(\mathrm{id}-\pi_H^E)(\mathbf{e}-\mathbf{e}_{H,m})\|_{\mathrm{curl},\omega} \\
&\quad\lesssim \big(H + \sqrt{C_{\mathrm{ol},m}}\,\beta^m\gamma^{-1}(\omega) + C_{\mathrm{ol},m}\,\beta^{2m}\gamma_{\mathrm{LOD}}^{-1}(\omega)\big)\|\mathbf{f}\|_{\mathbf{H}(\mathrm{div})} + \sqrt{C_{\mathrm{ol},m}}\,\beta^m\|\mathbf{e}\|_{\mathrm{curl},\omega}.
\end{aligned}$$

The last term can be hidden on the left-hand side and the third term can be absorbed in the second term. □

4 Heterogeneous Multiscale Methods for high contrast problems

In this chapter, we present and analyze the Heterogeneous Multiscale Method (HMM) for electromagnetic scattering problems with high contrast. More precisely, we study the problems (2.21) and (2.22) for the two-dimensional and three-dimensional setting, respectively, where the scatterer Ω exhibits a special (periodic) structure detailed below.

As already mentioned in the introduction, (locally) periodic media, such as photonic crystals, can have astonishing properties such as band gaps or negative refraction. The setting and studies of this chapter shed a light on the phenomenon of *artificial magnetism*. This describes the occurrence of an (effective) permeability $\mu \neq 1$ in an originally nonmagnetic material, i.e., $\mu = 1$. Clearly, such a material must exhibit some interior structure to allow this significant change of behavior. In [BBF17, BF04], a high contrast structure (see below) has been used to obtain a wavenumber-dependent permeability. The permeability can even have a negative real part, which is of particular interest: The corresponding wavenumbers form a so-called band gap where wave propagation is physically forbidden.

Inspired by [FB97] and the experimental setup of [OP02], the setting of [BF04] (two-dimensional case) is the following (see also Figure 4.1): A periodic array of rods with high permittivity is embedded in a lossless dielectric material. The three-dimensional extension in [BBF09, BBF17] consists of bulk inclusions with high permittivity embedded in a lossless dielectric material, see Figure 4.2. In both cases, denoting by the small parameter δ the periodicity, the high permittivity in the inclusions is modeled by setting $\varepsilon^{-1} = \delta^2 \varepsilon_1^{-1}$, see (4.1) for an exact definition. As in Section 2.1, we denote by k the wavenumber of the scattering problem and assume that there is $k_0 > 0$ such that $k \geq k_0$, which corresponds to medium and high frequencies. It is important to relate the scales introduced by k and δ: We basically have a three-scale structure with $\delta \ll \lambda \sim k^{-1} < 1$, i.e., the periodicity of the material (and hence the size of the inclusions) is much smaller than the wavelength of the incoming wave.

This chapter is structured as follows. The (geometric) setting is detailed in Section 4.1. In Section 4.2, we give the homogenization results for these problems in form of a two-scale and an effective homogenized equation each. These homogenized systems are analyzed with respect to stability and regularity in Section 4.3. In Section 4.4, we introduce the Heterogeneous Multiscale Method (HMM) and perform a rigorous a priori error analysis. Section 4.5 analyzes an additional Localized Orthogonal Decomposition (LOD) to relax the resolution condition

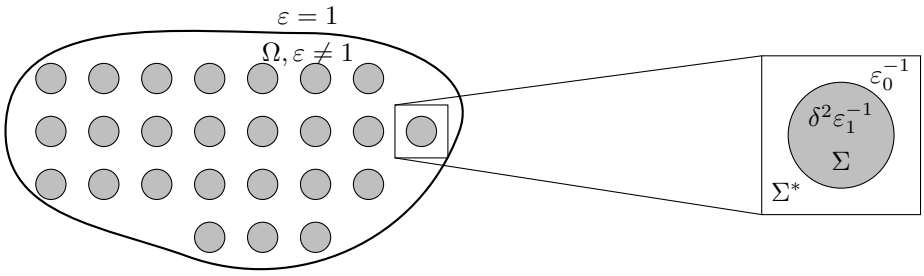

Figure 4.1: Left: Scatterer Ω with inclusions Σ_δ with high permittivity (in gray); Right: Zoom into one unit cell Y and scaling of the permittivity ε_δ^{-1}.

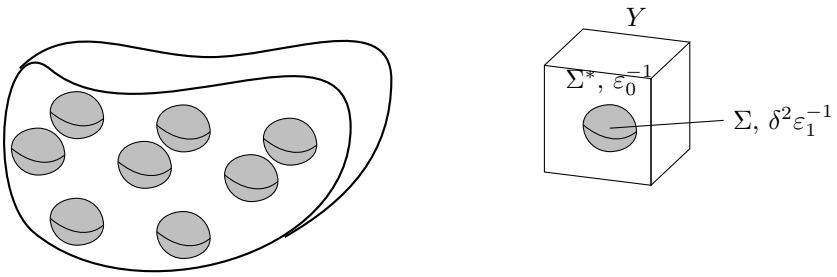

Figure 4.2: Left: Scatterer Ω with the high contrast inclusions Σ_δ (in gray); Right: Zoom into unit cell Y and scaling of ε_δ^{-1}.

between the mesh size and the wavenumber. Numerical experiments are given in Section 4.6. The results presented in this chapter have been published in [OV17, OV18] and as preprint in [Ver17a].

4.1 Problem setting

Let $\Omega \subset\subset G \subset \mathbb{R}^d$, $d \in \{2,3\}$, be bounded, simply connected domains with C^2-boundary and denote the outer unit normal of G by $\mathbf{n}$. We consider the following setting for the inverse relative permittivity ε^{-1}, see [BBF17,BF04]: Ω is composed of δ-periodically disposed inclusions, δ being a small parameter. Denoting by $\Sigma \subset\subset Y = (-\frac{1}{2},\frac{1}{2})^d$ a connected domain with C^2-boundary, the inclusions occupy a region $\Sigma_\delta = \cup_{j\in I}\delta(j+\Sigma)$ with $I = \{j \in \mathbb{Z}^d | \delta(j+Y) \subset \Omega\}$. The complement of Σ in Y, denoted by Σ^*, is connected. In the three-dimensional case, we additionally assume Σ^* to be simply connected. The inverse relative permittivity ε_δ^{-1} is then defined (possibly after rescaling) as (cf. Figures 4.1 and 4.2)

$$\varepsilon_\delta^{-1}(x) := \begin{cases} \delta^2\varepsilon_1^{-1}, & \text{if } x \in \Sigma_\delta \quad \text{with } \varepsilon_1 \in \mathbb{C},\ \mathrm{Im}(\varepsilon_1) > 0,\ \mathrm{Re}(\varepsilon_1) > 0, \\ \varepsilon_0^{-1}, & \text{if } x \in \Omega \setminus \Sigma_\delta \quad \text{with } \varepsilon_0 \in \mathbb{R},\ \varepsilon_0 > 0, \\ 1, & \text{if } x \in G \setminus \overline{\Omega}. \end{cases} \tag{4.1}$$

We assume $\mathrm{Re}(\varepsilon_1) > 0$ for simplicity; all results hold — up to minor modifications in the proofs — also for ε_1 with $\mathrm{Re}(\varepsilon_1) \le 0$. Physically speaking, this choice of ε_δ^{-1} means that the scatterer Ω consists of periodically disposed metallic inclusions Σ_δ embedded in a dielectric "matrix" medium.

We use the notation on Sobolev spaces from Section 2.1.2. We then consider the Helmholtz equation (2.21) and the Maxwell equation (2.22) with the coefficient ε_δ^{-1}. To be more precise, we consider the following situations.

Definition 4.1.1 (Weak solution for the Helmholtz equation)**.** Let ε_δ^{-1} be defined by (4.1) and let $g \in H^{1/2}(\partial G)$. We call $u_\delta \in H^1(G)$ a weak solution for $d = 2$ if it fulfills

$$\int_G \varepsilon_\delta^{-1}\nabla u_\delta \cdot \nabla\psi^* - k^2 u_\delta\psi^*\,dx - ik\int_{\partial G} u_\delta\psi^*\,d\sigma = \int_{\partial G} g\psi^*\,d\sigma \qquad \forall\psi \in H^1(G). \tag{4.2}$$

Definition 4.1.2 (Weak solution for the Maxwell equation)**.** Let ε_δ^{-1} be defined by (4.1) and let $\mathbf{g} \in L_T^2(\partial G)$. We call $\mathbf{u}_\delta \in \mathbf{H}_{\mathrm{imp}}(G)$ a weak solution for $d = 3$ if it fulfills

$$\int_G \varepsilon_\delta^{-1}\,\mathrm{curl}\,\mathbf{u}_\delta\cdot\mathrm{curl}\,\boldsymbol{\psi}^* - k^2\mathbf{u}_\delta\cdot\boldsymbol{\psi}^*\,dx - ik\int_{\partial G}(\mathbf{u}_\delta)_T\cdot\boldsymbol{\psi}_T^*\,d\sigma = \int_{\partial G}\mathbf{g}\cdot\boldsymbol{\psi}_T^*\,d\sigma \qquad \forall\boldsymbol{\psi} \in \mathbf{H}_{\mathrm{imp}}(G). \tag{4.3}$$

Both problems admit a unique solution for fixed δ, which can be shown by unique continuation principles and Fredholm theory, see Section 2.1.3. The spaces $H^1(G)$ and $\mathbf{H}_{\mathrm{imp}}$ are equipped with the k-weighted norms $\|\cdot\|_{1,k}$ (2.10) and $\|\cdot\|_{\mathrm{imp},k}$ (2.15).

4.2 Homogenization results

In this section we consider the homogenization process $\delta \to 0$ of problems (4.2) and (4.3) using the tool of two-scale convergence. We present a two-scale equation and a homogenized effective equation for each of the two problems: Section 4.2.1 deals with the Helmholtz equation (4.2) and Section 4.2.2 with the Maxwell equation (4.3). In Section 4.2.3, we compare our results and formulations with the existing ones in the literature, namely [All92, Section 4] and [BF04] for the two-dimensional case, and [BBF17, CC15] for the three-dimensional case.

Details on two-scale convergence can be found in Section 2.3.1 and [All92, LNW02]. We recall the short-hand notation $\overset{2}{\rightharpoonup}$. In addition to the (periodic) function spaces introduced in Definition 2.3.1, we denote by $H^1_{\sharp,0}(\Sigma^*)$ the restriction of functions in $H^1_{\sharp,0}(Y)$ to $\Sigma^* \subset Y$.

4.2.1 Homogenization results for the Helmholtz equation

The special scaling of ε_δ^{-1} with δ^2 on a part of Ω leads to a different behavior of the solution on Σ_δ and its complement, which can still be seen in the two-scale equation and the homogenized (effective) equation. More precisely, we obtain the standard two-scale convergences from Theorems 2.3.4 and 2.3.5 outside of the inclusions Σ_δ, whereas inside these inclusions the high contrast implies that an additional identity term "survives".

Theorem 4.2.1 (Two-scale equation)**.** *Let u_δ be the weak solution to (4.2). There are functions $u_0 \in H^1(G)$, $u_1 \in L^2(\Omega; H^1_{\sharp,0}(\Sigma^*))$, and $u_2 \in L^2(\Omega; H^1_0(\Sigma))$ such that the following two-scale convergences for $\delta \to 0$ hold*

$$u_\delta \overset{2}{\rightharpoonup} u_0 + \chi_\Sigma u_2, \qquad \chi_{\Omega\setminus\overline{\Sigma}_\delta} \nabla u_\delta \overset{2}{\rightharpoonup} \chi_{\Sigma^*}(\nabla u_0 + \nabla_y u_1),$$
$$\delta \chi_{\Sigma_\delta} \nabla u_\delta \overset{2}{\rightharpoonup} \chi_\Sigma \nabla_y u_2, \qquad \nabla u_\delta \overset{2}{\rightharpoonup} \nabla u_0 \quad \text{in} \quad G \setminus \overline{\Omega}.$$

The two-scale triple $\underline{\mathbf{u}} := (u_0, u_1, u_2) \in \mathcal{H}$ is the unique solution to

$$\mathcal{B}\big((u_0,u_1,u_2),(\psi_0,\psi_1,\psi_2)\big) = (g,\psi_0)_{L^2(\partial G)} \qquad \forall \underline{\boldsymbol{\psi}} := (\psi_0,\psi_1,\psi_2) \in \mathcal{H}, \tag{4.4}$$

where $\mathcal{H} := H^1(G) \times L^2(\Omega; H^1_{\sharp,0}(\Sigma^*)) \times L^2(\Omega; H^1_0(\Sigma))$ and

$$\begin{aligned}\mathcal{B}(\underline{\mathbf{v}}, \underline{\boldsymbol{\psi}}) := &\int_\Omega \int_{\Sigma^*} \varepsilon_0^{-1}(\nabla v_0 + \nabla_y v_1)\cdot(\nabla \psi_0^* + \nabla_y \psi_1^*)\,dydx + \int_\Omega \int_\Sigma \varepsilon_1^{-1} \nabla_y v_2 \cdot \nabla_y \psi_2^*\,dydx \\ &- k^2 \int_G \int_Y (v_0 + \chi_\Sigma v_2)(\psi_0^* + \chi_\Sigma \psi_2^*)\,dydx + \int_{G\setminus\overline{\Omega}} \nabla v_0 \cdot \nabla \psi_0^*\,dx - ik \int_{\partial G} v_0\, \psi_0^*\,d\sigma.\end{aligned}$$

The proof mainly follows the lines of [BF04] with the application of the two-scale convergences proved in [All92, Section 4] for a so-called highly heterogeneous diffusion problem. Note that u_1 and u_2 are zero outside Ω so that we have $u_\delta \rightharpoonup u_0$ in $H^1(G \setminus \overline{\Omega})$. We remark that the two-scale equation for a problem with high contrast includes an additional corrector in the identity part in comparison to the classical elliptic case, see [All92, LNW02].

The two-scale equation can be recast into a homogenized effective (macroscopic) equation which involves effective parameters computed from cell problems, as given in the next theorem.

Theorem 4.2.2 (Homogenized effective equation)**.** *Define for $j,l=1,2$ the effective parameters*

$$((\varepsilon^{-1})_{\mathrm{hom}}(x))_{jl} := \begin{cases} \int_{\Sigma^*} \varepsilon_0^{-1}(\mathbf{e}_j+\nabla_y w_j)\cdot(\mathbf{e}_l+\nabla_y w_l^*)\,dy, & \text{if} \quad x\in\Omega,\\ \mathrm{Id}_{jl}, & \text{if} \quad x\in G\setminus\overline{\Omega}, \end{cases}$$

$$\text{and} \quad \mu_{\mathrm{hom}}(x) := \begin{cases} \int_Y 1+k^2\chi_\Sigma\, w\,dy, & \text{if} \quad x\in\Omega,\\ 1, & \text{if} \quad x\in G\setminus\overline{\Omega}, \end{cases}$$

where w_j and w are solutions to the following cell problems: $w_j\in H^1_{\sharp,0}(\Sigma^*)$, $j=1,2$, solves

$$\int_{\Sigma^*}\varepsilon_0^{-1}(\mathbf{e}_j+\nabla_y w_j)\cdot\nabla_y\psi_1^*\,dy=0 \qquad \forall\psi_1\in H^1_{\sharp,0}(\Sigma^*) \tag{4.5}$$

and $w\in H^1_0(\Sigma)$ solves

$$\int_\Sigma \varepsilon_1^{-1}\nabla_y w\cdot\nabla_y\psi_2^* - k^2 w\psi_2^*\,dy=\int_\Sigma\psi_2^*\,dy \qquad \forall\psi_2\in H^1_0(\Sigma). \tag{4.6}$$

Then the triple (u_0,u_1,u_2) solves the two-scale equation (4.4) if and only if we set $u_1(x,y)=\sum_{j=1}^2\frac{\partial u_0}{\partial x_j}|_\Omega(x)w_j(y)$, $u_2(x,y)=k^2u_0|_\Omega(x)w(y)$, and $u_0\in H^1(G)$ solves

$$\mathcal{B}_{\mathrm{hom}}(u_0,\psi)=(g,\psi)_{L^2(\partial G)} \qquad \forall\psi\in H^1(G) \tag{4.7}$$

with the effective sesquilinear form

$$\mathcal{B}_{\mathrm{hom}}(v,\psi):=\int_G(\varepsilon^{-1})_{\mathrm{hom}}\nabla v\cdot\nabla\psi^* - k^2\mu_{\mathrm{hom}}v\,\psi^*\,dx - ik\int_{\partial G} v\,\psi^*\,d\sigma. \tag{4.8}$$

The presentation is oriented at the results for diffusion problems in [All92], which can be seen most prominently in the form of the effective permeability μ_{hom}. In Lemma 4.2.5, we prove that this formula for μ_{hom} is perfectly equivalent to the representation chosen in [BF04].

We emphasize that all cell problems are uniquely solvable due to the Theorem of Lax-Milgram. (For (4.6), note that the left-hand side is coercive because of $\mathrm{Im}(\varepsilon_1^{-1})<0$.) Unique solvability of the effetive macroscopic equation (4.7) again follows with Fredholm theory.

The foregoing theorem means that in the limit $\delta\to0$, the scatterer Ω can be described as a homogeneous material with the (effective) parameters $(\varepsilon^{-1})_{\mathrm{hom}}$ and μ_{hom}. Whereas $(\varepsilon^{-1})_{\mathrm{hom}}$ is a positive definite matrix (see Proposition 4.3.5), the effective permeability μ_{hom} exhibits some astonishing properties: First of all, its occurrence itself is surprising as the scatterer is nonmagnetic. This is the already discussed effect of artificial magnetism. Second, the permeability is wavenumber-dependent and its real part can have a positive or a negative sign. In the region with $\mathrm{Re}(\mu_{\mathrm{hom}})<0$ waves cannot propagate leading to photonic band gaps, see [BF04]. This effect is also studied numerically in detail in Section 4.6.

4.2.2 Homogenization results for the Maxwell equation

From the previous section, we also expect a different behavior of the solution $\mathbf{u}_\delta$ to (4.3) in- and outside Σ_δ. Moreover, we have to apply the two-scale convergences for $\mathbf{H}(\mathrm{curl})$ from Theorem 2.3.6, so that we already obtain a corrector in the identity term *outside* the inclusions. Hence, the Maxwell equation with high contrast finally has *three* correctors in the two-scale equation.

Similar to $H^1_{\sharp,0}(\Sigma^*)$, we denote by $\mathbf{H}_\sharp(\mathrm{curl},\Sigma^*)$ the restriction of functions in $\mathbf{H}_\sharp(\mathrm{curl},Y)$ to $\Sigma^*\subset Y$. Moreover, we introduce the space

$$\widetilde{\mathbf{H}}_\sharp(\mathrm{curl},\Sigma^*):=\mathbf{H}_\sharp(\mathrm{curl},\Sigma^*)/\ker(\mathrm{curl}_{y|_{\Sigma^*}}).$$

This is the space of functions $\mathbf{v} \in \mathbf{H}_\sharp(\operatorname{curl}, \Sigma^*)$ such that $\operatorname{curl}_y \mathbf{v}$ is uniquely determined in Σ^* or, in other words, such that $\mathbf{v}$ is determined up to a gradient (as Σ^* is simply connected). Note, however, that in practical applications, we will always be interested in $\operatorname{curl}_y \mathbf{v}$ solely, which is in $L^2_\sharp(\Sigma^*)$ and uniquely determined.

Theorem 4.2.3 (Two-scale equation)**.** *Let $\mathbf{u}_\delta$ be the solution to (4.3). There are functions $\mathbf{u}_0 \in \mathbf{H}_{\mathrm{imp}}(G)$, $\mathbf{u}_1 \in L^2(\Omega; \widetilde{\mathbf{H}}_\sharp(\operatorname{curl}, \Sigma^*))$, $u_2 \in L^2(\Omega; H^1_{\sharp,0}(\Sigma^*))$, and $\mathbf{u}_3 \in L^2(\Omega; \mathbf{H}_0(\operatorname{curl}, \Sigma))$, such that the following two-scale convergences hold*

$$\mathbf{u}_\delta \xrightarrow{2} \mathbf{u}_0 + \chi_{\Sigma^*} \nabla_y u_2 + \chi_\Sigma \mathbf{u}_3, \qquad \chi_{\Omega\setminus\overline{\Sigma}_\delta} \operatorname{curl} \mathbf{u}_\delta \xrightarrow{2} \chi_{\Sigma^*}(\operatorname{curl} \mathbf{u}_0 + \operatorname{curl}_y \mathbf{u}_1),$$
$$\delta \chi_{\Sigma_\delta} \operatorname{curl} \mathbf{u}_\delta \xrightarrow{2} \chi_\Sigma \operatorname{curl}_y \mathbf{u}_3, \qquad \operatorname{curl} \mathbf{u}_\delta \xrightarrow{2} \operatorname{curl} \mathbf{u}_0 \quad \text{in} \quad G \setminus \overline{\Omega}.$$

The quadruple $\underline{\mathbf{u}} := (\mathbf{u}_0, \mathbf{u}_1, u_2, \mathbf{u}_3) \in \mathcal{H}$ of two-scale limits is the unique solution to

$$\mathcal{B}((\mathbf{u}, \mathbf{u}_1, u_2, \mathbf{u}_3), (\boldsymbol{\psi}, \boldsymbol{\psi}_1, \psi_2, \boldsymbol{\psi}_3)) = (\mathbf{g}, \boldsymbol{\psi}_T)_{L^2(\partial G)} \qquad \forall (\boldsymbol{\psi}, \boldsymbol{\psi}_1, \psi_2, \boldsymbol{\psi}_3) \in \mathcal{H}, \tag{4.9}$$

where $\mathcal{H} := \mathbf{H}_{\mathrm{imp}}(G) \times L^2(\Omega; \widetilde{\mathbf{H}}_\sharp(\operatorname{curl}, \Sigma^*)) \times L^2(\Omega; H^1_{\sharp,0}(\Sigma^*)) \times L^2(\Omega; \mathbf{H}_0(\operatorname{curl}, \Sigma))$ and

$$\begin{aligned}
\mathcal{B}(\underline{\mathbf{v}}, \underline{\boldsymbol{\psi}}) := &\int_\Omega \int_{\Sigma^*} \varepsilon_0^{-1} (\operatorname{curl} \mathbf{v}_0 + \operatorname{curl}_y \mathbf{v}_1) \cdot (\operatorname{curl} \boldsymbol{\psi}_0^* + \operatorname{curl}_y \boldsymbol{\psi}_1^*) \, dy dx \\
&+ \int_\Omega \int_\Sigma \varepsilon_1^{-1} \operatorname{curl}_y \mathbf{v}_3 \cdot \operatorname{curl}_y \boldsymbol{\psi}_3^* \, dy dx \\
&- k^2 \int_G \int_Y (\mathbf{v}_0 + \chi_{\Sigma^*} \nabla_y v_2 + \chi_\Sigma \mathbf{v}_3) \cdot (\boldsymbol{\psi}_0^* + \chi_{\Sigma^*} \nabla_y \psi_2^* + \chi_\Sigma \boldsymbol{\psi}_3^*) \, dy dx \\
&+ \int_{G\setminus\overline{\Omega}} \operatorname{curl} \mathbf{v}_0 \cdot \operatorname{curl} \boldsymbol{\psi}_0^* \, dx - ik \int_{\partial G} (\mathbf{v}_0)_T \cdot (\boldsymbol{\psi}_0)_T^* \, d\sigma.
\end{aligned}$$

Proof. The proof closely follows [BBF17] and mainly differs in the form of the two-scale convergence, so that we focus on that part.

First step: A priori bounds. Assume that $\mathbf{u}_\delta$ is uniformly bounded in $L^2(G)$. We then easily deduce that $\sqrt{|\varepsilon_\delta^{-1}|} \operatorname{curl} \mathbf{u}_\delta$ is also uniformly bounded in $L^2(G)$.

Second step: Two-scale convergences. By the a priori bounds, $\mathbf{u}_\delta$ converges weakly in $\mathbf{H}(\operatorname{curl}, G \setminus \overline{\Omega})$ to some $\mathbf{u}_0$. Using [BBF17, Prop. 7.1], we deduce $\mathbf{u}_0 \in \mathbf{H}(\operatorname{curl}, G \setminus \overline{\Omega})$. Since $G \setminus \overline{\Sigma}_\delta$ is a simply connected domain, the two-scale convergences from Wellander et al. [Wel09, WK03] and Visintin [Vis07] can be applied (formally with the help of extension by zero in Σ_δ): There exist $\mathbf{u}_0 \in \mathbf{H}_{\mathrm{imp}}(G)$, $\mathbf{u}_1 \in L^2(\Omega; \widetilde{\mathbf{H}}_\sharp(\operatorname{curl}, \Sigma^*))$, and $u_2 \in L^2(\Omega; H^1_{\sharp,0}(\Sigma^*))$ such that, up to a subsequence,

$$\chi_{G\setminus\overline{\Sigma}_\delta} \mathbf{u}_\delta \xrightarrow{2} \chi_{\Sigma^*}(\mathbf{u}_0 + \nabla_y u_2) \qquad \text{and} \qquad \chi_{G\setminus\overline{\Sigma}_\delta} \operatorname{curl} \mathbf{u}_\delta \xrightarrow{2} \chi_{\Sigma^*}(\operatorname{curl} \mathbf{u}_0 + \operatorname{curl}_y \mathbf{u}_1).$$

The uniform a priori bound of $\mathbf{u}_\delta$ furthermore implies that there is $\widetilde{\mathbf{u}}_0 \in L^2(\Omega; \mathbf{H}_\sharp(\operatorname{curl}, \Sigma))$ such that, up to a subsequence,

$$\chi_{\Sigma_\delta} \mathbf{u}_\delta \xrightarrow{2} \chi_\Sigma \widetilde{\mathbf{u}}_0 \qquad \text{and} \qquad \delta \chi_{\Sigma_\delta} \operatorname{curl} \mathbf{u}_\delta \xrightarrow{2} \chi_\Sigma \operatorname{curl}_y \widetilde{\mathbf{u}}_0,$$

cf. [CC15]. Using all these two-scale convergences, we can deduce for any $\boldsymbol{\psi} \in C_0^\infty(\Omega; C_\sharp^\infty(Y))$

$$\begin{aligned}
&\int_\Omega \int_\Sigma \operatorname{curl}_y \widetilde{\mathbf{u}}_0 \cdot \boldsymbol{\psi} \, dy dx \longleftarrow \int_\Omega \delta \operatorname{curl} \mathbf{u}_\delta \cdot \boldsymbol{\psi}\big(x, \frac{x}{\delta}\big) \, dx \\
&\quad = \int_\Omega \delta \mathbf{u}_\delta \cdot \operatorname{curl}_y \boldsymbol{\psi}\big(x, \frac{x}{\delta}\big) \, dx \longrightarrow \int_\Omega \int_Y \operatorname{curl}_y \boldsymbol{\psi} \cdot (\chi_\Sigma \widetilde{\mathbf{u}}_0 + \chi_{\Sigma^*}(\mathbf{u}_0 + \nabla_y u_2)) \, dy dx.
\end{aligned}$$

Integrating then by parts on the right-hand side, we derive the continuity of the tangential traces over $\partial\Sigma$, i.e.,

$$\int_\Omega \int_{\partial\Sigma} \widetilde{\mathbf{u}}_0 \times \mathbf{n} \cdot \boldsymbol{\psi}\, d\sigma dx = \int_\Omega \int_{\partial\Sigma} (\mathbf{u}_0 + \nabla_y u_2) \times \mathbf{n} \cdot \boldsymbol{\psi}\, d\sigma dx \quad \forall \boldsymbol{\psi} \in C_0^\infty(\Omega; C_\sharp^\infty(Y)).$$

Therefore, there exists $\mathbf{u}_3 \in L^2(\Omega; \mathbf{H}_0(\mathrm{curl}, \Sigma))$ such that

$$\mathbf{u}_\delta \overset{2}{\rightharpoonup} \mathbf{u}_0 + \chi_{\Sigma^*} \nabla_y u_2 + \chi_\Sigma \mathbf{u}_3.$$

Third step: Two-scale equation and uniqueness. The two-scale equation follows from the two-scale limits by inserting a test function of the form $\boldsymbol{\psi}(x) + \delta \boldsymbol{\psi}_1(x, \frac{x}{\delta}) + \nabla_y \psi_2(x, \frac{x}{\delta}) + \boldsymbol{\psi}_3(x, \frac{x}{\delta})$ with smooth and locally periodic functions $\boldsymbol{\psi}_i$ and with $\boldsymbol{\psi}_3(\cdot, y) = 0$ for $y \in \Sigma^*$ and $\nabla_y \psi_2(\cdot, y) = 0$ for $y \in \Sigma$ into (4.3). Uniqueness of this problem can either be derived by the uniqueness of the effective equation (see Theorem 4.2.4) or by inserting appropriate test functions.

Fourth step: $L^2(G)$-bound on $\mathbf{u}_\delta$. Finally, the assumption that $\mathbf{u}_\delta$ is uniformly bounded in $L^2(G)$ is proved by a contradiction argument, for details we refer to [BBF17]. Note that we cannot argue in the same way as for Helmholtz problems in [BF04] since weak convergence in $\mathbf{H}(\mathrm{curl})$ does *not* imply strong convergence in L^2. □

Again, we decouple the influence of the micro- and macroscale by introducing effective parameters. We emphasize that the homogenized solution $\mathbf{u}_0$ is *not* the weak limit of $\mathbf{u}_\delta$.

Theorem 4.2.4 (Homogenized effective equation)**.** *Define for $j, l = 1, 2, 3$ the effective material parameters*

$$((\varepsilon^{-1})_{\mathrm{hom}})_{j,l} := \begin{cases} \int_{\Sigma^*} \varepsilon_0^{-1}(\mathbf{e}_l + \mathrm{curl}_y\, \mathbf{w}_l^1) \cdot \mathbf{e}_j\, dy, & \text{if} \quad x \in \Omega, \\ \mathrm{Id}_{jl}, & \text{if} \quad x \in G \setminus \overline{\Omega}, \end{cases}$$

$$\text{and} \quad (\mu_{\mathrm{hom}})_{j,l} := \begin{cases} \int_Y (\mathbf{e}_l + k^2 \chi_{\Sigma^*} \nabla_y w_l^2 + k^2 \chi_\Sigma \mathbf{w}_l^3) \cdot \mathbf{e}_j\, dy, & \text{if} \quad x \in \Omega, \\ \mathrm{Id}_{jl}, & \text{if} \quad x \in G \setminus \overline{\Omega}, \end{cases}$$

where $\mathbf{w}_l^1$, w_l^2, and $\mathbf{w}_l^3$ are solutions to the following cell problems: $\mathbf{w}_l^1 \in \widetilde{\mathbf{H}}_\sharp(\mathrm{curl}, \Sigma^*)$, $l = 1, 2, 3$, solves

$$\int_{\Sigma^*} \varepsilon_0^{-1}(\mathbf{e}_l + \mathrm{curl}_y\, \mathbf{w}_l^1) \cdot \mathrm{curl}_y\, \boldsymbol{\psi}_1^*\, dy = 0 \qquad \forall \boldsymbol{\psi}_1 \in \widetilde{\mathbf{H}}_\sharp(\mathrm{curl}, \Sigma^*), \tag{4.10}$$

and $w_l^2 \in H^1_{\sharp,0}(\Sigma^*)$ and $\mathbf{w}_l^3 \in \mathbf{H}_0(\mathrm{curl}, \Sigma)$, $l = 1, 2, 3$, solve

$$\int_{\Sigma^*} (\mathbf{e}_l + k^2 \nabla_y w_l^2) \cdot \nabla_y \psi_2^*\, dy = 0 \qquad \forall \psi_2 \in H^1_{\sharp,0}(\Sigma^*), \tag{4.11}$$

$$\int_\Sigma \varepsilon_1^{-1}\, \mathrm{curl}_y\, \mathbf{w}_l^3 \cdot \mathrm{curl}_y\, \boldsymbol{\psi}_3^* - k^2 \mathbf{w}_l^3 \cdot \boldsymbol{\psi}_3^*\, dy = \int_\Sigma \mathbf{e}_l \cdot \boldsymbol{\psi}_3^*\, dy \qquad \forall \boldsymbol{\psi}_3 \in \mathbf{H}_0(\mathrm{curl}, \Sigma). \tag{4.12}$$

Then the quadruple $(\mathbf{u}_0, \mathbf{u}_1, u_2, \mathbf{u}_3)$ is solution to the two-scale equation (4.9) if and only if $\mathbf{u}_0 \in \mathbf{H}_{\mathrm{imp}}(G)$ solves the effective macroscopic scattering problem

$$\int_G (\varepsilon^{-1})_{\mathrm{hom}}\, \mathrm{curl}\, \mathbf{u}_0 \cdot \mathrm{curl}\, \boldsymbol{\psi}^* - k^2 \mu_{\mathrm{hom}} \mathbf{u}_0 \cdot \boldsymbol{\psi}^*\, dx - ik \int_{\partial G} (\mathbf{u}_0)_T \cdot \boldsymbol{\psi}_T^*\, d\sigma = \int_{\partial G} \mathbf{g} \cdot \boldsymbol{\psi}_T^*\, d\sigma \quad \forall \boldsymbol{\psi} \in \mathbf{H}_{\mathrm{imp}}(G) \tag{4.13}$$

and the correctors are

$$\mathbf{u}_1 = \sum_j (\mathrm{curl}\, \mathbf{u}_0|_\Omega)_j\, \mathbf{w}_j^1, \quad u_2 = \sum_j k^2 (\mathbf{u}_0|_\Omega)_j\, w_j^2, \quad \text{and} \quad \mathbf{u}_3 = \sum_j k^2 (\mathbf{u}_0|_\Omega)_j\, \mathbf{w}_j^3. \tag{4.14}$$

With the same arguments as for the Helmholtz equation in Theorem 4.2.2, we again conclude existence and uniqueness of solutions to the cell problems. Unique solvability of the effective macroscopic equation (4.13) follows because $\operatorname{Im}(\mu_{\text{eff}})$ is positive-definite in Ω according to Proposition 4.3.5, see [BBF17] and [Mon03, Section 4] for details.

The effective macroscopic equation (4.13) again reveals the physical properties of the scatterer Ω, see the discussion after Theorem 4.2.2. The effective parameters are very similar to the two-dimensional case: $(\varepsilon^{-1})_{\text{hom}}$ is a positive definite matrix (see Proposition 4.3.5), while μ_{hom} is wavenumber-dependent and its real part can be positive or negative definite, see the numerical experiments in Section 4.6. However, there are also some striking differences to the two-dimensional case: μ_{hom} is now matrix-valued and does not only involve a cell problem inside Σ, but also a cell problem in Σ^*.

4.2.3 Comparison to the literature

In this section, we show the equivalence of our results and those available in the literature, namely [All92, BF04] for the two-dimensional case and [BBF17, CC15] for the three-dimensional case.

Helmholtz equation. As already mentioned, our presentation in Section 4.2.1 closely follows [All92, Section 4]. The main difference is that we deal with the Helmholtz equation, whereas [All92] considers an elliptic problem, i.e., with positive identity term $+\alpha$. Still, the two-scale equation (4.4) as well as the cell problem (4.6) and the representation of μ_{hom} in Theorem 4.2.2 can be transferred directly by formally setting $\alpha = -k^2$. Only the unique solvability of the two-scale equation (4.4) needs to be ascertained because the two-scale sesquilinear form is no longer coercive. Note that we do not have a volume term on the right-hand side and that our boundary condition differs from [All92].

Comparing with [BF04], we only observe a difference in the representation of μ_{hom}. The equivalence of both formulations is shown in the next lemma. Note that ε_1 is constant.

Lemma 4.2.5 (Representation of μ_{hom})**.** *The homogenized parameter μ_{hom} from Theorem 4.2.2 can be equivalently written as*

$$\mu_{\text{hom}} = 1 + \sum_{n\in\mathbb{N}} \frac{k^2\varepsilon_1}{\lambda_n - k^2\varepsilon_1} \Big(\int_\Sigma \phi_n \, dy \Big)^2,$$

where (λ_n, ϕ_n) are the eigenvalues and eigenfunctions of the Laplace operator on Σ with Dirichlet boundary conditions.

Proof. It is well known that the eigenfunctions of the Laplace operator on Σ with Dirichlet boundary conditions form an orthonormal basis of $L^2(\Sigma)$. The eigenvalues λ_n are sorted as a positive, increasing sequence of real numbers. We have the representation $1 = \sum_n \big(\int_\Sigma \phi_n \, dy\big)\phi_n$. Writing $w = \sum_n \alpha_n \phi_n$ and inserting this into (4.6) gives after a comparison of coefficients

$$w = \sum_n \Big(\frac{\varepsilon_1}{\lambda_n - k^2\varepsilon_1} \int_\Sigma \phi_n \, dy \Big) \phi_n \qquad \text{and hence,} \qquad \mu_{\text{hom}} = 1 + \sum_n \frac{k^2\varepsilon_1}{\lambda_n - k^2\varepsilon_1} \Big(\int_\Sigma \phi_n \, dy \Big)^2,$$

cf. [BF04]. See [LS16a, Appendix A] for a computation in the three-dimensional case. □

We stress two advantages of our choice of μ_{hom} over the representation in [BF04]: First, it still holds for nonconstant parameters ε_1. Second, it only involves the solution of one cell problem rather than determining all eigenvalues and eigenfunctions of the Dirichlet Laplacian, which is very useful for the numerical implementation.

Maxwell equation. For the Maxwell equation from Section 4.2.2, we combined the two approaches [BBF17] and [CC15], so that there are differences to both contributions. First of all, we want to emphasize a few new aspects and advantages of our formulations:

- Presentation of a two-scale equation: So far, this concise and elegant formulation has been hidden in the proofs of [CC15].
- Uniqueness of the two-scale solution: By a slightly modified definition of the correctors (in comparison to [CC15], see below), we are able to prove uniqueness in nevertheless simple and natural function spaces. This is a great advantage for analysis.
- A new formulation for μ_{hom}: As already discussed in [BBF17], the computation of μ_{hom} is very challenging, especially with respect to numerical implementations. In contrast to the two-dimensional case, μ_{hom} does not only depend on the behavior of the magnetic field inside the inclusions (as one might expect), but also the surrounding medium Σ^* has to be considered. This, of course, is also persistent in our formulation. Here, however, both parts decouple quite nicely. Moreover, in comparison to [BBF17], we are also able to use natural function spaces and cell problems which are easy to implement.

Cherednichenko and Cooper [CC15, Theorem 2.1] obtain a very similar homogenization result to Theorem 4.2.3. Note that in [CC15], the sign of the identity term is switched and a volume source term is present. Instead of the corrector $\mathbf{u}_1$, [CC15, Lemma 4.4] already includes the effective matrix $(\varepsilon^{-1})_{\text{hom}}$ (named A_{hom}) in the two-scale equation.

The only crucial difference between Theorem 4.2.3 and [CC15, Theorem 2.1] is the different choice or construction of u_2 and $\mathbf{u}_3$. Roughly speaking, our $\mathbf{u}_3$ fulfills $\mathbf{u}_3 = \nabla_y u^1 + u^2$ in Σ for the functions u^1, u^2 defined in [CC15, Theorem 2.1]. Basically, we cut off our u_2 at the boundary $\partial\Sigma$ and add the "remaining" normal boundary traces to $\mathbf{u}_3$, whereas in [CC15] the function u^1 (corresponding to our u_2) is present on the whole cube Y. Moreover, this different definition of the identity correctors leads to the lower regularity $\mathbf{u}_3 \in \mathbf{H}_0(\text{curl}, \Sigma)$ instead of $u^2 \in \mathbf{H}^1_0(\Sigma)$ in [CC15]. The great advantage of our new formulation is the uniqueness of the two-scale solution. In [CC15], only uniqueness of u and of $\nabla_y u^1 + u^2$ can be demonstrated.

Comparing with [BBF17], we have $(\varepsilon^{-1})_{\text{hom}} = (\varepsilon^{\text{eff}})^{-1}$ and $\mu_{\text{hom}} = \mu^{\text{eff}}$, where μ^{eff} and ε^{eff} are defined in [BBF17]. The relationship $(\varepsilon^{-1})_{\text{hom}} = (\varepsilon^{\text{eff}})^{-1}$ is shown in [CC15, Lemma 4.4]. Comparing the definition of μ_{hom} and the definition of μ^{eff} (via equations (5.23) and (5.21) of [BBF17]), we observe that we have to prove

$$\chi_{\Sigma^*} \nabla_y w_j^2 + \chi_\Sigma \mathbf{w}_j^3 = \mathbf{u}^j,$$

where w_j^2 and $\mathbf{w}_j^3$ are defined in Theorem 4.2.4 above and $\mathbf{u}^j$ is introduced in [BBF17, equation (5.21)]. Equivalently, this means to check that

$$\widetilde{\mathbf{w}}_j := \chi_{\Sigma^*} \nabla_y w_j^2 + \chi_\Sigma \mathbf{w}_j^3 \in X_0^{\text{div}} := \left\{ \mathbf{v} \in \mathbf{H}^1_\sharp(Y) | \, \text{div}_y \, \mathbf{v} = 0 \text{ in } Y, \text{curl}_y \, \mathbf{v} = 0 \text{ in } \Sigma, \oint \mathbf{v} = 0 \right\}$$

and that $\widetilde{\mathbf{w}}_j$ fulfills equation (5.18) of [BBF17]. For that, we first prove the following lemma.

Lemma 4.2.6. *Let w_j^2 and $\mathbf{w}_j^3$ be the solutions to* (4.11) *and* (4.12). *The function $\widetilde{\mathbf{w}}_j := \chi_{\Sigma^*} \nabla_y w_j^2 + \chi_\Sigma \mathbf{w}_j^3$ fulfills*

$$\widetilde{\mathbf{w}}_j \in \mathbf{H}^1_\sharp(Y) \text{ with } \text{div}_y \, \widetilde{\mathbf{w}}_j = 0.$$

Consequently, the same holds true for $\chi_{\Sigma^*} \nabla_y u_2 + \chi_\Sigma \mathbf{u}_3$ with the correctors $u_2, \mathbf{u}_3$ defined in (4.14).

Proof. We have $\text{div}_y \, \nabla_y w_j^2 = 0$ in Σ^* because of (4.11) tested with $\psi_2 \in H^1_{\sharp,0}(\Sigma^*)$ satisfying $\psi_2 = 0$ on $\partial\Sigma$. By inserting $\boldsymbol{\psi}_3 = \nabla_y \psi_3$ with $\psi_3 \in H^1_0(\Sigma)$ into (4.12), we obtain $\text{div}_y \, \mathbf{w}_j^3 = 0$ in Σ. Inserting then test functions as before, but without vanishing (normal) traces on $\partial\Sigma$, we deduce that the normal traces of $\nabla_y w_j^2$ and $\mathbf{w}_j^3$ coincide on $\partial\Sigma$. These properties together imply $\widetilde{\mathbf{w}}_j \in \mathbf{H}_\sharp(\text{div}, Y)$ with $\text{div}_y \, \widetilde{\mathbf{w}}_j = 0$. Since obviously $\widetilde{\mathbf{w}}_j \in \mathbf{H}_\sharp(\text{curl}, Y)$, the assertion follows with [BBF17, Lemma 4.7]. □

The inclusion $\widetilde{\mathbf{w}}_j \in X_0^{\mathrm{div}}$ follows from the previous lemma and because $\widetilde{\mathbf{w}}_j$ is given as a gradient on Σ^*. Equation (5.18) of [BBF17] follows from the two cell problems (4.11) and (4.12) by a direct calculation, which we omit here. Note that ε_0 and ε_1 are constants on Σ^* and Σ, respectively.

4.3 Analysis of the homogenized systems

This section is devoted to a detailed analysis of the homogenized formulations (two-scale equation and effective macroscopic equation) presented in the previous section. The aim is to obtain regularity and stability results and gain a better insight in the properties of the effective material parameters. We emphasize that this stability and regularity analysis is a prerequisite for the a priori estimates in Section 4.4.2.

In most of this section, we consider the two- and the three-dimensional case in parallel. Some notations may be ambiguous, but it should be always clear which case we consider. We analyze the cell problems and the macroscopic equation separately: Section 4.3.1 focuses on the cell problems and the effective parameters, while Section 4.3.2 presents the stability results for the homogenized macroscopic equations. The proofs of these (new) stability estimates are detailed in Section 4.3.3.

4.3.1 Analysis of the two-scale equation and the effective parameters

In this section, we give some results on the two-scale equations, analyze the effective parameters, and quantify higher regularity of all parts of the two-scale solutions. For the Helmholtz equation, we explicitly keep track of the appearing constants, which are re-used in Section 4.4.2. This also gives an idea on how the constants hidden in $\lesssim$ for the Maxwell equation look like.

Two-scale equations. We first introduce a so-called two-scale energy norm for both cases. $\mathcal{H}$ denotes the function space for the two-scale solution, i.e.,

$$\mathcal{H} = H^1(G) \times L^2(\Omega; H^1_{\sharp,0}(\Sigma^*)) \times L^2(\Omega; H^1_0(\Sigma))$$

for the Helmholtz equation and

$$\mathcal{H} = \mathbf{H}_{\mathrm{imp}}(G) \times L^2(\Omega; \widetilde{\mathbf{H}}_\sharp(\mathrm{curl}, \Sigma^*)) \times L^2(\Omega; H^1_{\sharp,0}(\Sigma^*)) \times L^2(\Omega; \mathbf{H}_0(\mathrm{curl}, \Sigma))$$

for the Maxwell equation. We recall that $\|\cdot\|_R$ denotes the $L^2(R)$-norm. The norms $\|\cdot\|_{1,k}$, $\|\cdot\|_{\mathrm{curl},k}$, and $\|\cdot\|_{\mathrm{imp},k}$ are defined in (2.10), (2.14), and (2.15), respectively. If these norms are applied to a locally periodic function $v(x,y)$, the derivatives are always taken w.r.t. y.

Lemma 4.3.1 (Two-scale energy norms)**.** *For the Helmholtz equation, the two-scale energy norm*

$$\|\underline{\mathbf{v}}\|_e^2 := \|\nabla v_0 + \nabla_y v_1\|^2_{G\times\Sigma^*} + \|\nabla_y v_2\|^2_{\Omega\times\Sigma} + k^2\|v_0 + \chi_\Sigma v_2\|^2_{G\times Y} \tag{4.15}$$

is equivalent to the k-weighted norm

$$\|\underline{\mathbf{v}}\|^2_{k,\mathcal{H}} := \|v_0\|^2_{1,k,G} + \|v_1\|^2_{L^2(\Omega;H^1(\Sigma^*))} + \|v_2\|^2_{1,k,\Omega\times\Sigma},$$

where the equivalence constants do not depend on k.

For the Maxwell equation, the two-scale energy norm

$$\begin{aligned}\|\underline{\mathbf{v}}\|_e^2 := {} & \|\operatorname{curl}\mathbf{v}_0 + \operatorname{curl}_y\mathbf{v}_1\|^2_{G\times\Sigma^*} + \|\operatorname{curl}_y\mathbf{v}_3\|^2_{\Omega\times\Sigma} \\ & + k^2\|\mathbf{v}_0 + \chi_{\Sigma^*}\nabla_y v_2 + \chi_\Sigma\mathbf{v}_3\|^2_{G\times Y} + k\|(\mathbf{v}_0)_T\|^2_{\partial G}\end{aligned} \tag{4.16}$$

is equivalent to the k-weighted norm

$$\|\underline{\mathbf{v}}\|_{k,\mathcal{H}}^2 := \|\mathbf{v}_0\|_{\mathrm{imp},k}^2 + \|\operatorname{curl}_y \mathbf{v}_1\|_{\Omega\times\Sigma^*}^2 + k^2\|\nabla_y v_2\|_{\Omega\times\Sigma^*}^2 + \|\mathbf{v}_3\|_{\mathrm{curl},k,\Omega\times\Sigma},$$

where the equivalence constants do not depend on k.

Proof. The essential ingredient is a sharpened Cauchy-Schwarz inequality for the mixed/non-orthogonal terms. More precisely, for the Helmholtz equation it holds that

$$\begin{aligned}\Big|\int_G\int_{\Sigma^*} \nabla v_0\cdot\nabla_y v_1\,dydx\Big| &\le \|\nabla v_0\|_{L^2(G\times\Sigma^*)}\|\nabla_y v_1\|_{L^2(G\times\Sigma^*)}\\ &= |\Sigma^*|^{1/2}\|\nabla v_0\|_{L^2(G)}\|\nabla_y v_1\|_{L^2(\Omega\times\Sigma^*)}\\ \text{and}\quad \Big|\int_G\int_Y v_0\ \chi_\Sigma\, v_2\,dydx\Big| &\le \|v_0\|_{L^2(G\times\Sigma)}\|v_2\|_{L^2(G\times\Sigma)} = |\Sigma|^{1/2}\|v\|_{L^2(G)}\|v_2\|_{L^2(\Omega\times\Sigma)},\end{aligned}$$

where $|\Sigma^*|, |\Sigma| < 1$. The proof for the three-dimensional case follows in the same manner. Note that due to the choices of $H^1_{\sharp,0}(\Sigma^*)$ and $\widetilde{\mathbf{H}}_\sharp(\operatorname{curl},\Sigma^*)$, the H^1- and $\mathbf{H}(\operatorname{curl})$-seminorms are norms on these function spaces, respectively. □

We prove Gårding-type inequalities for the two-scale sesquilinear forms, which play a crucial role for the numerical analysis.

Lemma 4.3.2. *For the Helmholtz equation, there exist constants $C_B > 0$ and $C_{\min} := \min\{1, \varepsilon_0^{-1}, \operatorname{Re}(\varepsilon_1^{-1})\} > 0$ depending only on the parameters and the geometry, such that the sesquilinear form $\mathcal{B}$ from Theorem 4.2.1 is continuous with constant C_B and fulfills a Gårding inequality with constant $C_{\min}$, i.e.,*

$$|\mathcal{B}(\underline{\mathbf{v}},\underline{\boldsymbol{\psi}})| \le C_B\|\underline{\mathbf{v}}\|_e\|\underline{\boldsymbol{\psi}}\|_e \quad \textit{and} \quad \operatorname{Re}\mathcal{B}(\underline{\mathbf{v}},\underline{\mathbf{v}}) + 2k^2\|v_0+\chi_\Sigma v_2\|_{G\times Y}^2 \ge C_{\min}\|\underline{\mathbf{v}}\|_e^2$$

for all $\underline{\mathbf{v}}, \underline{\boldsymbol{\psi}} \in \mathcal{H}$.

Proof. The Gårding inequality is obvious from the definition of $\mathcal{B}$ in Theorem 4.2.1. The continuity of $\mathcal{B}$ follows from the multiplicative trace inequality as in [Mel95]. □

Also for the Maxwell equation, the two-scale sesquilinear form $\mathcal{B}$ from Theorem 4.2.3 is obviously continuous w.r.t. the energy norm (4.16) with a k-independent constant. For the Gårding-type inequality, however, the situation is more intricate: Due to the large kernel of the curl-operator, the L^2-term is no compact perturbation of the curl-term. As a remedy, we have to use a Helmholtz-type splitting. We have the following decomposition of $(\mathbf{v}_0,\mathbf{v}_3) \in \mathbf{H}_{\mathrm{imp}}(G)\times L^2(\Omega;\mathbf{H}_0(\operatorname{curl},\Sigma))$:

$$\begin{aligned}\mathbf{v}_0+\chi_\Sigma\mathbf{v}_3 = \mathbf{z}_0+\chi_\Sigma\mathbf{z}_3+\nabla\theta_0+\chi_\Sigma\nabla_y\theta_3 \qquad &\text{with}\quad \theta_0\in H_0^1(G),\quad \theta_3\in L^2(\Omega;H_0^1(\Sigma)),\\ \text{and}\quad 0 = (\mathbf{z}_0+\chi_\Sigma\mathbf{z}_3, \nabla\eta_0+\chi_\Sigma\nabla_y\eta_3)_{L^2(G\times Y)} \qquad &\forall(\eta_0,\eta_3)\in H_0^1(G)\times L^2(\Omega;H_0^1(\Sigma)).\end{aligned} \tag{4.17}$$

The orthogonality in the last line implies a weak divergence-free constraint on $\mathbf{z}_0+\chi_\Sigma\mathbf{z}_3$. In fact, we have $\operatorname{div}(\mu_{\mathrm{hom}}\mathbf{z}_0) = 0$ and $\operatorname{div}_y\mathbf{z}_3 = 0$ in the weak sense. See [Hip15] for a similar approach using the regular decomposition.

Lemma 4.3.3. *For the Maxwell equation (4.9), define the sign-flip isomorphism $SF : \mathcal{H}\to\mathcal{H}$ via*

$$SF(\underline{\mathbf{v}}) := (\mathbf{z}_0-\nabla\theta, \mathbf{v}_1, -v_2, \mathbf{z}_3-\nabla_y\theta_3)$$

with the Helmholtz-type decomposition from (4.17). There exist $C_g > 0$ and $\gamma_{\mathrm{ell}} > 0$, both independent of k, such that

$$\Big|\mathcal{B}(\underline{\mathbf{v}}, SF(\underline{\mathbf{v}})) + C_g k^2\|\mathbf{z}_0+\chi_\Sigma\mathbf{z}_3\|_{L^2(G\times Y)}^2 + C_g k\|(\mathbf{z}_0)_T\|_{L^2(\partial G)}^2\Big| \ge \gamma_{\mathrm{ell}}\|\underline{\mathbf{v}}\|_e^2. \tag{4.18}$$

Proof. The sign-flip isomorphism and the added term correct the "wrong" sign of the sesquilinear form $\mathcal{B}$ and make it coercive. Mixed terms between θ_0 and $\mathbf{z}_0$, or θ_3 and $\mathbf{z}_3$, respectively, either vanish due to the orthogonality of the Helmholtz decomposition or can be absorbed using Cauchy-Schwarz and Young's inequalities. □

Cell problems and effective parameters. As discussed in Sections 4.2.1 and 4.2.2, all cell problems, for the Helmholtz equation as well as for the Maxwell equation, are coercive so that their stability is an easy consequence.

Lemma 4.3.4. *For the Helmholtz equation, there are $C_{\mathrm{stab},1}, C_{\mathrm{stab},2} > 0$ depending only on ε_1^{-1}, ε_0^{-1}, Σ, Σ^*, and k_0, such that the correctors u_1 and u_2 from Theorem 4.2.2 satisfy*

$$\|u_1\|_{L^2(\Omega;H^1(\Sigma^*))} \le C_{\mathrm{stab},1}\|\nabla u_0\|_G \quad \text{and} \quad \|u_2\|_{1,k,\Omega\times\Sigma} \le C_{\mathrm{stab},2}\|u_0\|_{1,k,G}.$$

For the Maxwell equation, the correctors $\mathbf{u}_1$, u_2, and $\mathbf{u}_3$ from (4.14) fulfill

$$\begin{aligned} \|\operatorname{curl}_y \mathbf{u}_1\|_{L^2(\Omega\times\Sigma^*)} &\lesssim \|\operatorname{curl}\mathbf{u}_0\|_{L^2(\Omega)}, \\ k\|\nabla_y u_2\|_{L^2(\Omega\times\Sigma^*)} &\lesssim \|\mathbf{u}_0\|_{\mathrm{imp},k,\Omega}, \\ \|\operatorname{curl}_y \mathbf{u}_3\|_{L^2(\Omega\times\Sigma)} + k\|\mathbf{u}_3\|_{L^2(\Omega\times\Sigma)} &\lesssim \|\mathbf{u}_0\|_{\mathrm{imp},k,\Omega}. \end{aligned}$$

With this knowledge on the cell problems, we analyze the homogenized parameters.

Proposition 4.3.5. *The effective parameters have the following properties:*

- $(\varepsilon^{-1})_{\mathrm{hom}}$ *is a real-valued, symmetric positive definite matrix;*
- μ_{hom} *is complex-valued and a scalar in the two-dimensional case and a symmetric (not hermitian!) matrix in the three-dimensional case;*
- $|\mu_{\mathrm{hom}}| \le C_\mu$ *with a k-independent constant C_μ, where $|\cdot|$ stands for a matrixnorm in the three-dimensional case;*
- *for the Helmholtz equation, it holds that*

$$\operatorname{Im}(\mu_{\mathrm{hom}}) \ge C(\varepsilon_1, \Sigma, Y)\, k^{-2} > 0; \tag{4.19}$$

- *for the Maxwell equation,* $\operatorname{Im}(\mu_{\mathrm{hom}})$ *is symmetric positive definite (and hence μ_{hom} is invertible) and moreover,*

$$\operatorname{Im}(\mu_{\mathrm{hom}})\xi\cdot\xi^* \gtrsim k^{-2}|\xi|^2 \qquad \forall \xi \in \mathbb{C}^3.$$

Proof. The characterization of $(\varepsilon^{-1})_{\mathrm{hom}}$ is well known and follows from the ellipticity of the corresponding cell problem, see [All92] (two-dimensional case) and [CFS17] (three-dimensional case).

The upper bound on μ_{hom} easily follows from the stability bounds on u_2 (Helmholtz equation) and u_2 and $\mathbf{u}_3$ (Maxwell equation), respectively, given in Lemma 4.3.4.

For the lower bound on μ_{hom} for the Helmholtz equation, we use the representation of Lemma 4.2.5. Due to the positivity of $\operatorname{Im}(\varepsilon_1)$ and of the eigenvalues of the Laplacian we can deduce that

$$\operatorname{Im}(\mu_{\mathrm{hom}}) = \sum_n \frac{k^2\lambda_n \operatorname{Im}(\varepsilon_1)}{|\lambda_n - k^2\varepsilon_1|^2}\Big(\int_\Sigma \phi_n\, dy\Big)^2 \ge \frac{k^2\lambda_0 \operatorname{Im}(\varepsilon_1)}{|\lambda_0 - k^2\varepsilon_1|^2}\Big(\int_\Sigma \phi_0\, dy\Big)^2.$$

The first eigenfunction of the Dirichlet Laplacian is zero-free, thus $(\int_\Sigma \phi_0)^2 > 0$. As we consider the high-frequency case, w.l.o.g., we can assume $\lambda_0 \le k^2|\varepsilon_1|$ and then obtain $|\lambda_0 - k^2\varepsilon_1|^2 \le 2k^4|\varepsilon_1|^2$. This finally gives

$$\operatorname{Im}(\mu_{\mathrm{hom}}) \ge \frac{k^2\lambda_0 \operatorname{Im}(\varepsilon_1)}{2k^4|\varepsilon_1|^2}\Big(\int_\Sigma \phi_0\, dy\Big)^2 \ge \frac{C(\varepsilon,\Sigma)}{k^2} > 0.$$

For the Maxwell equation, we also use the equivalence to the effective μ given in [BBF17] (cf. Subsection 4.2.3). Then, we can use the following representation, which is equation (6.16) of [BBF17] (see also [LS16a]),

$$(\mu_{\text{hom}})_{jl} = \text{Id}_{jl} + \sum_n \frac{\varepsilon_1 k^2}{\lambda_n - \varepsilon_1 k^2} \Big(\int_Y \boldsymbol{\phi}_n \cdot \mathbf{e}_j \, dy \Big) \Big(\int_Y \boldsymbol{\phi}_n \cdot \mathbf{e}_l \, dy \Big), \qquad j,l = 1,2,3.$$

Here, $(\boldsymbol{\phi}_n, \lambda_n)$ are eigenfunctions and eigenvalues of a vector-Laplacian on Y. Then, the lower bound can be shown similar to the two-dimensional case above. □

The upper and lower bound on μ_{hom} can only be obtained for $\text{Im}(\varepsilon_1) > 0$. If we have an ideal lossless material (i.e., $\text{Im}(\varepsilon_1) = 0$), μ_{hom} is unbounded, see [BF04]. Moreover, the positivity of $\text{Im}(\mu_{\text{hom}})$ can also be proved directly from our representations of μ_{hom} using the cell problems. Hence, it also holds for nonconstant ε_1. The lower bound(s) on $\text{Im}(\mu_{\text{hom}})$ might be improved using more advanced methods for estimating eigenvalues and averages of eigenfunctions of the Laplacian. We emphasize that our numerical experiments in Section 4.6 do not show this severe k-dependency of the lower bound.

Higher regularity. Well-known regularity theory for elliptic diffusion problems [GT77, Pet10] and the Maxwell equation [Hip02] directly implies higher regularity of the correctors. We recall the notation $\mathbf{H}^s(\text{curl})$ from (2.12).

Lemma 4.3.6 (Higher regularity for the correctors)**.** *For the Helmholtz equation* (4.4)*, there are* $t_1, t_2 \in (\frac{1}{2}, 1]$ *such that* $u_1 \in L^2(\Omega; H^{1+t_1}(\Sigma^*))$*,* $u_2 \in L^2(\Omega; H^{1+t_2}(\Sigma))$ *and*

$$\begin{aligned} \|u_1\|_{L^2(\Omega;H^{1+t_1}(\Sigma^*))} &\leq C_{\text{reg},1} \|\nabla u_0\|_{L^2(\Omega)}, \\ \|u_2\|_{L^2(\Omega;H^{1+t_2}(\Sigma))} &\leq C_{\text{reg},2}\, k \|u_0\|_{1,k,\Omega}. \end{aligned}$$

For the Maxwell equation (4.9)*, there are* $t_j \in (\frac{1}{2}, 1]$*,* $j = 1,2,3$*, such that* $\mathbf{u}_1 \in L^2(\Omega; \mathbf{H}^{t_1}(\text{curl}, \Sigma^*))$*,* $u_2 \in L^2(\Omega; H^{1+t_2}(\Sigma^*))$*,* $\mathbf{u}_3 \in L^2(\Omega; \mathbf{H}^{t_3}(\text{curl}, \Sigma))$ *and*

$$\begin{aligned} \|\operatorname{curl}_y \mathbf{u}_1\|_{L^2(\Omega;\mathbf{H}^{t_1}(\Sigma^*))} &\lesssim \|\mathbf{u}_0\|_{\text{curl},k,G}, \\ k\|u_2\|_{L^2(\Omega;H^{1+t_2}(\Sigma^*))} &\lesssim \|\mathbf{u}_0\|_{\text{imp},k,G}, \\ \|\operatorname{curl}_y \mathbf{u}_3\|_{L^2(\Omega;\mathbf{H}^{t_3}(\Sigma))} + k\|\mathbf{u}_3\|_{L^2(\Omega;\mathbf{H}^{t_3}(\Sigma))} &\lesssim (1+k)\|\mathbf{u}_0\|_{\text{imp},k,G}. \end{aligned}$$

The regularity indices t_j only depend on the geometry of Σ. With a C^2-boundary of Σ, we have $t_j = 1$ for all j and both problems. For the numerical treatment, Σ is approximated by a Lipschitz domain with polygonal/polyhedral boundary. In general, the maximal regularity of problems posed on such a Lipschitz domain with polygonal/polyhedral boundary depends on the domain's maximal interior angle, see [CD00, Pet10]. We give the regularity results in their general form as polygonal/polyhedral (nonconvex) domains have to be considered in the process of boundary approximation in Section 4.4.

As the effective parameters $(\varepsilon^{-1})_{\text{hom}}$ and μ_{hom} are piecewise constant, we can only expect piecewise higher regularity for the macroscopic solutions u_0 and $\mathbf{u}_0$. We recall the notations $H^{1+s}_{pw}(G)$ and $\mathbf{H}^s_{pw}(\text{curl}, G)$ from (2.11) and (2.16). The higher regularity for the effective Maxwell (scattering) problem (4.13) is more difficult to derive than for the Helmholtz equation. For the definition of trace spaces in the Maxwell case, we use the notations $\mathbf{H}^s_T(\partial G)$ (2.17), $\mathbf{H}^s_\parallel(\partial G)$ (2.18) and $\mathbf{H}(\text{curl}_{\partial G})$ (2.19). We again refer to [BC01, BCS02, Moi11] for details on the spaces.

Proposition 4.3.7 (Higher regularity for the Helmholtz equation)**.** *Let* u_0 *be the solution to* (4.7) *with additional volume term* $f \in L^2(G)$ *and let* $g \in H^{1/2}(\partial G)$*.*

- *If* Ω *has* C^2*-boundary and* G *is convex, then* $u_0 \in H^2_{pw}(G)$*.*

- *If Ω has a polygonal Lipschitz boundary and G is convex, there is $s \in (\frac{1}{2}, 1]$ such that $u_0 \in H^{1+s}_{pw}(G)$.*

Moreover, we have the regularity estimate

$$\|u_0\|_{H^{1+s}_{pw}(G)} \lesssim k\|u_0\|_{1,k,G} + \|f\|_{L^2(G)} + \|g\|_{H^{1/2}(\partial G)}. \tag{4.20}$$

Proof. The assertion follows from classical regularity theory for elliptic and interface problems, see [Pet10]. We also refer to regularity results for the standard Helmholtz equation as, for instance, in [Mel95]. □

Proposition 4.3.8 (Higher regularity for the Maxwell equation)**.** *Let $\mathbf{u}_0$ be the solution to (4.13) with additional volume term $\mathbf{f} \in \mathbf{H}(\operatorname{div} 0, G)$.*

- *If Ω and G have C^2-boundary and $\mathbf{g} \in \mathbf{H}^{1/2}_T(\partial G)$, then $\mathbf{u}_0 \in \mathbf{H}^1_{pw}(\operatorname{curl}, G)$.*
- *If G is convex and $\mathbf{g} \in \mathbf{H}^{s_g}_T(\partial G)$ for $s_g \in (0, \frac{1}{2})$, there is $s \in (\frac{1}{2}, \frac{1}{2} + s_g]$, only depending on the shape of Ω and G, such that $\mathbf{u}_0 \in \mathbf{H}^s_{pw}(\operatorname{curl}, G)$.*

If $\mathbf{u}_0 \in \mathbf{H}^s_{pw}(G)$ with $s \in (\frac{1}{2}, 1]$, it also holds $\mathbf{u}_0 \in \mathbf{H}^{s-1/2}_{\|}(\partial G) \cap \mathbf{H}(\operatorname{curl}_{\partial G})$ with the regularity estimates

$$\begin{aligned} \|\operatorname{curl} \mathbf{u}_0\|_{\mathbf{H}^s_{pw}(G)} + k\|\mathbf{u}_0\|_{\mathbf{H}^s_{pw}(G)} &\lesssim (1+k)\|\mathbf{u}_0\|_{\operatorname{curl},k,G} + \|\mathbf{f}\|_{L^2(G)} + \|\mathbf{g}\|_{\mathbf{H}^{s_g}(\partial G)}, \\ k^{1/2}(\|\mathbf{u}_0\|_{\mathbf{H}^{s-1/2}_{\|}(\partial G)} + \|\operatorname{curl}_{\partial G}((\mathbf{u}_0)_T)\|_{L^2(\partial G)}) &\lesssim k^{1/2}\|\mathbf{u}_0\|_{\mathbf{H}^s_{pw}(G)}. \end{aligned} \tag{4.21}$$

Proof. The proof can be easily adopted from the case of scalar-valued constant material parameters in [Moi11]. We refer to [BGL13, CDN99] for other results on higher regularity of curl-curl-problems with piecewise constant coefficients. The regularity on the boundary directly follows from the continuity of trace operators, see [BC01, BCS02, BH03]. □

We see that the impedance boundary condition for the Maxwell equation is quite intricate w.r.t. higher regularity: Maximal regularity of $s = 1$ is never possible for polyhedral G, even under the assumption of convexity. Note that $\mathbf{u}_0 \in \mathbf{H}^s_{pw}(G)$ even for $\mathbf{g} \in L^2_T(\partial G)$, due to [Cos90].

Remark 4.3.9. The arguments from Lemma 4.3.6 also imply $\mathbf{z}_3 \in L^2(\Omega, \mathbf{H}^{t_3}(\operatorname{curl}, \Sigma))$ for the divergence-free part in the decomposition (4.17). According to [Cos90], it also holds $\mathbf{z}_0 \in \mathbf{H}^{1/2}_{pw}(G)$. Moreover, if $(\mathbf{z}_0)_T \in \mathbf{H}^r_T(\partial G)$ with $r \in (0, \frac{1}{2})$ for some reason (for instance, higher regularity of the function which is decomposed), the arguments of Proposition 4.3.8 imply $\mathbf{z}_0 \in \mathbf{H}^{1/2+r}_{pw}(G)$.

4.3.2 Stability results

Looking at Propositions 4.3.7 and 4.3.8, we note that these do not yet provide full regularity estimates in terms of the data. We additionally need a stability result, i.e., the dependence of the solution in its natural norm ($\|\cdot\|_{1,k,G}$ or $\|\cdot\|_{\mathrm{imp},k,G}$, respectively) on the data. Fredholm theory ensures such a stability estimate, but without explicit dependency of the involved constant on the wavenumber k. Therefore, we assume an explicit polynomial (in k) stability constant from now on.

Assumption 4.3.10. Assume that there is $q \in \mathbb{N}_0$ and $C_{\mathrm{stab},0} > 0$ such that the solution u_0 to (4.7) with additional right-hand side $f \in L^2(G)$ fulfills

$$\|u_0\|_{1,k,G} \leq C_{\mathrm{stab},0}\, k^q (\|f\|_{L^2(G)} \|g\|_{H^{1/2}(\partial G)}).$$

Assumption 4.3.11. Assume that there is $q \in \mathbb{N}_0$ and $C_{\text{stab}} > 0$ such that the solution $\mathbf{u}_0$ to (4.13) with additional volume term $\mathbf{f} \in \mathbf{H}(\operatorname{div} 0, G)$ and $\mathbf{g} \in \mathbf{H}_T^{s_g}(\partial G)$ with $s_g \in (0, \frac{1}{2})$ fulfills

$$\|\mathbf{u}_0\|_{\text{imp},k,G} \leq C_{\text{stab}}\, k^q (\|\mathbf{f}\|_{L^2(G)} + \|\mathbf{g}\|_{\mathbf{H}^{s_g}(\partial G)}). \tag{4.22}$$

As discussed in Section 2.1.3, such stability results are not trivial and most studies in the literature concern the case of constant coefficients. We refer to Section 2.1.3 for a detailed overview of existing results. The setting of the effective homogenized equations (4.7) and (4.13) exhibits new challenges for the stability analysis: discontinuous, namely piecewise constant, matrix-valued coefficients, and a partly complex parameter μ. In order to cope with these challenges, we first generalize the known results to the class of matrix-valued, Lipschitz continuous coefficients. We have the following propositions, proved in Section 4.3.3.

Proposition 4.3.12. *Assume that there is $\gamma > 0$ such that*

$$x \cdot \mathbf{n}_G \geq \gamma \text{ on } \partial G, \qquad\qquad x \cdot \mathbf{n}_\Omega \geq 0 \text{ on } \partial\Omega, \tag{4.23}$$

where $\mathbf{n}$ denotes the outer normal of the domain specified in the subscript. Let $v \in H^1(G)$ be the unique solution to

$$(A\nabla v, \nabla\psi)_G - k^2(\mu v, \psi)_G - ik(v,\psi)_{\partial G} = (f,\psi)_G + (g,\psi)_{\partial G} \qquad \forall \psi \in H^1(G)$$

for $f \in L^2(G)$ and $g \in L^2(\partial G)$. Moreover, we assume for A and μ that

- *$A \in W^{1,\infty}(G, \mathbb{R}^{2\times 2})$ is symmetric, bounded, and uniformly elliptic;*
- *the matrix $DA \cdot x$ with $(DA \cdot x)_{jl} := \sum_{n=1}^2 x_n\, \partial_n A_{jl}$, $j,l = 1,2$, is negative semidefinite;*
- *$\mu \in L^\infty(G;\mathbb{C})$ is piecewise constant, namely $\mu|_{G\setminus\overline{\Omega}} = \mu_2 \in \mathbb{R}_+$ and $\mu|_\Omega = \mu_1 \in \mathbb{C}$ with $\operatorname{Im}(\mu_1) > c_0 > 0$.*

Then, there exists a constant $C > 0$, which depends on the geometry, the upper bounds on μ and A, the ellipticity constant of A, and on k_0, but not on the Lipschitz constant of A or any other constant involving the derivative of A, such that

$$\begin{aligned}\|v\|_{1,k,G} \leq C\Big(&k^{1/2}(c_0^{-1/2}+1)\|g\|_{\partial G} + \|f\|_G + (c_0^{-1/2}+c_0^{-1})\|f\|_\Omega \\ &+ \frac{1}{k}(1 + c_0^{-1/2} + c_0^{-1})\|f\|_G + \frac{k}{c_0}\|f\|_{G\setminus\overline{\Omega}}\Big).\end{aligned} \tag{4.24}$$

Proposition 4.3.13. *Let Ω and G satisfy (4.23). Let $\mathbf{v} \in \mathbf{H}_{\text{imp}}(G)$ be the unique solution to*

$$\int_G A \operatorname{curl}\mathbf{v}\cdot\operatorname{curl}\boldsymbol{\psi}^* - k^2 B\mathbf{v}\cdot\boldsymbol{\psi}^*\,dx - ik\int_{\partial G}\beta\mathbf{v}_T\cdot\boldsymbol{\psi}_T^*\,d\sigma = \int_G \mathbf{f}\cdot\boldsymbol{\psi}^*\,dx + \int_{\partial G}\mathbf{g}\cdot\boldsymbol{\psi}_T^*\,d\sigma \quad \forall\boldsymbol{\psi}\in\mathbf{H}_{\text{imp}} \tag{4.25}$$

for $\mathbf{f} \in \mathbf{H}(\operatorname{div} 0, G)$, $\mathbf{g} \in L_T^2(\partial G)$. Moreover, we assume for $A, B \in W^{1,\infty}(G)$ that

- *A, B are real-valued symmetric positive definite;*
- *$A = \alpha(x)\,\mathrm{Id}$, $B = \beta(x)\,\mathrm{Id}$ in a neighborhood of the boundary ∂G with $\alpha, \beta > 0$, uniformly in x;*
- *the matrix $DA \cdot \mathbf{x}$ is negative semi-definite and $DB \cdot \mathbf{x}$ is positive semi-definite, where $(DA \cdot \mathbf{x})_{jl} := \sum_n x_n\, \partial_n A_{jl}$ and $DB \cdot \mathbf{x}$ is defined analogously.*

Then, there exists a constant $C > 0$, depending only on G, k_0, and the upper and lower bounds (eigenvalues) of A and B, but not on k, the data $\mathbf{f}$ and $\mathbf{g}$, or any derivative information of A and B, such that

$$\|\mathbf{v}\|_{\text{imp},k,G} \leq C\big(\|\mathbf{f}\|_{L^2(G)} + \|\mathbf{g}\|_{L^2(\partial G)}\big). \tag{4.26}$$

The geometrical assumption (4.23) is the common assumption for scattering problems, see [EM12, Het07, HMP11, Moi11, MS14]. It can, for example, be fulfilled if Ω is convex (and w.l.o.g. $0 \in \Omega$) and G is chosen appropriately. Note that the condition on the derivatives of the coefficient A are quite similar for both propositions. In order to obtain the propositions, a weaker condition on the Lipschitz constant of A and B would be sufficient, but then the constant in the stability estimates would depend on this Lipschitz constant. This is not desirable because we use the Lipschitz continuous coefficients to approximate discontinuous coefficients, where this Lipschitz constant blows up. We emphasize that a similar condition on the derivative of A is also imposed in [BGP17, GPS18]. Previous works on the Helmholtz equation, e.g., [BGP17, EM12, Mel95, MS11], have shown stability with $q = 0$, whereas (4.24) gives (for c_0 independent of k) $q = 1$. This is due to the fact that μ is complex on a part of the domain, see the discussion in Section 4.3.3. For the Maxwell equation, we obtain the same stability result as the literature [HMP11, Moi11]. Hence, Propositions 4.3.12 and 4.3.13 generalize the existing results to a wider class of coefficients and may be of interest on their own.

We now prove Assumptions 4.3.10 and 4.3.11 with $q = 3$ for the setting of the homogenized equations (4.7) and (4.13), respectively.

Theorem 4.3.14 (Stability for (4.7))**.** *Assume that Ω and G fulfill* (4.23)*. Furthermore assume that the (constant) matrix $(\varepsilon^{-1})_{\mathrm{hom}}|_{G\setminus\overline{\Omega}} - (\varepsilon^{-1})_{\mathrm{hom}}|_{\Omega}$ is negative semidefinite. Let u_0 be the solution to* (4.7) *with additional volume term $\int_G f\psi^* \, dx$ on the right-hand side for $f \in L^2(G)$. Then, there is $C_{\mathrm{stab},0}$ only depending on the geometry, the parameters, and k_0, such that u_0 satisfies the stability estimate*

$$\|u_0\|_{1,k,G} \leq C_{\mathrm{stab},0}(k^3\|f\|_{L^2(G\setminus\overline{\Omega})} + k^2\|f\|_{L^2(\Omega)} + k^{3/2}\|g\|_{L^2(\partial G)} + k^{-1}\|g\|_{H^{1/2}(\partial G)}).$$

Theorem 4.3.15 (Stability for (4.13))**.** *Let G and Ω fulfill* (4.23)*. Furthermore assume that the (constant) matrix $(\varepsilon^{-1})_{\mathrm{hom}}|_{G\setminus\overline{\Omega}} - (\varepsilon^{-1})_{\mathrm{hom}}|_{\Omega}$ is negative semidefinite. Let $\mathbf{u}_0$ be the solution to* (4.13) *with additional volume term $\int_G \mathbf{f} \cdot \boldsymbol{\psi}^* \, dx$ on the right-hand side for $\mathbf{f} \in \mathbf{H}(\mathrm{div}\, 0, G)$ and $\mathbf{g} \in \mathbf{H}_T^{s_g}(\partial G)$ with $s_g \in (0, \frac{1}{2})$. Then, there is C_{stab} only depending on the geometry, the parameters, and k_0, such that $\mathbf{u}_0$ satisfies the stability estimate*

$$\|\mathbf{u}_0\|_{\mathrm{imp},k,G} \leq C_{\mathrm{stab}}(k^3\|\mathbf{f}\|_{L^2(\Omega)} + k^2\|\mathbf{f}\|_{L^2(G\setminus\overline{\Omega})} + k^{3/2}\|\mathbf{g}\|_{L^2(\partial G)} + k^{-1}\|\mathbf{g}\|_{\mathbf{H}^{s_g}(\partial G)}).$$

The assumption on $(\varepsilon^{-1})_{\mathrm{hom}}$ in fact is an assumption on ε_0^{-1} and can be fulfilled for appropriate choices of material inside and outside the scatterer. It originates in the conditions on the derivative of A in Propositions 4.3.12 and 4.3.13. The different power in k to the results in the literature are caused by the complex-valued μ_{hom} (see the discussion above) and the dependency of $\mathrm{Im}(\mu_{\mathrm{hom}})$ on k (see Proposition 4.3.5). Note that Theorems 4.3.14 and 4.3.15 exhibit the same power in k.

In the following, we work with the (abstract) polynomial stability of Assumptions 4.3.10 and 4.3.11 and keep in mind that we have obtained an explicit (maximal) q in Theorems 4.3.14 and 4.3.15, respectively. For the Helmholtz equation we can directly deduce the (final) stability and regularity estimates as well as a bound on the inf-sup constant of the two-scale sesquilinear form, which is obtained similarly to [Het07, Mel95, Pet17].

Proposition 4.3.16. *If Assumption 4.3.10 is satisfied, the following hold:*

1. *The two-scale solution to* (4.4) *satisfies*

$$\|(u_0, u_1, u_2)\|_e \leq C_{\mathrm{stab},e}\, k^q(\|f\|_G + \|g\|_{H^{1/2}(\partial G)})$$

   for $C_{\mathrm{stab},e} := C_{\mathrm{stab},0}(1 + C_{\mathrm{stab},1} + C_{\mathrm{stab},2})$ with $C_{stab,1}$ and $C_{\mathrm{stab},2}$ from Lemma 4.3.4.

2. *There is $C_{\mathrm{reg},0} > 0$ such that the solution u_0 to* (4.7) *satisfies*

$$\|u_0\|_{H^{1+s}_{pw}(G)} \leq C_{\mathrm{reg},0}\, k^{q+1}(\|f\|_G + \|g\|_{H^{1/2}(\partial G)}).$$

3. The inf-sup constant of $\mathcal{B}$ can be bounded below as follows:

$$\inf_{\underline{\mathbf{v}}\in\mathcal{H}} \sup_{\underline{\boldsymbol{\psi}}\in\mathcal{H}} \frac{\operatorname{Re}\mathcal{B}(\underline{\mathbf{v}},\underline{\boldsymbol{\psi}})}{\|\underline{\mathbf{v}}\|_e\|\underline{\boldsymbol{\psi}}\|_e} \geq C_{\mathrm{inf},e}k^{-(q+1)} \tag{4.27}$$

for $C_{\mathrm{inf},e} := \min\{C_{\min},1\}(k_0^{-(q+1)} + C_{\mathrm{stab},e})^{-1}$ with $C_{\min}$ from Lemma 4.3.2.

Also for the Maxwell equation, we can conclude that the regularity constant from Proposition 4.3.8 behaves like k^{q+1}. Using the Helmholtz-type decomposition (4.17), we can deduce the same form of the inf-sup constant as for the Helmholtz equation.

Proposition 4.3.17. *Under Assumption 4.3.11, the sesquilinear form $\mathcal{B}$ is inf-sup stable with*

$$\inf_{\underline{\mathbf{v}}\in\mathcal{H}} \sup_{\underline{\mathbf{w}}\in\mathcal{H}} \frac{|\mathcal{B}(\underline{\mathbf{v}},\underline{\mathbf{w}})|}{\|\underline{\mathbf{v}}\|_e\,\|\underline{\mathbf{w}}\|_e} \geq \frac{\gamma_{\mathrm{ell}}}{1+C_{\mathrm{stab},e}C_g k^{q+1}},$$

where $C_{\mathrm{stab},e}$ is a stability constant for the two-scale equation (4.9) *and is k-independent.*

Proof. Let $\underline{\mathbf{v}} = (\mathbf{v}_0,\mathbf{v}_1,v_2,\mathbf{v}_3) \in \mathcal{H}$ be arbitrary and consider its Helmholtz-type decomposition according to (4.17). Let $\underline{\mathbf{w}} \in \mathcal{H}$ be the solution to the adjoint two-scale problem with volume term $C_g k^2(\mathbf{z}_0+\chi_\Sigma\mathbf{z}_3)$ and boundary term $C_g k(\mathbf{z}_0)_T$ on the right-hand side. Note that $\mathbf{z}_0$ and $\mathbf{z}_3$ are divergence-free and therefore, Assumption 4.3.11 can be applied. Recall the sign-flip isomorphism SF and the Gårding inequality from Lemma 4.3.3. On the one hand, due to the orthogonality of the Helmholtz decomposition we have

$$\begin{aligned}
&\big|\mathcal{B}(\underline{\mathbf{v}},SF(\underline{\mathbf{v}})+\underline{\mathbf{w}})\big| \\
&\quad= \Big|\mathcal{B}(\underline{\mathbf{v}},SF(\underline{\mathbf{v}})) + C_g k^2(\mathbf{z}_0+\chi_\Sigma\mathbf{z}_3,\mathbf{v}_0+\chi_{\Sigma^*}\nabla_y v_2+\chi_\Sigma\mathbf{v}_3)_{G\times Y} + C_g k((\mathbf{z}_0)_T,(\mathbf{v}_0)_T)_{\partial G}\Big| \\
&\quad= \Big|\mathcal{B}(\underline{\mathbf{v}},SF(\underline{\mathbf{v}})) + C_g k^2\|\mathbf{z}_0+\chi_\Sigma\mathbf{z}_3\|^2_{G\times Y} + C_g k\|(\mathbf{z}_0)_T\|^2_{\partial G}\Big| \geq \gamma_{\mathrm{ell}}\|\underline{\mathbf{v}}\|_e^2.
\end{aligned}$$

On the other hand, it holds that

$$\begin{aligned}
\|SF(\underline{\mathbf{v}})+\underline{\mathbf{w}}\|_e &\leq \|SF(\underline{\mathbf{v}})\|_e + \|\underline{\mathbf{w}}\|_e \leq \|\underline{\mathbf{v}}\|_e + C_{\mathrm{stab},e}k^q C_g\big(k^2\|\mathbf{z}_0+\chi_\Sigma\mathbf{z}_3\|_{G\times Y} + k\|(\mathbf{z}_0)_T\|_{\partial G}\big) \\
&\leq (1+C_{\mathrm{stab},e}C_g k^{q+1})\|\underline{\mathbf{v}}\|_e.
\end{aligned}$$

Combining both estimates finishes the proof. □

4.3.3 Proofs of the stability results

In this section, we give detailed proofs of Theorems 4.3.14 and 4.3.15. First, we show the (general) stability results Propositions 4.3.12 and 4.3.13. The proofs are based on Rellich-Morawetz identities. For the proof of Proposition 4.3.12, we use these identities indirectly by testing the variational form with the special function $x\cdot\nabla v$. This requires higher regularity of v in order to be an admissible test function (see the proof below), which can be relaxed when starting with the original Rellich-Morawetz identities.

Proof of Proposition 4.3.12. First step: With $\psi = v$ and considering the imaginary part of the variational problem, we obtain with Hölder and Young's inequalities

$$k^2c_0\|v\|^2_\Omega + k\|v\|^2_{\partial G} \lesssim \frac{1}{k}\|g\|^2_{\partial G} + \frac{1}{k^2c_0}\|f\|^2_\Omega + \|f\|_{G\setminus\overline{\Omega}}\|u\|_{G\setminus\overline{\Omega}}. \tag{4.28}$$

Second step: With $\psi = v$ and considering the real part of the variational problem, we obtain due to the boundedness of μ and the uniform ellipticity of A

$$\|\nabla v\|^2_G \lesssim k^2\|v\|^2_G + \frac{1}{2k^2}\|f\|^2_G + \frac{k^2}{2}\|v\|^2_G + \|g\|_{\partial G}\|v\|_{\partial G}.$$

Inserting (4.28) yields

$$\|\nabla v\|_G^2 \lesssim k^2\|v\|_{G\setminus\overline{\Omega}}^2 + \frac{1}{k^2}\Big(1+\frac{1}{c_0^2}\Big)\|f\|_G + \frac{1}{k^2c_0}\|f\|_\Omega^2 + \frac{1}{k}\Big(\frac{1}{c_0}+1\Big)\|g\|_{\partial G}^2. \tag{4.29}$$

Third step: It remains to estimate $\|v\|_{G\setminus\overline{\Omega}}^2$. For this, we insert $\psi = x\cdot\nabla v$ and consider the real part of the variational problem. Note that $x\cdot\nabla v$ is an admissible test function because we have $v\in H^2(G)$ due to the convexity of G and the smoothness of A, see [GT77]. We moreover use the identity $\partial_j(|w|^2) = 2\,\mathrm{Re}(w\partial_j w^*)$. For the first term of the sesquilinear form we obtain

$$\begin{aligned}\mathrm{Re}\Big\{\int_G A\nabla v\cdot\nabla(x\cdot\nabla v^*)\,dx\Big\} &= \mathrm{Re}\Big\{\int_G A\nabla v\cdot\nabla v^* + A\nabla v\cdot(D^2v^*)x\,dx\Big\}\\ &= \int_G A\nabla v\cdot\nabla v^* + \frac{1}{2}\nabla(A\nabla v\cdot\nabla v^*)\cdot x - \frac{1}{2}(DA\cdot x)\nabla v\cdot\nabla v^*\,dx\\ &= -\frac{1}{2}\int_G (DA\cdot x)\nabla v\cdot\nabla v^*\,dx + \frac{1}{2}\int_{\partial G} A\nabla v\cdot\nabla v^* x\cdot n\,d\sigma,\end{aligned}$$

where in the last equality we integrated by parts. As $DA\cdot x$ is negative semidefinite by assumption, the first term is nonnegative.

For the second part of the sesquilinear form we obtain

$$\begin{aligned}&\mathrm{Re}\Big\{\int_G k^2\mu v x\cdot\nabla v^*\,dx\Big\}\\ &\quad= \mathrm{Re}\Big\{\int_\Omega k^2\mu_1 v x\cdot\nabla v^*\,dx\Big\} + \frac{\mu_2}{2}\int_{G\setminus\overline{\Omega}} k^2 x\cdot\nabla|v|^2\,dx\\ &\quad= \mathrm{Re}\Big\{\int_\Omega k^2\mu_1 v x\cdot\nabla v^*\,dx\Big\} + \frac{\mu_2}{2}\int_{\partial(G\setminus\overline{\Omega})} k^2|v|^2 x\cdot n\,d\sigma - \int_{G\setminus\overline{\Omega}} k^2\mu_2|v|^2\,dx.\end{aligned}$$

Hence, for the test function $\psi = x\cdot\nabla v$ and the real part we deduce by combining the foregoing calculations

$$\begin{aligned}&\frac{1}{2}\int_{\partial G} A\nabla v\cdot\nabla v^* x\cdot n\,d\sigma + \int_{G\setminus\overline{\Omega}} k^2\mu_2|v|^2\,dx\\ &\quad\le \frac{1}{2}\int_{\partial(G\setminus\overline{\Omega})} k^2\mu_2|v|^2 x\cdot n\,d\sigma + \mathrm{Re}\Big\{\int_\Omega k^2\mu_1 v x\cdot\nabla v^*\,dx + \int_{\partial G} ikvx\cdot\nabla v^*\,d\sigma\Big\}\\ &\qquad+ \mathrm{Re}\Big\{\int_G fx\cdot\nabla v^*\,dx + \int_{\partial G} gx\cdot\nabla v^*\,d\sigma\Big\}.\end{aligned}$$

The assumption (4.23) on G and Ω implies that the first term on the right-hand side can be bounded from above by $k^2\|v\|_{\partial G}^2$. This yields after application of Hölder and Young's inequalities

$$k^2\|v\|_{G\setminus\overline{\Omega}}^2 \lesssim k^2\|v\|_\Omega\|\nabla v\|_\Omega + k^2\|v\|_{\partial G}^2 + \|g\|_{\partial G}^2 + \|f\|_G\|\nabla u\|_G.$$

Inserting the estimates (4.28) and (4.29) gives

$$\begin{aligned}k^2\|v\|_{G\setminus\overline{\Omega}}^2 \lesssim \|g\|_{\partial G}^2 + \frac{1}{kc_0}\|f\|_\Omega^2 + \eta_1 k^2\|v\|_{G\setminus\overline{\Omega}}^2 + \frac{1}{\eta_1}\|f\|_{G\setminus\overline{\Omega}}^2 + \frac{1}{\eta_2}\|f\|_G^2 + \eta_2 k^2\|v\|_{G\setminus\overline{\Omega}}^2\\ + \frac{\eta_2}{k^2}(1+c_0^{-2})\|f\|_G^2 + \frac{\eta_2}{k^2c_0}\|f\|_\Omega^2 + \frac{\eta_2}{k}(1+c_0^{-1})\|g\|_{\partial G}^2 + \frac{k^4}{\eta_2}\|v\|_\Omega^2.\end{aligned}$$

We choose η_1, η_2 independent of k such that $k^2\|v\|_{G\setminus\overline{\Omega}}$ can be hidden on the left-hand side and insert once more (4.28) for the last term on the right-hand side to obtain

$$k^2\|v\|^2_{G\setminus\overline{\Omega}} \lesssim \|g\|^2_{\partial G} + \|f\|^2_G + \Big(\frac{1}{kc_0} + \frac{1}{k^2c_0}\Big)\|f\|^2_\Omega + \Big(\frac{1}{k^2} + \frac{1}{k^2c_0^2}\Big)\|f\|^2_G + \Big(\frac{1}{k} + \frac{1}{kc_0}\Big)\|g\|^2_{\partial G} + \frac{k}{c_0}\|g\|^2_{\partial G} + \frac{1}{c_0^2}\|f\|^2_\Omega + \eta_3 k^2\|v\|^2_{G\setminus\overline{\Omega}} + \frac{k^2}{\eta_3 c_0^2}\|f\|^2_{G\setminus\overline{\Omega}}.$$

Choosing finally η_3 appropriately gives the desired estimate for $k^2\|v\|^2_{G\setminus\overline{\Omega}}$ and combination with (4.28) and (4.29) finishes the proof. □

If c_0 is independent of k, we obtain

$$\|v\|_{1,k,G} \lesssim \|f\|_\Omega + k\|f\|_{G\setminus\overline{\Omega}} + k^{1/2}\|g\|_{\partial G}.$$

On the other hand, if $c_0 > k^{-2}$ as in the case of μ_{hom} (see Proposition 4.3.5), we obtain

$$\|v\|_{1,k,G} \lesssim k^2\|f\|_\Omega + k^3\|f\|_{G\setminus\overline{\Omega}} + k^{3/2}\|g\|_{\partial G}.$$

The dependency of c_0 on k contributes by a factor k for g and a factor k^2 for f. However, even without this critical dependency of c_0 on k, the stability estimate is worse than the classical versions by about a factor k for f and $k^{1/2}$ for g. Looking into the proof, we can see that this is due to the difficult term $\int_\Omega k^2\mu v x\cdot\nabla v$. The presented proof can also be transferred (with minor adaptations) to the case where μ is real-valued and then yields the known stability of k^0. Hence, this also contributes to the analysis of [BGP17, MS17] by covering the case of matrix-valued A and it coincides with the recent findings of [GPS18].

For the proof of Proposition 4.3.13 we generalize the Rellich-Morawetz identities of [Moi11] to the case of Lipschitz continuous coefficients.

Lemma 4.3.18. *Let G be an open, bounded domain satisfying* (4.23). *Let $A, B \in W^{1,\infty}(G)$ be symmetric positive definite such that $DA\cdot\mathbf{x}$ is negative semidefinite, $DB\cdot\mathbf{x}$ is positive semidefinite and it holds $A = \alpha(x)\,\mathrm{Id}$ and $B = \beta(x)\,\mathrm{Id}$ with real-valued, uniformly positive α, β in a neighborhood of the boundary ∂G.*

- *If $\boldsymbol{\xi} \in \mathbf{H}(\mathrm{div}, G)$ with $\mathrm{curl}(A\boldsymbol{\xi}) \in L^2(G)$ and $\boldsymbol{\xi}_T \in L^2_T(\partial G)$, then*

$$\|A^{1/2}\boldsymbol{\xi}\|^2_{L^2(G)} \le 2\Big|\int_G \mathrm{curl}(A\boldsymbol{\xi})\cdot(\boldsymbol{\xi}^*\times\mathbf{x}) + (A\boldsymbol{\xi}\cdot\mathbf{x})\,\mathrm{div}\,\boldsymbol{\xi}^*\,dx\Big| + C(G)\int_{\partial G}\alpha|\boldsymbol{\xi}_T|^2\,d\sigma. \quad (4.30)$$

- *If $\boldsymbol{\xi} \in \mathbf{H}_{\text{imp}}(G)$ with $\mathrm{div}(B\boldsymbol{\xi}) \in L^2(G)$, then*

$$\|B^{1/2}\boldsymbol{\xi}\|^2_{L^2(G)} \le 2\Big|\int_G \mathrm{curl}\,\boldsymbol{\xi}^*\cdot(B\boldsymbol{\xi}\times\mathbf{x}) + (\boldsymbol{\xi}^*\cdot\mathbf{x})\,\mathrm{div}(B\boldsymbol{\xi})\,dx\Big| + C(G)\int_{\partial G}\beta|\boldsymbol{\xi}_T|^2\,d\sigma. \quad (4.31)$$

Proof. We only prove (4.30), the procedure for (4.31) is similar.

First step: Assuming that A and $\boldsymbol{\xi}$ are C^1, we derive the pointwise identity

$$\begin{aligned} 2\,\mathrm{Re}\big\{\mathrm{curl}(A\boldsymbol{\xi})\cdot(\boldsymbol{\xi}^*\times\mathbf{x})\big\} = {} & 2\,\mathrm{Re}\big\{\mathrm{div}((A\boldsymbol{\xi}\cdot\mathbf{x})\boldsymbol{\xi}^*) - (A\boldsymbol{\xi}\cdot\mathbf{x})\,\mathrm{div}\,\boldsymbol{\xi}^*\big\} \\ & - \mathrm{div}((A\boldsymbol{\xi}\cdot\boldsymbol{\xi}^*)\,\mathbf{x}) + A\boldsymbol{\xi}\cdot\boldsymbol{\xi}^* - (DA\cdot\mathbf{x})\boldsymbol{\xi}\cdot\boldsymbol{\xi}^*. \end{aligned} \quad (4.32)$$

This is a direct computation using product rules for $\mathrm{curl}(\mathbf{a}\times\mathbf{b})$, $\mathrm{div}(\mathbf{a}\times\mathbf{b})$, the vector calculus identity $\mathbf{a}\times(\mathbf{b}\times\mathbf{c}) = (\mathbf{a}\cdot\mathbf{c})\mathbf{b} - (\mathbf{a}\cdot\mathbf{b})\mathbf{c}$, and

$$2\,\mathrm{Re}(A\boldsymbol{\xi}\cdot(\mathbf{x}\cdot\nabla)\boldsymbol{\xi}^*) = \mathbf{x}\cdot\nabla(A\boldsymbol{\xi}\cdot\boldsymbol{\xi}^*) - (DA\cdot\mathbf{x})\boldsymbol{\xi}\cdot\boldsymbol{\xi}^* = \mathrm{div}((A\boldsymbol{\xi}\cdot\boldsymbol{\xi}^*)\mathbf{x}) - 3A\boldsymbol{\xi}\cdot\boldsymbol{\xi}^* - (DA\cdot\mathbf{x})\boldsymbol{\xi}\cdot\boldsymbol{\xi}^*.$$

Second step: We then integrate (4.32) over G with partial integration in the divergence-terms. Splitting the vector $\boldsymbol{\xi}$ in its tangential and normal components, $\boldsymbol{\xi}_T$ and $\boldsymbol{\xi}_N$, respectively, and using their orthogonality, we obtain

$$\begin{aligned}
&\int_G A\boldsymbol{\xi}\cdot\boldsymbol{\xi}^* - (DA\cdot\mathbf{x})\boldsymbol{\xi}\cdot\boldsymbol{\xi}^*\,dx \\
&= 2\,\mathrm{Re}\Big\{\int_G \operatorname{curl}(A\boldsymbol{\xi})\cdot(\boldsymbol{\xi}^*\times\mathbf{x}) + (A\boldsymbol{\xi}\cdot\mathbf{x})\,\operatorname{div}\boldsymbol{\xi}^*\,dx\Big\} - 2\,\mathrm{Re}\Big\{\int_{\partial G}((A\boldsymbol{\xi})_T\cdot\mathbf{x}_T)\,(\boldsymbol{\xi}^*\cdot\mathbf{n})\,d\sigma\Big\} \\
&\quad + \mathrm{Re}\Big\{\int_{\partial G}((A\boldsymbol{\xi})_T\cdot\boldsymbol{\xi}_T^* - (A\boldsymbol{\xi})_N\cdot\boldsymbol{\xi}_N^*)\,(\mathbf{x}\cdot\mathbf{n})\,d\sigma\Big\}.
\end{aligned} \tag{4.33}$$

Third step: Using the assumptions of this lemma in (4.33) gives

$$\begin{aligned}
\|A^{1/2}\boldsymbol{\xi}\|_{L^2(G)}^2 \le 2\Big|\int_G \operatorname{curl}(A\boldsymbol{\xi})\cdot(\boldsymbol{\xi}^*\times\mathbf{x}) + (A\boldsymbol{\xi}\cdot\mathbf{x})\operatorname{div}\boldsymbol{\xi}^*\,dx\Big| \\
+ \int_{\partial G}\alpha(|\boldsymbol{\xi}_T|^2 - |\boldsymbol{\xi}_N|^2)(\mathbf{x}\cdot\mathbf{n})\,d\sigma - 2\,\mathrm{Re}\Big\{\int_{\partial G}\alpha(\boldsymbol{\xi}_T\cdot\mathbf{x}_T)(\boldsymbol{\xi}^*\cdot\mathbf{n})\,d\sigma\Big\}.
\end{aligned}$$

We apply Young's inequality with weight $\mathbf{x}\cdot\mathbf{n}$ to the last term and obtain

$$\|A^{1/2}\boldsymbol{\xi}\|_{L^2(G)}^2 \le 2\Big|\int_G \operatorname{curl}(A\boldsymbol{\xi})\cdot(\boldsymbol{\xi}^*\times\mathbf{x}) + (A\boldsymbol{\xi}\cdot\mathbf{x})\operatorname{div}\boldsymbol{\xi}^*\,dx\Big| + C(G)\int_{\partial G}\alpha|\boldsymbol{\xi}_T|^2|\mathbf{x}|^2\,d\sigma,$$

which directly yields (4.30). The claim is then obtained by a density argument. □

For this lemma it is essential that A and B reduce to scalar values near the boundary because otherwise no connection between $(A\boldsymbol{\xi})_T$ and $\boldsymbol{\xi}_T$ etc. can be drawn. The previous lemma eliminated all terms with normal components on the boundary, which is necessary in order to apply this lemma to functions in $\mathbf{H}_{\mathrm{imp}}$. In other words, we do not have any knowledge about $\mathbf{v}_N$ on ∂G for the solution $\mathbf{v}$ to (4.25).

Proof of Proposition 4.3.13. We test (4.25) with $\boldsymbol{\psi} = \mathbf{v}$ and take the imaginary part to obtain

$$k\|\mathbf{v}_T\|_{L^2(\partial G)}^2 \lesssim \|\mathbf{f}\|_{L^2(G)}\|\mathbf{v}\|_{L^2(G)} + k^{-1}\|\mathbf{g}\|_{L^2(\partial G)}^2 \tag{4.34}$$

with a constant independent of k. Next, we observe that by testing with $\nabla\phi$ for $\phi\in H_0^1(G)$, we deduce $\operatorname{div}(B\mathbf{v}) = 0$. We apply (4.30) with $\xi = \operatorname{curl}\mathbf{v}$ and (4.31) with $\xi = \mathbf{v}$ and obtain

$$\begin{aligned}
&\|\mathbf{v}\|_{\mathrm{curl},k,G}^2 \\
&\lesssim 2\Big|\int_G \operatorname{curl}(A\mathbf{v})\cdot(\operatorname{curl}\mathbf{v}^*\times\mathbf{x}) + k^2\operatorname{curl}\mathbf{v}^*\cdot(B\mathbf{v}\times\mathbf{x})\,dx\Big| + \int_{\partial G}\alpha|\operatorname{curl}\mathbf{v}_T|^2 + \beta k^2|\mathbf{v}_T|^2\,d\sigma \\
&= 2\Big|\int_G \operatorname{curl}(A\mathbf{v})\cdot(\operatorname{curl}\mathbf{v}^*\times\mathbf{x}) - k^2 B\mathbf{v}\cdot(\operatorname{curl}\mathbf{v}^*\times\mathbf{x})\,dx\Big| + \int_{\partial G}\alpha|\operatorname{curl}\mathbf{v}_T|^2 + \beta k^2|\mathbf{v}_T|^2\,d\sigma \\
&\lesssim 2\Big|\int_G \mathbf{f}\cdot(\operatorname{curl}\mathbf{v}^*\times\mathbf{x})\,dx\Big| + \int_{\partial G}k^2|\mathbf{v}_T|^2 + |\mathbf{g}|^2\,d\sigma,
\end{aligned}$$

where we used (the strong form of) the PDE and the boundary condition. Applying Hölder and Young's inequalities for the first term on the right-hand side, we deduce

$$\|\mathbf{v}\|_{\mathrm{curl},k,G}^2 \lesssim \|\mathbf{f}\|_{L^2(G)}^2 + \|\mathbf{g}\|_{L^2(\partial G)}^2 + k^2\|\mathbf{v}_T\|_{L^2(\partial G)}^2.$$

Plugging in (4.34) and using once more Young's inequality we finally obtain the asserted estimate (4.26). □

We can now prove our main results, namely Theorems 4.3.14 and 4.3.15. For the Helmholtz equation, we only have to deal with the discontinuity of $(\varepsilon^{-1})_{\mathrm{hom}}$ across $\partial\Omega$, which is treated by a smoothing/approximation procedure, see [GPS18] for a similar idea.

Proof of Theorem 4.3.14. Because of the density of smooth functions in L^p for $p \in [1,\infty)$, for every $\eta > 0$ there exists $A_\eta \in C^\infty(\overline{G})$ such that $\|A_\eta - (\varepsilon^{-1})_{\mathrm{hom}}\|_{L^p} \leq \eta$. Furthermore, A_η can be chosen symmetric and uniformly elliptic with constants independent of η. Because of the additional assumption on $(\varepsilon^{-1})_{\mathrm{hom}}$ and the geometric setting, the assumption "$DA_\eta \cdot x$ is negative semidefinite" can also be fulfilled for all η small enough.

According to Proposition 4.3.12, the solution v_η to the Helmholtz problem with diffusion coefficient A_η (and sesquilinear form B_η) satisfies

$$\|v_\eta\|_{1,k,G} \lesssim k^3\|f\|_{G\setminus\overline{\Omega}} + k^2\|f\|_\Omega + k^{3/2}\|g\|_{\partial G}.$$

$u_0 - v_\eta$ satisfies $B_\eta(u_0 - v_\eta, \psi) = \int_G (A_\eta - (\varepsilon^{-1})_{\mathrm{hom}})\nabla u_0 \cdot \nabla\psi^*\,dx$ for all $\psi \in H^1(G)$. As the inf-sup constant of B_η is bounded below by k^{-4}, this gives

$$\|u_0 - v_\eta\|_{1,k,G} \lesssim k^4\|(A_\eta - (\varepsilon^{-1})_{\mathrm{hom}})\nabla u_0\|_G.$$

By the Hölder inequality, we have

$$\|(A_\eta - (\varepsilon^{-1})_{\mathrm{hom}})\nabla u_0\|_G \lesssim \|A_\eta - (\varepsilon^{-1})_{\mathrm{hom}}\|_{L^p(G)}\|\nabla u_0\|_{L^q(G)}$$

for all p, q with $1/p + 1/q = 1/2$. Choose q such that $L^q \subset H^s$ for some $s \in (0, 1/2]$ (e.g., $q = p = 4$ or $q = 8/3$, $p = 8$). Because of $\|A_\eta - (\varepsilon^{-1})_{\mathrm{hom}}\|_{L^p} \leq \eta$ and the estimate for the H^s-norm of u (see Proposition 4.3.7), we get

$$\|u_0 - v_\eta\|_{1,k,G} \lesssim k^4\eta(k\|u_0\|_{1,k,G} + \|f\|_G + \|g\|_{H^{1/2}(\partial G)}).$$

Then, choose $\eta = O(k^{-5})$ small enough. By the triangle inequality we finally obtain

$$\begin{aligned}\|u_0\|_{1,k,G} &\leq \|u_0 - v_\eta\|_{1,k,G} + \|v_\eta\|_{1,k,G} \\ &\lesssim \frac{1}{2}\|u_0\|_{1,k,G} + k^{-1}(\|f\|_G + \|g\|_{H^{1/2}(\partial G)}) + k^3\|f\|_{G\setminus\overline{\Omega}} + k^2\|f\|_\Omega + k^{3/2}\|g\|_{\partial G},\end{aligned}$$

which gives the claim. □

The same smoothing/approximation argument is also used for $(\varepsilon^{-1})_{\mathrm{hom}}$ for the Maxwell equation, while μ_{hom} is treated with a modified (auxiliary) problem. The procedure for μ_{hom} presented below could have also been used for the Helmholtz equation.

Proof of Theorem 4.3.15. Let $\widetilde{\mathbf{u}} \in \mathbf{H}_{\mathrm{imp}}$ be the solution to (4.13) with μ_{hom} replaced by $\tilde{\mu} = \mathrm{Id}$ on all of G. Using the higher regularity of $\widetilde{\mathbf{u}}$ (see Proposition 4.3.8) and an approximation argument for $(\varepsilon^{-1})_{\mathrm{hom}}$ similar to the one above gives the following stability

$$\|\widetilde{\mathbf{u}}\|_{\mathrm{imp},k,G} \lesssim \|\mathbf{f}\|_{L^2(G)} + \|\mathbf{g}\|_{L^2(\partial G)} + k^{-1}\|\mathbf{g}\|_{\mathbf{H}^{sg}(\partial G)}.$$

This also implies that the inf-sup constant behaves like k^{-1}, so that the above stability estimate holds also for $\tilde{\mathbf{f}} \in L^2(G)$ without the divergence-free constraint.

The difference function $\mathbf{u}_0 - \widetilde{\mathbf{u}}$ solves (4.13) with μ_{hom} replaced by $\tilde{\mu}$ and right-hand side (volume term) $k^2(\tilde{\mu} - \mu_{\mathrm{hom}})\mathbf{u}_0 \in L^2(G)$. Note that the right-hand side vanishes outside Ω. Hence, the previous arguments together with the triangle inequality yield

$$\|\mathbf{u}_0\|_{\mathrm{imp},k,G} \lesssim \|\mathbf{f}\|_{L^2(G)} + \|\mathbf{g}\|_{L^2(\partial G)} + k^{-1}\|\mathbf{g}\|_{\mathbf{H}^{sg}(\partial G)} + k^2\|\mathbf{u}\|_{L^2(\Omega)}.$$

It thus remains to bound $\|\mathbf{u}_0\|_{L^2(\Omega)}$. Inserting $\boldsymbol{\psi} = \mathbf{u}_0$ into (4.13) and considering the imaginary part gives

$$k^2 c_0 \|\mathbf{u}_0\|^2_{L^2(\Omega)} \lesssim k^{-1}\|\mathbf{g}\|^2_{L^2(\partial G)} + k^{-2}c_0^{-1}\|\mathbf{f}\|^2_{L^2(\Omega)} + \|\mathbf{f}\|_{L^2(G\setminus\overline{\Omega})}\|\mathbf{u}_0\|_{L^2(G\setminus\overline{\Omega})},$$

where c_0 denotes the lower bound on $\mathrm{Im}(\mu_{\mathrm{hom}})$. Together with Young's inequality and the foregoing estimates this finally gives

$$\|\mathbf{u}_0\|_{\mathrm{imp},k,G} \lesssim c_0^{-1}\|\mathbf{f}\|_{L^2(\Omega)} + kc_0^{-1}\|\mathbf{f}\|_{L^2(G\setminus\overline{\Omega})} + k^{1/2}c_0^{-1/2}\|\mathbf{g}\|_{L^2(\partial G)} + k^{-1}\|\mathbf{g}\|_{\mathbf{H}^{sg}(\partial G)}.$$

Setting $c_0 = k^{-2}$ according to Proposition 4.3.5 finishes the proof. □

The proof shows that if the lower bound c_0 on $\mathrm{Im}(\mu_{\mathrm{hom}})$ is independent of k, we get the improved stability estimate

$$\|\mathbf{u}_0\|_{\mathrm{imp},k,G} \lesssim \|\mathbf{f}\|_{L^2(\Omega)} + k\|\mathbf{f}\|_{L^2(G\setminus\overline{\Omega})} + k^{1/2}\|\mathbf{g}\|_{L^2(\partial G)} + k^{-1}\|\mathbf{g}\|_{\mathbf{H}^{sg}(\partial G)}.$$

Here again, the powers in k agree with the Helmholtz case, cf. the estimates after the proof of Proposition 4.3.12.

4.4 Multiscale method and numerical analysis

As explained in the introduction and in Section 2.3.2, a direct discretization of the heterogeneous problems (4.2) and (4.3) is infeasible due to the necessary small mesh width. We study the Heterogeneous Multiscale Method (HMM) for high contrast problems in this section. The method is introduced in Section 4.4.1 for the Helmholtz and the Maxwell equation. A rigorous numerical analysis is performed in Section 4.4.2. The proofs are detailed in Section 4.4.3 for the Helmholtz equation and in Section 4.4.4 for the Maxwell equation.

4.4.1 The Heterogeneous Multiscale Method

Following the original idea of [Ohl05] for elliptic diffusion problems, we concentrate on the direct discretization of the two-scale equations (4.4) and (4.9). This point of view is vital for the numerical analysis in Section 4.4.2. However, we also shortly explain how this direct discretization can be decoupled into macroscopic and microscopic computations in the fashion of the HMM as originally presented in [EE03, EE05]. We also refer to Section 2.3.3 for details about this equivalence and how it can be proved.

In this and the next section, we assume that Σ, Ω, and G are polygonally bounded (in contrast to the C^2-boundaries in the analytic sections). The reason is that the C^2-boundaries can be approximated by a series of more and more fitting polygonal boundaries. This procedure of boundary approximation results in nonconforming methods, i.e., the discrete function spaces are no subspaces of the analytic ones. We avoid this difficulty in our numerical analysis by assuming polygonally bounded domains by now. The new assumption reduces the possible higher regularity of solutions as discussed in Section 4.3. However, we can always obtain the maximal regularity in the limit of polygonal approximation of C^2-boundaries, which we have in mind as an application case. We assume throughout this section that G has been chosen as a convex domain.

Denote by $\mathcal{T}_H = \{T_j | j \in J\}$ and $\mathcal{T}_h = \{S_l | l \in I\}$ with index sets J, I regular and shape regular simplicial partitions of G and Y, respectively. Additionally, we assume that $\mathcal{T}_H$ resolves the partition into Ω and $G \setminus \overline{\Omega}$ and that $\mathcal{T}_h$ resolves the partition of Y into Σ and Σ^* and is periodic in the sense of Section 2.3.3 (no hanging nodes or edges over the periodic boundary). By $\mathcal{T}_h(\Sigma^*)$ and $\mathcal{T}_h(\Sigma)$, we denote the parts of the triangulation $\mathcal{T}_h$ belonging to Σ^* and Σ, respectively. We define the global mesh sizes $H := \max_{j\in J} \mathrm{diam}(T_j)$ and $h := \max_{l\in I} \mathrm{diam}(S_l)$.

We use the following (standard) conforming finite element spaces, associated with the meshes $\mathcal{T}_H$ or $\mathcal{T}_h$,

- classical linear Lagrange elements $\mathcal{S}(\mathcal{T}_H) \subset H^1(G)$, $\widetilde{\mathcal{S}}(\mathcal{T}_h(\Sigma^*)) \subset H^1_{\sharp,0}(\Sigma^*)$ (adopted to periodic boundary conditions and zero mean value), and $\mathring{\mathcal{S}}(\mathcal{T}_h(\Sigma)) \subset H^1_0(\Sigma)$;
- Nédélec edge elements of lowest order $\mathcal{N}(\mathcal{T}_H) \subset \mathbf{H}_{\mathrm{imp}}(G)$, $\widetilde{\mathcal{N}}(\mathcal{T}_h(\Sigma^*)) \subset \widetilde{\mathbf{H}}_\sharp(\mathrm{curl}, \Sigma^*)$, and $\mathring{\mathcal{N}}(\mathcal{T}_h(\Sigma)) \subset \mathbf{H}_0(\mathrm{curl}, \Sigma)$.

The linear Lagrange space $\mathcal{S}$ and the lowest order Nédélec space $\mathcal{N}$ are defined in Section 2.2.2. The space $\widetilde{\mathcal{N}}(\mathcal{T}_h(\Sigma^*))$ is used to discretize the first corrector $\mathbf{u}_1$ for the Maxwell equation. As discussed in Section 4.2.2, we are only interested in its curl. In order to obtain a unique solution $\mathbf{u}_{h,1}$, we have to apply a suitable stabilization procedure to the corresponding cell problem, such as a Lagrange multiplier or weighted divergence regularization, see [CD00, CD02]. As an alternative, we can also directly discretize $\mathrm{curl}_y \mathbf{u}_1(x, \cdot)$ in a suitable finite element space.

These function spaces are used to build up a two-scale function space $\mathbf{V}_{H,h}$ for the Galerkin method.

Definition 4.4.1 (HMM).

- For the Helmholtz equation, set

$$\mathbf{V}_{H,h} := \mathcal{S}(\mathcal{T}_H) \times L^2(\Omega; \widetilde{\mathcal{S}}(\mathcal{T}_h(\Sigma^*))) \times L^2(\Omega; \mathring{\mathcal{S}}(\mathcal{T}_h(\Sigma))).$$

  We then seek the discrete two-scale solution $\mathbf{u}_{H,h} := (u_H, u_{h,1}, u_{h,2}) \in \mathbf{V}_{H,h}$ such that

$$\mathcal{B}(\mathbf{u}_{H,h}, \boldsymbol{\psi}_{H,h}) = (g, \psi_H)_{L^2(\partial G)} \qquad \forall \boldsymbol{\psi}_{H,h} := (\psi_H, \psi_{h,1}, \psi_{h,2}) \in \mathbf{V}_{H,h} \tag{4.35}$$

  with the two-scale sesquilinear form defined in Theorem 4.2.1.

- For the Maxwell equation, set

$$\mathbf{V}_{H,h} := \mathcal{N}(\mathcal{T}_H) \times L^2(\Omega; \widetilde{\mathcal{N}}(\mathcal{T}_h(\Sigma))) \times L^2(\Omega; \widetilde{\mathcal{S}}(\mathcal{T}_h(\Sigma^*))) \times L^2(\Omega; \mathring{\mathcal{N}}(\mathcal{T}_h(\Sigma))).$$

  We then seek the discrete two-scale solution $\mathbf{u}_{H,h} := (\mathbf{u}_H, \mathbf{u}_{h,1}, u_{h,2}, \mathbf{u}_{h,3}) \in \mathbf{V}_{H,h}$ such that

$$\mathcal{B}(\mathbf{u}_{H,h}, \boldsymbol{\psi}_{H,h}) = (\mathbf{g}, (\boldsymbol{\psi}_H)_T)_{L^2(\partial G)} \qquad \forall \boldsymbol{\psi}_{H,h} := (\boldsymbol{\psi}_H, \boldsymbol{\psi}_{h,1}, \psi_{h,2}, \boldsymbol{\psi}_{h,3}) \in \mathbf{V}_{H,h} \tag{4.36}$$

  with the two-scale sesquilinear form defined in Theorem 4.2.3.

In order to evaluate the integrals over G in $\mathcal{B}$ for both cases, we introduce quadrature rules, which are exact for the given ansatz and test spaces. In our case of piecewise linear functions, it suffices to choose the one-point rule $\{|T_j|, x_j\}$ with the barycenters x_j for the part with the differential operator and a second order quadrature rule $Q_j^{(2)} := \{q_l, x_l\}_l$ with $l = 1, \ldots, d+1$ on each simplex T_j for the identity part. As a consequence, the functions $u_{h,1}$ and $u_{h,2}$ as well as $\mathbf{u}_{h,1}$, $u_{h,2}$ and $\mathbf{u}_{h,3}$ are also discretized w.r.t. the macroscopic variable x: In fact, we have

- $u_{h,1} \in \mathcal{P}^0(\mathcal{T}_H(\Omega); \widetilde{\mathcal{S}}(\mathcal{T}_h(\Sigma^*)))$ and $u_{h,2} \in \mathcal{P}^1(\mathcal{T}_H(\Omega); \mathring{\mathcal{S}}(\mathcal{T}_h(\Sigma)))$ for the Helmholtz equation;
- for the Maxwell equation: $\mathbf{u}_{h,1} \in \mathcal{P}^0(\mathcal{T}_H(\Omega); \widetilde{\mathcal{N}}(\mathcal{T}_h(\Sigma^*)))$, $u_{h,2} \in \mathcal{P}^1(\mathcal{T}_H(\Omega); \widetilde{\mathcal{S}}(\mathcal{T}_h(\Sigma^*)))$, and $\mathbf{u}_{h,3} \in \mathcal{P}^1(\mathcal{T}_H(\Omega); \mathring{\mathcal{N}}(\mathcal{T}_h(\Sigma)))$.

The space of discontinuous, piecewise p-polynomial (w.r.t. x) discrete functions $\mathcal{P}^p$ is defined in Section 2.2.2. Note that $u_{h,2}$ (for both cases) and $\mathbf{u}_{h,3}$ (for the Maxwell equation) are piecewise x-linear discrete functions, since $Q^{(2)}$ consists of $d+1$ quadrature points on each simplex.

The functions $u_{h,1}$ and $u_{h,2}$ as well as $\mathbf{u}_{h,1}$, $u_{h,2}$, and $\mathbf{u}_{h,3}$ are the discrete counterparts of the analytical correctors u_1 and u_2 and $\mathbf{u}_1$, u_2, and $\mathbf{u}_3$, respectively. These corrections are an important part of the HMM-approximation and cannot be neglected as higher order

terms: For the Maxwell equation, we saw in Chapter 3 that $u_{h,2}$ is necessary to obtain good L^2-approximations. Additionally, the correctors $u_{h,2}$ for the Helmholtz equation and $u_{h,2}$ and $\mathbf{u}_{h,3}$ for the Maxwell equation, respectively, encode the behavior of the solution inside the inclusions, see Section 4.6.

The discrete correctors depend on the macroscopic discrete function u_H or $\mathbf{u}_H$, respectively, and solve discretized cell problems. These cell problems, posed on the unit cell Y, can be transferred back to δ-scaled and shifted cells $Y_j^\delta = x_j + \delta Y$, where x_j is a macroscopic quadrature point. This finally gives an equivalent formulation of (4.35) and (4.36) in the form of a (traditional) HMM. The formulation using a macroscopic sesquilinear form with local cell reconstructions is used in practical implementations. We emphasize that the presented HMM also works for locally periodic ε_0^{-1} and ε_1^{-1} depending on x and y. The HMM and its interpretation as discretization of a fully coupled two-scale equation can even be applied to nonperiodic problems, as demonstrated in [HO15].

4.4.2 Numerical analysis

Based on the definition of the HMM as direct discretization of the two-scale equation (Definition 4.4.1), we analyze its well-posedness and quasi-optimality in Theorems 4.4.2 and 4.4.3. This quasi-optimality is a kind of Céa lemma for indefinite sesquilinear forms and directly leads to a priori estimates in Corollaries 4.4.4 and 4.4.5 as well as Theorem 4.4.6.

All estimates are derived in the two-scale energy norms (4.15) and (4.16). Let us furthermore define the (discretization) error $\mathbf{e} := \underline{\mathbf{u}} - \mathbf{u}_{H,h}$, where $\underline{\mathbf{u}}$ solves the (analytical) two-scale equation (4.4) or (4.9), respectively, and $\mathbf{u}_{H,h}$ is the discrete two-scale solution solving (4.35) or (4.36), respectively. For the Helmholtz equation, $\mathbf{e} = (e_0, e_1, e_2)$ with $e_0 = u_0 - u_H$, $e_1 = u_1 - u_{h,1}$, $e_2 = u_2 - u_{h,2}$; for the Maxwell equation $\mathbf{e} = (e_0, e_1, e_2, e_3)$ with $e_0 = \mathbf{u}_0 - \mathbf{u}_H$, $e_1 = \mathbf{u}_1 - \mathbf{u}_{h,1}$, $e_2 = u_2 - u_{h,2}$ and $e_3 = \mathbf{u}_3 - \mathbf{u}_{h,3}$. We only estimate these (discretization) errors and leave the modeling error, introduced by homogenization, apart. Unfortunately, there is no estimate in δ available in the literature for this homogenization error.

In the h-version of the Finite Element method we consider in this thesis, the meshes $\mathcal{T}_H$ and $\mathcal{T}_h$ are refined (thus H and h are decreased) in order to obtain a better approximation. Hence, we introduce constants $H_{\max} > 0$ and $h_{\max} > 0$ such that $H \leq H_{\max}$ and $h \leq h_{\max}$ for all considered grids.

For the Helmholtz equation, we explicitly keep track of the appearing constants. This also gives an idea on how the constants hidden in $\lesssim$ (which are independent of k, H and h) for the Maxwell equation look like. We recall the following notations on constants: C_B is the continuity constant of $\mathcal{B}$ (for both cases), s and t_j are the regularity exponents from Lemma 4.3.6 and Propositions 4.3.7 and 4.3.8, and k_0 is the lower bound on k. C_{approx} denotes the approximation properties constant, see (4.43) and Lemma 4.4.7 below. For the Helmholtz equation, we have the regularity constants $C_{\text{reg},j}$, $j = 0, 1, 2$ (Lemma 4.3.6 and Proposition 4.3.16), the stability constant $C_{\text{stab},e}$ (Proposition 4.3.16), and the constant $C_{\min}$ from the Gårding inequality (Lemma 4.3.2). For the Maxwell equation, we recall the constants C_g and γ_{ell} from the Gårding-type inequality (Lemma 4.3.3).

Theorem 4.4.2 (Quasi-optimality for the Helmholtz equation)**.** *Let Assumption 4.3.10 be satisfied. If the wavenumber k and the mesh widths H and h are coupled by*

$$\begin{aligned}
k^{q+2}H^s &\leq -\frac{k_0^{q+1}}{2H_{\max}^{1-s}} + \sqrt{\frac{k_0^{q+1}}{H_{\max}^{1-s}}\Big(\frac{C_{\min}}{12C_BC_{\text{approx}}C_{\text{reg},0}} + \frac{k_0^{q+1}}{4H_{\max}^{1-s}}\Big)},\\
k^{q+1}h^{t_1} &\leq \frac{C_{\min}}{12C_BC_{\text{approx}}C_{\text{reg},1}C_{\text{stab},e}},\\
k^{q+2}h^{t_2} &\leq -\frac{k_0^{q+1}}{2h_{\max}^{1-t_2}} + \sqrt{\frac{k_0^{q+1}}{h_{\max}^{1-t_2}}\Big(\frac{C_{\min}}{12C_BC_{\text{approx}}C_{\text{reg},2}C_{\text{stab},e}} + \frac{k_0^{q+1}}{4h_{\max}^{1-t_2}}\Big)},
\end{aligned} \tag{4.37}$$

we have the discrete inf-sup condition

$$\inf_{\mathbf{v}_{H,h}\in\mathbf{V}_{H,h}}\sup_{\boldsymbol{\psi}_{H,h}\in\mathbf{V}_{H,h}}\frac{\operatorname{Re}\mathcal{B}(\mathbf{v}_{H,h},\boldsymbol{\psi}_{H,h})}{\|\mathbf{v}_{H,h}\|_e\,\|\boldsymbol{\psi}_{H,h}\|_e}\geq\frac{C_{\mathrm{HMM}}}{k^{q+1}}\tag{4.38}$$

with $C_{\mathrm{HMM}}:=\frac{C_{\min}}{2}(k_0^{-(q+1)}(1+\frac{C_{\min}}{2C_B})+C_{\mathrm{stab},e})^{-1}$ *and the error between the analytical and discrete two-scale solution satisfies*

$$\|(e_0,e_1,e_2)\|_e\leq\frac{2C_B}{C_{\min}}\inf_{\mathbf{v}_{H,h}\in\mathbf{V}_{H,h}}\|\underline{\mathbf{u}}-\mathbf{v}_{H,h}\|_e.\tag{4.39}$$

The proof is postponed to Section 4.4.3. The resolution conditions (4.37) can (roughly) be summarized as $k^{q+2}(H^s+h^{t_1}+h^{t_2})\lesssim 1$, this is discussed in detail further below. A similar result as Theorem 4.4.2 is also obtained in the three-dimensional case. However, the resolution condition includes a second part due to the boundary terms, which are part of the energy norm for the Maxwell equation.

Theorem 4.4.3 (Quasi-optimality for the Maxwell equation)**.** *Let Assumption 4.3.11 be fulfilled. Under the resolution condition*

$$C_BC_{\mathrm{approx}}(C_g+2)(k^{q+2}(H^s+h^{t_1}+h^{t_2}+h^{t_3})+k^{q+3/2}H^{s-1/2})\leq\gamma_{\mathrm{ell}}/2,\tag{4.40}$$

we have the discrete inf-sup condition

$$\inf_{\mathbf{v}_{H,h}\in\mathbf{V}_{H,h}}\sup_{\boldsymbol{\psi}_{H,h}\in\mathbf{V}_{H,h}}\frac{|\mathcal{B}(\mathbf{v}_{H,h},\boldsymbol{\psi}_{H,h})|}{\|\mathbf{v}_{H,h}\|_e\|\boldsymbol{\psi}_{H,h}\|_e}\geq\frac{\gamma_{\mathrm{ell}}}{2+\gamma_{\mathrm{ell}}/C_B+2C_gC_{\mathrm{stab},e}k^{q+1}}\sim k^{-(q+1)}\tag{4.41}$$

and the error between the analytical and discrete two-scale solution satisfies

$$\|(e_0,e_1,e_2,e_3)\|_e\leq\frac{2C_B}{\gamma_{\mathrm{ell}}}\inf_{\mathbf{v}_{H,h}\in\mathbf{V}_{H,h}}\|\underline{\mathbf{u}}-\mathbf{v}_{H,h}\|_e.\tag{4.42}$$

The proof is postponed to Section 4.4.4. Together with the approximation results (4.43) and of Lemma 4.4.7, the quasi-optimality yields explicit convergence rates.

Corollary 4.4.4 (A priori estimate for the Helmholtz equation)**.** *Let the assumptions of Theorem 4.4.2 be fulfilled. Then, the energy error can be estimated as*

$$\|(e_0,e_1,e_2)\|_e\lesssim\big((H^s+h^{t_2})k^{q+1}+k^qh^{t_1}\big)\|g\|_{H^{1/2}(\partial G)}.$$

Assuming the maximal possible regularity $s=t_1=t_2=1$ *as discussed in Section 4.3.1, the energy error converges with rate* $k^{q+1}(H+h)$ *under the resolution assumption that* $k^{q+2}(H+h)$ *is sufficiently small.*

Corollary 4.4.5 (A priori estimate for the Maxwell equation I)**.** *Let the assumptions of Theorem 4.4.3 be fulfilled. Then, the energy error can be estimated as*

$$\|(e_0,e_1,e_2,e_3)\|_e\lesssim(k^{q+1}(H^s+h^{t_1}+h^{t_2}+h^{t_3})+k^{q+1/2}H^{s-1/2})\|\mathbf{g}\|_{\mathbf{H}^{s_g}(\partial G)}.$$

Assuming the maximal possible regularity $s=t_1=t_2=t_3=1$ *as discussed in Section 4.3.1, the energy error converges with rate* $k^{q+1}(H+h)+k^{q+1/2}H^{1/2}$ *under the resolution assumption that* $k^{q+2}(H+h)+k^{q+3/2}H^{1/2}$ *is sufficiently small.*

The a priori estimates give linear convergence for the volume terms and, in the case of the Maxwell equation, a convergence rate of $H^{1/2}$ for the boundary terms. These are classical optimal convergence rates under mesh refinement for the Helmholtz equation, see [MS11, Sau06] and for problems posed in $\mathbf{H}(\mathrm{curl})$, see [EG17a, GM12].

For the Helmholtz equation, dual problems can be used to obtain the estimate

$$\|e_0 + \chi_\Sigma e_2\|_{L^2(G\times Y)} \lesssim (k^{q+1}(H^s + h^{t_2}) + k^q h^{t_1})\|(e_0, e_1, e_2)\|_e$$

as it will be done in the proof of Theorem 4.4.2. This is the classical Aubin–Nitsche argument to obtain higher convergence rates in the L^2-norm, for details see [EM14, MS11] for classical Helmholtz problems. However, for the Maxwell equation, we have to go over to dual norms to obtain higher order convergence, as discussed in [GHV18, HOV16b].

Theorem 4.4.6 (A priori estimate for the Maxwell equation II)**.** *Under the assumptions of Theorem 4.4.3, let $e_0 + \chi_\Sigma e_3 = \mathbf{z}_0 + \chi_\Sigma \mathbf{z}_3 + \nabla\theta_0 + \chi_\Sigma \nabla_y \theta_3$ be the Helmholtz decomposition of the error according to* (4.17)*. This decomposition satisfies the following a priori estimate*

$$\|\mathbf{z}_0+\chi_\Sigma \mathbf{z}_3\|_{L^2(G\times Y)} + \|\theta_0+\chi_\Sigma \theta_3\|_{L^2(G\times Y)} \lesssim (k^{q+1}(H^s+h^{t_1}+h^{t_2}+h^{t_3}) + k^{q+1/2}H^{s-1/2})\|\mathbf{e}\|_e.$$

The proof is postponed to Section 4.4.4.

As has already been remarked in [HOV16b, Ohl05], the definition of the HMM as a direct discretization of the two-scale equation, see (4.35) and (4.36), is the crucial starting point for all kinds of error estimates and, in particular, enables us to derive a posteriori error estimates. Concerning a posteriori error estimates in general, we refer to [DS13, IB01] for the Helmholtz equation and to [HOV16b, Sch08] for the Maxwell equation.

Discussion of the resolution conditions. Under the stability estimate from Assumption 4.3.10, the resolution conditions (4.37) for the Helmholtz equation are optimal/unavoidable for standard finite element methods and the multiscale setting: As the second cell problem depends on k, it is natural that h enters the condition (4.37). We emphasize that h denotes the mesh width of the unit square mesh and is thus not coupled to δ in any way. Assuming $q = 0$, as is the case for classical Helmholtz problems, we regain the usual condition "$k^2(H+h)$ sufficiently small", cf., e.g., [EM12, Het07, Ihl98, Mel95, MS11]. This latter resolution condition is also what we experience in our numerical experiments in Section 4.6.1.

The resolution condition (4.40) for the Maxwell equation reads $k^2(H + h) + k^{3/2}H^{1/2} \lesssim 1$ if we assume maximal regularity $s = t_1 = t_2 = t_3 = 1$ and optimal stability $q = 0$. The first part $k^2(H + h)$ comes from the volume terms and is unavoidable as just discussed for the Helmholtz equation. The second part $k^{3/2}H^{1/2}$ is caused by the boundary terms, which are an essential part of the energy norm for the Maxwell equation. In contrast to the Helmholtz equation, they cannot be estimated against the volume terms by a trace inequality and thus, seem to be unavoidable as well. The powers in k and H for the resolution condition caused by the boundary terms are consistent with the volume terms: for both, k and H, the power is reduced by $1/2$. Unfortunately, despite this consistency, the part $k^{3/2}H^{1/2}$ is the dominating part in the resolution condition and finally, leads to a condition like "k^3H small".

Our explicit stability estimates in Theorems 4.3.14 and 4.3.15 yield $q = 3$. This is a kind of "worst case" resolution condition which is certainly sufficient for the quasi-optimality and a priori error results presented above, but can well be suboptimal (as the numerical experiments indicate). We emphasize that this gap between the optimal and worst case resolution condition is no defect of the numerical method, but can be closed if better stability results are proved, which is outside the scope of our work. For instance, the influence of $\mathrm{Im}(\mu_{\mathrm{hom}})$ may still be overestimated. For the Maxwell equation, we moreover underline that previous works [GM12, Hip02, Hip15, Mon03] so far have only proved well-posedness for sufficiently fine meshes without explicit k-dependent resolution condition.

As also supported by our numerical experiments, the HMM is much more efficient than a direct discretization of the heterogeneous problems (4.2) and (4.3). In order to get an accurate solution, a grid with mesh size h_{ref} satisfying $h_{\mathrm{ref}} < \delta \ll 1$ is required from the multiscale point of view. On top of that, at least $k^2 h_{\mathrm{ref}} < C$ has to be satisfied to rule out pre-asymptotic effects. Note that the heterogeneous problems do not fulfill the assumptions for any available stability estimate, so that the resolution condition may even be worse.

Reduction of the pollution effect. Although the above described so-called pollution effect is not avoidable for the classical Helmholtz equation in dimension $d \geq 2$ as shown in [BS00], much work in its reduction has been invested: Examples of the proposed methods are the *hp*-version of the finite element method [EM12, MS11], (hybridizable) discontinuous Galerkin methods [CLX13, GM11], or plane wave Trefftz methods [HMP16a, HMP16b, PPR16], just to name a few. For the Maxwell equation, attempts to reduce the pollution effect include *hp*-FEM [MS18], (hybridizable) discontinuous Galerkin methods [FLX16, FW14b, LCQ17], or (plane wave) Trefftz methods [HMP13]. Recently, it has been shown that the resolution condition for the Helmholtz equation can be relaxed to the natural assumption "kh sufficiently small" by applying a Localized Orthogonal Decomposition (LOD), see [BGP17, GP15, Pet17]. To that end, the function space is decomposed into a coarse space, where the solution is sought, and a remainder space. The coarse space is spanned by pre-computable basis functions with local support, which include some information from the remainder space by the solution of localized corrector problems, see Section 2.3.4 for details. Only recently, the LOD has also been discussed for $\mathbf{H}(\mathrm{curl})$-problems [GHV18, Ver17b]. The definition of the HMM as a direct discretization of the two-scale equation makes it possible to apply an additional LOD, see Section 4.5.

4.4.3 Proofs for the Helmholtz equation

In this section we give the proof of Theorem 4.4.2. The finite element function space $\mathbf{V}_{H,h}$ for the Helmholtz equation (see first part of Definition 4.4.1) has the following approximation property: There is C_{approx} such that for all $\frac{1}{2} < s \leq 1$ and given $(v_0, v_1, v_2) \in H^{1+s}_{pw}(G) \times L^2(\Omega; H^{1+s}(\Sigma^*)) \times L^2(\Omega; H^{1+s}(\Sigma))$ it holds

$$\begin{aligned} \|v_0 - v_H\|_G + H\|\nabla(v - v_H)\|_G &\leq C_{\mathrm{approx}} H^{1+s} |v|_{H^{1+s}_{pw}(G)}, \\ \|v_1 - v_{h,1}\|_{\Omega\times\Sigma^*} + h\|\nabla_y(v_1 - v_{h,1})\|_{\Omega\times\Sigma^*} &\leq C_{\mathrm{approx}} h^{1+s} |v_1|_{L^2(\Omega;H^{1+s}(\Sigma^*))}, \\ \|v_2 - v_{h,2}\|_{\Omega\times\Sigma} + h\|\nabla_y(v_2 - v_{h,2})\|_{\Omega\times\Sigma} &\leq C_{\mathrm{approx}} h^{1+s} |v_2|_{L^2(\Omega;H^{1+s}(\Sigma))} \end{aligned} \tag{4.43}$$

for all $\mathbf{v}_{H,h} := (v_H, v_{h,1}, v_{h,2}) \in \mathbf{V}_{H,h}$. Note that the regularity coefficient s does not necessarily have to be the same in all three estimates.

Proof of Theorem 4.4.2. Proof of the inf-sup condition (4.38): Let $\mathbf{v}_{H,h} := (v_H, v_{h,1}, v_{h,2}) \in \mathbf{V}_{H,h}$ be given and let $\underline{\mathbf{w}} := (w_0, w_1, w_2) \in \mathcal{H}$ solve

$$\mathcal{B}(\underline{\boldsymbol{\psi}}, \underline{\mathbf{w}}) = 2k^2(\psi_0 + \chi_\Sigma \psi_2, v_H + \chi_D v_{h,2})_{G\times Y} \qquad \forall \underline{\boldsymbol{\psi}} := (\psi_0, \psi_1, \psi_2) \in \mathcal{H}.$$

Due to the regularity of the cell problems (Lemma 4.3.6), Assumption 4.3.10 on the stability, and the resulting estimates from Proposition 4.3.16 it holds that

$$\begin{aligned} \|\underline{\mathbf{w}}\|_e &\leq 2C_{\mathrm{stab},e} k^{q+1} \|\mathbf{v}_{H,h}\|_e, \\ \|w_0\|_{H^{1+s}_{pw}(G)} &\leq 2C_{\mathrm{reg},0} k^{q+2} \|\mathbf{v}_{H,h}\|_e, \\ \|w_1\|_{L^2(\Omega;H^{1+t_1}(\Sigma^*))} \leq C_{\mathrm{reg},1} \|\underline{\mathbf{w}}\|_e &\leq 2C_{\mathrm{reg},1} C_{\mathrm{stab},e} k^{q+1} \|\mathbf{v}_{H,h}\|_e, \\ \|w_2\|_{L^2(\Omega;H^{1+t_2}(\Sigma))} \leq C_{\mathrm{reg},2} k \|\underline{\mathbf{w}}\|_e &\leq 2C_{\mathrm{reg},2} C_{\mathrm{stab},e} k^{q+2} \|\mathbf{v}_{H,h}\|_e. \end{aligned} \tag{4.44}$$

Due to (4.43) we can choose $\mathbf{w}_{H,h} := (w_H, w_{h,1}, w_{h,2}) \in \mathbf{V}_{H,h}$ such that

$$\begin{aligned} \|\underline{\mathbf{w}} - \mathbf{w}_{H,h}\|_e &\leq C_{\mathrm{approx}} \Big(H^s(1 + kH) \|w_0\|_{H^{1+s}_{pw}(G)} + h^{t_1} \|w_1\|_{L^2(\Omega;H^{1+t_1}(\Sigma^*))} \\ &\qquad + h^{t_2}(1 + kh) \|w_2\|_{L^2(\Omega;H^{1+t_2}(\Sigma))} \Big) \\ &\overset{(4.44)}{\leq} 2C_{\mathrm{approx}} \Big(C_{\mathrm{reg},0} k^{q+2} H^s (1 + kH) + C_{\mathrm{reg},1} C_{\mathrm{stab},e} k^{q+1} h^{t_1} \\ &\qquad + C_{\mathrm{reg},2} C_{\mathrm{stab},e} k^{q+2} h^{t_2} (1 + kh) \Big) \|\mathbf{v}_{H,h}\|_e. \end{aligned} \tag{4.45}$$

With this $\mathbf{w}_{H,h}$ we obtain

$$\begin{aligned}\operatorname{Re}\mathcal{B}(\mathbf{v}_{H,h},\mathbf{v}_{H,h}+\mathbf{w}_{H,h}) &= \operatorname{Re}\mathcal{B}(\mathbf{v}_{H,h},\mathbf{v}_{H,h}+\underline{\mathbf{w}}-\underline{\mathbf{w}}+\mathbf{w}_{H,h})\\ &= \operatorname{Re}\mathcal{B}(\mathbf{v}_{H,h},\mathbf{v}_{H,h}+\underline{\mathbf{w}})-\operatorname{Re}\mathcal{B}(\mathbf{v}_{H,h},\underline{\mathbf{w}}-\mathbf{w}_{H,h})\\ &\geq C_{\min}\|\mathbf{v}_{H,h}\|_e^2 - C_B\|\mathbf{v}_{H,h}\|_e\,\|\underline{\mathbf{w}}-\mathbf{w}_{H,h}\|_e.\end{aligned}$$

Inserting (4.45) yields

$$\begin{aligned}&\operatorname{Re}\mathcal{B}(\mathbf{v}_{H,h},\mathbf{v}_{H,h}+\mathbf{w}_{H,h})\\ &\geq C_{\min}\Big(1-\frac{2C_BC_{\text{approx}}}{C_{\min}}\Big(C_{\text{reg},0}k^{q+2}H^s(1+kH)+C_{\text{reg},2}C_{\text{stab},e}k^{q+2}h^{t_2}(1+kh)\\ &\qquad\qquad +C_{\text{reg},1}C_{\text{stab},e}k^{q+1}h^{t_1}\Big)\Big)\|\mathbf{v}_{H,h}\|_e^2.\end{aligned}$$

Hence, this gives $\operatorname{Re}\mathcal{B}(\mathbf{v}_{H,h},\mathbf{v}_{H,h}+\mathbf{w}_{H,h}) \geq \frac{1}{2}C_{\min}\|\mathbf{v}_{H,h}\|_e^2$ under the resolution conditions (4.37). Finally, observing that

$$\begin{aligned}&\|\mathbf{v}_{H,h}+\mathbf{w}_{H,h}\|_e \leq \|\mathbf{v}_{H,h}\|_e+\|\underline{\mathbf{w}}\|_e+\|\underline{\mathbf{w}}-\mathbf{w}_{H,h}\|_e\\ &\leq \Big(1+2C_{\text{stab},e}k^{q+1}+2C_{\text{approx}}\Big(C_{\text{reg},0}k^{q+2}H^s(1+kH)+C_{\text{reg},1}C_{\text{stab},e}k^{q+1}h^{t_1}\\ &\qquad\qquad +C_{\text{reg},2}C_{\text{stab},e}k^{q+2}h^{t_2}(1+kh)\Big)\Big)\|\mathbf{v}_{H,h}\|_e\\ &\overset{(4.37)}{\leq} \Big(1+2C_{\text{stab},e}k^{q+1}+\frac{C_{\min}}{2C_B}\Big)\|\mathbf{v}_{H,h}\|_e\\ &\leq \Big(k_0^{-(q+1)}\Big(1+\frac{C_{\min}}{2C_B}\Big)+2C_{\text{stab},e}\Big)k^{q+1}\|\mathbf{v}_{H,h}\|_e\end{aligned}$$

finishes the proof of the inf-sup condition.

Proof of the quasi-optimality (4.39)*:* Consider the following (auxiliary) dual problem for $\underline{\mathbf{w}} := (w_0,w_1,w_2) \in \mathcal{H}$

$$\mathcal{B}(\underline{\boldsymbol{\psi}},\underline{\mathbf{w}}) = k^2(\psi_0+\chi_\Sigma\psi_2, e_0+\chi_\Sigma e_2)_{G\times Y} \qquad \forall \underline{\boldsymbol{\psi}} := (\psi_0,\psi_1,\psi_2)\in\mathcal{H}.$$

As already argued in the proof of the discrete inf-sup constant, $w_0 \in H^{1+s}_{pw}(G)$ fulfills the estimate $\|w_0\|_{H^{1+s}_{pw}} \leq C_{\text{reg},0}k^{q+2}\|(e_0,e_1,e_2)\|_e$ due to Proposition 4.3.16. For all $\mathbf{w}_{H,h}\in\mathbf{V}_{H,h}$, the standard Galerkin orthogonality gives

$$k^2\|e_0+\chi_\Sigma e_2\|^2_{L^2(G\times Y)} = \mathcal{B}(\mathbf{e},\underline{\mathbf{w}}) = \mathcal{B}(\mathbf{e},\underline{\mathbf{w}}-\mathbf{w}_{H,h}).$$

The continuity of $\mathcal{B}$ w.r.t. the energy norm and an approximation argument like (4.45) yield

$$\begin{aligned}k^2\|e+\chi_\Sigma e_2\|^2_{L^2(G\times Y)} &\leq C_B\|(e_0,e_1,e_2)\|_e\,\|\underline{\mathbf{z}}-\mathbf{z}_{H,h}\|_e\\ &\leq C_BC_{\text{approx}}\Big(C_{\text{reg},0}k^{q+2}H^s(1+kH)+C_{\text{reg},1}C_{\text{stab},e}k^{q+1}h^{t_1}\\ &\qquad +C_{\text{reg},2}C_{\text{stab},e}k^{q+2}h^{t_2}(1+kh)\Big)\|(e_0,e_1,e_2)\|_e^2.\end{aligned}$$

With the Gårding inequality, we get for any $\mathbf{w}_{H,h}\in\mathbf{V}_{H,h}$

$$\begin{aligned}\|(e_0,e_1,e_2)\|_e^2 &\leq C_{\min}^{-1}\big(\operatorname{Re}\mathcal{B}(\mathbf{e},\mathbf{e})+2k^2\|e_0+\chi_\Sigma e_2\|^2_{L^2(G\times Y)}\big)\\ &= C_{\min}^{-1}\big(\operatorname{Re}\mathcal{B}(\mathbf{e},\underline{\mathbf{u}}-\mathbf{w}_{H,h})+2k^2\|e_0+\chi_\Sigma e_2\|^2_{L^2(G\times Y)}\big)\\ &\leq \frac{C_B}{C_{\min}}\|\underline{\mathbf{u}}-\mathbf{w}_{H,h}\|_e\,\|(e_0,e_1,e_2)\|_e\\ &\quad+\frac{2C_BC_{\text{approx}}}{C_{\min}}\Big(C_{\text{reg},0}k^{q+2}H^s(1+kH)+C_{\text{reg},1}C_{\text{stab},e}k^{q+1}h^{t_1}\\ &\qquad +C_{\text{reg},2}C_{\text{stab},e}k^{q+2}h^{t_2}(1+kh)\Big)\|(e_0,e_1,e_2)\|_e^2.\end{aligned}$$

Together with the resolution conditions (4.37) this gives

$$\|(e_0,e_1,e_2)\|_e^2 \leq \frac{C_B}{C_{\min}}\|\underline{\mathbf{u}}-\mathbf{w}_{H,h}\|_e\|(e_0,e_1,e_2)\|_e + \frac{1}{2}\|(e_0,e_1,e_2)\|_e^2$$

and, hence, (4.39). □

4.4.4 Proofs for the Maxwell equation

In this section, we prove Theorems 4.4.3 and 4.4.6. We introduce the following dual problem: For $\mathbf{f} \in \mathbf{H}(\operatorname{div}0,G)$, $\mathbf{f}_3 \in L^2(\Omega;\mathbf{H}(\operatorname{div}0,\Sigma))$ and $\widetilde{\mathbf{g}} \in \mathbf{H}_T^r(\partial G)$ with $r \in (0,\frac{1}{2})$, find $\underline{\mathbf{w}} = (\mathbf{w}_0,\mathbf{w}_1,w_2,\mathbf{w}_3) \in \mathcal{H}$ such that

$$\mathcal{B}(\underline{\boldsymbol{\psi}},\underline{\mathbf{w}}) = (\boldsymbol{\psi}+\chi_\Sigma\boldsymbol{\psi}_3,\mathbf{f}+\chi_\Sigma\mathbf{f}_3)_{L^2(G\times Y)} + (\boldsymbol{\psi}_T,\widetilde{\mathbf{g}})_{L^2(\partial G)} \qquad \forall \underline{\boldsymbol{\psi}} = (\boldsymbol{\psi}_0,\boldsymbol{\psi}_1,\psi_2,\boldsymbol{\psi}_3) \in \mathcal{H}. \tag{4.46}$$

Dual problem (4.46) is very similar to the two-scale limit equation (4.9) and we thereby know that it is uniquely solvable. Note that we can also apply our theory from Section 4.3, in particular Assumption 4.3.11, since the right-hand side is divergence-free. We have the following approximation result for the dual problem.

Lemma 4.4.7. *Under Assumption 4.3.11, the solution* $\underline{\mathbf{w}} \in \mathcal{H}$ *to* (4.46) *satisfies*

$$\begin{aligned}\inf_{\mathbf{w}_{H,h}\in\mathbf{V}_{H,h}} \|\underline{\mathbf{w}}-\mathbf{w}_{H,h}\|_e \leq C_{\text{approx}}\big(&k^{q+1}(H^s+h^{t_1}+h^{t_2}+h^{t_3}) \\ &+ k^{q+1/2}H^{s-1/2}\big)\big(\|\mathbf{f}+\chi_\Sigma\mathbf{f}_3\|_{L^2(G\times Y)} + \|\widetilde{\mathbf{g}}\|_{\mathbf{H}^r(\partial G)}\big).\end{aligned} \tag{4.47}$$

Proof. Interpolation and best approximation estimates in $\mathbf{H}_{\text{imp}}$, see [EG17b, GM12], yield

$$\begin{aligned}\inf_{\mathbf{w}_{H,h}\in\mathbf{V}_{H,h}} \|\underline{\mathbf{w}}-\mathbf{w}_{H,h}\|_e \lesssim{}& (H^s+h^{t_1}+h^{t_2}+h^{t_3})\|\underline{\mathbf{w}}\|_{k,\mathcal{H}^{s,t}} \\ &+ k^{1/2}H^{s-1/2}(\|\mathbf{w}_T\|_{\mathbf{H}_\parallel^s(\partial G)} + \|\operatorname{curl}_{\partial G}\mathbf{w}_T\|_{L^2(\partial G)}),\end{aligned}$$

where we abbreviated by $\|\cdot\|_{k,\mathcal{H}^{s,t}}$ the (weighted) higher order norms. Inserting the regularity and stability results from Section 4.3 and using Assumption 4.3.11 finishes the proof. □

With these preliminaries, we prove the inf-sup condition and the quasi-optimality of Theorem 4.4.3.

Proof of Theorem 4.4.3. Proof of the inf-sup condition (4.41)*:* Let $\mathbf{v}_{H,h} \in \mathbf{V}_{H,h}$ be arbitrary and apply the Helmholtz decomposition (4.17) to $\mathbf{v}_H = \mathbf{z}_0 + \nabla\theta_0$ and $\mathbf{v}_{h,3} = \mathbf{z}_3 + \nabla_y\theta_3$. We write in short $\mathbf{v}_{H,h} = \underline{\mathbf{z}} + \nabla\boldsymbol{\theta}$ with $\underline{\mathbf{z}} = (\mathbf{z}_0,\mathbf{v}_{h,1},0,\mathbf{z}_3)$ and $\nabla\boldsymbol{\theta} := (\nabla\theta_0,0,\nabla_y v_{h,2},\nabla_y\theta_3)$. Let $\underline{\mathbf{w}} = (\mathbf{w}_0,\mathbf{w}_1,w_2,\mathbf{z}_3) \in \mathcal{H}$ be the solution to dual problem (4.46) with $\mathbf{f} = C_g k^2\mathbf{z}_0$, $\mathbf{f}_3 = C_g k^2\mathbf{z}_3$, and $\widetilde{\mathbf{g}} = C_g k(\mathbf{z}_0)_T$. Note that $(\mathbf{z}_0)_T \in \mathbf{H}_T^r(\partial G)$ for all $r < \frac{1}{2}$ due to the boundary regularity of edge element functions. Let $\mathbf{w}_{H,h} \in \mathbf{V}_{H,h}$ be the best approximation to $\underline{\mathbf{w}}$ in the two-scale energy norm $\|\cdot\|_e$.

Imitating the proof of the analytical inf-sup condition in Proposition 4.3.17, we would like to choose the test function $SF(\mathbf{v}_{H,h})+\mathbf{w}_{H,h}$ with the sign-flip isomorphism SF. Unfortunately, $SF(\mathbf{v}_{H,h})$ is not discrete any more, so that we have to apply an additional interpolation operator. We choose the corresponding standard (nodal) interpolation operator for each of the single spaces of $\mathbf{V}_{H,h}$ (see Section 2.2.2) and call the resulting operator $\mathbf{I}_{H,h}$. Hence, we obtain

$$\begin{aligned}&\big|\mathcal{B}(\mathbf{v}_{H,h},\mathbf{I}_{H,h}(SF(\mathbf{v}_{H,h}))+\mathbf{w}_{H,h})\big| \\ &\quad\geq \big|\mathcal{B}(\mathbf{v}_{H,h},SF(\mathbf{v}_{H,h})+\underline{\mathbf{w}})\big| - \big|\mathcal{B}(\mathbf{v}_{H,h},(\mathbf{I}_{H,h}-\mathrm{id})SF(\mathbf{v}_{H,h})\big| - \big|\mathcal{B}(\mathbf{v}_{H,h},\mathbf{w}_{H,h}-\underline{\mathbf{w}})\big|.\end{aligned}$$

Due to the orthogonality of the Helmholtz decomposition, the first term can be estimated as

$$\begin{aligned}
&\big|\mathcal{B}(\mathbf{v}_{H,h}, SF(\mathbf{v}_{H,h}) + \underline{\mathbf{w}})\big| \\
&\quad = \big|\mathcal{B}(\mathbf{v}_{H,h}, SF(\mathbf{v}_{H,h})) + C_g k^2 (\mathbf{z}_0 + \chi_\Sigma \mathbf{z}_3, \mathbf{v}_H + \chi_\Sigma \mathbf{v}_{h,3})_{G\times Y} + C_g k((\mathbf{z}_0)_T, (\mathbf{v}_H)_T)_{\partial G}\big| \\
&\quad = \big|\mathcal{B}(\mathbf{v}_{H,h}, SF(\mathbf{v}_{H,h})) + C_g k^2 \|\mathbf{z}_0 + \chi_\Sigma \mathbf{z}_3\|^2_{G\times Y} + C_g k \|(\mathbf{z}_0)_T\|^2_{\partial G}\big| \geq \gamma_{\mathrm{ell}} \|\mathbf{v}_{H,h}\|_e^2.
\end{aligned}$$

Using the continuity of $\mathcal{B}$ and Lemma 4.4.7, we deduce for the third term

$$\begin{aligned}
&\big|\mathcal{B}(\mathbf{v}_{H,h}, \mathbf{w}_{H,h} - \underline{\mathbf{w}})\big| \\
&\quad \leq C_c C_{\mathrm{approx}} C_g (k^{q+2}(H^s + h^{t_1} + h^{t_2} + h^{t_3}) + k^{q+3/2} H^{s-1/2}) \|\mathbf{v}_{H,h}\|_e \\
&\qquad \cdot \big(k\|\mathbf{z}_0 + \chi_\Sigma \mathbf{z}_3\|_{G\times Y} + k^{1/2} \|(\mathbf{z}_0)_T\|_{L^2_T(\partial G)}\big) \\
&\quad \leq C_c C_{\mathrm{approx}} C_g (k^{q+2}(H^s + h^{t_1} + h^{t_2} + h^{t_3}) + k^{q+3/2} H^{s-1/2}) \|\mathbf{v}_{H,h}\|_e^2,
\end{aligned}$$

where we used the stability of the Helmholtz decomposition in the last step.

For the second term we note that $SF(\mathbf{v}_{H,h}) = 2\underline{\mathbf{z}} - \mathbf{v}_{H,h}$. It holds that $\operatorname{curl}(\mathbf{I}_{H,h} - \mathrm{id})\underline{\mathbf{z}} = 0$ because the nodal interpolation operator is a commuting projector and $\operatorname{curl} \underline{\mathbf{z}} = \operatorname{curl} \mathbf{v}_{H,h}$. In particular, this means that the curl and the tangential curl of $\mathbf{z}_0 + \chi_\Sigma \mathbf{z}_3$ are discrete functions, so that we can apply the modified interpolation estimates [GM12, Lemmas 5.1 and 5.3]. Together with the regularity of the decomposition discussed in Remark 4.3.9, this yields for the second term

$$\begin{aligned}
&\big|\mathcal{B}(\mathbf{v}_{H,h}, (\mathbf{I}_{H,h} - \mathrm{id}) SF(\mathbf{v}_{H,h}))\big| \\
&\quad \leq 2C_c \|\mathbf{v}_{H,h}\|_e \big(k\|(\mathbf{I}_{H,h} - \mathrm{id})(\mathbf{z}_0 + \chi_\Sigma \mathbf{z}_3)\|_{G\times Y} + k^{1/2} \|(\mathbf{I}_{H,h} - \mathrm{id})(\mathbf{z}_0)_T\|_{\partial G}\big) \\
&\quad \leq 2C_c C_{\mathrm{approx}} (k(H^s + h^{t_3}) + k^{1/2} H^{s-1/2}) \|\mathbf{v}_{H,h}\|_e.
\end{aligned}$$

The term $|\mathcal{B}(\mathbf{v}_{H,h}, (\mathbf{I}_{H,h} - \mathrm{id}) SF(\mathbf{v}_{H,h}))|$ thus is of lower order than term $|\mathcal{B}(\mathbf{v}_{H,h}, \mathbf{w}_{H,h} - \underline{\mathbf{w}})|$ and can be absorbed in the latter because of $k \geq k_0$. All in all, this gives

$$\begin{aligned}
&\big|\mathcal{B}(\mathbf{v}_{H,h}, \mathbf{I}_{H,h}(SF(\mathbf{v}_{H,h})) + \mathbf{w}_{H,h})\big| \\
&\quad \geq (\gamma_{\mathrm{ell}} - C_c C_{\mathrm{approx}} (C_g + 2)(k^{q+2}(H^s + h^{t_1} + h^{t_2} + h^{t_3}) + k^{q+3/2} H^{s-1/2})) \|\mathbf{v}_{H,h}\|_e^2 \\
&\quad \geq \gamma_{\mathrm{ell}}/2 \|\mathbf{v}_{H,h}\|_e^2,
\end{aligned}$$

where we used the resolution condition (4.40) in the last step.

Furthermore, it holds – with the same arguments as before – that

$$\begin{aligned}
&\|\mathbf{I}_{H,h}(SF(\mathbf{v}_{H,h})) + \mathbf{w}_{H,h}\|_e \\
&\quad \leq \|SF(\mathbf{v}_{H,h})\|_e + \|\underline{\mathbf{w}}\|_e + \|\underline{\mathbf{w}} - \mathbf{w}_{H,h}\|_e + \|(\mathbf{I}_{H,h} - \mathrm{id}) SF(\mathbf{v}_{H,h})\|_e \\
&\quad \leq \Big(1 + C_g C_{\mathrm{stab},e} k^{q+1} \\
&\qquad + (C_g + 2) C_{\mathrm{approx}} (k^{q+2}(H^s + h^{t_1} + h^{t_2} + h^{t_3}) + k^{q+3/2} H^{s-1/2})\Big) \|\mathbf{v}_{H,h}\|_e^2,
\end{aligned}$$

which finishes the proof of the inf-sup condition.

Proof of the quasi-optimality (4.42)*:* Let $\mathbf{e} := (e_0, e_1, e_2, e_3)$ and apply the Helmholtz decomposition (4.17) to $e_0 + \chi_\Sigma e_3 = \mathbf{z}_0 + \chi_\Sigma \mathbf{z}_3 + \nabla\theta_0 + \chi_\Sigma \nabla_y \theta_3$. We write in short $\mathbf{e} = \underline{\mathbf{z}} + \nabla\boldsymbol{\theta}$ with $\underline{\mathbf{z}} = (\mathbf{z}_0, e_1, 0, \mathbf{z}_3)$ and $\nabla\boldsymbol{\theta} := (\nabla\theta_0, 0, \nabla_y e_2, \nabla_y \theta_3)$.

Using the Gårding-type inequality (4.18), we have that

$$\begin{aligned}
\gamma_{\mathrm{ell}} \|\mathbf{e}\|_e^2 &\leq |\mathcal{B}(\mathbf{e}, SF(\mathbf{e})) + C_g k^2 \|\mathbf{z}_0 + \chi_\Sigma \mathbf{z}_3\|^2_{G\times Y} + C_g k \|(\mathbf{z}_0)_T\|^2_{\partial G}| \\
&\leq |\mathcal{B}(\mathbf{e}, \mathbf{e})| + (C_g + 2) k^2 \|\mathbf{z}_0 + \chi_\Sigma \mathbf{z}_3\|^2_{G\times Y} + (C_g + 2) k \|(\mathbf{z}_0)_T\|^2_{\partial G}.
\end{aligned} \tag{4.48}$$

The main work is to bound the second and third term. For this, let $\underline{\mathbf{w}} \in \mathcal{H}$ be the solution to dual problem (4.46) with $\mathbf{f} = k\mathbf{z}_0$, $\mathbf{f}_3 = k\mathbf{z}_3$ and $\widetilde{\mathbf{g}} = k^{1/2}(\mathbf{z}_0)_T$. Note that $(\mathbf{z}_0)_T \in \mathbf{H}_T^{s-1/2}(\partial G)$

due to the regularity of $\mathbf{u}_0$ from Proposition 4.3.8 and the regularity of functions in $\mathbf{V}_{H,h}$. Because of the orthogonality in the Helmholtz decomposition of (4.17) and $\nabla_T \theta_0 = 0$ it holds that

$$\begin{aligned} k\|\mathbf{z}_0 + \chi_\Sigma \mathbf{z}_3\|^2_{G\times Y} + k^{1/2}\|(\mathbf{z}_0)_T\|^2_{\partial G} &= k(\mathbf{z}_0 + \chi_\Sigma \mathbf{z}_3, e_0 + \chi_\Sigma e_3)_{G\times Y} + k^{1/2}((\mathbf{z}_0)_T, (e_0)_T)_{\partial G} \\ &= \mathcal{B}(\mathbf{e}, \underline{\mathbf{w}}). \end{aligned}$$

Using Galerkin orthogonality and Lemma 4.4.7, we obtain for any $\mathbf{w}_{H,h} \in \mathbf{V}_{H,h}$ that

$$\begin{aligned} k\|\mathbf{z}_0 + \chi_\Sigma \mathbf{z}_3\|^2_{G\times Y} + k^{1/2}\|(\mathbf{z}_0)_T\|^2_{\partial G} &= \mathcal{B}(\mathbf{e}, \underline{\mathbf{w}}) = \mathcal{B}(\mathbf{e}, \underline{\mathbf{w}} - \mathbf{w}_{H,h}) \\ &\leq C_c C_{\text{approx}}(k^{q+2}(H^s + h^{t_1} + h^{t_2} + h^{t_3}) + k^{q+3/2}H^{s-1/2})\|\mathbf{e}\|_e \\ &\quad \cdot (\|(\mathbf{z}_0 + \chi_\Sigma \mathbf{z}_3)\|_{G\times Y} + \|(\mathbf{z}_0)_T\|_{\partial G}) \end{aligned}$$

and thus

$$\begin{aligned} &k\|(\mathbf{z}_0 + \chi_\Sigma \mathbf{z}_3)\|_{G\times Y} + k^{1/2}\|(\mathbf{z}_0)_T\|_{\partial G} \\ &\quad \leq C_c C_{\text{approx}}(k^{q+2}(H^s + h^{t_1} + h^{t_2} + h^{t_3}) + k^{q+3/2}H^{s-1/2})\|\mathbf{e}\|_e. \end{aligned} \tag{4.49}$$

Inserting (4.49) into (4.48) and applying Galerkin orthogonality, we get

$$\begin{aligned} \gamma_{\text{ell}}\|\mathbf{e}\|^2_e &\leq \left|\mathcal{B}(\mathbf{e}, \mathbf{e})\right| + (C_g + 2)k^2\|\mathbf{z}_0 + \chi_\Sigma \mathbf{z}_3\|^2_{G\times Y} + (C_g + 2)k\|(\mathbf{z}_0)_T\|^2_{\partial G} \\ &\leq \left|\mathcal{B}(\mathbf{e}, \underline{\mathbf{u}} - \mathbf{v}_{H,h})\right| + (C_g + 2)\|\mathbf{e}\|_e \left(k\|\mathbf{z}_0 + \chi_\Sigma \mathbf{z}_3\|_{G\times Y} + k^{1/2}\|(\mathbf{z}_0)_T\|_{\partial G}\right) \\ &\leq C_c\|\mathbf{e}\|_e\|\underline{\mathbf{u}} - \mathbf{v}_{H,h}\| \\ &\quad + (C_g + 2)C_c C_{\text{approx}}(k^{q+2}(H^s + h^{t_1} + h^{t_2} + h^{t_3}) + k^{q+3/2}H^{s-1/2})\|\mathbf{e}\|^2_e, \end{aligned}$$

which gives the claim using resolution condition (4.40). □

The proof of the quasi-optimality already showed that the compact perturbation is of higher order (w.r.t. the rates in the mesh size) than the energy error. This kind of Aubin-Nitsche trick can be extended to the whole Helmholtz decomposition.

Proof of Theorem 4.4.6. The estimate for $\mathbf{z}_0 + \chi_\Sigma \mathbf{z}_3$ is already given by (4.49) (considering only the volume term and dividing by k). To estimate $\theta_0 + \chi_\Sigma \theta_3$, we pose another dual problem (cf. [HOV16b]): Find $\mathbf{w} := (w_0, w_2, w_3) \in X := H^1_0(G) \times L^2(\Omega; H^1_{\sharp,0}(\Sigma^*)) \times L^2(\Omega; H^1_0(\Sigma))$ such that

$$\begin{aligned} \mathcal{A}(\boldsymbol{\psi}, \mathbf{w}) &:= -k^2 \int_G \int_Y (\nabla \psi_0 + \chi_{\Sigma^*} \nabla_y \psi_2 + \chi_\Sigma \nabla_y \psi_3) \cdot (\nabla w_0^* + \chi_{\Sigma^*} \nabla_y w_2^* + \chi_\Sigma \nabla_y w_3^*)\, dydx \\ &= \int_G \int_Y (\psi_0 + \chi_\Sigma \psi_3) \cdot (\theta_0^* + \chi_\Sigma \theta_3^*)\, dydx \qquad \forall \boldsymbol{\psi} = (\psi_0, \psi_2, \psi_3) \in X. \end{aligned}$$

Let us denote by $\mathbf{w}_{H,h} = (w_H, w_{h,2}, w_{h,3})$ the solution to the corresponding discrete problem over the Lagrange finite element spaces $\mathring{\mathcal{S}}(\mathcal{T}_H) \subset H^1_0(G)$, $\widetilde{\mathcal{S}}(\mathcal{T}_h(\Sigma^*)) \subset H^1_{\sharp,0}(\Sigma^*)$, and $\mathring{\mathcal{S}}(\mathcal{T}_h(\Sigma)) \subset H^1_0(\Sigma)$. It is a well-known fact in finite element exterior calculus that $\nabla \mathcal{S}(\mathcal{T}_H) \subset \mathcal{N}(\mathcal{T}_H)$, etc. We obtain with the Galerkin orthogonality and the orthogonality of the Helmholtz decomposition

$$\begin{aligned} \|\theta_0 + \chi_\Sigma \theta_3\|^2_{G\times Y} &= \mathcal{A}((\theta_0, e_2, \theta_3), \mathbf{w}) = \mathcal{B}((\nabla\theta_0, e_1, e_2, \nabla_y \theta_3), (\nabla w_0, 0, w_2, \nabla_y w_3)) \\ &= \mathcal{B}(\mathbf{e}, (\nabla w_0, 0, w_2, \nabla_y w_3)) - \mathcal{B}((\mathbf{z}_0, 0, 0, \mathbf{z}_3), (\nabla w_0, 0, w_2, \nabla_y w_3)) \\ &= \mathcal{B}(\mathbf{e}, (\nabla(w_0 - w_H), 0, w_2 - w_{h,2}, \nabla_y(w_3 - w_{h,3})). \end{aligned}$$

Using the approximation properties of the Lagrange finite element spaces and the regularity and stability of elliptic diffusion two-scale problems, we deduce

$$\begin{aligned} \|\theta_0 + \chi_\Sigma \theta_3\|^2_{G\times Y} &\lesssim \|\mathbf{e}\|_e\, k\|\nabla(w_0 - w_H) + \chi_{\Sigma^*} \nabla_y (w_2 - w_{h,2}) + \chi_\Sigma \nabla_y (w_3 - w_{h,3})\|_{G\times Y} \\ &\lesssim (H^s + h^{t_2} + h^{t_3} + H^{s-1/2})\|\mathbf{e}\|_e \|\theta_0 + \chi_\Sigma \theta_3\|_{G\times Y}, \end{aligned}$$

which in combination with (4.49) finishes the proof. □

4.5 Two-scale Localized Orthogonal Decomposition for Helmholtz-type problems

In this section, we present how the Localized Orthogonal Decomposition (LOD) can be applied to two-scale Helmholtz-type problems to relax the resolution conditions (4.37), following the ideas in [GP15]. Here, we have to deal with coupled functional spaces and sesquilinear forms. This coupling has to be taken care of in all new definitions of (again coupled) spaces and also in the estimates, where we have to jump back and forth between the two-scale norms and the properties of each individual space and interpolation operator. Furthermore, our coupled two-scale functional spaces involve periodic boundary conditions on the unit cell, which also have to be paid attention at when defining the interpolation operators and the oversampling patches at the boundary.

We consider the two-scale equation (4.4) over the two-scale space $\mathcal{H}$. Again, we estimate errors in the two-scale energy norm (4.15). Furthermore, we introduce a version $\|\cdot\|_{1,e}$ of the H^1-seminorm on $\mathcal{H}$ via

$$\|(v_0, v_1, v_2)\|^2_{1,e,\omega\times R} := \|\nabla v_0 + \nabla_y v_1\|^2_{\omega\times R_1} + \|\nabla_y v_2\|^2_{\omega\times R_2} \tag{4.50}$$

for a subdomain $\omega \times R \subset G \times Y$ with $R_1 := R \cap \Sigma^*$ and $R_2 := R \cap \Sigma$. This norm is induced by the sesquilinear form

$$(\underline{\mathbf{v}}, \underline{\boldsymbol{\psi}})_{1,e,\omega\times R} := (\nabla v_0 + \nabla_y v_1, \nabla \psi_0 + \nabla_y \psi_1)_{\omega\times R_1} + (\nabla_y v_2, \nabla_y \psi_2)_{\omega\times R_2} \qquad \forall \underline{\mathbf{v}}, \underline{\boldsymbol{\psi}} \in \mathcal{H}.$$

Recall that the sesquilinear form $\mathcal{B}$ fulfills a Gårding inequality, see Lemma 4.3.2.

For the error analysis, we compare the solution of the LOD to a discrete reference solution, which is only needed for the theory and is never computed in practical implementations. This reference solution is the discrete two-scale solution $\mathbf{u}_{H,h} \in \mathbf{V}_{H,h}$ to (4.35), see Definition 4.4.1. It is computed over the meshes $\mathcal{T}_H$ for G and $\mathcal{T}_h$ for Y, as introduced in Section 4.4.1. We assume that this discretization is stable in the following sense: The (fine) mesh sizes H and h are small enough (in dependence on the wavenumber k) such that there is a constant C_{HMM} with

$$(C_{\mathrm{HMM}}\, k^{q+1})^{-1} \leq \inf_{\mathbf{v}_{H,h}\in\mathbf{V}_{H,h}} \sup_{\boldsymbol{\psi}_{H,h}\in\mathbf{V}_{H,h}} \frac{\operatorname{Re}\mathcal{B}(\mathbf{v}_{H,h}, \boldsymbol{\psi}_{H,h})}{\|\mathbf{v}_{H,h}\|_e \|\boldsymbol{\psi}_{h,h}\|_e}. \tag{4.51}$$

In Theorem 4.4.2, we proved that this discrete inf-sup condition holds under the classical resolution condition $k^{q+2}(H + h) = O(1)$.

Remark 4.5.1. We demonstrate the LOD at the specific example of the two-scale Helmholtz problem obtained in Theorem 4.2.1. However, the theory can easily be extended to more general two-scale Helmholtz problems, which fulfill the following assumptions:

- The variational problem (4.4) involves a continuous sesquilinear form with Gårding inequality.
- The analytical solution fulfills a stability estimate of order k^q (see Assumption 4.3.10).
- The (direct) Galerkin discretization (4.35) is stable (4.51) for sufficiently fine meshes.

This section is organized as follows: The LOD is introduced in Section 4.5.1 and its rigorous a priori error analysis is performed in Section 4.5.2. The proof of the exponential decay of the correctors is detailed in Section 4.5.3.

4.5.1 Localized Orthogonal Decomposition

In this section, we introduce the notation on meshes and (quasi)-interpolation operators and define the LOD in Petrov-Galerkin formulation for the two-scale setting. We close with some remarks regarding an implementation of the two-scale LOD.

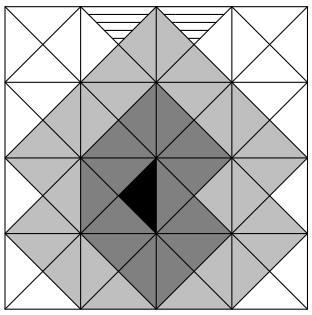

Figure 4.3: Triangle T (in black) and its first and second order patches. Striped triangles belong to $\mathrm{N}^2(T)$ in the case of periodic boundary conditions.

Meshes and interpolation operator. Let the (fine) meshes $\mathcal{T}_H$ of G and $\mathcal{T}_h$ of Y be given as in Section 4.4.1, we assume that H and h are small enough such that (4.51) is fulfilled. We consider a second, coarse discretization scale $H_c > H$ and $h_c > h$: Let $\mathcal{T}_{H_c}$ and $\mathcal{T}_{h_c}$ denote corresponding regular, quasi-uniform, and shape regular triangulations of G and Y, respectively. As for the fine grids, we additionally assume that $\mathcal{T}_{h_c}$ is periodic and that $\mathcal{T}_{H_c}$ and $\mathcal{T}_{h_c}$ resolve the partition of G into Ω and its complement and of Y into Σ and Σ^*, respectively. We denote by $\mathcal{T}_{h_c}(\Sigma^*)$ and $\mathcal{T}_{h_c}(\Sigma)$ the parts of $\mathcal{T}_{h_c}$ triangulating Σ^* and Σ, respectively. The global mesh sizes are defined as $H_c := \max\{\mathrm{diam}(T)|T \in \mathcal{T}_{H_c}\}$ and $h_c := \max\{\mathrm{diam}(S)|S \in \mathcal{T}_{h_c}\}$. For the sake of simplicity we assume that $\mathcal{T}_H$ and $\mathcal{T}_h$ are derived from $\mathcal{T}_{H_c}$ and $\mathcal{T}_{h_c}$, respectively, by some regular, possibly nonuniform, mesh refinement including at least one global refinement. We consider simplicial partitions, but the theory of this paper carries over to quadrilateral partitions [GP15] and even meshless methods would be possible [HMP15].

We use the notation $\mathrm{N}^m(\omega)$ for the mth layer patch around a subdomain $\omega \subset G$, as introduced in Definition 2.2.4. In this context, we also recall the overlap constants $C_{\mathrm{ol},m}$ (2.25) and $C_{\mathrm{ol}} := C_{\mathrm{ol},1}$. The patches can also be defined in a similar way for a subdomain $R \subset \overline{Y}$. Here, we split $R = R_1 \cup R_2$ with $R_1 = R \cap \Sigma$ and $R_2 = R \cap \Sigma^*$, where R_1 or R_2 may be empty, and we write in short $\mathrm{N}^m(R) := \mathrm{N}^m(R_1) \cup \mathrm{N}^m(R_2)$. $\mathrm{N}^m(R_1)$ is defined in the same way as before, in particular, it ends at the boundary $\partial\Sigma$. For the patch $\mathrm{N}^m(R_2)$ we interpret $\overline{\Sigma^*}$ as part of the torus. This implies that $\mathrm{N}^m(R_2)$ ends at the inner boundary $\partial\Sigma$, but is continued periodically over the outer boundary ∂Y. This means that also the striped triangles in Figure 4.3 belong to the second patch for the periodic setting. We denote the overlap constants by $C_{\mathrm{ol},m,Y}$ and $C_{\mathrm{ol},Y}$. By slight abuse of notation, we write $\mathrm{N}^m(\omega \times R) := \mathrm{N}^m(\omega) \times \mathrm{N}^m(R)$ for a subdomain $\omega \times R \subset \overline{G} \times \overline{Y}$.

We denote the conforming FE triple space consisting of lowest order Lagrange elements w.r.t. the meshes $\mathcal{T}_{H_c}$ and $\mathcal{T}_{h_c}$ by $\mathbf{V}_{H_c,h_c}$ as in Section 4.4. Again, we have $\mathbf{V}_{H_c,h_c} := \mathcal{S}(\mathcal{T}_H) \times L^2(\Omega; \widetilde{\mathcal{S}}(\mathcal{T}_{h_c}(\Sigma^*))) \times L^2(\Omega; \mathring{\mathcal{S}}(\mathcal{T}_{h_c}(\Sigma)))$ and we moreover note that $\mathbf{V}_{H_c,h_c} \subset \mathbf{V}_{H,h} \subset \mathcal{H}$.

A key tool in the definition and the analysis is a bounded linear surjective (quasi)-interpolation operator $\mathbf{\Pi}_{H_c,h_c} : \mathbf{V}_{H,h} \to \mathbf{V}_{H_c,h_c}$ that acts as a stable quasi-local projection in the following sense. It is a projection, i.e., $\mathbf{\Pi}_{H_c,h_c} \circ \mathbf{\Pi}_{H_c,h_c} = \mathbf{\Pi}_{H_c,h_c}$, and it is constructed as $\mathbf{\Pi}_{H_c,h_c} := (\Pi_{H_c}, \Pi_{h_c}^{\Sigma^*}, \Pi_{h_c}^{\Sigma})$, where each (quasi)-interpolation operator fulfills the following. There exist constants $C_{\Pi_{H_c}}$, $C_{\Pi_{h_c}^{\Sigma^*}}$, and $C_{\Pi_{h_c}^{\Sigma}}$ such that for all $\mathbf{v}_{H,h} := (v_H, v_{h,1}, v_{h,2}) \in \mathbf{V}_{H,h}$ and for all $T \in \mathcal{T}_{H_c}$, $S_1 \in \mathcal{T}_{h_c}(\Sigma^*)$, and $S_2 \in \mathcal{T}_{h_c}(\Sigma)$

$$\begin{aligned} H_c^{-1}\|v_H - \Pi_{H_c}(v_H)\|_T + \|\nabla \Pi_{H_c}(v_H)\|_T &\leq C_{\Pi_{H_c}} \|\nabla v_H\|_{\mathrm{N}(T)}, \\ h_c^{-1}\|v_{h,1} - \Pi_{h_c}^{\Sigma^*}(v_{h,1})\|_{T\times S_1} + \|\nabla_y \Pi_{h_c}^{\Sigma^*}(v_{h,1})\|_{T\times S_1} &\leq C_{\Pi_{H_c}^{\Sigma^*}} \|\nabla_y v_{h,1}\|_{T\times \mathrm{N}(S_1)}, \\ h_c^{-1}\|v_{h,2} - \Pi_{h_c}^{\Sigma}(v_{h,2})\|_{T\times S_2} + \|\nabla_y \Pi_{h_c}^{\Sigma}(v_{h,2})\|_{T\times S_2} &\leq C_{\Pi_{H_c}^{\Sigma}} \|\nabla_y v_{h,2}\|_{T\times \mathrm{N}(S_2)}. \end{aligned} \tag{4.52}$$

We abbreviate $C_{\mathbf{\Pi}} := \max\{C_{\Pi_{H_c}}, C_{\Pi^{\Sigma^*}_{h_c}}, C_{\Pi^{\Sigma}_{H_c}}\}$. Under the mesh condition that $k(H_c + h_c) \lesssim 1$, this implies stability in the two-scale energy norm

$$\|\mathbf{\Pi}_{H_c,h_c}\mathbf{v}_{H,h}\|_e \leq C_{\mathbf{\Pi},e}\|\mathbf{v}_{H,h}\|_e \qquad \forall \mathbf{v}_{H,h} \in \mathbf{V}_{H,h}. \tag{4.53}$$

The quasi-interpolation operator $\mathbf{\Pi}_{H_c,h_c}$ is not unique: A different choice might lead to a different Localized Orthogonal Decomposition and this can even affect the practical performance of the method [Pet17]. One popular choice is the concatenation of the L^2-projection onto piecewise polynomials and the Oswald interpolation operator, see also Section 2.2.3. Other choices are discussed in [EHMP16, Pet16]. Note that the operators $\Pi^{\Sigma^*}_{h_c}$ and $\Pi^{\Sigma}_{h_c}$ only act w.r.t. the second variable y. For $\Pi^{\Sigma^*}_{h_c}$, the averaging process of the Oswald interpolation operator has to be continued over the periodic boundary (as for the patches before) to preserve periodicity.

Definition of the LOD. The method approximates the discrete two-scale solution $\mathbf{u}_{H,h} := (u_H, u_{h,1}, u_{h,2})$ to (4.35) for given (fine) mesh sizes H, h. It is determined by the choice of the coarse mesh sizes H_c and h_c and the oversampling parameter m explained in the following. We assign to any $(T, S_1, S_2) \in \mathcal{T}_{H_c} \times \mathcal{T}_{h_c}(\Sigma^*) \times \mathcal{T}_{h_c}(\Sigma)$ its mth order patch $G_T \times \Sigma^*_S \times \Sigma_S = \mathrm{N}^m(T) \times \mathrm{N}^m(S_1) \times \mathrm{N}^m(S_2)$ and define for any $\mathbf{v}_{H,h} = (v_H, v_{h,1}, v_{h,2}), \boldsymbol{\psi}_{H,h} = (\psi_H, \psi_{h,1}, \psi_{h,2}) \in \mathbf{V}_{H,h}$ the localized sesquilinear form

$$\begin{aligned}
&\mathcal{B}_{G_T \times Y_S}(\mathbf{v}_{H,h}, \boldsymbol{\psi}_{H,h}) \\
&\quad := (\varepsilon_0^{-1}(\nabla v_H + \nabla_y v_{h,1}), \nabla \psi_H + \nabla_y \psi_{h,1})_{(G_T \cap \Omega) \times \Sigma^*_S} + (\varepsilon_1^{-1} \nabla_y v_{h,2}, \nabla_y \psi_{h,2})_{G_T \times \Sigma_S} \\
&\qquad + (\nabla v_H, \nabla \psi_H)_{G_T \cap (G \setminus \overline{\Omega})} - k^2 (v_H + \chi_D v_{h,2}, \psi_H, + \chi_D \psi_{h,2})_{G_T \times Y_S} \\
&\qquad - ik(v_H, \psi_H)_{\partial G_T \cap \partial G}
\end{aligned}$$

with $Y_S := \Sigma \cup \Sigma^*_S$. For $m = 0$ (i.e., $\mathrm{N}^m(T) = T$), we write $\mathcal{B}_{T \times S}$ with $S = S_1 \cup S_2$. Note that the oversampling parameter does not necessarily have to be the same for G, Σ^*, and Σ. We could as well introduce patches $\mathrm{N}^{m_0}(T) \times \mathrm{N}^{m_1}(S_1) \times \mathrm{N}^{m_2}(S_2)$, but we choose $m_0 = m_1 = m_2 =: m$ for simplicity of presentation and to improve readability.

We define the (truncated) finite element functions on the fine-scale meshes as

$$\begin{aligned}
\mathcal{S}(\mathcal{T}_H(G_T)) &:= \{v_H \in \mathcal{S}(\mathcal{T}_H) | v_H = 0 \text{ outside } G_T\}, \\
L^2(\Omega; \widetilde{\mathcal{S}}(\mathcal{T}_h(\Sigma^*_S))) &:= \{v_{h,1} \in L^2(\Omega; \widetilde{\mathcal{S}}(\mathcal{T}_h(\Sigma^*))) | v_{h,1} = 0 \text{ outside } (G_T \cap \Omega) \times \Sigma^*_S\},
\end{aligned}$$

and $L^2(\Omega; \mathring{\mathcal{S}}(\mathcal{T}_h(\Sigma_S)))$ in a similar way. Define the null space

$$\begin{aligned}
&\mathbf{W}_{H,h}(G_T \times Y_S) \\
&\quad := \{\mathbf{w}_{H,h} \in \mathcal{S}(\mathcal{T}_H(G_T)) \times L^2(\Omega; \widetilde{\mathcal{S}}(\mathcal{T}_h(\Sigma^*_S))) \times L^2(\Omega; \mathring{\mathcal{S}}(\mathcal{T}_h(\Sigma_S))) | \mathbf{\Pi}_{H_c,h_c}(\mathbf{w}_{H,h}) = 0\}
\end{aligned}$$

and note that $\mathbf{W}_{H,h}(G_T \times Y_S) := W_H(G_T) \times L^2(\Omega; W_h(\Sigma^*_S)) \times L^2(\Omega; W_h(\Sigma_S))$, where W_H and W_h are defined as the kernels of the corresponding (single) interpolation operators Π_{H_C} and $\Pi^{\Sigma^*}_{h_c}$ and $\Pi^{\Sigma}_{h_c}$, respectively. For given $\mathbf{v}_{H_c,h_c} \in \mathbf{V}_{H_c,h_c}$ we define the localized correction $\mathbf{Q}_m(\mathbf{v}_{H_c,h_c}) := (Q_m(v_{H_c}), Q_{m,1}(v_{h_c,1}), Q_{m,2}(v_{h_c,2}))$ as

$$\mathbf{Q}_m(\mathbf{v}_{H_c,h_c}) := \sum_{(T,S_1,S_2) \in \mathcal{T}_{H_c} \times \mathcal{T}_{h_c}(\Sigma^*) \times \mathcal{T}_{h_c}(\Sigma)} \mathbf{Q}_{T \times S, m}(\mathbf{v}_{H_c,h_c}|_{T \times S}),$$

where $\mathbf{Q}_{T \times S, m}(\mathbf{v}_{H_c,h_c}|_{T \times S}) \in \mathbf{W}_{H,h}(G_T \times Y_S)$ solves the following subscale corrector problem

$$\mathcal{B}_{G_T \times Y_S}(\mathbf{w}_{H,h}, \mathbf{Q}_{T \times S, m}(\mathbf{v}_{H_c,h_c}|_{T \times S})) = \mathcal{B}_{T \times S}(\mathbf{w}_{H,h}, \mathbf{v}_{H_c,h_c}) \quad \forall \mathbf{w}_{H,h} \in \mathbf{W}_{H,h}(G_T \times Y_S). \tag{4.54}$$

The space of test functions then reads

$$\overline{\mathbf{V}}_{H_c,h_c,m} := (\mathrm{id} - \mathbf{Q}_m)(\mathbf{V}_{H_c,h_c})$$

and can be written as triple

$$\overline{\mathbf{V}}_{H_c,h_c,m} = \overline{V}_{H_c,m} \times L^2(\Omega; \overline{V}_{h_c,m}(\Sigma^*)) \times L^2(\Omega; \overline{V}_{h_c,m}(\Sigma)).$$

We emphasize that $\dim \overline{\mathbf{V}}_{H_c,h_c,m} = \dim \mathbf{V}_{H_c,h_c}$ and hence, $\overline{\mathbf{V}}_{H_c,h_c,m}$ is low-dimensional. Moreover, the dimension does not depend on H, h, or m.

Definition 4.5.2. For the two-scale Localized Orthogonal Decomposition in Petrov-Galerkin formulation we seek $\mathbf{u}_{H_c,h_c} \in \mathbf{V}_{H_c,h_c}$ such that

$$\mathcal{B}(\mathbf{u}_{H_c,h_c}, \overline{\boldsymbol{\psi}}_{H_c,h_c}) = (g, \overline{\psi}_{H_c})_{\partial G} \qquad \forall \overline{\boldsymbol{\psi}}_{H_c,h_c} := (\overline{\psi}_{H_c}, \overline{\psi}_{h_c,1}, \overline{\psi}_{h_c,2}) \in \overline{\mathbf{V}}_{H_c,h_c,m}. \tag{4.55}$$

The error analysis will show that the choice $k(H_c + h_c) \lesssim 1$ and $m \approx \log k$ suffices to guarantee stability and quasi-optimality of the method, provided that the direct discretization (4.35) (with mesh widths H, h) is stable.

As discussed in [Pet17], further stable variants of the method are possible: The local subscale correction procedure can be applied only to the test functions, only to the ansatz functions, or to both ansatz and test functions.

Remarks on implementation aspects. The present approach of the LOD exploits the two-scale structure of the underlying problem. In practice, we cannot work with the space triples such as $\mathbf{V}_{H_c,h_c}$, but look at each of the function spaces separately. The LOD consists of two main steps: First, the modified basis functions of $\overline{\mathbf{V}}_{H_c,h_c,m}$ have to be determined, which includes the solution of the localized subscale corrector problems (4.54). Second, the actual LOD-approximation is computed as solution to (4.55). In both steps, the computations for the macroscopic domain and the unit square can be decoupled. For general considerations on how to implement an LOD, for example algebraic realizations of the problems, we refer to [EHMP16].

Computation of modified bases. We observe that due to the sesquilinearity of $\mathcal{B}$ the following linearity fof the correction operators $\mathbf{Q}_m$ holds

$$\begin{aligned}\mathbf{Q}_m \mathbf{v}_{H_c,h_c} &= \mathbf{Q}_m(v_{H_c}, 0, 0) + \mathbf{Q}_m(0, v_{h_c,1}, 0) + \mathbf{Q}_m(0, 0, v_{h_c,2}) \\ &= (Q_m(v_{H_c}), 0, 0) + (0, Q_{m,1}(v_{h_c}), 0) + (0, 0, Q_{m,2}(v_{h_c,2})).\end{aligned}$$

This means that the corrections of the basis functions in $\mathcal{S}(\mathcal{T}_{H_c})$, $\widetilde{\mathcal{S}}(\mathcal{T}_{h_c}(\Sigma^*))$, and $\mathring{\mathcal{S}}(\mathcal{T}_{h_c}(\Sigma))$ can be computed separately in the following way:

1. Choose bases $\{\lambda_x\}$ of $\mathcal{S}(\mathcal{T}_{H_c})$, $\{\lambda_{y,1}\}$ of $\widetilde{\mathcal{S}}(\mathcal{T}_{h_c}(\Sigma^*))$, and $\{\lambda_{y,2}\}$ of $\mathring{\mathcal{S}}(\mathcal{T}_{h_c}(\Sigma))$.
2. For each basis function λ_x, $\lambda_{y,1}$, and $\lambda_{y,2}$:
   a) Find the solutions $Q_{T\times S,m}(\lambda_x)$, $Q_{T\times S,m,1}(\lambda_{y,1})$, and $Q_{T\times S,m,2}(\lambda_{y,2})$ to the corrector problem (4.54) for each $T \in \mathcal{T}_{H_c}$, $S_1 \in \mathcal{T}_{h_c}(\Sigma^*)$, and $S_2 \in \mathcal{T}_{h_c}(\Sigma)$. This needs the determination of $W_H(G_T)$, $W_h(\Sigma_S^*)$, and $W_h(\Sigma_S)$.
   b) Build up the modified bases $\overline{\lambda}_x$ of $\overline{V}_{H_c,m}$, $\overline{\lambda}_{y,1}$ of $\overline{V}_{h_c,m}(\Sigma^*)$, and $\overline{\lambda}_{y,2}$ of $\overline{V}_{h_c,m}(\Sigma)$ via $\overline{\lambda}_x := \lambda_x - \sum_{(T,S_1,S_2)\in\mathcal{T}_{H_c}\times\mathcal{T}_{h_c}(\Sigma^*)\times\mathcal{T}_{h_c}(\Sigma)} Q_{T\times S,m}(\lambda_x)$, etc.

Note that no communication between the basis functions on G, Σ^*, and Σ is needed and therefore, the computation of the modified bases can be easily parallelized. Only if the parameters ε_1 and ε_0 are constant w.r.t. x as here, the corrections $Q_{T\times S,m,1}$ and $Q_{T\times S,m,2}$ are x-independent. Depending on the choice of the interpolation operator, Lagrange multipliers can be employed to decode if a function belongs to W_H or W_h, see [EHMP16].

We can further decrease the computational complexity of the localized corrector problems by decoupling the integrals over G and Y and by reducing the number of corrector problems. The potential gain of course hinges on (additional) structure of the parameters and the meshes with the following general observations:

- The corrections $Q_{T\times S,m,1}$ and $Q_{T\times S,m,2}$ only have to be computed for $T \in \mathcal{T}_{H_c}$ with $T \cap \Omega \neq \emptyset$.
- It is sufficient to choose test functions of the form $\mathbf{w} = (w, 0, 0)$ for $Q_{T\times S,m}$, $\mathbf{w} = (0, w_1, 0)$ for $Q_{T\times S,m,1}$, and $\mathbf{w} = (0, 0, w_2)$ for $Q_{T\times S,m,2}$.
- In the case of constant parameters ε_1 and ε_0, the corrector problems for $Q_{T\times S,m,1}$ and $Q_{T\times S,m,2}$ include information on T only in form of the weights $|T|$ and $|\Omega|$; and the problems for $Q_{T\times S,m}$ only depend on S in form of the weights $|S_1|$ and $|\Sigma_S^*|$.
- In case of structured meshes $\mathcal{T}_{H_c}$ and $\mathcal{T}_{h_c}$ and constant parameters, we can exploit symmetries to reduce the number of corrector problems [GP15].

Computation of the LOD-approximation. The LOD-approximation is defined as the solution to (4.55). This problem is similar to the discrete two-scale equation (4.35), only the test functions have been modified. Therefore, the LOD-approximation can be re-interpreted as an HMM-approximation with modified test functions and corrector problems. To be more explicit, $\mathbf{u}_{H_c,h_c} \in \mathbf{V}_{H_c,h_c}$ from Definition 4.5.2 can be characterized as $\mathbf{u}_{H_c,h_c} = (u_{H_c}, K_{h_c,1}(u_{H_c}), K_{h_c,2}(u_{H_c}))$, where $u_{H_c} \in V^1_{H_c}$ is the solution to an HMM with modified test functions and the corrections $K_{h_c,1}(u_{H_c})$ and $K_{h_c,2}(u_{H_c})$ are computed from u_{H_c} and its reconstructions; see Section 2.3.3 and [HOV16b, Ohl05] for similar reformulations in different settings. The HMM with modified test functions involves the following two steps:

1. Solve the cell problems for the reconstructions around each quadrature point of the macroscopic triangulation $\mathcal{T}_{H_c}$ using test functions in $\overline{V}_{h_c,m}(\Sigma^*)$ and $\overline{V}_{h_c,m}(\Sigma)$.
2. Assemble the macroscopic sesquilinear form with the computed reconstructions and the test functions in $\overline{V}_{H_c,m}$.

Note that the reconstructions as well as the fine-scale correctors $K_{h,1}$ and $K_{h,2}$ are different from those of a standard HMM for this problem because of the modified test functions. This reformulation of the LOD-approximation as solution to a (modified) HMM decouples the computations on Y and G and no triple function spaces have to be considered. This is one great advantage of the present Petrov-Galerkin ansatz for the LOD in comparison to a Galerkin ansatz: We only need to compute reconstructions of standard Lagrange basis functions in $\mathcal{S}(\mathcal{T}_{H_c})$, but not of the basis functions in $\overline{V}_{H_c,m}$.

4.5.2 Error analysis

The error analysis is based on the observation that the localized subscale corrector problems (4.54) can be seen as perturbation of idealized subscale problems posed on the whole domain $G \times Y$. Let us introduce idealized counterparts of the correction operators $\mathbf{Q}_{T\times S,m}$ and $\mathbf{Q}_m$ where the patch $G_T \times Y_S$ equals $G \times Y$, roughly speaking "$m = \infty$". Define the null space

$$\mathbf{W}_{H,h} := W_H \times L^2(\Omega; W_h(\Sigma^*)) \times L^2(\Omega; W_h(\Sigma)) := \{\mathbf{v}_{H,h} \in \mathbf{V}_{H,h} | \mathbf{\Pi}_{H_c,h_c}(\mathbf{v}_{H,h}) = 0\}.$$

For any $\mathbf{v}_{H,h} \in \mathbf{V}_{H,h}$, the idealized element corrector problem seeks $\mathbf{Q}_{T\times S,\infty}\mathbf{v}_{H,h} \in \mathbf{W}_{H,h}$ such that

$$\mathcal{B}(\mathbf{w}_{H,h}, \mathbf{Q}_{T\times S,\infty}\mathbf{v}_{H,h}) = \mathcal{B}_{T\times S}(\mathbf{w}_{H,h}, \mathbf{v}_{H,h}) \qquad \forall \mathbf{w}_{H,h} \in \mathbf{W}_{H,h}, \tag{4.56}$$

and we define

$$\mathbf{Q}_\infty(\mathbf{v}_{H,h}) := \sum_{(T,S_1,S_2)\in\mathcal{T}_{H_c}\times\mathcal{T}_{h_c}(\Sigma^*)\times\mathcal{T}_{h_c}(\Sigma)} \mathbf{Q}_{T\times S,\infty}(\mathbf{v}_{H,h}). \tag{4.57}$$

The following result implies the well-posedness of the idealized corrector problems.

Lemma 4.5.3. *Under the assumption*

$$k(C_{\Pi_{H_c}}\sqrt{C_{\mathrm{ol},G}}\,H_c + C_{\Pi^\Sigma_{h_c}}\sqrt{C_{\mathrm{ol},Y}}\,h_c) \le \sqrt{C_{\min}/2}, \tag{4.58}$$

we have for all $\mathbf{w}_{H,h} := (w_H, w_{h,1}, w_{h,2}) \in \mathbf{W}_{H,h}$ *the following equivalence of norms*

$$\|(w_H, w_{h,1}, w_{h,2})\|_{1,e} \le \|(w_H, w_{h,1}, w_{h,2})\|_e \le \sqrt{1 + C_{\min}/2}\,\|(w_H, w_{h,1}, w_{h,2})\|_{1,e},$$

and coercivity

$$C_{\min}/2\,\|(w_H, w_{h,1}, w_{h,2})\|^2_{1,e} \le \operatorname{Re}\mathcal{B}(\mathbf{w}_{H,h}, \mathbf{w}_{H,h}),$$

where the H^1*-seminorm* $\|\cdot\|_{1,e}$ *is defined in* (4.50).

Proof. The essential observation is that for any $(w_H, w_{h,1}, w_{h,2}) \in \mathbf{W}_{H,h}$ the property of the quasi-interpolation operators (4.52) implies that

$$\begin{aligned} k^2\|w_H + \chi_\Sigma w_{h,2}\|^2_{G\times Y} &\le k^2\big(\|w_H\|_G + \|w_{h,2}\|_{G\times\Sigma}\big)^2 \\ &= k^2\big(\|w_H - \Pi_{H_c}(w_H)\|_G + \|w_{h,2} - \Pi^\Sigma_{h_c}(w_{h,2})\|_{G\times\Sigma}\big)^2 \\ &\le k^2\big(H_c\,C_{\Pi_{H_c}}\sqrt{C_{\mathrm{ol},G}}\,\|\nabla w_H\|_G + h_c\,C_{\Pi^\Sigma_{h_c}}\sqrt{C_{\mathrm{ol},Y}}\|\nabla_y w_{h,2}\|_{G\times\Sigma}\big)^2. \end{aligned}$$

This directly yields the equivalence of norms on $\mathbf{W}_{H,h}$ under the resolution condition (4.58). For the coercivity we observe that

$$\operatorname{Re}\mathcal{B}(\mathbf{w}_{H,h}, \mathbf{w}_{H,h}) \ge C_{\min}\|\mathbf{w}_{H,h}\|^2_{1,e} - k^2\|w_H + \chi_\Sigma w_{h,2}\|^2_{G\times Y}. \qquad \square$$

As the sesquilinear form $\mathcal{B}$ is also continuous (see Lemma 4.3.2), Lemma 4.5.3 implies that the idealized corrector problem (4.56) is well-posed and that the idealized correctors $\mathbf{Q}_\infty$ defined by (4.57) are continuous w.r.t. the two-scale energy norm

$$\|\mathbf{Q}_\infty(\mathbf{v}_{H,h})\|_e \le C_{\mathbf{Q}}\,\|\mathbf{v}_{H,h}\|_e \qquad \forall \mathbf{v}_{H,h} \in \mathbf{V}_{H,h}.$$

Since the inclusion $\mathbf{W}_{H,h}(G_T \times Y_S) \subset \mathbf{W}_{H,h}$ holds, the well-posedness result carries over to the localized corrector problems (4.54) with the same constant.

The proof of the well-posedness of the two-scale LOD in Petrov-Galerkin formulation (4.55) relies on the fact that $(\mathbf{Q}_\infty - \mathbf{Q}_m)(\mathbf{v})$ decays exponentially with the distance from $\operatorname{supp}(\mathbf{v})$. The difference between idealized and localized correctors is quantified in the next theorem. The proof is given in Section 4.5.3 and is based on the observation that $\mathbf{Q}_\infty(\mathbf{v}|_{T\times S})$ decays exponentially with distance from $T \times S$.

Theorem 4.5.4 (Error of corrector localization)**.** *Under the resolution condition* (4.58) *there exist constants* C_1*,* C_2*, and* $0 < \beta < 1$*, independent of* H_c*,* h_c*,* H*, and* h*, such that for any* $\mathbf{v}_{H_c,h_c} \in \mathbf{V}_{H_c,h_c}$*, any* $(T, S_1, S_2) \in \mathcal{T}_{H_c} \times \mathcal{T}_{h_c}(\Sigma^*) \times \mathcal{T}_{h_c}(\Sigma)$*, and any* $m \in \mathbb{N}$ *it holds*

$$\|(\mathbf{Q}_{T\times S,\infty} - \mathbf{Q}_{T\times S,m})(\mathbf{v}_{H_c,h_c})\|_{1,e} \le C_1\beta^m\|\mathbf{v}_{H_c,h_c}\|_{1,e,T\times S}, \tag{4.59}$$

$$\|(\mathbf{Q}_\infty - \mathbf{Q}_m)(\mathbf{v}_{H_c,h_c})\|_{1,e} \le C_2(\sqrt{C_{\mathrm{ol},m,G}} + \sqrt{C_{\mathrm{ol},m,Y}})\beta^m\|\mathbf{v}_{H_c,h_c}\|_{1,e}. \tag{4.60}$$

The stability of the LOD requires the coupling of the oversampling parameter m to the stability/inf-sup constant of the HMM. Therefore, we assume that H and h are small enough such that (4.51) holds.

Theorem 4.5.5 (Well-posedness of the LOD)**.** *Under the resolution conditions* (4.51) *and* (4.58)*, and the following oversampling condition*

$$m \geq \frac{(q+1)\log(k)+\log\big(2C_2C_{\mathbf{\Pi}}C_{\mathbf{\Pi},e}C_{\mathrm{HMM}}C_B\sqrt{1+C_{\min}/2}\big(\sqrt{C_{\mathrm{ol},m,G}}+\sqrt{C_{\mathrm{ol},m,Y}}\big)\big)}{|\log(\beta)|}, \quad (4.61)$$

the two-scale LOD (4.55) *is well-posed and with the constant* $C_{\mathrm{LOD}} := 2C_{\mathrm{HMM}}C_{\mathbf{\Pi},e}^2(1+C_{\mathbf{Q}})$ *it holds*

$$(C_{\mathrm{LOD}}\, k^{q+1})^{-1} \leq \inf_{\mathbf{v}_{H_c,h_c}\in\mathbf{V}_{H_c,h_c}} \sup_{\overline{\boldsymbol{\psi}}_{H_c,h_c}\in\overline{\mathbf{V}}_{H_c,h_c,m}} \frac{\mathrm{Re}\,\mathcal{B}(\mathbf{v}_{H_c,h_c},\overline{\boldsymbol{\psi}}_{H_c,h_c})}{\|\mathbf{v}_{H_c,h_c}\|_e\|\overline{\boldsymbol{\psi}}_{H_c,h_c}\|_e}.$$

As $C_{\mathrm{ol},m,G}$ and $C_{\mathrm{ol},m,Y}$ grow at most polynomially with m because of the quasi-uniformity of $\mathcal{T}_{H_c}$ and $\mathcal{T}_{h_c}$, condition (4.61) is indeed satisfiable and the choice of the oversampling parameter m is dominated by the logarithm of the wavenumber, i.e., $m \approx \log k$ is a good choice. This condition for the oversampling parameter is standard for the LOD of Helmholtz problems, see, for instance, [Pet17, equation (5.12)]. In the numerical examples, moderate choices of m were sufficient, see Remark 4.5.9.

Proof. Let $\mathbf{v}_{H_c,h_c} \in \mathbf{V}_{H_c,h_c}$ be given. From (4.51) we infer that there is $\boldsymbol{\psi}_{H,h} \in \mathbf{V}_{H,h}$ such that

$$\mathrm{Re}\,\mathcal{B}(\mathbf{v}_{H_c,h_c}-(\mathbf{Q}_\infty(\mathbf{v}^*_{H_c,h_c}))^*,\boldsymbol{\psi}_{H,h}) \geq C_{\mathrm{HMM}}^{-1}k^{-(q+1)}\|\mathbf{v}_{H_c,h_c}-(\mathbf{Q}_\infty(\mathbf{v}^*_{H_c,h_c}))^*\|_e\,\|\boldsymbol{\psi}_{H,h}\|_e.$$

It follows from the structure of the sesquilinear form $\mathcal{B}$ that $(\mathbf{Q}_\infty(\mathbf{v}^*_{H_c,h_c}))^*$ solves the following adjoint corrector problem

$$\mathcal{B}((\mathbf{Q}_\infty(\mathbf{v}^*_{H_c,h_c}))^*,\mathbf{w}_{H,h}) = \mathcal{B}(\mathbf{v}_{H_c,h_c},\mathbf{w}_{H,h}) \qquad \forall \mathbf{w}_{H,h}\in\mathbf{W}_{H,h}.$$

Let $\overline{\boldsymbol{\psi}}_{H_c,h_c} := (\mathrm{id}-\mathbf{Q}_m)\mathbf{\Pi}_{H_c,h_c}\boldsymbol{\psi}_{H,h} \in \overline{\mathbf{V}}_{H_c,h_c,m}$. It obviously holds that

$$\mathcal{B}(\mathbf{v}_{H_c,h_c},\overline{\boldsymbol{\psi}}_{H_c,h_c}) = \mathcal{B}(\mathbf{v}_{H_c,h_c},(\mathrm{id}-\mathbf{Q}_\infty)\mathbf{\Pi}_{H_c,h_c}\boldsymbol{\psi}_{H,h}) + \mathcal{B}(\mathbf{v}_{H_c,h_c},(\mathbf{Q}_\infty-\mathbf{Q}_m)\mathbf{\Pi}_{H_c,h_c}\boldsymbol{\psi}_{H,h}). \quad (4.62)$$

Since $\mathbf{Q}_\infty$ is a projection onto $\mathbf{W}_{H,h}$ and $(\mathrm{id}-\mathbf{\Pi}_{H_c,h_c})\boldsymbol{\psi}_{H,h} \in \mathbf{W}_{H,h}$, we have

$$(\mathrm{id}-\mathbf{Q}_\infty)(\mathrm{id}-\mathbf{\Pi}_{H_c,h_c})\boldsymbol{\psi}_{H,h} = 0$$

and thus, $(\mathrm{id}-\mathbf{Q}_\infty)\mathbf{\Pi}_{H_c,h_c}\boldsymbol{\psi}_{H,h} = (\mathrm{id}-\mathbf{Q}_\infty)\boldsymbol{\psi}_{H,h}$. The solution property of $(\mathbf{Q}_\infty(\mathbf{v}^*_{H_c,h_c}))^*$ and the definition of $\mathbf{Q}_\infty$ in (4.56)–(4.57) gives

$$\begin{aligned}\mathcal{B}((\mathbf{Q}_\infty(\mathbf{v}^*_{H_c,h_c}))^*,\boldsymbol{\psi}_{H,h}) &= \mathcal{B}((\mathbf{Q}_\infty(\mathbf{v}^*_{H_c,h_c}))^*,\mathbf{Q}_\infty\boldsymbol{\psi}_{H,h}) + \mathcal{B}((\mathbf{Q}_\infty(\mathbf{v}^*_{H_c,h_c}))^*,(\mathrm{id}-\mathbf{Q}_\infty)\boldsymbol{\psi}_{H,h})\\ &= \mathcal{B}(\mathbf{v}_{H_c,h_c},\mathbf{Q}_\infty\boldsymbol{\psi}_{H,h}).\end{aligned}$$

Hence, we obtain

$$\begin{aligned}\mathrm{Re}\,\mathcal{B}(\mathbf{v}_{H_c,h_c},(\mathrm{id}-\mathbf{Q}_\infty)\mathbf{\Pi}_{H_c,h_c}\boldsymbol{\psi}_{H,h}) &= \mathrm{Re}\,\mathcal{B}(\mathbf{v}_{H_c,h_c}-(\mathbf{Q}_\infty(\mathbf{v}^*_{H_c,h_c}))^*,\boldsymbol{\psi}_{H,h})\\ &\geq (C_{\mathrm{HMM}}\,k^{q+1})^{-1}\,\|\mathbf{v}_{H_c,h_c}-(\mathbf{Q}_\infty(\mathbf{v}^*_{H_c,h_c}))^*\|_e\,\|\boldsymbol{\psi}_{H,h}\|_e.\end{aligned}$$

Furthermore, the estimate (4.53) implies

$$\|\mathbf{v}_{H_c,h_c}\|_e = \|\mathbf{\Pi}_{H_c,h_c}(\mathbf{v}_{H_c,h_c}-(\mathbf{Q}_\infty(\mathbf{v}^*_{H_c,h_c}))^*)\|_e \leq C_{\mathbf{\Pi},e}\|\mathbf{v}_{H_c,h_c}-(\mathbf{Q}_\infty(\mathbf{v}^*_{H_c,h_c}))^*\|_e$$

and

$$\|\overline{\boldsymbol{\psi}}_{H_c,h_c}\|_e \leq C_{\mathbf{\Pi},e}(1+C_{\mathbf{Q}})\,\|\boldsymbol{\psi}_{H,h}\|_e.$$

The second term on the right-hand side of (4.62) satisfies with Lemma 4.5.3 and Theorem 4.5.4 that

$$\begin{aligned}
&|\mathcal{B}(\mathbf{v}_{H_c,h_c}, (\mathbf{Q}_\infty - \mathbf{Q}_m)\boldsymbol{\Pi}_{H_c,h_c}\boldsymbol{\psi}_{H,h})| \\
&\quad \leq \sqrt{1 + C_{\min}/2}\, C_B \, \|(\mathbf{Q}_\infty - \mathbf{Q}_m)\boldsymbol{\Pi}_{H_c,h_c}\boldsymbol{\psi}_{H,h}\|_{1,e} \, \|\mathbf{v}_{H_c,h_c}\|_e \\
&\quad \leq \sqrt{1 + C_{\min}/2}\, C_B C_2 \big(\sqrt{C_{\mathrm{ol},m,G}} + \sqrt{C_{\mathrm{ol},m,Y}}\big)\beta^m C_{\boldsymbol{\Pi}} \, \|\boldsymbol{\psi}_{H,h}\|_e \, \|\mathbf{v}_{H_c,h_c}\|_e.
\end{aligned}$$

Altogether, this yields

$$\begin{aligned}
&\operatorname{Re} \mathcal{B}(\mathbf{v}_{H_c,h_c}, \overline{\boldsymbol{\psi}}_{H_c,h_c}) \\
&\quad \geq \Big(\frac{1}{C_{\boldsymbol{\Pi},e} C_{\mathrm{HMM}} k^{q+1}} - \sqrt{1 + C_{\min}/2}\, C_B C_2 \big(\sqrt{C_{\mathrm{ol},m,G}} + \sqrt{C_{\mathrm{ol},m,Y}}\big)\beta^m C_{\boldsymbol{\Pi}}\Big) \\
&\qquad \cdot \|\mathbf{v}_{H_c,h_c}\|_e \, \|\boldsymbol{\psi}_{H,h}\|_e \\
&\quad \geq \Big(\frac{1}{C_{\boldsymbol{\Pi},e} C_{\mathrm{HMM}} k^{q+1}} - \sqrt{1 + C_{\min}/2}\, C_B C_2 \big(\sqrt{C_{\mathrm{ol},m,G}} + \sqrt{C_{\mathrm{ol},m,Y}}\big)\beta^m C_{\boldsymbol{\Pi}}\Big) \\
&\qquad \cdot \frac{1}{C_{\boldsymbol{\Pi},e}(1 + C_{\mathbf{Q}})} \, \|\mathbf{v}_{H_c,h_c}\|_e \, \|\overline{\boldsymbol{\psi}}_{H_c,h_c}\|_e.
\end{aligned}$$

Hence, the condition (4.61) implies the assertion. □

Remark 4.5.6 (Adjoint problem)**.** Under the assumption of Theorem 4.5.5, problem (4.55) is well-posed. Thus, it follows from a dimension argument that also the adjoint problem to (4.55) is well-posed with the same stability constant as in Theorem 4.5.5, cf. [GP15, Rem. 1].

Theorem 4.5.7 (Quasi-optimality)**.** *Under the resolution conditions* (4.51) *and* (4.58)*, and the oversampling conditions* (4.61) *and*

$$m \geq \big((q+1)\log(k) + \log(2\sqrt{1 + C_{\min}/2}\, C_B^2 C_2 C_{\mathrm{LOD}})\big)/|\log(\beta)|, \tag{4.63}$$

the LOD-approximation $\mathbf{u}_{H_c,h_c}$*, solution to* (4.55)*, and the solution* $\mathbf{u}_{H,h}$ *to the direct discretization* (4.35) *satisfy*

$$\|\mathbf{u}_{H,h} - \mathbf{u}_{H_c,h_c}\|_e \leq C \min_{\mathbf{v}_{H_c,h_c} \in \mathbf{V}_{H_c,h_c}} \|\mathbf{u}_{H,h} - \mathbf{v}_{H_c,h_c}\|_e$$

with a generic constant C *depending only on* $C_{\boldsymbol{\Pi},e}$*.*

Proof. Let $\mathbf{e} := \mathbf{u}_{H,h} - \mathbf{u}_{H_c,h_c}$. We prove that $\|\mathbf{e}\|_e \leq 2\|(\mathrm{id} - \boldsymbol{\Pi}_{H_c,h_c})\mathbf{u}_{H,h}\|_e$, which gives the assertion because $\boldsymbol{\Pi}_{H_c,h_c}$ is a projection. By the triangle inequality and the fact that $\boldsymbol{\Pi}_{H_c,h_c}$ is a projection onto $\mathbf{V}_{H_c,h_c}$, we obtain

$$\|\mathbf{e}\|_e \leq \|(\mathrm{id} - \boldsymbol{\Pi}_{H_c,h_c})\mathbf{u}_{H,h}\|_e + \|\boldsymbol{\Pi}_{H_c,h_c}\mathbf{e}\|_e,$$

so that it only remains to bound the second term on the right-hand side. The proof employs a standard duality argument, the stability of the idealized method, and the fact that the actual two-scale LOD can be seen as a perturbation of the idealized method. Let $\mathbf{z}_{H_c,h_c} \in \mathbf{V}_{H_c,h_c}$ be the solution to the dual problem

$$\mathcal{B}(\boldsymbol{\psi}_{H_c,h_c}, (\mathrm{id} - \mathbf{Q}_\infty)\mathbf{z}_{H_c,h_c}) = (\boldsymbol{\psi}_{H_c,h_c}, \boldsymbol{\Pi}_{H_c,h_c}\mathbf{e})_e \qquad \forall \boldsymbol{\psi}_{H_c,h_c} \in \mathbf{V}_{H_c,h_c},$$

where $(\cdot,\cdot)_e$ denotes the scalar product which induces the two-scale energy norm (4.15). This adjoint problem is uniquely solvable as explained in Remark 4.5.6. Choosing the test function $\boldsymbol{\psi}_{H_c,h_c} = \boldsymbol{\Pi}_{H_c,h_c}\mathbf{e}$ implies

$$\begin{aligned}
\|\boldsymbol{\Pi}_{H_c,h_c}\mathbf{e}\|_e^2 &= \mathcal{B}(\boldsymbol{\Pi}_{H_c,h_c}\mathbf{e}, (\mathrm{id} - \mathbf{Q}_\infty)\mathbf{z}_{H_c,h_c}) \\
&= \mathcal{B}(\boldsymbol{\Pi}_{H_c,h_c}\mathbf{e}, (\mathbf{Q}_m - \mathbf{Q}_\infty)\mathbf{z}_{H_c,h_c}) + \mathcal{B}(\boldsymbol{\Pi}_{H_c,h_c}\mathbf{e}, (\mathrm{id} - \mathbf{Q}_m)\mathbf{z}_{H_c,h_c}).
\end{aligned} \tag{4.64}$$

Since $(\mathrm{id}-\mathbf{Q}_m)\mathbf{z}_{H_c,h_c} \in \overline{\mathbf{V}}_{H_c,h_c,m}$ by definition, we have the Galerkin orthogonality

$$\mathcal{B}(\mathbf{u}_{H,h}-\mathbf{u}_{H_c,h_c},(\mathrm{id}-\mathbf{Q}_m)\mathbf{z}_{H_c,h_c})=0.$$

Using this orthogonality and the fact that $\mathbf{\Pi}_{H_c,h_c}\mathbf{u}_{H,h}-\mathbf{u}_{H,h} \in \mathbf{W}_{H,h}$ together with the definition of $\mathbf{Q}_\infty$ (4.56)–(4.57) implies for the second term

$$\begin{aligned}\mathcal{B}(\mathbf{\Pi}_{H_c,h_c}\mathbf{e},(\mathrm{id}-\mathbf{Q}_m)\mathbf{z}_{H_c,h_c}) &= \mathcal{B}(\mathbf{\Pi}_{H_c,h_c}\mathbf{u}_{H,h}-\mathbf{u}_{H,h},(\mathrm{id}-\mathbf{Q}_m)\mathbf{z}_{H_c,h_c})\\ &= \mathcal{B}(\mathbf{\Pi}_{H_c,h_c}\mathbf{u}_{H,h}-\mathbf{u}_{H,h},(\mathbf{Q}_\infty-\mathbf{Q}_m)\mathbf{z}_{H_c,h_c}).\end{aligned}$$

The first and the (modified) second term of (4.64) are similar now and can be treated with the same procedure. First, we note that $(\mathbf{Q}_\infty-\mathbf{Q}_m)\mathbf{z}_{H_c,h_c} \in \mathbf{W}_{H,h}$. Applying Lemma 4.5.3 and then the decay estimate (4.60) from Theorem 4.5.4, we obtain (for the second term)

$$\begin{aligned}&|\mathcal{B}(\mathbf{\Pi}_{H_c,h_c}\mathbf{u}_{H,h}-\mathbf{u}_{H,h},(\mathbf{Q}_\infty-\mathbf{Q}_m)\mathbf{z}_{H_c,h_c})|\\ &\quad\le \sqrt{1+C_{\min}/2}\,C_B\|(\mathrm{id}-\mathbf{\Pi}_{H_c,h_c})\mathbf{u}_{H,h}\|_e\,\|(\mathbf{Q}_\infty-\mathbf{Q}_m)\mathbf{z}_{H_c,h_c}\|_{1,e}\\ &\quad\le \sqrt{1+C_{\min}/2}\,C_BC_2\big(\sqrt{C_{\mathrm{ol},m,G}}+\sqrt{C_{\mathrm{ol},m,Y}}\big)\beta^m\,\|(\mathrm{id}-\mathbf{\Pi}_{H_c,h_c})\mathbf{u}_{H,h}\|_e\,\|\mathbf{z}_{H_c,h_c}\|_{1,e}.\end{aligned}$$

The stability of the adjoint problem from Remark 4.5.6 implies

$$\|\mathbf{z}_{H_c,h_c}\|_{1,e} \le C_{\mathrm{LOD}}k^{q+1}C_B\|\mathbf{\Pi}_{H_c,h_c}\mathbf{e}\|_e.$$

Thus, we obtain for (4.64) after division by $\|\mathbf{\Pi}_{H_c,h_c}\mathbf{e}\|_e$ that

$$\begin{aligned}\|\mathbf{\Pi}_{H_c,h_c}\mathbf{e}\|_e \le \sqrt{1+C_{\min}/2}\,C_B^2C_2\big(\sqrt{C_{\mathrm{ol},m,G}}+\sqrt{C_{\mathrm{ol},m,Y}}\big)\beta^mC_{\mathrm{LOD}}k^{q+1}\\ \cdot\big(\|(\mathrm{id}-\mathbf{\Pi}_{H_c,h_c})\mathbf{u}_{H,h}\|_e+\|\mathbf{\Pi}_{H_c,h_c}\mathbf{e}\|_e\big).\end{aligned}$$

The oversampling condition (4.63) implies that the constants can be bounded by $1/2$ and hence, the term $\|\mathbf{\Pi}_{H_c,h_c}\mathbf{e}\|_e$ can be absorbed on the left-hand side. □

Corollary 4.5.8 (Full error)**.** *Let $\underline{\mathbf{u}} := (u_0,u_1,u_2) \in \mathcal{H}$ be the two-scale solution to* (4.4)*. Under the assumptions of Theorem 4.5.7, the two-scale LOD-approximation $\mathbf{u}_{H_c,h_c}$, solution to* (4.55)*, satisfies with some generic constant C*

$$\|\underline{\mathbf{u}}-\mathbf{u}_{H_c,h_c}\|_e \le \|\underline{\mathbf{u}}-\mathbf{u}_{H,h}\|_e + C\min_{\mathbf{v}_{H_c,h_c}\in\mathbf{V}_{H_c,h_c}}\|\mathbf{u}_{H,h}-\mathbf{v}_{H_c,h_c}\|_e.$$

The full error is dominated by the best approximation error of $\mathbf{V}_{H_c,h_c}$, which can be quantified using standard interpolation operators and regularity results. The error of the HMM-approximation $\underline{\mathbf{u}}-\mathbf{u}_{H,h}$ is estimated in Theorem 4.4.2. As we consider the HMM-approximation as an (overkill) reference solution only needed for the error estimates and *not in practical computations*, H and h are much smaller than the actual mesh sizes H_c and h_c, so that the error $\underline{\mathbf{u}}-\mathbf{u}_{H,h}$ indeed becomes negligible.

Remark 4.5.9 (Choice of LOD parameters in practice)**.** Although this is a purely theoretical section, we want to give a few comments on the practical choice of H_c, h_c, and m. Our numerical experiment in Section 4.6 reveals a resolution condition of $k^2(H+h) \lesssim 1$, so that for a wavenumber $k=2^6$, grids with mesh width of about $H=h=2^{-9}$ up to $H=h=2^{-12}$ are required for a reliable HMM-approximation. Numerical experiments by other authors in [BGP17, GP15, Pet17] for the standard Helmholtz problem showed that the LOD only needs meshes of about $H_c=h_c=2^{-5}$ to give a good approximation for a wavenumber $k=2^6$. Furthermore, an oversampling parameter of $m=2$ was already sufficient for various wavenumbers and no problems with the well-posedness of the discrete scheme have been reported. This is a significant reduction of the mesh size, which might outweigh the overhead of the additional corrector computations, in particular when taking the decoupling of Section 4.5.1 into account.

4.5.3 Proof of the decay of the corrector

In this section, we give a proof of the exponential decay result of Theorem 4.5.4, which is central for this method. The idea of the proof is the same as in the previous proofs for the Helmholtz equation [BGP17, GP15, Pet17] or in the context of diffusion problems [MP14]. As in the previous sections, we have to take into account the two-scale nature of the problem and the spaces.

Let $\mathbf{I}_{H,h} := (I_H, I_h^{\Sigma^*}, I_h^{\Sigma})$ with $I_H \colon C^0(G) \to \mathcal{S}(\mathcal{T}_H)$, $I_h^{\Sigma^*} \colon L^2(\Omega; C^0(\Sigma^*)) \to L^2(\Omega; \widetilde{\mathcal{S}}(\mathcal{T}_h(\Sigma^*)))$, and $I_h^{\Sigma} : L^2(\Omega; C^0(\Sigma)) \to L^2(\Omega; \mathring{\mathcal{S}}(\mathcal{T}_h(\Sigma)))$ denote the nodal Lagrange interpolation operators (see Section 2.2.2), where $I_h^{\Sigma^*}$ and I_h^{Σ} only act on the second variable. We note that periodicity is preserved when identifying degrees of freedom on the periodic boundary. Recall that the nodal Lagrange interpolation operator I is L^2- and H^1-stable on piecewise polynomials $\mathcal{P}^p$ on shape regular meshes due to inverse inequalities. Hence, for any $(T, S_1, S_2) \in \mathcal{T}_{H_c} \times \mathcal{T}_{h_c}(\Sigma^*) \times \mathcal{T}_{h_c}(\Sigma)$ and all $\mathbf{q} \in \mathcal{P}^2(T) \times L^2(T; \mathcal{P}^2(S_1)) \times L^2(T; \mathcal{P}^2(S_2))$ we have the stability estimate

$$\|\mathbf{I}_{H,h}\mathbf{q}\|_{1,e,T\times S} \leq C_{\mathbf{I}} \|\mathbf{q}\|_{1,e,T\times S}. \tag{4.65}$$

In this section, we do not explicitly give the constants in the estimates. Instead we use a generic constant C, which is independent of the mesh sizes and the oversampling parameter, but may depend on the (quasi)-interpolation operators' norms, the overlap constants $C_{\mathrm{ol},G}$ and $C_{\mathrm{ol},Y}$ (not on $C_{\mathrm{ol},m,G}$ and $C_{\mathrm{ol},m,Y}$!), the constant for the cut-off functions (see below), and $C_{\min}$.

In the proofs, we frequently use cut-off functions. We collect some basic properties in the following lemma, see also [GP15, Appendix A, Lemma 2].

Lemma 4.5.10. *Let $\boldsymbol{\eta} := (\eta_0, \eta_1, \eta_2) \in \mathbf{V}_{H_c,h_c}$ be a function triple with η_j, $j = 0, 1, 2$, having values in the interval $[0, 1]$ and satisfying the bounds*

$$\|\nabla\eta_0\|_{L^\infty(G)} \leq C_\eta H_c^{-1} \qquad \text{and} \qquad \|\nabla_y\eta_j\|_{L^2(\Omega;L^\infty(Y))} \leq C_\eta h_c^{-1}, \quad j = 1, 2. \tag{4.66}$$

By writing $\nabla\boldsymbol{\eta}$, we mean the triple $(\nabla\eta_0, \nabla_y\eta_1, \nabla_y\eta_2)$. Let $\mathbf{w}_{H,h} := (w_H, w_{h,1}, w_{h,2}) \in \mathbf{W}_{H,h}$ be arbitrary and define $\boldsymbol{\eta}\mathbf{w}_{H,h} := (\eta_0 w_H, \eta_1 w_{h,1}, \eta_2 w_{h,2})$. Given any subset $(K_0, K_1, K_2) \subset \mathcal{T}_{H_c} \times \mathcal{T}_{h_c}(\Sigma^*) \times \mathcal{T}_{h_c}(\Sigma)$, $\mathbf{w}_{H,h}$ fulfills for $\mathcal{R} := K_0 \times (K_1 \cup K_2)$ that

$$\|\mathbf{w}_{H,h}\|_{\mathcal{R}} \leq C(H_c\|\nabla w_H\|_{\mathrm{N}(R_0)} + \sum_{j=1}^{2} h_c\|\nabla_y w_{h,j}\|_{R_0\times\mathrm{N}(R_j)}), \tag{4.67}$$

$$\|\boldsymbol{\eta}\mathbf{w}_{H,h}\|_{1,e,\mathcal{R}} \leq C(\|\mathbf{w}_{H,h}\|_{1,e,\mathcal{R}\cap\mathrm{supp}(\boldsymbol{\eta})} + \|\mathbf{w}_{H,h}\|_{1,e,\mathrm{N}(\mathcal{R}\cap\mathrm{supp}(\nabla\boldsymbol{\eta}))}), \tag{4.68}$$

$$\|(\mathrm{id} - \boldsymbol{\Pi}_{H_c,h_c})\mathbf{I}_{H,h}(\boldsymbol{\eta}\mathbf{w}_{H,h})\|_{\mathcal{R}} \leq C(H_c + h_c)\|\boldsymbol{\eta}\mathbf{w}_{H,h}\|_{1,e,\mathrm{N}(\mathcal{R})}. \tag{4.69}$$

Proof. The properties (4.52) directly imply (4.67). For the proof of (4.68) the product rule and (4.66) yield

$$\begin{aligned}\|\boldsymbol{\eta}\mathbf{w}_{H,h}\|_{1,e,\mathcal{R}} \leq \|\mathbf{w}_{H,h}\|_{1,e,\mathcal{R}\cap\mathrm{supp}(\boldsymbol{\eta})} &+ C_\eta H_c^{-1}\|w_H\|_{R_0\cap\mathrm{supp}(\nabla\eta_0)} \\ &+ \sum_{j=1}^{2} C_\eta h_c^{-1}\|w_{h,j}\|_{R_0\times(R_j\cap\mathrm{supp}(\nabla\eta_j))}.\end{aligned}$$

The combination with (4.67) gives the assertion. For a proof of (4.69), apply (4.52). The estimate then follows from the H^1-stability of $\mathbf{I}_{H,h}$ (4.65) on the piecewise polynomial function $\boldsymbol{\eta}\mathbf{w}_{H,h}$. □

Proposition 4.5.11. *Under the resolution condition (4.58), there exists $0 < \beta < 1$ such that for any $\mathbf{v}_{H_c,h_c} \in \mathbf{V}_{H_c,h_c}$, all $(T, S_1, S_2) \in \mathcal{T}_{H_c} \times \mathcal{T}_{h_c}(\Sigma^*) \times \mathcal{T}_{h_c}(\Sigma)$, and $m \in \mathbb{N}$*

$$\|\mathbf{Q}_{T\times S,\infty}\mathbf{v}_{H_c,h_c}\|_{1,e,(G\times Y)\setminus\mathrm{N}^m(T\times S)} \leq C\beta^m\|\mathbf{v}_{H_c,h_c}\|_{1,e,T\times S}.$$

Proof. We define the cut-off functions $\eta_0 \in \mathcal{S}(\mathcal{T}_{H_c})$, $\eta_1 \in L^2(\Omega;\widetilde{\mathcal{S}}(\mathcal{T}_{h_c}(\Sigma^*)))$, and $\eta_2 \in L^2(\Omega;\mathring{\mathcal{S}}(\mathcal{T}_{h_c}(\Sigma)))$ via

$$\begin{aligned}
&\eta_0 = 0 \quad \text{in } \mathrm{N}^{m-3}(T) && \text{and} && \eta_0 = 1 \quad \text{in } G \setminus \mathrm{N}^{m-2}(T),\\
&\eta_1 = 0 \quad \text{in } \mathrm{N}^{m-3}(T\times S_1) && \text{and} && \eta_1 = 1 \quad \text{in } (\Omega\times\Sigma^*) \setminus \mathrm{N}^{m-2}(T\times S_1),\\
&\eta_2 = 0 \quad \text{in } \mathrm{N}^{m-3}(T\times S_2) && \text{and} && \eta_2 = 1 \quad \text{in } (\Omega\times\Sigma) \setminus \mathrm{N}^{m-2}(T\times S_2),
\end{aligned}$$

where w.l.o.g. η_1 and η_2 are chosen piecewise x-constant. The shape regularity implies that each η_j satisfies (4.66). Denote $\boldsymbol{\eta} := (\eta_0,\eta_1,\eta_2)$ and $\mathcal{R} := \operatorname{supp}(\nabla\boldsymbol{\eta})$. Let $\mathbf{v}_{H_c,h_c} \in \mathbf{V}_{H_c,h_c}$ and denote $\boldsymbol{\phi} := \mathbf{Q}_{T\times S,\infty}\mathbf{v}_{H_c,h_c} \in \mathbf{W}_{H,h}$. Elementary estimates yield

$$\begin{aligned}
&\|\boldsymbol{\phi}\|^2_{1,e,(G\times Y)\setminus \mathrm{N}^m(T\times S)}\\
&\quad = |\operatorname{Re}(\boldsymbol{\phi},\boldsymbol{\phi})_{1,e,(G\times Y)\setminus \mathrm{N}^m(T\times S)}|\\
&\quad \le |\operatorname{Re}\big((\nabla\phi_0+\nabla_y\phi_1,\eta_0\nabla\phi_0+\eta_1\nabla_y\phi_1)_{G\times\Sigma^*}+(\nabla_y\phi_2,\eta_2\nabla_y\phi_2)_{G\times\Sigma}\big)|\\
&\quad \le |\operatorname{Re}(\boldsymbol{\phi},\boldsymbol{\eta}\boldsymbol{\phi})_{1,e}|+|\operatorname{Re}\big((\nabla\phi_0+\nabla_y\phi_1,\phi_0\nabla\eta_0+\phi_1\nabla_y\eta_1)_{G\times\Sigma^*}+(\nabla_y\phi_2,\phi_2\nabla_y\eta_2)_{G\times\Sigma}\big)|\\
&\quad \le M_1+M_2+M_3+M_4
\end{aligned}$$

for

$$\begin{aligned}
M_1 &:= \Big|\operatorname{Re}\big(\boldsymbol{\phi},(\mathrm{id}-\mathbf{I}_{H,h})(\boldsymbol{\eta}\boldsymbol{\phi})\big)_{1,e}\Big|,\\
M_2 &:= \Big|\operatorname{Re}\big(\boldsymbol{\phi},(\mathrm{id}-\boldsymbol{\Pi}_{H_c,h_c})\mathbf{I}_{H,h}(\boldsymbol{\eta}\boldsymbol{\phi})\big)_{1,e}\Big|,\\
M_3 &:= \Big|\operatorname{Re}\big(\boldsymbol{\phi},\boldsymbol{\Pi}_{H_c,h_c}\mathbf{I}_{H,h}(\boldsymbol{\eta}\boldsymbol{\phi})\big)_{1,e}\Big|,\\
M_4 &:= \Big|\operatorname{Re}\big((\nabla\phi_0+\nabla_y\phi_1,\phi_0\nabla\eta_0+\phi_1\nabla_y\eta_1)_{G\times\Sigma^*}+(\nabla_y\phi_2,\phi_2\nabla_y\eta_2)_{G\times\Sigma}\big)\Big|.
\end{aligned}$$

With the stability of $\mathbf{I}_{H,h}$ on polynomials (4.65) and estimate (4.68) we obtain

$$M_1 \le C\|\boldsymbol{\phi}\|_{1,e,\mathcal{R}}\,\|\boldsymbol{\eta}\boldsymbol{\phi}-\mathbf{I}_{H,h}(\boldsymbol{\eta}\boldsymbol{\phi})\|_{1,e,\mathcal{R}} \le C\|\boldsymbol{\phi}\|_{1,e,\mathcal{R}}\,\|\boldsymbol{\phi}\|_{1,e,\mathrm{N}(\mathcal{R})}.$$

Since $\mathbf{w} := (\mathrm{id}-\boldsymbol{\Pi}_{H_c,h_c})\mathbf{I}_{H,h}(\boldsymbol{\eta}\boldsymbol{\phi}) \in \mathbf{W}_{H,h}$, the idealized corrector problem (4.56) and the fact that $\mathbf{w}$ has support only outside $T\times S$ imply $\mathcal{B}(\mathbf{w},\boldsymbol{\phi}) = \mathcal{B}_{T\times S}(\mathbf{w},\mathbf{v}_{H_c,h_c}) = 0$. Therefore, we obtain

$$\begin{aligned}
M_2 := |\operatorname{Re}(\boldsymbol{\phi},\mathbf{w})_{1,e}| &\le C_{\min}^{-1}\,|\operatorname{Re}\big(\mathcal{B}(\mathbf{w},\boldsymbol{\phi})+k^2(w_0+\chi_\Sigma w_2,\phi_0+\chi_\Sigma\phi_2)_{G\times Y}\big)|\\
&= C_{\min}^{-1}|\operatorname{Re} k^2(w_0+\chi_\Sigma w_2,\phi_0+\chi_\Sigma\phi_2)_{G\times Y}|.
\end{aligned}$$

Hence, estimates (4.68) and(4.69) give with the resolution condition (4.58)

$$\begin{aligned}
M_2 &\le C_{\min}^{-1}k^2(H_c^2C^2_{\Pi_{H_c}}C_{\mathrm{ol},G}+h_c^2C^2_{\Pi^\Sigma_{h_c}}C_{\mathrm{ol},Y})\|\boldsymbol{\phi}\|^2_{1,e,(G\times Y)\setminus \mathrm{N}^m(T\times S)}\\
&\quad + C_{\min}^{-1}k^2(H_c^2C^2_{\Pi_{H_c}}C_{\mathrm{ol},G}+h_c^2C^2_{\Pi^\Sigma_{h_c}}C_{\mathrm{ol},Y})C_{\boldsymbol{\Pi}}C_{\mathbf{I}}C_\eta\|\boldsymbol{\phi}\|^2_{1,e,\mathrm{N}^2(\mathcal{R})}\\
&\le \frac{1}{2}\|\boldsymbol{\phi}\|^2_{1,e,(G\times Y)\setminus \mathrm{N}^m(T\times S)} + C\|\boldsymbol{\phi}\|^2_{1,e,\mathrm{N}^2(\mathcal{R})},
\end{aligned}$$

so that the first term can be absorbed. Because of $\operatorname{supp}(\boldsymbol{\Pi}_{H_c,h_c}\mathbf{I}_{H,h}(\boldsymbol{\eta}\boldsymbol{\phi})) \subset \mathrm{N}(\mathcal{R})$, the properties (4.52) of $\boldsymbol{\Pi}_{H_c,h_c}$, (4.65) of $\mathbf{I}_{H,h}$, and estimate (4.68) lead to

$$M_3 \le \|\boldsymbol{\phi}\|_{1,e,\mathrm{N}(\mathcal{R})}\,\|\boldsymbol{\Pi}_{H_c,h_c}\mathbf{I}_{H,h}(\boldsymbol{\eta}\boldsymbol{\phi})\|_{1,e,\mathrm{N}(\mathcal{R})} \le C\|\boldsymbol{\phi}\|^2_{1,e,\mathrm{N}^2(\mathcal{R})}.$$

For the last term, the Lipschitz bound (4.66) on the cut-off functions and estimate (4.67) show

$$M_4 \le C_\eta\big(H_c^{-1}\|\phi_0\|_{\operatorname{supp}(\nabla\eta_0)}+\sum_{j=1}^{2}h_c^{-1}\|\phi_j\|_{\operatorname{supp}(\nabla\eta_j)}\big)\|\boldsymbol{\phi}\|_{1,e,\mathcal{R}} \le C\|\boldsymbol{\phi}\|^2_{1,e,\mathrm{N}(\mathcal{R})}.$$

All in all, it follows for some $\tilde{C} > 0$ that

$$\frac{1}{2}\|\boldsymbol{\phi}\|^2_{1,e,(G\times Y)\setminus \mathrm{N}^m(T\times S)} \leq \tilde{C}\|\boldsymbol{\phi}\|^2_{1,e,\mathrm{N}^2(\mathcal{R})},$$

where we recall that $\mathrm{N}^2(\mathcal{R}) = \mathrm{N}^m(T\times S)\setminus \mathrm{N}^{m-5}(T\times S)$. Because of

$$\|\boldsymbol{\phi}\|^2_{1,e,(G\times Y)\setminus \mathrm{N}^m(T\times S)} + \|\boldsymbol{\phi}\|^2_{1,e,\mathrm{N}^m(T\times S)\setminus \mathrm{N}^{m-5}(T\times S)} = \|\boldsymbol{\phi}\|^2_{1,e,(G\times Y)\setminus \mathrm{N}^{m-5}(T\times S)},$$

we obtain

$$(1+(2\tilde{C})^{-1})\|\boldsymbol{\phi}\|^2_{1,e,(G\times Y)\setminus \mathrm{N}^m(T\times S)} \leq \|\boldsymbol{\phi}\|^2_{1,e,(G\times Y)\setminus \mathrm{N}^{m-5}(T\times S)}.$$

Repeated application of this argument gives for $\tilde{\beta} := 2\tilde{C}/(2\tilde{C}+1) < 1$ together with the stability of $\mathbf{Q}_{T\times S,\infty}$ that

$$\|\boldsymbol{\phi}\|^2_{1,e,(G\times Y)\setminus \mathrm{N}^m(T\times S)} \leq \tilde{\beta}^{\lfloor m/5\rfloor}\|\boldsymbol{\phi}\|^2_{1,e} \leq C_{\mathbf{Q}}\tilde{\beta}^{\lfloor m/5\rfloor}\|\mathbf{v}_{H_c,h_c}\|^2_{1,e,T\times S},$$

which gives the assertion after some algebraic manipulations. □

As the localized correctors $\mathbf{Q}_m$ are the Galerkin approximations of the idealized correctors $\mathbf{Q}_\infty$, the decay property carries over to $\mathbf{Q}_m$. This is the main observation for the proof of Theorem 4.5.4.

Proof of Theorem 4.5.4. We define the cut-off functions $\eta_0 \in \mathcal{S}(\mathcal{T}_{H_c})$, $\eta_1 \in L^2(\Omega;\widetilde{\mathcal{S}}(\mathcal{T}_{h_c}(\Sigma^*)))$, and $\eta_2 \in L^2(\Omega;\mathring{\mathcal{S}}(\mathcal{T}_{h_c}(\Sigma)))$ via

$$\begin{aligned}
&\eta_0 = 0 \quad \text{in } G\setminus \mathrm{N}^{m-1}(T) && \text{and} && \eta_0 = 1 \quad \text{in } \mathrm{N}^{m-2}(T),\\
&\eta_1 = 0 \quad \text{in } (\Omega\times\Sigma^*)\setminus \mathrm{N}^{m-1}(T\times S_1) && \text{and} && \eta_1 = 1 \quad \text{in } \mathrm{N}^{m-2}(T\times S_1),\\
&\eta_2 = 0 \quad \text{in } (\Omega\times\Sigma)\setminus \mathrm{N}^{m-1}(T\times S_2) && \text{and} && \eta_2 = 1 \quad \text{in } \mathrm{N}^{m-2}(T\times S_2),
\end{aligned}$$

where again w.l.o.g. η_1 and η_2 are piecewise x-constant. The cut-off functions η_j satisfy the bounds (4.66). Set again $\boldsymbol{\eta} := (\eta_0,\eta_1,\eta_2)$. As already discussed, $\mathbf{Q}_{T\times S,m}$ can be interpreted as Galerkin approximation of $\mathbf{Q}_{T\times S,\infty}$ in the discrete subspace $\mathbf{W}_{H,h}(G_T\times Y_S) \subset \mathbf{W}_{H,h}$. Hence, Céa's Lemma gives for any $\mathbf{w}_{H,h} \in \mathbf{W}_{H,h}(G_T\times Y_S)$

$$\|(\mathbf{Q}_{T\times S,\infty}-\mathbf{Q}_{T\times S,m})\mathbf{v}\|^2_{1,e} \leq C\|\mathbf{Q}_{T\times S,\infty}\mathbf{v}-\mathbf{w}_{H,h}\|^2_e.$$

We choose $\mathbf{w}_{H,h} := (\mathrm{id}-\boldsymbol{\Pi}_{H_c,h_c})\mathbf{I}_{H,h}(\boldsymbol{\eta}\mathbf{Q}_{T\times S,\infty}\mathbf{v}) \in \mathbf{W}_{H,h}(G_T\times Y_S)$ and obtain with the identity $\boldsymbol{\Pi}_{H_c,h_c}\mathbf{Q}_{T\times S,\infty}\mathbf{v} = 0$, the estimate (4.69), the approximation and stability estimates (4.52) and (4.65), the resolution condition (4.58), and estimate (4.68) that

$$\begin{aligned}
&\|(\mathbf{Q}_{T\times S,\infty}-\mathbf{Q}_{T\times S,m})\mathbf{v}\|^2_{1,e}\\
&\quad\leq C\|\mathbf{Q}_{T\times S,\infty}\mathbf{v}-(\mathrm{id}-\boldsymbol{\Pi}_{H_c,h_c})\mathbf{I}_{H,h}(\boldsymbol{\eta}\mathbf{Q}_{T\times S,\infty}\mathbf{v})\|^2_e\\
&\quad= C\|(\mathrm{id}-\boldsymbol{\Pi}_{H_c,h_c})\mathbf{I}_{H,h}(\mathbf{Q}_{T\times S,\infty}\mathbf{v}-\boldsymbol{\eta}\mathbf{Q}_{T\times S,\infty}\mathbf{v})\|^2_{e,(G\times Y)\setminus\{\boldsymbol{\eta}=1\}}\\
&\quad\leq C\|(1-\boldsymbol{\eta})\mathbf{Q}_{T\times S,\infty}\mathbf{v}\|^2_{1,e,\mathrm{N}((G\times Y)\setminus\{\boldsymbol{\eta}=1\})}\\
&\quad\leq C\|\mathbf{Q}_{T\times S,\infty}\mathbf{v}\|^2_{1,e,\mathrm{N}((G\times Y)\setminus\{\boldsymbol{\eta}=1\})}.
\end{aligned}$$

Note that $\mathrm{N}((G\times Y)\setminus\{\boldsymbol{\eta}=1\}) = (G\times Y)\setminus \mathrm{N}^{m-3}(T\times S)$. Together with Proposition 4.5.11, this proves (4.59).

Define $\mathbf{z} := (\mathbf{Q}_\infty-\mathbf{Q}_m)\mathbf{v}$ and $\mathbf{z}_{T\times S} := (\mathbf{Q}_{T\times S,\infty}-\mathbf{Q}_{T\times S,m})\mathbf{v}$. The ellipticity from Lemma 4.5.3 yields

$$\|\mathbf{z}\|^2_{1,e} \leq C\Big|\sum_{(T,S_1,S_2)\in\mathcal{T}_{H_c}\times\mathcal{T}_{h_c}(\Sigma^*)\times\mathcal{T}_{h_c}(\Sigma)} \mathcal{B}(\mathbf{z},\mathbf{z}_{T\times S})\Big|.$$

We (re-)define the cut-off functions $\eta_0 \in \mathcal{S}(\mathcal{T}_{H_c})$, $\eta_1 \in L^2(\Omega; \widetilde{\mathcal{S}}(\mathcal{T}_{h_c}(\Sigma^*)))$, and $\eta_2 \in L^2(\Omega; \mathring{\mathcal{S}}(\mathcal{T}_{h_c}(\Sigma)))$ via

$$\begin{aligned}
&\eta_0 = 1 \quad \text{in } G \setminus \mathrm{N}^{m+2}(T) \qquad \text{and} \qquad \eta_0 = 0 \quad \text{in } \mathrm{N}^{m+1}(T),\\
&\eta_1 = 1 \quad \text{in } (\Omega \times \Sigma^*) \setminus \mathrm{N}^{m+2}(T \times S_1) \qquad \text{and} \qquad \eta_1 = 0 \quad \text{in } \mathrm{N}^{m+1}(T \times S_1),\\
&\eta_2 = 1 \quad \text{in } (\Omega \times \Sigma) \setminus \mathrm{N}^{m+2}(T \times S_2) \qquad \text{and} \qquad \eta_2 = 0 \quad \text{in } \mathrm{N}^{m+1}(T \times S_2),
\end{aligned}$$

where again η_1 and η_2 are w.l.o.g. piecewise x-constant. The cut-off functions satisfy the bounds (4.66) and we set $\boldsymbol{\eta} := (\eta_0, \eta_1, \eta_2)$. For any $(T, S_1, S_2) \in \mathcal{T}_{H_c} \times \mathcal{T}_{h_c}(\Sigma^*) \times \mathcal{T}_{h_c}(\Sigma)$ we have $(\mathrm{id} - \boldsymbol{\Pi}_{H_c,h_c})\mathbf{I}_{H,h}(\boldsymbol{\eta}\mathbf{z}) \in \mathbf{W}_{H,h}$ with support outside $G_T \times Y_S$. Hence, we deduce with $\mathbf{z} = \mathbf{I}_{H,h}\mathbf{z}$ that

$$\mathcal{B}(\mathbf{z}, \mathbf{z}_{T\times S}) = \mathcal{B}(\mathbf{I}_{H,h}(\mathbf{z} - \boldsymbol{\eta}\mathbf{z}), \mathbf{z}_{T\times S}) + \mathcal{B}(\boldsymbol{\Pi}_{H_c,h_c}\mathbf{I}_{H,h}(\boldsymbol{\eta}\mathbf{z}), \mathbf{z}_{T\times S}).$$

The function $\mathbf{z} - \mathbf{I}_{H,h}(\boldsymbol{\eta}\mathbf{z})$ vanishes on $\{\boldsymbol{\eta} = 1\}$. Thus, the first term on the right-hand side satisfies

$$|\mathcal{B}(\mathbf{I}_{H,h}(\mathbf{z} - \boldsymbol{\eta}\mathbf{z}), \mathbf{z}_{T\times S})| \leq C_B \|\mathbf{I}_{H,h}(\mathbf{z} - \boldsymbol{\eta}\mathbf{z})\|_{e,\mathrm{supp}(1-\boldsymbol{\eta})} \|\mathbf{z}_{T\times S}\|_e.$$

The L^2- and H^1-stability of $\mathbf{I}_{H,h}$ on piecewise polynomials together with the estimate (4.68) applied to the cut-off function $1 - \boldsymbol{\eta}$ gives

$$\|\mathbf{I}_{H,h}(\mathbf{z} - \boldsymbol{\eta}\mathbf{z})\|_{e,\mathrm{supp}(1-\boldsymbol{\eta})} \leq C\|\mathbf{z}\|_{e,\mathrm{N}(\mathrm{supp}(1-\boldsymbol{\eta}))}.$$

Furthermore, $\boldsymbol{\Pi}_{H_c,h_c}\mathbf{I}_{H,h}(\boldsymbol{\eta}\mathbf{z})$ vanishes on $(G \times Y) \setminus \mathrm{N}(\mathrm{supp}(1 - \boldsymbol{\eta}))$. Therefore, we infer from the stability (4.53) of $\boldsymbol{\Pi}_{H_c,h_c}$, the stability of $\mathbf{I}_{H,h}$ as before, and estimate (4.68) that

$$|\mathcal{B}(\boldsymbol{\Pi}_{H_c,h_c}\mathbf{I}_{H,h}(\boldsymbol{\eta}\mathbf{z}), \mathbf{z}_{T\times S})| \leq C\|\mathbf{z}\|_{e,\mathrm{N}^2(\mathrm{supp}(1-\boldsymbol{\eta}))} \|\mathbf{z}_{T\times S}\|_e.$$

Because of the resolution condition (4.58) and Lemma 4.5.3, it holds $\|\mathbf{z}\|_e \leq C\|\mathbf{z}\|_{1,e}$. Summing up over $(T, S_1, S_2) \in \mathcal{T}_{H_c} \times \mathcal{T}_{h_c}(\Sigma^*) \times \mathcal{T}_{h_c}(\Sigma)$ yields with the Cauchy-Schwarz inequality and the finite overlap of patches that

$$\begin{aligned}
\|\mathbf{z}\|_{1,e}^2 &\leq C \sum_{(T,S_1,S_2)\in\mathcal{T}_{H_c}\times\mathcal{T}_{h_c}(\Sigma^*)\times\mathcal{T}_{h_c}(\Sigma)} \|\mathbf{z}\|_{1,e,\mathrm{N}^2(\mathrm{supp}(1-\boldsymbol{\eta}))} \|\mathbf{z}_{T\times S}\|_e\\
&\leq C\big(\sqrt{C_{\mathrm{ol},m,G}} + \sqrt{C_{\mathrm{ol},m,Y}}\big)\|\mathbf{z}\|_{1,e} \sqrt{\sum_{(T,S_1,S_2)\in\mathcal{T}_{H_c}\times\mathcal{T}_{h_c}(\Sigma^*)\times\mathcal{T}_{h_c}(\Sigma)} \|\mathbf{z}_{T\times S}\|_e^2}.
\end{aligned}$$

Combining the last estimate with (4.59) concludes the proof. □

4.6 Numerical experiments

In this section we analyze the HMM numerically with particular respect to the convergence order, the resolution condition for the Helmholtz equation (see (4.37)), and the behavior of solutions for different values of μ_{hom}. The implementation has been done based on the module dune-gdt [MS15] of the DUNE software framework [BBD+08a, BBD+08b]. The corresponding code can be found on Github[1]. The examples are located in test/helmholtz.cc for Section 4.6.1 and in test/hmm-maxwell.cc for Section 4.6.2.

The overall setting is similar for the Helmholtz and Maxwell equation: We consider box-type domains G and Ω and also the inclusion Σ in the unit cell Y is a square or cube, respectively. The boundary condition is computed from incoming waves. As the inclusion Σ is quadratic or cubic, the eigenvalues of the Laplacian are explicitly known. The analytical predictions coincide nicely with our computed behavior of μ_{hom} for changing wavenumbers k.

[1] `github.com/BarbaraV/dune-gdt/tree/dissertation`

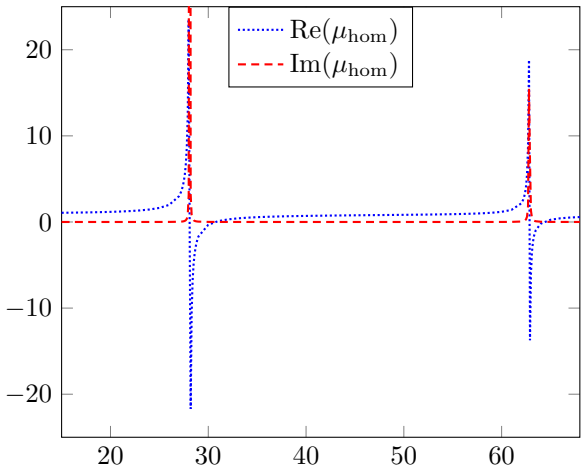

Figure 4.4: Real and imaginary parts of μ_{hom} for changing wavenumber k (Helmholtz equation).

In order to verify the predicted convergence rates, we compare the macroscopic part of the HMM-approximation with a homogenized reference solution. Besides the (absolute) errors we also give the experimental order of convergence (EOC), which is defined for two mesh sizes $H_1 > H_2$ and corresponding error values $e_{H,1}$ and $e_{H,2}$ as $\text{EOC}(e) := \ln(\frac{e_{H,1}}{e_{H,2}})/\ln(\frac{H_1}{H_2})$. In the tables, we list the EOC for $H_1 > H_2$ in the row of the smaller mesh size H_2. Finally, we compare wavenumbers with $\text{Re}(\mu_{\text{hom}}) > 0$ and $\text{Re}(\mu_{\text{hom}}) < 0$, both for the two- and the three-dimensional case. As physically expected, $\text{Re}(\mu_{\text{hom}}) > 0$ corresponds to normal transmission, whereas for $\text{Re}(\mu_{\text{hom}}) < 0$ the wave amplitude decays exponentially inside the scatter. This prohibited wave propagation is caused by the incited eigen resonances inside the inclusions.

The results of the numerical experiment for the Helmholtz equation are given in Section 4.6.1 and for the Maxwell equation in Section 4.6.2.

4.6.1 Experiments for the Helmholtz equation

We consider the macroscopic domain $G = (0.25, 0.75)^2$ with scatterer $\Omega = (0.375, 0.625)^2$. The boundary condition g is computed as $g = \nabla u_{\text{inc}} \cdot n - iku_{\text{inc}}$ from the (left-going) incoming plane wave $u_{\text{inc}} = \exp(-ikx_1)$. The unit square Y has the inclusion $\Sigma = (0.25, 0.75)^2$ and the inverse permittivities are chosen as $\varepsilon_0^{-1} = 10$ and $\varepsilon_1^{-1} = 10 - 0.01i$. Obviously, the real parts of both parameters are of the same order and, moreover, ε_1 is only slightly dissipative.

Behavior of the effective permeability. As discussed before, the eigenvalues of the Dirichlet Laplacian on Σ are explicitly known. Only the eigenvalues where the associated eigenfunctions have nonzero mean contribute to the expansion of μ_{hom}. For our setup, the first interesting values are at $k \approx 28.1$ and $k \approx 62.8$. We compute μ_{hom} using cell problem (4.6) with a grid consisting of 131,072 elements on Σ. Figure 4.4 shows the behavior of the real and the imaginary part. As predicted, we can see a significant change of behavior around the Laplace eigenvalues, where the real part changes sign and also the imaginary part has large values. Note that for this example, we do not see that $\text{Im}(\mu_{\text{hom}})$ behaves like k^{-2}, as proved in Proposition 4.3.5.

Resolution condition. In order to analyze the resolution condition, we use a reference homogenized solution by computing the effective parameters of Theorem 4.2.2 with 524,288 entities on Y and then solving the effective homogenized equation (4.7) on G with the same number of entities. We compare the macroscopic part u_H of our HMM-approximation (see Definition 4.4.1) with this reference solution in the weighted H^1-norm $\|\cdot\|_{1,k,G}$ for a sequence of simultaneously refined meshes on G and Y and three different wavenumbers $k = 34, 48, 68$,

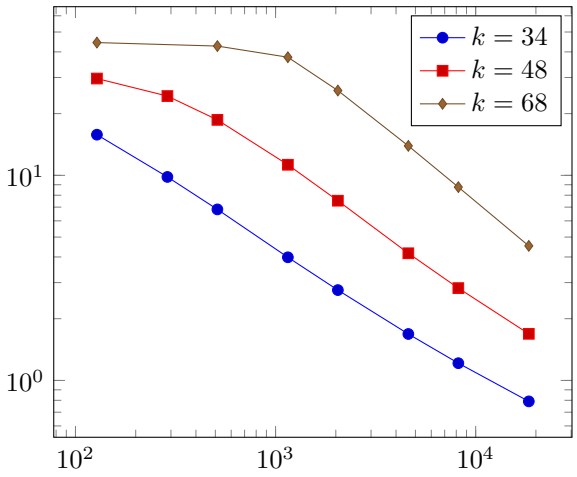

Figure 4.5: Error between the homogenized reference solution and the HMM-approximation in the weighted H^1-norm versus number of grid entities for different wavenumbers k for the Helmholtz equation.

see Figure 4.5. Note that these wavenumbers are all away from any resonant behavior of μ_{hom}. For higher wavenumbers, finer meshes are needed to obtain convergence: Whereas for $k = 34$, the error converges for all considered grids, the threshold value for $k = 48 \approx \sqrt{2} \cdot 34$ is 288 entities; and for $k = 68 = 2 \cdot 34$, it is 1,152 entities. This indicates a resolution condition of "$k^2(H + h)$ small" in practice, which is standard for continuous Galerkin discretizations of Helmholtz problems.

Convergence rates. We then take a closer look at the convergence of the errors and verify the predictions of Theorem 4.4.2 and Corollary 4.4.4. We choose the wavenumber $k = 29$, which corresponds to $\text{Re}(\mu_{\text{hom}}) < 0$ and is thus also interesting from a physical point of view. Table 4.1 shows the error between the macroscopic part u_H of the HMM-approximation and the reference homogenized solution (as before) in the k-weighted $H^1(G)$-norm and the $L^2(G)$-norm. The experimental order of convergence (EOC) verifies the linear convergence in the H^1-norm predicted theoretically in Corollary 4.4.4, and the quadratic convergence in the L^2-norm discussed afterwards. Note that from the geometry one might expect a reduced regularity of the analytical solution and, therefore, a sublinear convergence of the H^1-error. We believe that the linear convergence observed in the experiment does not imply a suboptimality of the error bound in Theorem 4.4.2 and Corollary 4.4.4, but that in fact, the analytical solution in this special case has full $H^2_{pw}(G)$ regularity, probably because of the boundary condition. This clearly shows that our general theory holds for all regimes of wavenumbers even if they result in unusual effective parameters. However, we observe a small pre-asymptotic effect for coarse meshes, which indicates that the resolution condition may be stricter for such resonant settings.

Furthermore, we compare the HMM-approximation with a detailed reference solution to the heterogeneous problem for $\delta = 1/32$, solved on a fine grid with 524,288 entities. The "homogenization" error between this (heterogenous) reference solution and the homogenized reference solution is 0.348659 in the L^2-norm. Table 4.2 compares the error to the reference solution for the macroscopic part u_H of the HMM-approximation and for the zeroth order L^2-approximation $u^0_{\text{HMM}} := u_H + u_{h,2}(\cdot, \frac{\cdot}{\delta})$. Whereas the error stagnates for u_H, we almost recover the quadratic convergence for u^0_{HMM} with a saturation effect for fine meshes where we enter the regime of the homogenization error. This clearly underlines the necessity of the correctors in the HMM to faithfully approximate the true solution. Note that we do not have results on the homogenization error: We expect strong convergence of u_δ to u^0_{HMM} in the L^2-norm according to [All92], but the proof is not applicable to the Helmholtz case.

Table 4.1: Convergence history and EOC for the error between the HMM-approximation and the reference homogenized solution in the L^2-norm and k-weighted H^1-norm for the Helmholtz equation with $k = 29$.

$H = 2h$	$\|e_0\|_{L^2(G)}$	$\|e_0\|_{1,k,G}$	EOC($\|e_0\|_{L^2}$)	EOC($\|e_0\|_{1,k}$)
$\sqrt{2} \cdot 1/8$	0.270474	11.780290	—	—
$\sqrt{2} \cdot 1/16$	0.110372	5.373207	1.293	1.132
$\sqrt{2} \cdot 1/24$	0.051400	2.970250	1.885	1.461
$\sqrt{2} \cdot 1/32$	0.029671	2.019241	1.910	1.341
$\sqrt{2} \cdot 1/48$	0.013506	1.235815	1.941	1.211
$\sqrt{2} \cdot 1/64$	0.007672	0.886311	1.967	1.155

Table 4.2: Error between the reference solution and the HMM- and zeroth order approximation in the L^2-norm for the Helmholtz equation with $k = 29$.

$H = 2h$	$\|u_\delta - u_H\|_{L^2(G)}$	$\|u_\delta - u^0_{\text{HMM}}\|_{L2(G)}$	EOC($u_\delta - u^0_{\text{HMM}}$)
$\sqrt{2} \cdot 1/8$	0.418463	0.565853	—
$\sqrt{2} \cdot 1/16$	0.351655	0.174724	1.696
$\sqrt{2} \cdot 1/24$	0.345950	0.061964	2.556
$\sqrt{2} \cdot 1/32$	0.346266	0.034091	2.077
$\sqrt{2} \cdot 1/48$	0.347330	0.027245	0.553
$\sqrt{2} \cdot 1/64$	0.347862	0.029764	−0.307

Comparison of wavenumbers. We compare two wavenumbers with very different physical meaning: $k = 38$ corresponds to normal transmission, whereas $k = 29$ has $\text{Re}(\mu_{\text{hom}}) < 0$ and thus corresponds to a wavenumber in the band gap where propagation inside the scatterer is physically forbidden. We consider the macroscopic part u_H of the HMM-approximation (with $H = 2h = \sqrt{2} \cdot 1/64$) and the zeroth order reconstruction u^0_{HMM} (plotted on a well-resolved mesh with 524,288 entities) and depict both functions on the whole two-dimensional domain as well as over the line $x_2 = 0.545$, which cuts through a row of inclusions. For $k = 38$, wave propagation with low speed takes place inside the scatterer, see the macroscopic part u_H depicted in Figures 4.6a and 4.6b. In contrast to that, we see the expected exponential decay of the wave amplitude inside the scatterer for $k = 29$, see the macroscopic part u_H depicted in Figures 4.7a and 4.7b. The zeroth order reconstruction u^0_{HMM} can explain this behavior by approximating the heterogeneous solution also inside the inclusions. For $k = 38$, the amplitudes inside the inclusions are as high as the amplitude of the incoming wave, see Figures 4.6c and 4.6d. However, we observe very high amplitudes inside the inclusions for $k = 29$, see Figures 4.7c and 4.7d. These are caused by eigen resonances incited inside the inclusions. Moreover, these incited waves from neighboring inclusions interfere destructively with each other so that over the whole scatterer, no wave can propagate.

Plane wave at an oblique angle. So far, we considered an incoming plane wave propagating in x_1-direction, which consequently hits the faces of the scatterer in either a perpendicular or parallel way. However, the observation of a frequency band gap should not depend on the angle of the incoming wave according to the presented homogenization theory. Therefore, we change the boundary condition to $g = \nabla u_{\text{inc}} \cdot n - iku_{\text{inc}}$, but now with the incoming plane wave $u_{\text{inc}} = \exp(-ik\nu \cdot x)$ with $\nu = (0.6, 0.8)^T$. All other parameters are left unchanged. The transmission wavenumber $k = 38$ and the band gap wavenumber $k = 29$ are compared in Figure 4.8. Again, we see no wave propagation inside the scatterer for $k = 29$, as predicted. The zeroth order approximation reveals that the incited eigen resonances inside the inclusions account for the decay of the wave amplitude for $k = 29$ also in this case. This confirms the theoretical prediction that the artificial magnetism and the band gap do not depend on the

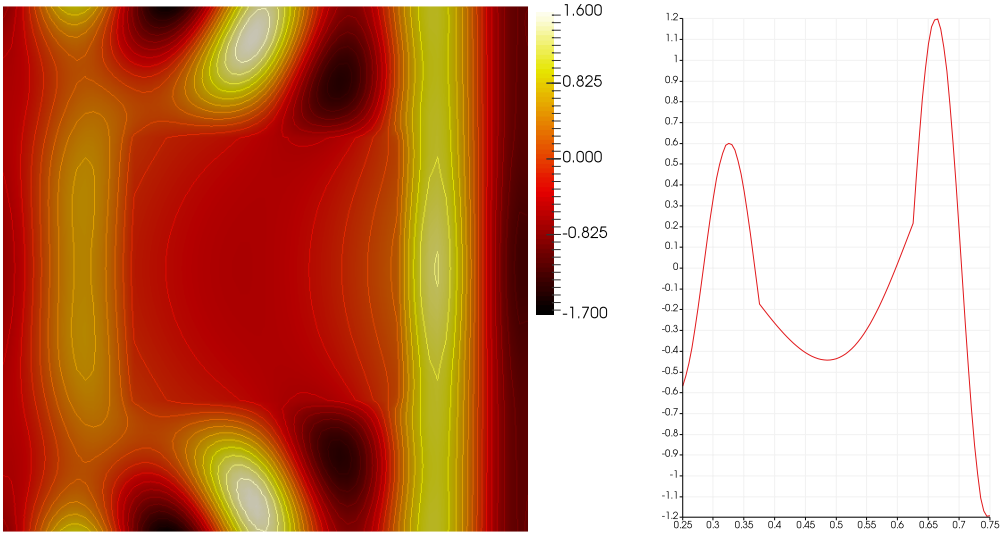

(a) u_H (b) line plot of u_H

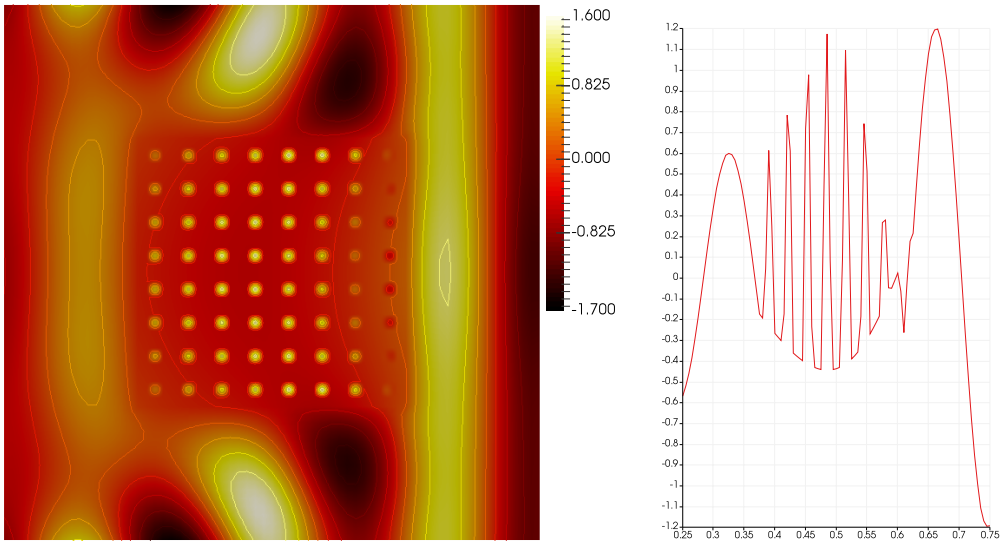

(c) u^0_{HMM} (d) line plot of u^0_{HMM}

Figure 4.6: Helmholtz equation for $k = 38$: Macroscopic part $\mathrm{Re}(u_H)$ of the HMM-approximation and zeroth order approximation $\mathrm{Re}(u^0_{\mathrm{HMM}})$, both on the whole domain (left column) and over the line $x_2 = 0.545$ (right column); incoming wave in $-x_1$-direction

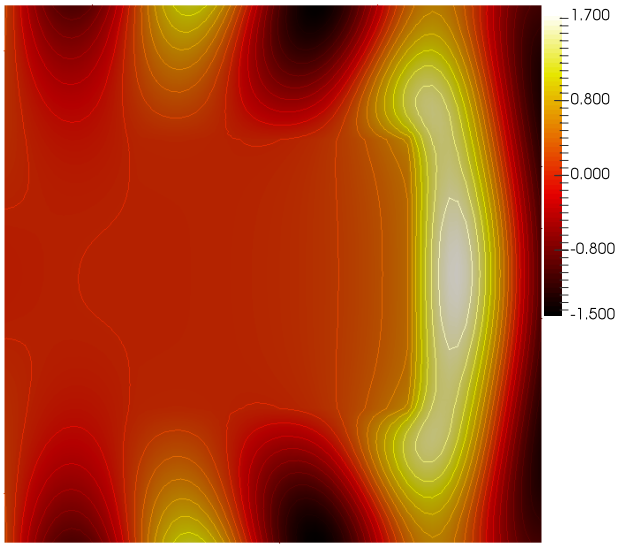

(a) u_H

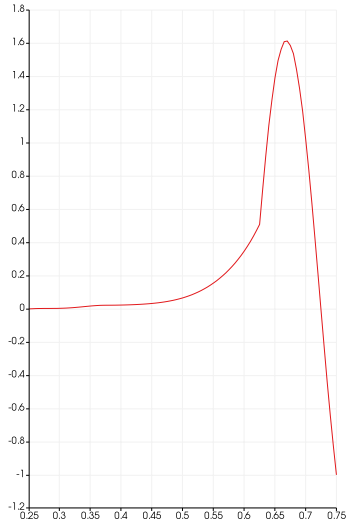

(b) line plot of u_H

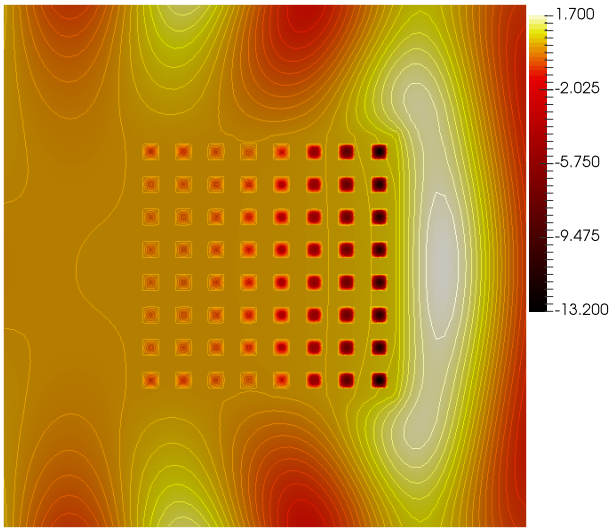

(c) u^0_{HMM}

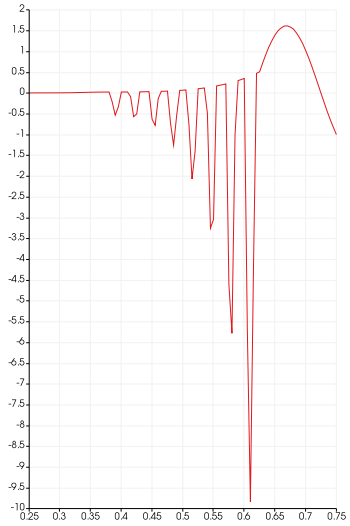

(d) line plot of u^0_{HMM}

Figure 4.7: Helmholtz equation for $k = 29$: Macroscopic part $\mathrm{Re}(u_H)$ of the HMM-approximation and zeroth order approximation $\mathrm{Re}(u^0_{\mathrm{HMM}})$, both on the whole domain (left column) and over the line $x_2 = 0.545$ (right column); incoming wave in $-x_1$-direction

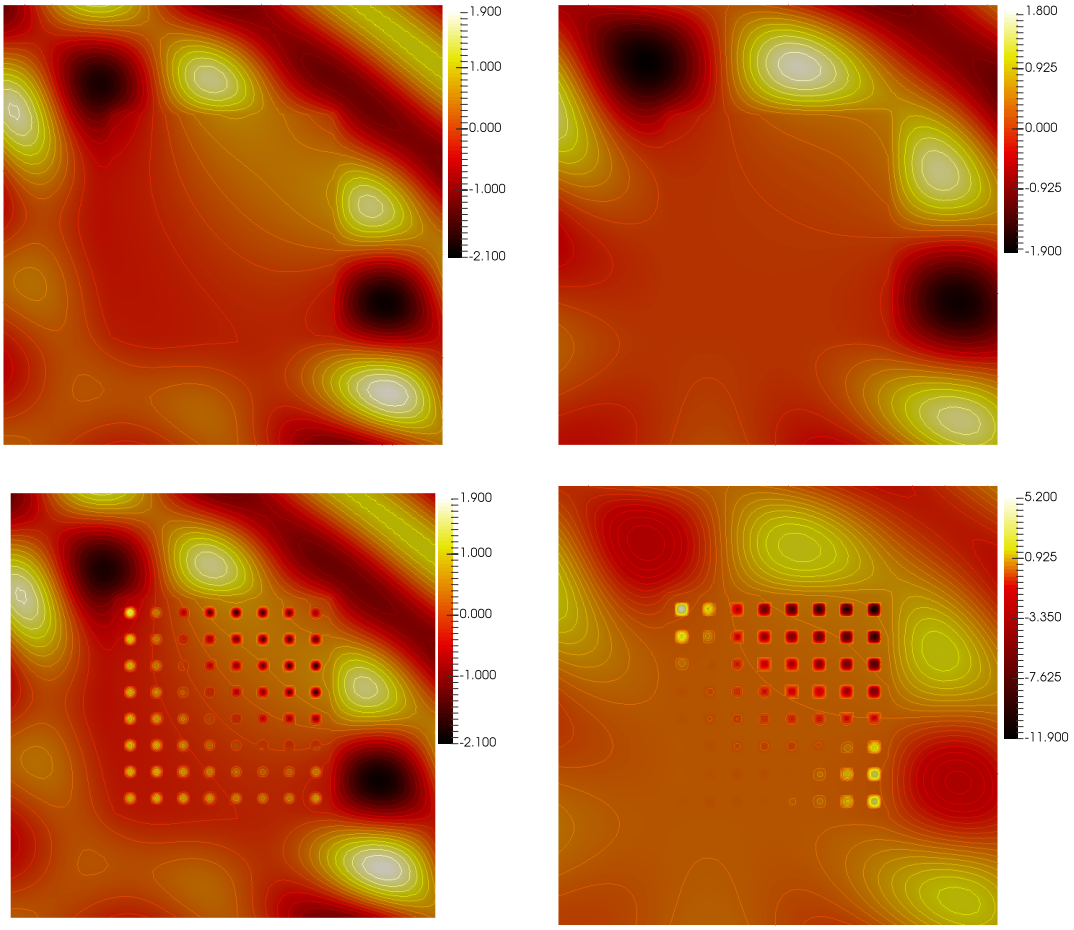

Figure 4.8: Macroscopic part $\mathrm{Re}(u_H)$ of the HMM-approximation (top row) and zeroth-order approximation $\mathrm{Re}(u^0_{\mathrm{HMM}})$ (bottom row) for $k = 38$ (left column) and $k = 29$ (right column); Helmholtz equation with incoming wave at an oblique angle

angle of the incoming wave. Moreover, it shows that our numerical method works regardless of the chosen boundary condition. We note that similar convergence behavior as in Tables 4.1 and 4.2 can also be observed for the oblique angle.

4.6.2 Experiments for the Maxwell equation

We consider the macroscopic domain $G = (0,1)^3$ with embedded scatterer $\Omega = (0.25, 0.75)^3$. The boundary condition $\mathbf{g}$ is computed as $\mathbf{g} = \operatorname{curl} \mathbf{u}_{\mathrm{inc}} \times \mathbf{n} - ik\mathbf{n} \times (\mathbf{u}_{\mathrm{inc}} \times \mathbf{n})$ with the (left-going), $\mathbf{e}_2$-polarized incoming plane wave $\mathbf{u}_{\mathrm{inc}} = \exp(-ikx_1)\mathbf{e}_2$. The unit cube Y has the inclusion $\Sigma = (0.25, 0.75)^3$ and we choose the inverse permittivities as $\varepsilon_0^{-1} = 1.0$ and $\varepsilon_1^{-1} = 1.0 - 0.01i$. Obviously, the real parts of both parameters are of the same order and ε_1 is only slightly dissipative.

Behavior of the effective permeability. The contribution to μ_{hom} from the second cell problem (4.11) in Σ^* is independent of k, as expected. The wavenumber dependence is wholly caused by cell problem (4.12) inside Σ. As discussed before, significant changes in μ_{hom} are expected around the eigenvalues of the vector Laplacian. Only some of the eigenvalues, namely those where the mean value of the eigenfunction(s) is not the zero vector, eventually lead to resonances in the behavior of the effective permeability. For our setup, the first interesting values are $k \approx 8.9$ and $k \approx 19.9$. We compute μ_{hom} using cell problems (4.11) and (4.12) with

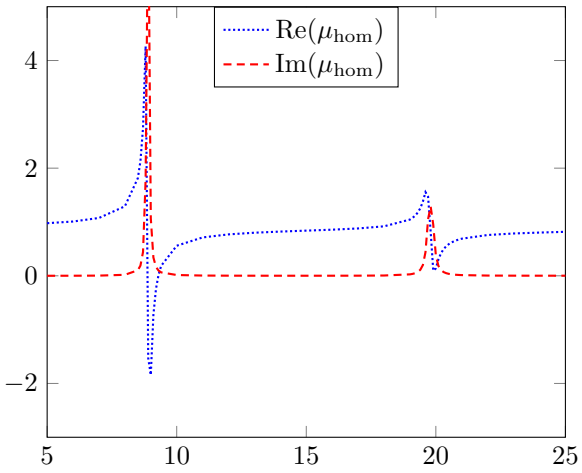

Figure 4.9: Dependency of the effective permeability μ_{hom} on the wavenumber k (Maxwell equation).

a mesh consisting of 196,608 elements on Y. Figure 4.9 depicts the behavior of the diagonal entries of $\text{Re}(\mu_{\text{hom}})$ and $\text{Im}(\mu_{\text{hom}})$ (all three diagonal entries are the same due to symmetry) for changing k. As predicted, we see a significant change of behavior around the eigenvalues, where the imaginary part has large values and the real part shows resonances. For the first eigenvalue, this resonance is strong enough to produce a negative real part, while this is not the case for the second eigenvalue in our setup.

Convergence rates. We then take a closer look at the convergence of errors and verify the predictions of Theorem 4.4.3/Corollary 4.4.5 and Theorem 4.4.6. We use a reference homogenized solution by computing the effective parameters of Theorem 4.2.4 with 196,608 elements on Y and then solving the effective homogenized equation (4.13) with these parameters using a mesh with 663,552 elements for G. This reference homogenized solution is compared to the macroscopic part $\mathbf{u}_H$ of the HMM-approximation on a sequence of simultaneously refined macro- and microscale meshes for the frequencies $k = 9$ and $k = 12$. Note that $k = 12$ corresponds to "standard" effective parameters, while for $k = 9$, $\text{Re}(\mu_{\text{hom}})$ is negative definite. The errors in the L^2- and $\mathbf{H}(\text{curl})$-seminorm are shown in Table 4.3 for $k = 12$ and in Table 4.4 for $k = 9$. In order to verify Theorem 4.4.6, we compute an approximation of the gradient part θ of the Helmholtz decomposition: We solve the Poisson problem determining θ (with right-hand side e_0) using linear Lagrange elements on the reference mesh (with 663,552 elements). The L^2-norms of this resulting θ are also shown in Tables 4.3 and Table 4.4, respectively. The experimental order of convergence (EOC) verifies the linear convergence in L^2 and $\mathbf{H}(\text{curl})$, predicted in Theorem 4.4.3 and Corollary 4.4.5, and the quadratic convergence of the Helmholtz decomposition, predicted in Theorem 4.4.6. As for the Helmholtz equation, we might expect reduced regularity of the exact solution and a sublinear error convergence from the geometry. We believe that the linear convergence observed in the experiment can be explained by full $\mathbf{H}^1_{pw}(\text{curl}, G)$ regularity of the analytical homogenized solution, cf. the discussion for the Helmholtz equation. This clearly shows that our general theory holds for all regimes of wavenumbers even if they result in unusual effective parameters. This is consistent with the observations made for the two-dimensional case in Section 4.6.1.

Comparison of wavenumbers. As in Section 4.6.1, we compare two wavenumber with different physical meaning in more detail: $k = 12$ (normal transmission) and $k = 9$ (band gap because of ($\text{Re}(\mu_{\text{hom}})$ negative definite). We consider the magnitude of the real part of $\mathbf{u}_H$ (the macroscopic part of the HMM-approximation with $H = h = \sqrt{3} \cdot 1/16$) in Figure 4.10. The isosurfaces are almost parallel planes for $k = 12$ indicating normal, almost undisturbed propagation of the wave through the scatterer. Note that the effective wave speed inside the

Table 4.3: Convergence history and EOC for the error between the macroscopic part of the HMM-approximation and the reference homogenized solution for the Maxwell equation with $k = 12$.

$H = h$	$\|e_0\|_{L^2(G)}$	$\|\operatorname{curl} e_0\|_{L^2(G)}$	$\|\theta\|_{L^2(G)}$	EOC(e_0)	EOC($\operatorname{curl} e_0$)	EOC(θ)
$\sqrt{3} \cdot 1/4$	0.945214	11.60030	0.015550	—	—	—
$\sqrt{3} \cdot 1/8$	0.531599	5.76452	0.009633	0.830	1.009	0.691
$\sqrt{3} \cdot 1/12$	0.321809	3.36067	0.004100	1.238	1.331	2.107
$\sqrt{3} \cdot 1/16$	0.230797	2.38167	0.002201	1.156	1.197	2.163

Table 4.4: Convergence history and EOC for the error between the macroscopic part of the HMM-approximation and the reference homogenized solution for the Maxwell equation with $k = 9$.

$H = h$	$\|e_0\|_{L^2(G)}$	$\|\operatorname{curl} e_0\|_{L^2(G)}$	$\|\theta\|_{L^2(G)}$	EOC(e_0)	EOC($\operatorname{curl} e_0$)	EOC(θ)
$\sqrt{3} \cdot 1/4$	0.697211	5.54104	0.024216	—	—	—
$\sqrt{3} \cdot 1/8$	0.410991	2.94379	0.010455	0.762	0.913	1.212
$\sqrt{3} \cdot 1/12$	0.285928	1.85786	0.005747	0.895	1.135	1.476
$\sqrt{3} \cdot 1/16$	0.216505	1.31478	0.003328	0.967	1.202	1.899

scatterer does not differ greatly from the one outside in our choice of material parameters. In contrast, the scatterer has a significant influence on the wave propagation for $k = 9$, as we can deduce from the distorted wavefronts in Figure 4.10, right.

To compare this in more detail, we study two-dimensional representations in the plane $x_2 = 0.545$ in Figure 4.11. There we depict the x_2-component, which is the principal one due to the polarization of the incoming wave. The top row shows again the macroscopic part $\mathbf{u}_H$ of the HMM-approximation and we see the expected exponential decay of the amplitude inside the scatterer for $k = 9$ (top right), while the amplitude is not affected for $k = 12$. The zeroth order approximation $\mathbf{u}^0_{\mathrm{HMM}} := \mathbf{u}_H + \nabla_y u_{h,2}(\cdot, \frac{\cdot}{\delta}) + \mathbf{u}_{h,3}(\cdot, \frac{\cdot}{\delta})$ in the bottom row of Figure 4.11 (depicted for $\delta = 1/8$ on a grid with 1,572,864 entities) explains this effect. In consistency with the observations of Section 4.6.1, the eigen resonance of the inclusions for $k = 9$ causes very high amplitudes, which confines the energy of the wave to the inclusions. The amplitudes in the inclusions for $k = 12$ are solely due to the different material parameters and do not disturb the overall wave propagation.

The comparison of the HMM- and zeroth order approximation to a (full) reference solution to the original (heterogeneous) problems (4.3) is a task for future research.

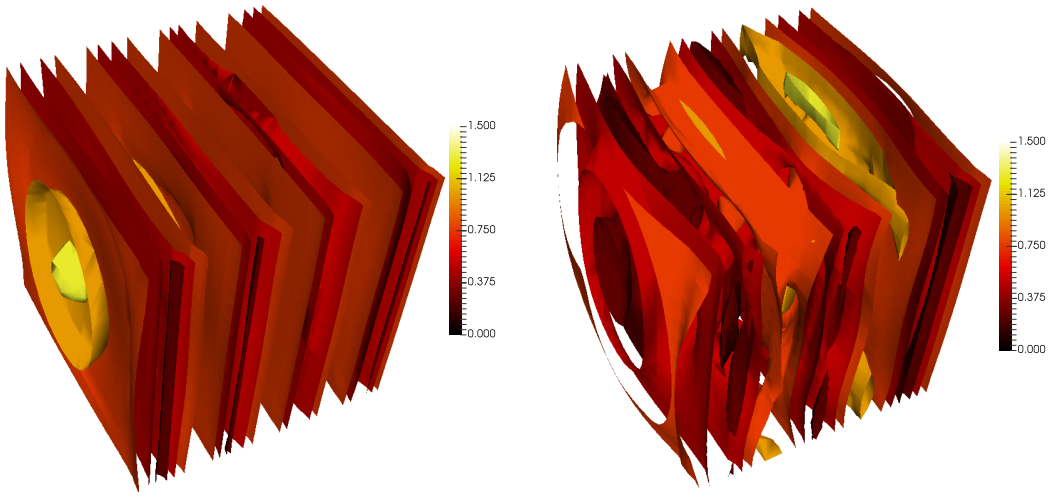

Figure 4.10: Maxwell equation: Isosurfaces for the magnitude of the HMM-approximation $\mathrm{Re}(\mathbf{u}_H)$ for $k = 12$ (left) and $k = 9$ (right).

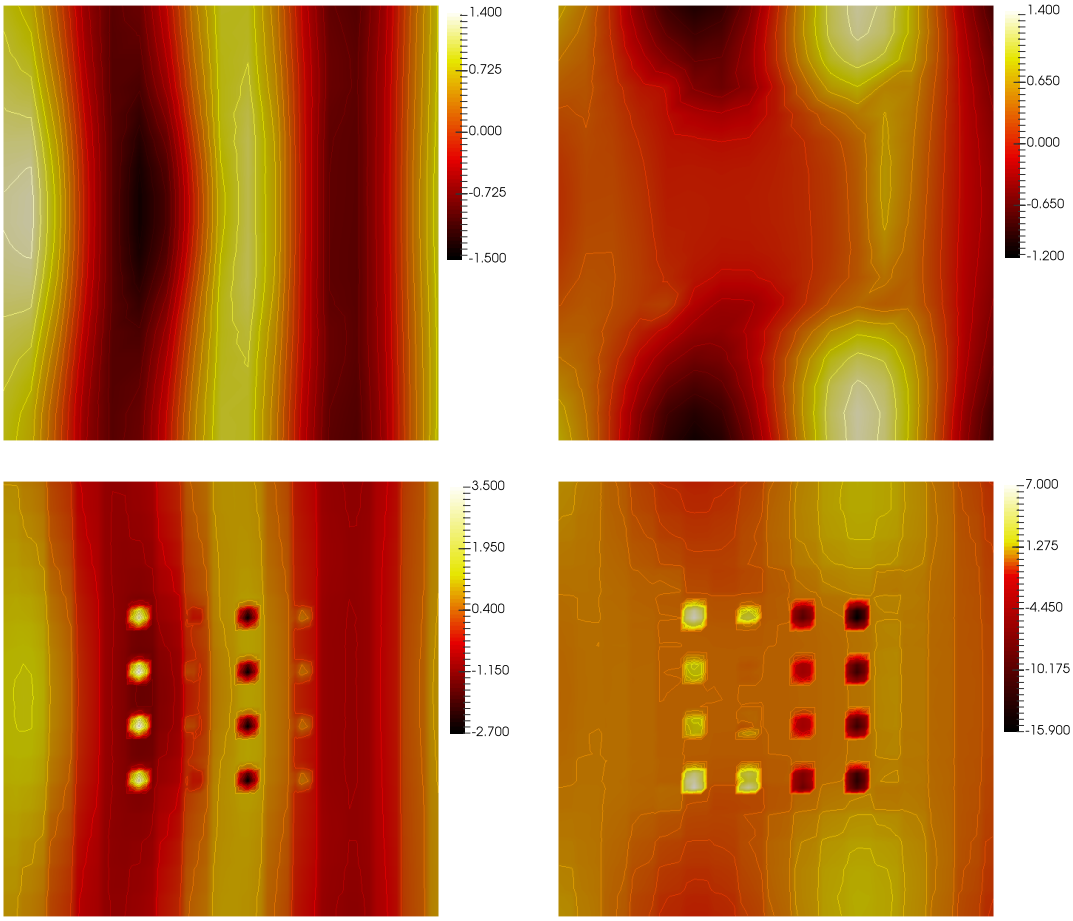

Figure 4.11: In the plane $x_2 = 0.545$: x_2-component of $\mathrm{Re}(\mathbf{u}_H)$ (top row) and of $\mathrm{Re}(\mathbf{u}^0_{\mathrm{HMM}})$ (bottom row) for the Maxwell equation with $k = 12$ (left column) and $k = 9$ (right column).

5 Conclusion and Outlook

5.1 Conclusion

In this thesis, we were concerned with two different classes of problems arising from time-harmonic Maxwell's equations in heterogeneous media.

At first, we considered $\mathbf{H}(\mathrm{curl})$-elliptic problems with homogeneous boundary conditions and rapidly oscillating coefficients μ and κ

$$\begin{aligned} \operatorname{curl}\big(\mu(x)\operatorname{curl}\mathbf{u}(x)\big) + \kappa(x)\mathbf{u}(x) &= \mathbf{f}(x) \qquad \text{in} \quad \Omega, \\ \mathbf{u}(x)\times\mathbf{n}(x) &= 0 \qquad \text{on} \quad \partial\Omega. \end{aligned}$$

We proposed and analyzed two multiscale methods: the Heterogeneous Multiscale (Finite Element) Method and the Localized Orthogonal Decomposition.

For locally periodic coefficients μ and κ, we suggested the Heterogeneous Multiscale Method and proved a priori error estimates. Based upon existing homogenization results, we formulated a two-scale equation as well as a decoupled macroscopic homogenized equation with cell problems. Particularly, we proposed a divergence regularization to cope with the cumbersome divergence-free constraint in one of the cell problems. The Heterogeneous Multiscale Method (for locally periodic coefficients) was reformulated as a discretization of the two-scale equation with numerical quadrature. Based on this framework, optimal convergence rates for the error to the solution to the two-scale limit equation were proved: linear convergence in the $\mathbf{H}(\mathrm{curl})$-norm and quadratic convergence in the $\mathbf{H}(\mathrm{div})'$-norm (based on a Helmholtz decomposition of the error). In order to confirm the convergence rates and to demonstrate the applicability of the method, we also gave numerical experiments. One model problem covered the $\mathbf{H}(\mathrm{curl})$-elliptic case and one dealt with the indefinite problem.

For general heterogeneous coefficients even without (local) periodicity and scale separation, we considered the Localized Orthogonal Decomposition. We showed that the exact solution can be decomposed into a coarse part (spanned by standard edge elements on a coarse mesh) and a fine part, using the Falk-Winther interpolation operator. The error between the coarse part and the exact solution converged linearly in the $\mathbf{H}(\mathrm{div})'$-norm. Adding a so-called Corrector Green's operator to the coarse functions, we obtained linear convergence of the error in the $\mathbf{H}(\mathrm{curl})$-norm and also quadratic convergence in the $\mathbf{H}(\mathrm{div})'$-norm. We discussed that these approximations results are optimal by revisiting the periodic case. We defined the Corrector Green's Operator as a projection onto the kernel of the interpolation operator, which is orthogonal with respect to the energy scalar product. Exponential decay of the corrector was shown so that its computation could be localized to patches of coarse elements. Adding these (local) corrections to the standard finite element basis, we defined a generalized finite element method. Under a suitable (logarithmic) coupling of the patch size to the (coarse) mesh size, linear convergence of the method in the $\mathbf{H}(\mathrm{curl})$-norm was proved. Furthermore, we showed that the same error convergence is obtained for indefinite problems.

As a second and even more challenging problem class, we were dealing with time-harmonic scattering problems with high contrast:

$$\begin{cases} -\nabla\cdot\big(\varepsilon_\delta^{-1}(x)\nabla u_\delta(x)\big) - k^2 u_\delta(x) &= 0 \qquad \text{in } G, \\ \nabla u_\delta(x)\cdot\mathbf{n}(x) - iku_\delta(x) &= g(x) \qquad \text{on } \partial G, \end{cases}$$

or

$$\begin{cases} \operatorname{curl}\big(\varepsilon_\delta^{-1}(x)\operatorname{curl}\mathbf{u}_\delta(x)\big) - k^2\mathbf{u}_\delta(x) & = 0 \qquad \text{in } G, \\ \operatorname{curl}\mathbf{u}_\delta(x)\times\mathbf{n}(x) - ik\big(\mathbf{n}(x)\times\mathbf{u}_\delta(x)\big)\times\mathbf{n}(x) & = \mathbf{g}(x) \qquad \text{on } \partial G, \end{cases}$$

where outside Ω, $\varepsilon_\delta^{-1} = 1$ and inside Ω, $\varepsilon_\delta^{-1}(x) = \varepsilon_0^{-1}\chi_{\Sigma^*}(\frac{x}{\delta}) + \varepsilon_1^{-1}\chi_\Sigma(\frac{x}{\delta})$.

Here, we proposed and analyzed a Heterogeneous Multiscale Method, which was directly formulated as the discretization of the corresponding two-scale equation. Hence, as a first step, we revisited the existing homogenization results for these problems and restated and proved them for our setting. The high contrast structure causes the occurrence of an additional homogenized (or effective) parameter in the identity term. This effective permeability depends on the wavenumber k and can have a positive or a negative sign. A negative effective permeability completely changes the mathematical structure of the equation and physically implies that wave propagation is forbidden inside the scatterer in that case, leading to a so-called band gap. Moreover, we were concerned with the stability and regularity of the homogenized macroscopic problems. Particularly, we proved stability estimates with k-explicit constants for the Helmholtz equation and the time-harmonic Maxwell equation with piecewise constant coefficients, respectively.

Using these results, we proved the well-posedness (stability) and quasi-optimality of the Heterogeneous Multiscale Method under a (standard) resolution condition between the wavenumber and the mesh size. As a consequence of the quasi-optimality, we deduced linear convergence in the energy norm (k-weighted H^1 or k-weighted $\mathbf{H}(\operatorname{curl})$) and quadratic convergence in the L^2-norm (Helmholtz equation) and $\mathbf{H}(\operatorname{div})'$-norm (Maxwell equation), respectively. Even though the discovered resolution condition between the wavenumber and the mesh size is standard in the literature, it can become prohibitive for large wavenumbers. As a remedy, we studied the additional application of a Localized Orthogonal Decomposition directly in the two-scale setting.

Numerical experiments for both problems demonstrated the applicability of the Heterogeneous Multiscale Method and confirmed the convergence rates. For wavenumbers with associated *negative* effective permeability, the (physically expected) exponential decay of the wave amplitude inside the scatterer was observed. Furthermore, this behavior could be explained by incited eigen resonances inside the inclusions Σ. For the Helmholtz equation, we also observed nice convergence behavior of a numerical zeroth order approximation to the heterogeneous reference solution.

5.2 Outlook

The problems arising from time-harmonic Maxwell's equations and the associated multiscale methods presented in this thesis offer several starting points for future research.

With view to negative refraction, homogenization results from the literature [LS16a] tell us that the three-dimensional setting of Chapter 4 needs to be complemented with long and thin wires. Building upon the method of Chapter 4, a Heterogeneous Multiscale Method for this setting could be proposed and analyzed. The vanishing diameter of the wires in the limit, however, might pose additional difficulties for discretization. In this context, we also mention high contrast structures with topology change in the limit (e.g., split rings), for which the formulation of a multiscale method is another task for the future and might be helpful for tackling the long and thin wires in the end.

Since in practice, no material is perfectly periodic, the extension of the Localized Orthogonal Decomposition of Section 3.2 should be studied – theoretically as well as in numerical experiments. First, impedance boundary conditions for Maxwell's equation need to be incorporated in the method. This might relax the resolution condition for time-harmonic Maxwell's problems, as it has already been achieved for the Helmholtz equation. Furthermore, we plan

to investigate the application of the Localized Orthogonal Decomposition to the high contrast problems of Chapter 4. Results and strategies obtained for high contrast diffusion problems in the literature are very promising. They can be combined with the (homogenization) analysis in Section 4.2 as well as the analysis of the Localized Orthogonal Decomposition for $\mathbf{H}(\mathrm{curl})$-problems in Section 3.2.

Furthermore, all problems considered in this thesis make use of the time-harmonic ansatz. The presented numerical analysis is an important building block for the long-time goal of studying multiscale methods for time-dependent Maxwell's equations, possibly also with high contrast or singular structures.

Finally, an even more challenging generalization are random media, where the coefficients of the problem are random fields. This modeling ansatz may be useful if the material properties are subject to uncertainties, for instance, if they are derived from measurements. In this context, the correlation length of the random coefficients plays an important role, comparable to the characteristic length of the spatial oscillations in our multiscale problems. Depending on the relation of wavelength and correlation length, random media may trigger astonishing phenomena in wave propagation problems, such as wave localization or time reversal, see [FGPS07] for an overview. In the numerical approximation of these random or stochastic PDEs one is interested in the extraction of deterministic quantities, such as the expected value, of the solutions. This is a challenging task since typically the problem has to be solved for several realizations of the coefficients. Under certain assumptions on the coefficients, stochastic homogenization [JKO94] provides an analytical tool for the identification of effective deterministic models, which can be used in the numerical approximation. We refer to [ACL+12] for an overview of analytical and numerical approaches in that direction.

List of Symbols

$\mathcal{B}$	sesquilinear form associated with a variational problem	16, 17
$C_{\mathrm{ol},m}$	upper bound on the number of elements in the mth level patch	22
conv	convex hull	23
curl	(weak) curl	13
δ	fine-scale parameter	2
Δ_0, Δ_1	set of vertices and edges, respectively	23
diam	diameter	21
div	(weak) divergence	13
$\mathbf{e}_j$	jth unit vector	28
$\|\cdot\|_e$	two-scale energy norm	42
$\|\cdot\|_{1,e}$	H^1-seminorm on the two-scale space $\mathcal{H}$ for the Helmholtz equation	101
ε	electric permittivity	10
$\approx$	equal up to a constant	9
η	cut-off function	59
$\mathcal{G}$	Corrector Green's operator	52
$\mathcal{G}_m$	approximation of the Corrector Green's operator	56
$\gtrsim$	greater or equal than up to a constant	9
H	(coarse) global mesh size	32
h	global mesh size either of a fine triangulation (LOD) or of the triangulation of the unit cell (HMM)	32, 58
$\|\cdot\|_{1,k}$	k-weighted H^1-norm	13
$\mathbf{H}(\mathrm{curl})$	space of functions with weak curl	13
$\mathbf{H}_0(\mathrm{curl})$	space of functions in $\mathbf{H}(\mathrm{curl})$ with zero tangential traces	15
$\|\cdot\|_{\mathrm{curl},k}$	k-weighted $\mathbf{H}(\mathrm{curl})$-norm	14
$\mathbf{H}(\mathrm{curl}_\Gamma)$	space of functions with surface curl	15
$\mathbf{H}^s(\mathrm{curl})$	space of functions in $\mathbf{H}^s$ with weak curl in $\mathbf{H}^s$	14
$\mathbf{H}^s_{pw}(\mathrm{curl})$	space of functions in $\mathbf{H}(\mathrm{curl})$, which are piecewise in $\mathbf{H}^s(\mathrm{curl})$ for $s > 0$	14
$\mathbf{H}(\mathrm{div})$	space of functions with weak divergence	13
$\mathbf{H}_0(\mathrm{div})$	space of functions in $\mathbf{H}(\mathrm{div})$ with zero normal traces	15
$\mathbf{H}(\mathrm{div}\,0)$	space of divergence-free functions	14
$\mathcal{H}$	two-scale space	79
$\mathbf{H}_{\mathrm{imp}}$	impedance function space	14
$\|\cdot\|_{\mathrm{imp},k}$	k-weighted $\mathbf{H}_{\mathrm{imp}}$-norm	14
hom	(as subscript) indicates homogenized (effective) parameters	30
H^s	space of functions with (fractional) weak derivatives up to order s in L^2	13
$\mathbf{H}^s$	vector-valued version of H^s	13
$\mathbf{H}^s_\parallel$	image space of the tangential trace	15
$H^s_{pw}(G)$	space of functions in $H^1(G)$, which are piecewise in H^s for $s > 1$	13
$H^s_{\sharp,0}(Y)$	space of periodic H^s functions on Y with zero average	28

$\mathbf{H}^s_T$	space of tangential $\mathbf{H}^s$ functions	15
id	identity operator	33
Id	identity matrix	74
I_h	nodal interpolation operator	24
Im	imaginary part	72
im	image of an operator	49
$\mathcal{K}$	corrector operator for $\mathbf{H}$(curl)-problems	53
k	wavenumber	12
ker	kernel of an operator	49
$\mathcal{K}_m$	approximation to the corrector operator for $\mathbf{H}$(curl)-problems	56
L^2_T	space of tangential L^2 functions on the boundary	14
λ_a	Lagrange basis function (hat function) associated with vertex a	23
$\lesssim$	less or equal than up to a constant	9
$\mathcal{L}$	differential operator associated with sesquilinear form $\mathcal{B}$	52
$L^p(\Omega; X)$	Bochner-Lebesgue space	28
m	oversampling constant	34
μ	magnetic permeability; for $\mathbf{H}$(curl)-elliptic problems: inverse permeability	10, 12
$\mathbf{n}$	unit outer normal of the domain	10
$\mathcal{N}(\mathcal{T}_h)$	lowest order edge elements on the mesh $\mathcal{T}_h$	23
N^m	mth level patch	21
ω_a	vertex patch associated with vertex a (support of the corresponding hat function)	26
ω_E^{ext}	extended edge patch of edge E (union of the two vertex patches for the vertices of E)	26
$\mathcal{P}^p(\mathcal{T}_h)$	piecewise polynomials of degree p on the mesh $\mathcal{T}_h$	24
$\boldsymbol{\phi}_E$	Nédélec basis function associated with edge E	23
Π	H^1-stable interpolation operator onto linear Lagrange elements	25
π^E	Falk-Winther interpolation operator	26
$\mathcal{Q}$	corrector operator for H^1-problems	33
$\mathcal{Q}_m$	approximation to the corrector operator for H^1-problems	34
Re	real part	11
$\rightharpoonup$	weak convergence	29
$\overset{2}{\rightharpoonup}$	two-scale convergence	29
$\mathcal{RT}(\mathcal{T}_h)$	Raviart-Thomas elements on the mesh $\mathcal{T}_h$	24
SF	sign-flip isomorphism	18
$\mathcal{S}(\mathcal{T}_h)$	linear Lagrange elements on the mesh $\mathcal{T}_h$	23
$\sharp$	(as subscript) indicates periodic function spaces	28
$\mathbf{v}_T$	tangential component of $\mathbf{v}$	14
$\mathcal{T}$	regular and shape regular triangulation	21
$\underline{\mathbf{u}}$	analytical two-scale solution	38, 73, 75
$\mathbf{u}_{H,h}$	discrete two-scale solution	92
$\mathbf{V}_{H,h}$	discrete two-scale space	92
X'	dual space of the Hilbert space X	12
Y	unit cell	28
Y_j^δ	δ-scaled and shifted unit cell	31

Acronyms

EOC	experimental order of convergence	43
FE	finite element	21
FEM	Finite Element Method	20
gFEM	generalized Finite Element Method	5
gMsFEM	generalized Multiscale Finite Element Method	6
HMM	Heterogeneous Multiscale Method	5
LOD	Localized Orthogonal Decomposition	5
LRBMS	Localized Reduced Basis Multiscale Method	6
MsFEM	Multiscale Finite Element Method	6
PDE	partial differential equation	2
VMM	Variational Multiscale Method	6

Bibliography

[AB15] A. Abdulle, O. Budáč. *An adaptive finite element heterogeneous multiscale method for Stokes flow in porous media.* Multiscale Model. Simul. 13(1), pp. 256–290, 2015. doi:10.1137/130950136.

[AB16] A. Abdulle, O. Budáč. *A reduced basis finite element heterogeneous multiscale method for Stokes flow in porous media.* Comput. Methods Appl. Mech. Engrg. 307, pp. 1–31, 2016. doi:10.1016/j.cma.2016.03.016.

[Abd05] A. Abdulle. *On a priori error analysis of fully discrete heterogeneous multiscale FEM.* Multiscale Model. Simul. 4(2), pp. 447–459, 2005. doi:10.1137/040607137.

[Abd09] A. Abdulle. *The finite element heterogeneous multiscale method: a computational strategy for multiscale PDEs.* In *Multiple scales problems in biomathematics, mechanics, physics and numerics*, vol. 31 of *GAKUTO Internat. Ser. Math. Sci. Appl.*, pp. 133–181. Gakkōtosho, Tokyo, 2009.

[ABDG98] C. Amrouche, C. Bernardi, M. Dauge, V. Girault. *Vector potentials in three-dimensional non-smooth domains.* Math. Methods Appl. Sci. 21(9), pp. 823–864, 1998. doi:10.1002/(SICI)1099-1476(199806)21:9<823::AID-MMA976>3.0.CO;2-B.

[ABV16] G. Allaire, M. Briane, M. Vanninathan. *A comparison between two-scale asymptotic expansions and Bloch wave expansions for the homogenization of periodic structures.* SeMA J. 73(3), pp. 237–259, 2016. doi:10.1007/s40324-016-0067-z.

[ACL+12] A. Anantharaman, R. Costaouec, C. Le Bris, F. Legoll, F. Thomines. *Introduction to numerical stochastic homogenization and the related computational challenges: some recent developments.* In *Multiscale modeling and analysis for materials simulation*, vol. 22 of *Lect. Notes Ser. Inst. Math. Sci. Natl. Univ. Singap.*, pp. 197–272. World Sci. Publ., Hackensack, NJ, 2012. doi:10.1142/9789814360906_0004.

[AE03] A. Abdulle, W. E. *Finite difference heterogeneous multi-scale method for homogenization problems.* J. Comput. Phys. 191(1), pp. 18–39, 2003. doi:10.1016/S0021-9991(03)00303-6.

[AEEV12] A. Abdulle, W. E, B. Engquist, E. Vanden-Eijnden. *The heterogeneous multiscale method.* Acta Numer. 21, pp. 1–87, 2012. doi:10.1017/S0962492912000025.

[AFW06] D. N. Arnold, R. S. Falk, R. Winther. *Finite element exterior calculus, homological techniques, and applications.* Acta Numer. 15, pp. 1–155, 2006. doi:10.1017/S0962492906210018.

[AFW10] D. N. Arnold, R. S. Falk, R. Winther. *Finite element exterior calculus: from Hodge theory to numerical stability.* Bull. Amer. Math. Soc. 47(2), pp. 281–354, 2010. doi:10.1090/S0273-0979-10-01278-4.

[AG11] A. Abdulle, M. J. Grote. *Finite element heterogeneous multiscale method for the wave equation.* Multiscale Model. Simul. 9(2), pp. 766–792, 2011. doi: 10.1137/100800488.

[AGJ17] A. Abdulle, M. J. Grote, O. Jecker. *FE-HMM for elastic waves in heterogeneous media.* preprint EPFL, 2017. `https://infoscience.epfl.ch/record/231083/files/Abdulle_Grote_Jecker_elawaves_rev.pdf`.

[AGS14] A. Abdulle, M. J. Grote, C. Stohrer. *Finite element heterogeneous multiscale method for the wave equation: long-time effects.* Multiscale Model. Simul. 12(3), pp. 1230–1257, 2014. doi:10.1137/13094195X.

[AH17a] A. Abdulle, P. Henning. *Localized orthogonal decomposition method for the wave equation with a continuum of scales.* Math. Comp. 86(304), pp. 549–587, 2017. doi:10.1090/mcom/3114.

[AH17b] A. Abdulle, P. Henning. *Multiscale methods for wave problems in heterogeneous media.* In *Handbook of numerical methods for hyperbolic problems*, vol. 18 of *Handb. Numer. Anal.*, pp. 545–576. Elsevier/North-Holland, Amsterdam, 2017.

[AHKO12] F. Albrecht, B. Haasdonk, S. Kaulmann, M. Ohlberger. *The localized reduced basis multiscale method.* In *Proceedings of Algoritmy 2012, Conference on Scientific Computing, Vysoke Tatry, Podbanske*, pp. 393–403. Slovak University of Technology, Bratislava, 2012.

[Ale12] G. Alessandrini. *Strong unique continuation for general elliptic equations in 2D.* J. Math. Anal. Appl. 386(2), pp. 669–676, 2012. doi:10.1016/j.jmaa.2011.08.029.

[All92] G. Allaire. *Homogenization and two-scale convergence.* SIAM J. Math. Anal. 23(6), pp. 1482–1518, 1992. doi:10.1137/0523084.

[AN09] A. Abdulle, A. Nonnenmacher. *A posteriori error analysis of the heterogeneous multiscale method for homogenization problems.* C. R. Math. Acad. Sci. Paris 347(17-18), pp. 1081–1086, 2009. doi:10.1016/j.crma.2009.07.004.

[AP16a] A. Abdulle, T. N. Pouchon. *Effective models for the multidimensional wave equation in heterogeneous media over long time and numerical homogenization.* Math. Models Methods Appl. Sci. 26(14), pp. 2651–2684, 2016. doi:10.1142/S0218202516500627.

[AP16b] A. Abdulle, T. N. Pouchon. *A priori error analysis of the finite element heterogeneous multiscale method for the wave equation over long time.* SIAM J. Numer. Anal. 54(3), pp. 1507–1534, 2016. doi:10.1137/15M1025633.

[AP17] A. Abdulle, T. N. Pouchon. *Effective models for long time wave propagation in locally periodic media.* preprint EPFL, 2017. `https://infoscience.epfl.ch/record/231084/files/wave_long_time_loc_per_abdulle_pouchon.pdf`.

[AR14] D. Arjmand, O. Runborg. *Analysis of heterogeneous multiscale methods for long time wave propagation problems.* Multiscale Model. Simul. 12(3), pp. 1135–1166, 2014. doi:10.1137/140957573.

[AS05] A. Abdulle, C. Schwab. *Heterogeneous multiscale FEM for diffusion problems on rough surfaces.* Multiscale Model. Simul. 3(1), pp. 195–220, 2004/05. doi: 10.1137/030600771.

[AS11] Y. Amirat, V. Shelukhin. *Homogenization of time harmonic Maxwell equations and the frequency dispersion effect.* J. Math. Pures Appl. 95(4), pp. 420–443, 2011. doi:10.1016/j.matpur.2010.10.007.

[Bab71] I. Babuška. *Error-bounds for finite element method.* Numer. Math. 16(4), pp. 322–333, 1970/1971. doi:10.1007/BF02165003.

[BB12] G. Bouchitté, C. Bourel. *Multiscale nanorod metamaterials and realizable permittivity tensors.* Commun. Comput. Phys. 11(2), pp. 489–507, 2012. doi:10.4208/cicp.171209.110810s.

[BBD+08a] P. Bastian, M. Blatt, A. Dedner, C. Engwer, R. Klöfkorn, R. Kornhuber, M. Ohlberger, O. Sander. *A generic grid interface for parallel and adaptive scientific computing. II. Implementation and tests in DUNE.* Computing 82(2-3), pp. 121–138, 2008. doi:10.1007/s00607-008-0004-9.

[BBD+08b] P. Bastian, M. Blatt, A. Dedner, C. Engwer, R. Klöfkorn, M. Ohlberger, O. Sander. *A generic grid interface for parallel and adaptive scientific computing. I. Abstract framework.* Computing 82(2-3), pp. 103–119, 2008. doi:10.1007/s00607-008-0003-x.

[BBF09] G. Bouchitté, C. Bourel, D. Felbacq. *Homogenization of the 3D Maxwell system near resonances and artificial magnetism.* C. R. Math. Acad. Sci. Paris 347(9–10), pp. 571–576, 2009. doi:10.1016/j.crma.2009.02.027.

[BBF17] G. Bouchitté, C. Bourel, D. Felbacq. *Homogenization near resonances and artificial magnetism in three dimensional dielectric metamaterials.* Arch. Ration. Mech. Anal. 225(3), pp. 1233–1277, 2017. doi:10.1007/s00205-017-1132-1.

[BC01] A. Buffa, P. Ciarlet, Jr. *On traces for functional spaces related to Maxwell's equations. I. An integration by parts formula in Lipschitz polyhedra.* Math. Methods Appl. Sci. 24(1), pp. 9–30, 2001. doi:10.1002/1099-1476(20010110)24:1<9::AID-MMA191>3.0.CO;2-2.

[BC13] J. Baiges, R. Codina. *A variational multiscale method with subscales on the element boundaries for the Helmholtz equation.* Internat. J. Numer. Methods Engrg. 93(6), pp. 664–684, 2013. doi:10.1002/nme.4406.

[BCG+11] T. Betcke, S. N. Chandler-Wilde, I. G. Graham, S. Langdon, M. Lindner. *Condition number estimates for combined potential integral operators in acoustics and their boundary element discretisation.* Numer. Methods Partial Differential Equations 27(1), pp. 31–69, 2011. doi:10.1002/num.20643.

[BCG17] H. Barucq, T. Chaumont-Frelet, C. Gout. *Stability analysis of heterogeneous Helmholtz problems and finite element solution based on propagation media approximation.* Math. Comp. 86(307), pp. 2129–2157, 2017. doi:10.1090/mcom/3165.

[BCS02] A. Buffa, M. Costabel, D. Sheen. *On traces for* $\mathbf{H}(\mathbf{curl}, \Omega)$ *in Lipschitz domains.* J. Math. Anal. Appl. 276(2), pp. 845–867, 2002. doi:10.1016/S0022-247X(02)00455-9.

[BDE03] W. L. Barnes, A. Dereux, T. W. Ebbesen. *Surface plasmon subwavelength optics.* Nature 424, pp. 824–830, 2003. doi:10.1038/nature01937.

[BEOR17a] A. Buhr, C. Engwer, M. Ohlberger, S. Rave. *ArbiLoMod, a simulation technique designed for arbitrary local modifications.* SIAM J. Sci. Comput. 39(4), pp. A1435–A1465, 2017. doi:10.1137/15M1054213.

[BEOR17b] A. Buhr, C. Engwer, M. Ohlberger, S. Rave. *ArbiLoMod: local solution spaces by random training in electrodynamics.* In *Model reduction of parametrized systems*, vol. 17 of *MS&A. Model. Simul. Appl.*, pp. 137–148. Springer, Cham, 2017.

[BF04] G. Bouchitté, D. Felbacq. *Homogenization near resonances and artificial magnetism from dielectrics.* C. R. Math. Acad. Sci. Paris 339(5), pp. 377–382, 2004. doi:10.1016/j.crma.2004.06.018.

[BF06] G. Bouchitté, D. Felbacq. *Homogenization of a wire photonic crystal: the case of small volume fraction.* SIAM J. Appl. Math. 66(6), pp. 2061–2084, 2006. doi:10.1137/050633147.

[BFHR97] F. Brezzi, L. P. Franca, T. J. R. Hughes, A. Russo. $b = \int g$. Comput. Methods Appl. Mech. Engrg. 145(3-4), pp. 329–339, 1997. doi:10.1016/S0045-7825(96)01221-2.

[BG16] D. L. Brown, D. Gallistl. *Multiscale sub-grid correction method for time-harmonic high-frequency elastodynamics with wavenumber explicit bounds.* arXiv preprint, 2016. `arXiv:1608.04243`.

[BGL13] A. Bonito, J.-L. Guermond, F. Luddens. *Regularity of the Maxwell equations in heterogeneous media and Lipschitz domains.* J. Math. Anal. Appl. 408(2), pp. 498–512, 2013. doi:10.1016/j.jmaa.2013.06.018.

[BGP17] D. L. Brown, D. Gallistl, D. Peterseim. *Multiscale Petrov-Galerkin Method for High-Frequency Heterogeneous Helmholtz Equations.* In M. Griebel, M. A. Schweitzer, eds., *Meshfree Methods for Partial Differential Equations VIII*, vol. 115 of *Lect. Notes Comput. Sci. Eng.*, pp. 85–115. Springer, Cham, 2017. doi:10.1007/978-3-319-51954-8_6.

[BH03] A. Buffa, R. Hiptmair. *Galerkin boundary element methods for electromagnetic scattering.* In *Topics in computational wave propagation*, vol. 31 of *Lect. Notes Comput. Sci. Eng.*, pp. 83–124. Springer, Berlin, 2003. doi:10.1007/978-3-642-55483-4_3.

[BLP78] A. Bensoussan, J.-L. Lions, G. Papanicolaou. *Asymptotic analysis for periodic structures*, vol. 5 of *Studies in Mathematics and its Applications.* North-Holland Publishing Co., Amsterdam-New York, 1978.

[BO83] I. Babuška, J. E. a. Osborn. *Generalized finite element methods: their performance and their relation to mixed methods.* SIAM J. Numer. Anal. 20(3), pp. 510–536, 1983. doi:10.1137/0720034.

[Bos98] A. Bossavit. *Computational electromagnetism: Variational formulations, complementarity, edge elements.* Electromagnetism, Academic Press, Inc., San Diego, CA, 1998.

[BS00] I. Babuška, S. A. Sauter. *Is the pollution effect of the FEM avoidable for the Helmholtz equation considering high wave numbers?* SIAM Rev. 42(3), pp. 451–484 (electronic), 2000. doi:10.1137/S0036142994269186. Reprint of SIAM J. Numer. Anal. **34** (1997), no. 6, 2392–2423.

[BS08] S. C. Brenner, L. R. Scott. *The mathematical theory of finite element methods*, vol. 15 of *Texts in Applied Mathematics.* Springer, New York, 3rd edn., 2008. doi:10.1007/978-0-387-75934-0.

[BS10] G. Bouchitté, B. Schweizer. *Homogenization of Maxwell's equations in a split ring geometry.* Multiscale Model. Simul. 8(3), pp. 717–750, 2010. doi:10.1137/09074557X.

[BSS11] H. Brandsmeier, K. Schmidt, C. Schwab. *A multiscale hp-FEM for 2D photonic crystal bands.* J. Comput. Phys. 230(2), pp. 349–374, 2011. doi:10.1016/j.jcp.2010.09.018.

[BSW16] D. Baskin, E. A. Spence, J. Wunsch. *Sharp high-frequency estimates for the Helmholtz equation and applications to boundary integral equations.* SIAM J. Math. Anal. 48(1), pp. 229–267, 2016. doi:10.1137/15M102530X.

[CC15] K. Cherednichenko, S. Cooper. *Homogenization of the system of high-contrast Maxwell equations.* Mathematika 61(2), pp. 475–500, 2015. doi:10.1112/S0025579314000424.

[CCZ02] L.-Q. Cao, J.-Z. Cui, D.-C. Zhu. *Multiscale asymptotic analysis and numerical simulation for the second order Helmholtz equations with rapidly oscillating coefficients over general convex domains.* SIAM J. Numer. Anal. 40(2), pp. 543–577, 2002. doi:10.1137/S0036142900376110.

[CD99] D. Cioranescu, P. Donato. *An introduction to homogenization*, vol. 17 of *Oxford Lecture Series in Mathematics and its Applications.* The Clarendon Press, Oxford University Press, New York, 1999.

[CD00] M. Costabel, M. Dauge. *Singularities of electromagnetic fields in polyhedral domains.* Arch. Ration. Mech. Anal. 151, pp. 221–276, 2000. doi:10.1007/s002050050197.

[CD02] M. Costabel, M. Dauge. *Weighted regularization of Maxwell equations in polyhedral domains. A rehabilitation of nodal finite elements.* Numer. Math. 93(2), pp. 239–277, 2002. doi:10.1007/s002110100388.

[CDN99] M. Costabel, M. Dauge, S. Nicaise. *Singularities of Maxwell interface problems.* M2AN Math. Model. Numer. Anal. 33(3), pp. 627–649, 1999. doi:10.1051/m2an:1999155.

[CEH16] E. Chung, Y. Efendiev, T. Y. Hou. *Adaptive multiscale model reduction with generalized multiscale finite element methods.* J. Comput. Phys. 320, pp. 69–95, 2016. doi:10.1016/j.jcp.2016.04.054.

[CEL14] E. T. Chung, Y. Efendiev, W. T. Leung. *Generalized multiscale finite element methods for wave propagation in heterogeneous media.* Multiscale Model. Simul. 12(4), pp. 1691–1721, 2014. doi:10.1137/130926675.

[CF06] P. Cummings, X. Feng. *Sharp regularity coefficient estimates for complex-valued acoustic and elastic Helmholtz equations.* Math. Models Methods Appl. Sci. 16(1), pp. 139–160, 2006. doi:10.1142/S021820250600108X.

[CFS17] P. Ciarlet, Jr., S. Fliss, C. Stohrer. *On the approximation of electromagnetic fields by edge finite elements. Part 2: A heterogeneous multiscale method for Maxwell's equations.* Comput. Math. Appl. 73(9), pp. 1900–1919, 2017. doi:10.1016/j.camwa.2017.02.043.

[CG07] K. D. Cherednichenko, S. Guenneau. *Bloch-wave homogenization for spectral asymptotic analysis of the periodic Maxwell operator.* Waves Random Complex Media 17(4), pp. 627–651, 2007. doi:10.1080/17455030701551930.

[CGH10] C.-C. Chu, I. G. Graham, T. Y. Hou. *A new multiscale finite element method for high-contrast elliptic interface problems.* Math. Comp. 79(272), pp. 1915–1955, 2010. doi:10.1090/S0025-5718-2010-02372-5.

[CH15] V. T. Chu, V. H. Hoang. *Homogenization error for two scale Maxwell equations.* arXiv preprint, 2015. `arXiv:1512.02788`.

[CH18] V. T. Chu, V. H. Hoang. *High-dimensional finite elements for multiscale Maxwell-type equations.* IMA Journal of Numerical Analysis 38(1), pp. 227–270, 2018. doi:10.1093/imanum/drx001.

[CHHS17] L. A. Caudillo-Mata, E. Haber, L. J. Heagy, C. Schwarzbach. *A framework for the upscaling of the electrical conductivity in the quasi-static Maxwell's equations.* J. Comput. Appl. Math. 317, pp. 388–402, 2017. doi:10.1016/j.cam.2016.11.051.

[Chr07] S. H. Christiansen. *Stability of Hodge decompositions in finite element spaces of differential forms in arbitrary dimension.* Numer. Math. 107(1), pp. 87–106, 2007. doi:10.1007/s00211-007-0081-2.

[Cia78] P. G. Ciarlet. *The finite element method for elliptic problems.* North-Holland Publishing Co., Amsterdam-New York-Oxford, 1978. Studies in Mathematics and its Applications, Vol. 4.

[Cia16] P. Ciarlet, Jr. *On the approximation of electromagnetic fields by edge finite elements. Part 1: Sharp interpolation results for low-regularity fields.* Comput. Math. Appl. 71(1), pp. 85–104, 2016. doi:10.1016/j.camwa.2015.10.020.

[CL18] E. Chung, Y. Li. *Adaptive generalized multiscale finite element methods for H(curl)-elliptic problems with heterogeneous coefficients.* arXiv preprint, 2018. `1802.02989`.

[CLX13] H. Chen, P. Lu, X. Xu. *A hybridizable discontinuous Galerkin method for the Helmholtz equation with high wave number.* SIAM J. Numer. Anal. 51(4), pp. 2166–2188, 2013. doi:10.1137/120883451.

[Cos90] M. Costabel. *A remark on the regularity of solutions of Maxwell's equations on Lipschitz domains.* Math. Methods Appl. Sci. 12(4), pp. 365–368, 1990. doi:10.1002/mma.1670120406.

[CS14] P. Ciarlet, Jr., C. Stohrer. *Finite-element heterogeneous multiscale method for the Helmholtz equation.* C. R. Math. Acad. Sci. Paris 352(9), pp. 755–760, 2014. doi:10.1016/j.crma.2014.07.006.

[CV97] C. Conca, M. Vanninathan. *Homogenization of periodic structures via Bloch decomposition.* SIAM J. Appl. Math. 57(6), pp. 1639–1659, 1997. doi:10.1137/S0036139995294743.

[CW08] S. H. Christiansen, R. Winther. *Smoothed projections in finite element exterior calculus.* Math. Comp. 77(262), pp. 813–829, 2008. doi:10.1090/S0025-5718-07-02081-9.

[CZAL10] L. Cao, Y. Zhang, W. Allegretto, Y. Lin. *Multiscale asymptotic method for Maxwell's equations in composite materials.* SIAM J. Numer. Anal. 47(6), pp. 4257–4289, 2010. doi:10.1137/080741276.

[DB05] L. Demkowicz, A. Buffa. *H^1, $H(curl)$ and $H(div)$-conforming projection-based interpolation in three dimensions. Quasi-optimal p-interpolation estimates.* Comput. Methods Appl. Mech. Engrg. 194(2-5), pp. 267–296, 2005. doi:10.1016/j.cma.2004.07.007.

[DE12] D. A. Di Pietro, A. Ern. *Mathematical aspects of discontinuous Galerkin methods*, vol. 69 of *Mathématiques & Applications (Berlin)*. Springer, Heidelberg, 2012. doi:10.1007/978-3-642-22980-0.

[DH14] A. Demlow, A. N. Hirani. *A posteriori error estimates for finite element exterior calculus: the de Rham complex.* Found. Comput. Math. 14(6), pp. 1337–1371, 2014. doi:10.1007/s10208-014-9203-2.

[DLS14] T. Dohnal, A. Lamacz, B. Schweizer. *Bloch-wave homogenization on large time scales and dispersive effective wave equations.* Multiscale Model. Simul. 12(2), pp. 488–513, 2014. doi:10.1137/130935033.

[DLS15] T. Dohnal, A. Lamacz, B. Schweizer. *Dispersive homogenized models and coefficient formulas for waves in general periodic media.* Asymptot. Anal. 93(1-2), pp. 21–49, 2015. doi:10.3233/ASY-141280.

[DLTZ12] H. Duan, S. Li, R. C. E. Tan, W. Zheng. *A delta-regularization finite element method for a double curl problem with divergence-free constraint.* SIAM J. Numer. Anal. 50(6), pp. 3208–3230, 2012. doi:10.1137/110850578.

[DS13] W. Dörfler, S. A. Sauter. *A posteriori error estimation for highly indefinite Helmholtz problems.* Comput. Methods Appl. Math. 13(3), pp. 333–347, 2013. doi:10.1515/cmam-2013-0008.

[DS17] T. Dohnal, B. Schweizer. *A Bloch wave numerical scheme for scattering problems in periodic wave-guides.* preprint TU Dortmund, 2017. `https://eldorado.tu-dortmund.de/bitstream/2003/36118/1/Preprint%202017-03.pdf`, accepted at SIAM J. Numer. Anal.

[EE03] W. E, B. Engquist. *The heterogeneous multiscale methods.* Commun. Math. Sci. 1(1), pp. 87–132, 2003.

[EE05] W. E, B. Engquist. *The heterogeneous multi-scale method for homogenization problems.* In *Multiscale methods in science and engineering*, vol. 44 of *Lect. Notes Comput. Sci. Eng.*, pp. 89–110. Springer, Berlin, 2005. doi:10.1007/3-540-26444-2_4.

[EEL+07] W. E, B. Engquist, X. Li, W. Ren, E. Vanden-Eijnden. *Heterogeneous multiscale methods: a review.* Commun. Comput. Phys. 2(3), pp. 367–450, 2007.

[EG16] A. Ern, J.-L. Guermond. *Mollification in strongly Lipschitz domains with application to continuous and discrete de Rham complexes.* Comput. Methods Appl. Math. 16(1), pp. 51–75, 2016. doi:10.1515/cmam-2015-0034.

[EG17a] A. Ern, J.-L. Guermond. *Analysis of the edge finite element approximation of the Maxwell equations with low regularity solutions.* Computers & Mathematics with Applications 15(3), pp. 918–932, 2017. doi:10.1016/j.camwa.2017.10.017.

[EG17b] A. Ern, J.-L. Guermond. *Finite element quasi-interpolation and best approximation.* ESAIM Math. Model. Numer. Anal. 51(4), pp. 1367–1385, 2017. doi:10.1051/m2an/2016066.

[EGH13] Y. Efendiev, J. Galvis, T. Y. Hou. *Generalized multiscale finite element methods (GMsFEM).* J. Comput. Phys. 251, pp. 116–135, 2013. doi:10.1016/j.jcp.2013.04.045.

[EGH15] D. Elfverson, V. Ginting, P. Henning. *On multiscale methods in Petrov-Galerkin formulation.* Numer. Math. 131(4), pp. 643–682, 2015. doi:10.1007/s00211-015-0703-z.

[EH09] Y. Efendiev, T. Y. Hou. *Multiscale finite element methods: Theory and applications*, vol. 4 of *Surveys and Tutorials in the Applied Mathematical Sciences*. Springer, New York, 2009.

[EHG04] Y. Efendiev, T. Y. Hou, V. Ginting. *Multiscale finite element methods for nonlinear problems and their applications.* Commun. Math. Sci. 2(4), pp. 553–589, 2004.

[EHMP16] C. Engwer, P. Henning, A. Målqvist, D. Peterseim. *Efficient implementation of the Localized Orthogonal Decomposition method.* arXiv preprint, 2016. `arXiv:1602.01658`.

[EHR11] B. Engquist, H. Holst, O. Runborg. *Multi-scale methods for wave propagation in heterogeneous media.* Commun. Math. Sci. 9(1), pp. 33–56, 2011.

[EHR12] B. Engquist, H. Holst, O. Runborg. *Multiscale methods for wave propagation in heterogeneous media over long time.* In *Numerical analysis of multiscale computations*, vol. 82 of *Lect. Notes Comput. Sci. Eng.*, pp. 167–186. Springer, Heidelberg, 2012. doi:10.1007/978-3-642-21943-6_8.

[EIL+09] R. Ewing, O. Iliev, R. Lazarov, I. Rybak, J. Willems. *A simplified method for upscaling composite materials with high contrast of the conductivity.* SIAM J. Sci. Comput. 31(4), pp. 2568–2586, 2009. doi:10.1137/080731906.

[EM12] S. Esterhazy, J. M. Melenk. *On stability of discretizations of the Helmholtz equation.* In *Numerical analysis of multiscale problems*, vol. 83 of *Lect. Notes Comput. Sci. Eng.*, pp. 285–324. Springer, Heidelberg, 2012. doi:10.1007/978-3-642-22061-6_9. Extended version on arXiv, arXiv:1105.2112.

[EM14] S. Esterhazy, J. M. Melenk. *An analysis of discretizations of the Helmholtz equation in L^2 and in negative norms.* Comput. Math. Appl. 67(4), pp. 830–853, 2014. doi:10.1016/j.camwa.2013.10.005.

[EMZ05] W. E, P. Ming, P. Zhang. *Analysis of the heterogeneous multiscale method for elliptic homogenization problems.* J. Amer. Math. Soc. 18, pp. 121–156, 2005. doi:10.1090/S0894-0347-04-00469-2.

[EP04] A. Efros, A. Pokrovsky. *Dielectroc photonic crystal as medium with negative electric permittivity and magnetic permeability.* Solid State Communications 129(10), pp. 643–647, 2004. doi:10.1016/j.ssc.2003.12.022.

[FB97] D. Felbacq, G. Bouchitté. *Homogenization of a set of parallel fibres.* Waves Random Media 7(2), pp. 245–256, 1997. doi:10.1088/0959-7174/7/2/006.

[FGPS07] J.-P. Fouque, J. Garnier, G. Papanicolaou, K. Sølna. *Wave propagation and time reversal in randomly layered media*, vol. 56 of *Stochastic Modelling and Applied Probability.* Springer, New York, 2007.

[FJ16] S. Fliss, P. Joly. *Solutions of the time-harmonic wave equation in periodic waveguides: asymptotic behaviour and radiation condition.* Arch. Ration. Mech. Anal. 219(1), pp. 349–386, 2016. doi:10.1007/s00205-015-0897-3.

[FLX16] X. Feng, P. Lu, X. Xu. *A hybridizable discontinuous Galerkin method for the time-harmonic Maxwell equations with high wave number.* Comput. Methods Appl. Math. 16(3), pp. 429–445, 2016. doi:10.1515/cmam-2016-0021.

[FR05] P. Fernandes, M. Raffetto. *Existence, uniqueness and finite element approximation of the solution of time-harmonic electromagnetic boundary value problems involving meta-materials.* COMPEL 24(4), pp. 1450–1469, 2005. doi:10.1108/03321640510615724.

[FW14a] R. S. Falk, R. Winther. *Local bounded cochain projections.* Math. Comp. 83(290), pp. 2631–2656, 2014. doi:10.1090/S0025-5718-2014-02827-5.

[FW14b] X. Feng, H. Wu. *An absolutely stable discontinuous Galerkin method for the indefinite time-harmonic Maxwell equations with large wave number.* SIAM J. Numer. Anal. 52(5), pp. 2356–2380, 2014. doi:10.1137/120902112.

[FW15] R. S. Falk, R. Winther. *Double complexes and local cochain projections.* Numer. Methods Partial Differential Equations 31(2), pp. 541–551, 2015. doi:10.1002/num.21922.

[GGS12] L. Grasedyck, I. Greff, S. Sauter. *The AL basis for the solution of elliptic problems in heterogeneous media.* Multiscale Model. Simul. 10(1), pp. 245–258, 2012. doi:10.1137/11082138X.

[GHV18] D. Gallistl, P. Henning, B. Verfürth. *Numerical homogenization of H(curl)-problems.* SIAM J. Numer. Anal. 56, pp. 1570–1596, 2018. doi:10.1137/17M1133932.

[Glo06] A. Gloria. *An analytical framework for the numerical homogenization of monotone elliptic operators and quasiconvex energies.* Multiscale Model. Simul. 5(3), pp. 996–1043, 2006. doi:10.1137/060649112.

[GM11] R. Griesmaier, P. Monk. *Error analysis for a hybridizable discontinuous Galerkin method for the Helmholtz equation.* J. Sci. Comput. 49(3), pp. 291–310, 2011. doi:10.1007/s10915-011-9460-z.

[GM12] G. N. Gatica, S. Meddahi. *Finite element analysis of a time harmonic Maxwell problem with an impedance boundary condition.* IMA J. Numer. Anal. 32(2), pp. 534–552, 2012. doi:10.1093/imanum/drq041.

[GP15] D. Gallistl, D. Peterseim. *Stable multiscale Petrov-Galerkin finite element method for high frequency acoustic scattering.* Comput. Methods Appl. Mech. Engrg. 295, pp. 1–17, 2015. doi:10.1016/j.cma.2015.06.017.

[GP17a] D. Gallistl, D. Peterseim. *Computation of quasi-local effective diffusion tensors and connections to the mathematical theory of homogenization.* Multiscale Model. Simul. 15(4), pp. 1530–1552, 2017. doi:10.1137/16M1088533.

[GP17b] D. Gallistl, D. Peterseim. *Numerical stochastic homogenization by quasi-local effective diffusion tensors.* arXiv preprint, 2017. `arXiv:1702.08858`.

[GPS18] I. G. Graham, O. R. Pembery, E. A. Spence. *The Helmholtz equation in heterogeneous media: a priori bounds, well-posedness, and resonances.* arXiv preprint, 2018. `arXiv:1801.08095`.

[Gri85] P. Grisvard. *Elliptic problems in nonsmooth domains*, vol. 24 of *Monographs and Studies in Mathematics*. Pitman (Advanced Publishing Program), Boston, MA, 1985.

[GT77] D. Gilbarg, N. S. Trudinger. *Elliptic partial differential equations of second order*. Springer-Verlag, Berlin-New York, 1977. Grundlehren der Mathematischen Wissenschaften, Vol. 224.

[GZN07] S. Guenneau, F. Zolla, A. Nicolet. *Homogenization of 3D finite photonic crystals with heterogeneous permittivity and permeability*. Waves Random Complex Media 17(4), pp. 653–697, 2007. doi:10.1080/17455030701607013.

[Hen11] P. Henning. *Heterogeneous multiscale finite element methods for advection diffusion and nonlinear elliptic multiscale problems*. Ph.D. thesis, Westfälische Wilhelms-Universität Münster, 2011.

[Het07] U. Hetmaniuk. *Stability estimates for a class of Helmholtz problems*. Commun. Math. Sci. 5(3), pp. 665–678, 2007.

[HFMQ98] T. J. R. Hughes, G. R. Feijóo, L. Mazzei, J.-B. Quincy. *The variational multiscale method—a paradigm for computational mechanics*. Comput. Methods Appl. Mech. Engrg. 166(1-2), pp. 3–24, 1998. doi:10.1016/S0045-7825(98)00079-6.

[HHM16] F. Hellman, P. Henning, A. Målqvist. *Multiscale mixed finite elements*. Discrete Contin. Dyn. Syst. Ser. S 9(5), pp. 1269–1298, 2016. doi:10.3934/dcdss.2016051.

[Hip02] R. Hiptmair. *Finite elements in computational electromagnetism*. Acta Numer. 11, pp. 237–339, 2002. doi:10.1017/S0962492902000041.

[Hip15] R. Hiptmair. *Maxwell's equations: continuous and discrete*. In *Computational electromagnetism*, vol. 2148 of *Lecture Notes in Math.*, pp. 1–58. Springer, Cham, 2015. doi:10.1007/978-3-319-19306-9_1.

[HM14] P. Henning, A. Målqvist. *Localized orthogonal decomposition techniques for boundary value problems*. SIAM J. Sci. Comput. 36(4), pp. A1609–A1634, 2014. doi:10.1137/130933198.

[HM17] F. Hellman, A. Målqvist. *Contrast independent localization of multiscale problems*. Multiscale Model. Simul. 15(4), pp. 1325–1355, 2017. doi:10.1137/16M1100460.

[HMP11] R. Hiptmair, A. Moiola, I. Perugia. *Stability results for the time-harmonic Maxwell equations with impedance boundary conditions*. Math. Models Methods Appl. Sci. 21(11), pp. 2263–2287, 2011. doi:10.1142/S021820251100574X.

[HMP13] R. Hiptmair, A. Moiola, I. Perugia. *Error analysis of Trefftz-discontinuous Galerkin methods for the time-harmonic Maxwell equations*. Math. Comp. 82(281), pp. 247–268, 2013. doi:10.1090/S0025-5718-2012-02627-5.

[HMP15] P. Henning, P. Morgenstern, D. Peterseim. *Multiscale partition of unity*. In *Meshfree methods for partial differential equations VII*, vol. 100 of *Lect. Notes Comput. Sci. Eng.*, pp. 185–204. Springer, Cham, 2015.

[HMP16a] R. Hiptmair, A. Moiola, I. Perugia. *Plane wave discontinuous Galerkin methods: exponential convergence of the hp-version*. Found. Comput. Math. 16(3), pp. 637–675, 2016. doi:10.1007/s10208-015-9260-1.

[HMP16b] R. Hiptmair, A. Moiola, I. Perugia. *A Survey of Trefftz Methods for the Helmholtz Equation.* In *Building bridges: connections and challenges in modern approaches to numerical partial differential equations*, vol. 114 of *Lect. Notes Comput. Sci. Eng.*, pp. 237–278. Springer Cham, 2016.

[HO09] P. Henning, M. Ohlberger. *The heterogeneous multiscale finite element method for elliptic homogenization problems in perforated domains.* Numer. Math. 113(4), pp. 601–629, 2009. doi:10.1007/s00211-009-0244-4.

[HO15] P. Henning, M. Ohlberger. *Error control and adaptivity for heterogeneous multiscale approximations of nonlinear monotone problems.* Discrete Contin. Dyn. Syst. Ser. S 8(1), pp. 119–150, 2015. doi:10.3934/dcdss.2015.8.119.

[HOV16a] P. Henning, M. Ohlberger, B. Verfürth. *Analysis of multiscale methods for time-harmonic Maxwell's equations.* Proc. Appl. Math. Mech. 16(1), pp. 559–560, 2016. doi:10.1002/pamm.201610268.

[HOV16b] P. Henning, M. Ohlberger, B. Verfürth. *A new Heterogeneous Multiscale Method for time-harmonic Maxwell's equations.* SIAM J. Numer. Anal. 54(6), pp. 3493–3522, 2016. doi:10.1137/15M1039225.

[HP13] P. Henning, D. Peterseim. *Oversampling for the multiscale finite element method.* Multiscale Model. Simul. 11(4), pp. 1149–1175, 2013. doi:10.1137/120900332.

[HS05] V. H. Hoang, C. Schwab. *High-dimensional finite elements for elliptic problems with multiple scales.* Multiscale Model. Simul. 3(1), pp. 168–194, 2004/05. doi:10.1137/030601077.

[HS07] T. J. R. Hughes, G. Sangalli. *Variational multiscale analysis: the fine-scale Green's function, projection, optimization, localization, and stabilized methods.* SIAM J. Numer. Anal. 45(2), pp. 539–557, 2007. doi:10.1137/050645646.

[HS17] M. Hochbruck, C. Stohrer. *Finite element heterogeneous multiscale method for time-dependent Maxwell's equations.* In M. Bittencourt, N. Dumont, J. Hesthaven, eds., *Spectral and High Order Methods for Partial Differential Equations ICOSAHOM 2016*, vol. 119 of *Lect. Notes Comput. Sci. Eng.*, pp. 269–281. Springer, Cham, 2017. doi:10.1007/978-3-319-65870-4_18.

[HW97] T. Y. Hou, X.-H. Wu. *A multiscale finite element method for elliptic problems in composite materials and porous media.* J. Comput. Phys. 134(1), pp. 169–189, 1997. doi:10.1006/jcph.1997.5682.

[IB01] S. Irimie, P. Bouillard. *A residual a posteriori error estimator for the finite element solution of the Helmholtz equation.* Comput. Methods Appl. Mech. Engrg. 190(31), pp. 4027–4042, 2001. doi:10.1016/S0045-7825(00)00314-5.

[Ihl98] F. Ihlenburg. *Finite element analysis of acoustic scattering*, vol. 132 of *Applied Mathematical Sciences.* Springer-Verlag, New York, 1998. doi:10.1007/b98828.

[JE12] L. Jiang, Y. Efendiev. *A priori estimates for two multiscale finite element methods using multiple global fields to wave equations.* Numer. Methods Partial Differential Equations 28(6), pp. 1869–1892, 2012. doi:10.1002/num.20706.

[JEG10] L. Jiang, Y. Efendiev, V. Ginting. *Analysis of global multiscale finite element methods for wave equations with continuum spatial scales.* Appl. Numer. Math. 60(8), pp. 862–876, 2010. doi:10.1016/j.apnum.2010.04.011.

[JJWM08] J. D. Joannapolous, S. G. Johnson, J. N. Winn, R. D. Meade. *Photonic Crystals: Molding the Flow of Light*. Princeton University Press, Princeton, 2nd edn., 2008.

[JKO94] V. V. Jikov, S. M. Kozlov, O. A. Oleĭnik. *Homogenization of differential operators and integral functionals*. Springer-Verlag, Berlin, 1994. Translated from the Russian by G. A. Yosifian.

[KPY18] R. Kornhuber, D. Peterseim, H. Yserentant. *An analysis of a class of variational multiscale methods based on subspace decomposition*. Math. Comp. , 2018. doi:10.1090/mcom/3302. In press.

[KY16] R. Kornhuber, H. Yserentant. *Numerical homogenization of elliptic multiscale problems by subspace decomposition*. Multiscale Model. Simul. 14(3), pp. 1017–1036, 2016. doi:10.1137/15M1028510.

[LCQ17] P. Lu, H. Chen, W. Qiu. *An absolutely stable hp-HDG method for the time-harmonic Maxwell equations with high wave number*. Math. Comp. 86(306), pp. 1553–1577, 2017. doi:10.1090/mcom/3150.

[Li16] J. Li. *A literature review of mathematical study of metamaterials*. Int. J. Numer. Anal. Model. 13(2), pp. 230–243, 2016.

[LJJP02] C. Luo, S. G. Johnson, J. Joannopolous, J. Pendry. *All-angle negative refraction without negative effective index*. Phys. Rev. B 65(2001104), 2002.

[LM05] M. G. Larson, A. Målqvist. *Adaptive variational multiscale methods based on a posteriori error estimation: duality techniques for elliptic problems*. In *Multiscale methods in science and engineering*, vol. 44 of *Lect. Notes Comput. Sci. Eng.*, pp. 181–193. Springer, Berlin, 2005. doi:10.1007/3-540-26444-2_9.

[LM07] M. G. Larson, A. Målqvist. *Adaptive variational multiscale methods based on a posteriori error estimation: energy norm estimates for elliptic problems*. Comput. Methods Appl. Mech. Engrg. 196(21-24), pp. 2313–2324, 2007. doi:10.1016/j.cma.2006.08.019.

[LNW02] D. Lukkassen, G. Nguetseng, P. Wall. *Two-scale convergence*. Int. J. Pure Appl. Math. 2(1), pp. 35–86, 2002.

[LS13] A. Lamacz, B. Schweizer. *Effective Maxwell equations in a geometry with flat rings of arbitrary shape*. SIAM J. Math. Anal. 45(3), pp. 1460–1494, 2013. doi:10.1137/120874321.

[LS16a] A. Lamacz, B. Schweizer. *A negative index meta-material for Maxwell's equations*. SIAM J. Math. Anal. 48(6), pp. 4155–4174, 2016. doi:10.1137/16M1064246.

[LS16b] A. Lamacz, B. Schweizer. *Outgoing wave conditions in photonic crystals and transmission properties at interfaces*. preprint TU Dortmund, 2016. `http://www.mathematik.uni-dortmund.de/lsi/schweizer/Preprints/bloch-transmission-rev2016-12.pdf`, accepted at ESAIM Math. Model. Numer. Anal.

[LS16c] R. Lipton, B. Schweizer. *Effective Maxwell's equations for perfectly conducting split ring resonators*. preprint TU Dortmund, 2016. `http://www.mathematik.uni-dortmund.de/lsi/schweizer/Preprints/perfectcondrings-preprint.pdf`, accepted at Arch. Rat. Mech.

[MBS00] A.-M. Matache, I. Babuška, C. Schwab. *Generalized p-FEM in homogenization.* Numer. Math. 86(2), pp. 319–375, 2000. doi:10.1007/PL00005409.

[Mel95] J. M. Melenk. *On generalized finite-element methods.* ProQuest LLC, Ann Arbor, MI, 1995. Thesis (Ph.D.)–University of Maryland, College Park.

[ML68] C. S. Morawetz, D. Ludwig. *An inequality for the reduced wave operator and the justification of geometrical optics.* Comm. Pure Appl. Math. 21(2), pp. 187–203, 1968. doi:10.1002/cpa.3160210206.

[Moi11] A. Moiola. *Trefftz-Discontinuous Galerkin methods for time-harmonic wave problems.* Ph.D. thesis, ETH Zürich, 2011.

[Mon03] P. Monk. *Finite element methods for Maxwell's equations.* Numerical Mathematics and Scientific Computation, Oxford University Press, New York, 2003. doi:10.1093/acprof:oso/9780198508885.001.0001.

[Mor75] C. S. Morawetz. *Decay for solutions of the exterior problem for the wave equation.* Comm. Pure Appl. Math. 28(2), pp. 229–264, 1975. doi:10.1002/cpa.3160280204.

[MP14] A. Målqvist, D. Peterseim. *Localization of elliptic multiscale problems.* Math. Comp. 83(290), pp. 2583–2603, 2014. doi:10.1090/S0025-5718-2014-02868-8.

[MP15] A. Målqvist, D. Peterseim. *Computation of eigenvalues by numerical upscaling.* Numer. Math. 130(2), pp. 337–361, 2015. doi:10.1007/s00211-014-0665-6.

[MP18] A. Målqvist, A. Persson. *Multiscale techniques for parabolic equations.* Numer. Math. 138(1), pp. 191–217, 2018. doi:10.1007/s00211-017-0905-7.

[MS02] A.-M. Matache, C. Schwab. *Two-scale FEM for homogenization problems.* M2AN Math. Model. Numer. Anal. 36(4), pp. 537–572, 2002. doi:10.1051/m2an:2002025.

[MS11] J. M. Melenk, S. A. Sauter. *Wavenumber explicit convergence analysis for Galerkin discretizations of the Helmholtz equation.* SIAM J. Numer. Anal. 49(3), pp. 1210–1243, 2011. doi:10.1137/090776202.

[MS14] A. Moiola, E. A. Spence. *Is the Helmholtz equation really sign-indefinite?* SIAM Rev. 56(2), pp. 274–312, 2014. doi:10.1137/120901301.

[MS15] R. Milk, F. Schindler. *dune-gdt*, 2015. doi:10.5281/zenodo.35389.

[MS17] A. Moiola, E. A. Spence. *Acoustic transmission problems: Wavenumber-explicit bounds and resonance-free regions.* arXiv preprint, 2017. `arXiv:1702.00745`.

[MS18] J. M. Melenk, S. Sauter. *Wavenumber-explicit hp-FEM analysis for Maxwell's equations with transperant boundary conditions.* arXiv preprint, 2018. `arXiv:1803.01619`.

[Ngu89] G. Nguetseng. *A general convergence result for a functional related to the theory of homogenization.* SIAM J. Math. Anal. 20(3), pp. 608–623, 1989. doi:10.1137/0520043.

[NW12] T. Nguyen, J.-N. Wang. *Quantitative uniqueness estimate for the Maxwell system with Lipschitz anisotropic media.* Proc. Amer. Math. Soc. 140(2), pp. 595–605, 2012. doi:10.1090/S0002-9939-2011-11137-7.

[Ohl05] M. Ohlberger. *A posteriori error estimates for the heterogeneous multiscale finite element method for elliptic homogenization problems.* Multiscale Model. Simul. 4(1), pp. 88–114, 2005. doi:10.1137/040605229.

[OP98] A. A. Oberai, P. M. Pinsky. *A multiscale finite element method for the Helmholtz equation.* Comput. Methods Appl. Mech. Engrg. 154(3-4), pp. 281–297, 1998. doi:10.1016/S0045-7825(97)00130-8.

[OP02] S. O'Brien, J. B. Pendry. *Photonic band-gap effects and magnetic activity in dielectric composites.* J. Phys.: Condens. Matter 14(15), p. 4035, 2002. doi:10.1088/0953-8984/14/15/317.

[OS15] M. Ohlberger, F. Schindler. *Error control for the localized reduced basis multiscale method with adaptive on-line enrichment.* SIAM J. Sci. Comput. 37(6), pp. A2865–A2895, 2015. doi:10.1137/151003660.

[OV17] M. Ohlberger, B. Verfürth. *Localized Orthogonal Decomposition for two-scale Helmholtz-type problems.* AIMS Mathematics 2(3), pp. 458–478, 2017. doi:10.3934/Math.2017.2.458.

[OV18] M. Ohlberger, B. Verfürth. *A new Heterogeneous Multiscale Method for the Helmholtz equation with high contrast.* Mulitscale Model. Simul. 16(1), pp. 385–411, 2018. doi:10.1137/16M1108820.

[Owh17] H. Owhadi. *Multigrid with rough coefficients and multiresolution operator decomposition from hierarchical information games.* SIAM Rev. 59(1), pp. 99–149, 2017. doi:10.1137/15M1013894.

[OZ11] H. Owhadi, L. Zhang. *Localized bases for finite-dimensional homogenization approximations with nonseparated scales and high contrast.* Multiscale Model. Simul. 9(4), pp. 1373–1398, 2011. doi:10.1137/100813968.

[OZ17] H. Owhadi, L. Zhang. *Gamblets for opening the complexity-bottleneck of implicit schemes for hyperbolic and parabolic ODEs/PDEs with rough coefficients.* J. Comput. Phys. 347, pp. 99–128, 2017. doi:10.1016/j.jcp.2017.06.037.

[OZB14] H. Owhadi, L. Zhang, L. Berlyand. *Polyharmonic homogenization, rough polyharmonic splines and sparse super-localization.* ESAIM Math. Model. Numer. Anal. 48(2), pp. 517–552, 2014. doi:10.1051/m2an/2013118.

[PE03] A. Pokrovsky, A. Efros. *Diffraction theory and focusing of light by a slab of left-handed material.* Physica B: Condensed Matter 338(1-4), pp. 333–337, 2003. Proceedings of the Sixth International Conference on Electrical Transport and Optical Properties of Inhomogeneous Media.

[Pen00] J. B. Pendry. *Negative refraction makes a perfect lens.* Phys. Rev. Lett. 85(18), pp. 3966–3969, 2000. doi:10.1103/PhysRevLett.85.3966.

[Pet10] M. Petzold. *Regularity and error estimators for elliptic problems with discontinuous coefficients.* Ph.D. thesis, Freie Universität Berlin, 2010.

[Pet16] D. Peterseim. *Variational multiscale stabilization and the exponential decay of fine-scale correctors.* In *Building bridges: connections and challenges in modern approaches to numerical partial differential equations*, vol. 114 of *Lect. Notes Comput. Sci. Eng.*, pp. 341–367. Springer, Cham, 2016.

[Pet17] D. Peterseim. *Eliminating the pollution effect in Helmholtz problems by local subscale correction.* Math. Comp. 86(305), pp. 1005–1036, 2017. doi:10.1090/mcom/3156.

[PPR16] I. Perugia, P. Pietra, A. Russo. *A plane wave virtual element method for the Helmholtz problem.* ESAIM Math. Model. Numer. Anal. 50(3), pp. 783–808, 2016. doi:10.1051/m2an/2015066.

[PS16] D. Peterseim, R. Scheichl. *Robust numerical upscaling of elliptic multiscale problems at high contrast.* Comput. Methods Appl. Math. 16(4), pp. 579–603, 2016. doi:10.1515/cmam-2016-0022.

[PS17] D. Peterseim, M. Schedensack. *Relaxing the CFL condition for the wave equation on adaptive meshes.* J. Sci. Comput. 72(3), pp. 1196–1213, 2017. doi:10.1007/s10915-017-0394-y.

[PSS06] J. B. Pendry, D. Schurig, D. R. Smith. *Controlling electromagnetic fields.* Science 312(5781), pp. 1780–1782, 2006. doi:10.1126/science.1125907.

[PZ02] J. E. Pasciak, J. Zhao. *Overlapping Schwarz methods in H(curl) on polyhedral domains.* J. Numer. Math. 10(3), pp. 221–234, 2002. doi:10.1515/JNMA.2002.221.

[Sau06] S. A. Sauter. *A refined finite element convergence theory for highly indefinite Helmholtz problems.* Computing 78(2), pp. 101–115, 2006. doi:10.1007/s00607-006-0177-z.

[Sch74] A. H. Schatz. *An observation concerning Ritz-Galerkin methods with indefinite bilinear forms.* Math. Comp. 28, pp. 959–962, 1974. doi:10.2307/2005357.

[Sch05] J. Schöberl. *A multilevel decomposition result in $H(curl)$.* In P. H. P. Wesseling, C.W. Oosterlee, ed., *Multigrid, Multilevel and Multiscale Methods, Proceedings of the 8th European Multigrid Conference, EMG*, 2005.

[Sch08] J. Schöberl. *A posteriori error estimates for Maxwell equations.* Math. Comp. 77(262), pp. 633–649, 2008. doi:10.1090/S0025-5718-07-02030-3.

[Sch17] B. Schweizer. *Resonance meets homogenization: construction of metamaterials with astonishing properties.* Jahresber. Dtsch. Math.-Ver. 119(1), pp. 31–51, 2017. doi:10.1365/s13291-016-0153-2.

[Spe14] E. A. Spence. *Wavenumber-explicit bounds in time-harmonic acoustic scattering.* SIAM J. Math. Anal. 46(4), pp. 2987–3024, 2014. doi:10.1137/130932855.

[SPV+00] D. R. Smith, W. J. Padilla, D. C. Vier, S. C. Nemat-Nasser, S. Schultz. *Composite Medium with Simultaneously Negative Permeability and Permittivity.* Phys. Rev. Lett. 84(18), pp. 4184–4187, 2000. doi:10.1103/PhysRevLett.84.4184.

[SPW04] D. R. Smith, J. B. Pendry, M. C. K. Wiltshire. *Metamaterials and negative refractive index.* Science 305(5685), pp. 788–792, 2004. doi:10.1126/science.1096796.

[ST17] S. A. Sauter, C. Torres. *Stability estimate for the Helmholtz equation with rapidly jumping coefficients.* arXiv preprint, 2017. `arXiv:1711.05430`.

[SU17] B. Schweizer, M. Urban. *Effective Maxwell's equations in general periodic microstructures.* Applicable Analysis pp. 1–21, 2017. doi:10.1080/00036811.2017.1359563. In press.

[Ver17a] B. Verfürth. *Heterogeneous Multiscale Method for the Maxwell equations with high contrast.* arXiv preprint, 2017. `arXiv:1710.09609`.

[Ver17b] B. Verfürth. *Numerical Homogenization for indefinite H(curl)-problems.* In K. Mikula, D. Sevcovic, J. Urban, eds., *Proceedings of Equadiff 2017 conference*, pp. 137–146. Slovak University of Technology, Bratislava, 2017.

[Ves68] V. G. Veselago. *The electrodynamics of substances with simultaneously negative values of ε and μ.* Soviet Physics Uspekhi 10(4), pp. 509–514, 1968. doi: 10.1070/PU1968v010n04ABEH003699.

[Vis07] A. Visintin. *Two-scale convergence of first-order operators.* Z. Anal. Anwend. 26(2), pp. 133–164, 2007. doi:10.4171/ZAA/1315.

[Wel01] N. Wellander. *Homogenization of the Maxwell equations. Case I. Linear theory.* Appl. Math. 46(1), pp. 29–51, 2001. doi:10.1023/A:1013727504393.

[Wel09] N. Wellander. *The two-scale Fourier transform approach to homogenization; periodic homogenization in Fourier space.* Asymptot. Anal. 62(1-2), pp. 1–40, 2009. doi:10.3233/ASY-2008-0914.

[Wey17] M. Weymuth. *Adaptive Local (AL) basis for elliptic problems with L^∞-coefficients.* arXiv preprint, 2017. `arXiv:1703.06325`.

[WK03] N. Wellander, G. Kristensson. *Homogenization of the Maxwell equations at fixed frequency.* SIAM J. Appl. Math. 64(1), pp. 170–195, 2003. doi:10.1137/S0036139902403366.

[WW14] C. Wieners, B. Wohlmuth. *Robust operator estimates and the application to substructuring methods for first-order systems.* ESAIM Math. Model. Numer. Anal. 48(5), pp. 1473–1494, 2014. doi:10.1051/m2an/2014006.

[XH14] B. Xia, V. H. Hoang. *High dimensional finite elements for multiscale wave equations.* Multiscale Model. Simul. 12(4), pp. 1622–1666, 2014. doi:10.1137/120902409.

[Zag06] S. Zaglmayr. *High order finite element methods for electromagnetic field computation.* Ph.D. thesis, Universität Linz, 2006.

[ZCW10] Y. Zhang, L.-Q. Cao, Y.-S. Wong. *Multiscale ccomputation for 3D time-dependent Maxwell's equations in composite materials.* SIAM J. Sci. Comput. 32, pp. 2560–2583, 2010. doi:10.1137/080740337.